

A THEORETICAL INVESTIGATION OF
SURFACE PHENOMENA

Thesis

by

Wilson Ho

In Partial Fulfillment of the Requirements for
the Degree of Master of Science

California Institute of Technology
Pasadena, California

1975

(Submitted June 6, 1975)

*This thesis is dedicated to
My Father, Mother, Dorian,
WenChi and Jack.*

ACKNOWLEDGMENTS

It has been indeed a most enjoyable year working with Dr. Steve Cunningham and Professor Henry Weinberg. The guidance they provided me throughout this work has been most inspiring. They have installed a great deal of confidence in me and encouraged me by their constant belief in my ability to do science. I thank them for spending their time and energy in perfecting my talk at the AVS conference last October and teaching me how to do science and write technical papers. In addition, they showed a great deal of responsibility for the members of this research group. Besides providing me a constant companionship at work, they further spent time with me in the basketball or the tennis courts. I am most grateful to Professor Weinberg for pointing out and photocopying for me the interesting current articles and spending time talking with me often in the evenings. During this past year, Henry and Steve have become two of my best friends.

To Professor Wilse Robinson, I owe much to him for teaching me what to do in science. He also taught me not to get discouraged when things get rough in the laboratory. I thank him for his generous support and for letting me have the picosecond laser almost completely to myself during the summer of 1973. The bike ride with him up Mt. Wilson was a memorable experience.

To Professor Aron Kuppermann, I thank him for providing me a Teaching Assistant's position in Chemistry 125c. It was a fun experience. I am grateful to him for serving as my undergraduate advisor and for letting me do research in vacuum ultraviolet photochemistry during my freshman year.

To Professor Bill Goddard, I am most grateful to him for teaching me quantum molecular calculations. I am sure that some of these ideas will

be of great use to me in my future work in surface science.

I am grateful to the National Science Foundation Undergraduate Research Program for its support during the summer of 1974. It was during this time that this work was undertaken. The generous support throughout my undergraduate years from the California State Scholarship and Loan Commission, the George H. Mayr Educational Foundation and the California Institute of Technology are also gratefully acknowledged.

I would like to thank Caltech and, in particular, the Division of Chemistry and Chemical Engineering for the education and the research opportunities it provided me. I am most grateful for the freedom I enjoyed. In many respects, save for the smog in the summer, Caltech is indeed an ideal place to do research.

My association with Page House has been a most enjoyable one. It was the center of my social life for the last four years. I am grateful for the friendship with the people in the house and in particular, Tak Sing Lo, Wai Cheng, Doug Schladweiler, Jack Stemple, Mark Hueschen, Gary Wakai, Joe Fahle, George Hendrickson and Ben Chun before his most unfortunate departure from us.

Finally, this thesis could not have appeared in its final form without the able, efficient, critical and beautiful typing of the second chapter by Carla Willard and the rest by Jennifer Burkhart. Special thanks go to Jennifer Burkhart for her most willing cooperation during the final preparation of this thesis.

Rocky

ABSTRACT

Using the Linear Combination of Atomic Orbitals (LCAO) formalism and the tight-binding approximation, we have investigated three separate types of surface phenomena via the Green's function method and the phase shift technique. We obtain the shift in the energy levels due to the following: (1) creation of the surface, (2) surface reconstruction, and (3) the adsorption of a single atom. In the first two parts, we study the (001) face of a two-band crystal with the CsCl structure, simulating the surface properties of semiconductors or insulators. In the third part, we study the interaction of a single atom with the (001) surface of a bcc metal. The results obtained are contrasted with those obtained from a one-band calculation for the (001) surface of a simple cubic crystal. We find that the second unoccupied band is of utmost importance in understanding these surface phenomena.

TABLE OF CONTENTS

	Page
Acknowledgments	iii
Abstract	v
I. INTRODUCTION	1
II. ELECTRONIC STRUCTURE OF CLEAN SURFACES	7
A. An Overview of the Calculation and Results	8
B. Green's Function Calculation of the Surface Properties of a Two-Band Crystal	11
III. ATOMIC REARRANGEMENT ON CLEAN CRYSTAL SURFACES	79
A. Lowering of the Electronic Energy Due to Surface Reconstruction	80
B. Effect of Surface Reconstruction on the Electronic Energy of a Two-Band Crystal	92
IV. SINGLE ATOM CHEMISORPTION ON A BCC METAL	156
V. CONCLUSIONS	191
VI. APPENDICES	194
A. Quantum Molecular Calculation of the Low Lying States of Cyclobutadiene	195
B. Picosecond Spectroscopy - A Study of Nonlinear Optical Phenomena	206

CHAPTER I
INTRODUCTION

I. INTRODUCTION

Chemisorption and chemical reactions on solid surfaces depend crucially upon the electronic structure and the geometry of the surface atoms. At the present time, we have at our disposal the experimental techniques to determine the composition and atomic geometry of the surface species (e.g., Auger electron spectroscopy and low-energy electron diffraction) as well as the surface electronic structure (e.g., photoemission and ion neutralization spectroscopy). This is largely due to the new instrumentation available to study processes occurring on solid surfaces under ultra-high vacuum conditions. However, the theories concerning these processes are still very rudimentary at the present time. At best, they give only semi-quantitative agreement with experimental results. More often, the calculations are carried out with assumptions which lead to a great deal of simplification. These model calculations can only give us qualitative understanding of surface phenomena.

The difficulties in the theories arise from the enormous number of particles involved in the problem. As such, one has to consider many-body effects. In molecules with several electrons, the electrons are correlated in their motion. The correlation is achieved by incorporating the distance between two electrons r_{ij} , or mixing excited states into the wave function. For a many-electron system, such an approach would be desirable but, for obvious reasons, has not been successfully implemented. The response of the system to an external perturbation, e.g., the creation of a surface, surface reconstruction or chemisorption, involves the participation of all electrons to varying degrees. In addition, a crystal with a surface has a reduced symmetry compared to the infinite crystal. This is due to the loss

of translational symmetry in the direction perpendicular to the surface. The discontinuity in the periodicity of the atoms requires that we know the potential energy in the surface region. Such a potential would decay away from the surface and into the vacuum.

In principle, one can write down a many-body Hamiltonian that includes the interaction of all the electrons plus the correct potential energy with the proper boundary conditions. As far as we know, the solutions of the Schrödinger equation with this Hamiltonian would give us complete and accurate solutions that would agree with experiment to arbitrary accuracy. However, this is a hopeless task. Instead, a great deal of simplification is made if we assume the electrons to move independently of one another. The interactions between the electrons are approximated such that the Hamiltonian becomes a one-electron Hamiltonian. Within this one-electron picture, the energy levels form energy bands and provide us an interpretation of many physically observed facts. An important consequence of the band picture is the occurrence of energy gaps in some crystals. Crystals with energy gaps are called semiconductors or insulators. Semiconductors, such as Si and Ge, are of great importance, especially in the electronics industry. Consequently, a great deal of research aimed at understanding these materials has been carried forward both in industrial and university laboratories.

Since the one-electron picture has given us much insight into the properties of an infinite crystal, it is natural to apply it to the study of surface phenomena. Throughout the calculations in this thesis, the valence electrons are assumed to be moving independently of one another. Each electron moves in the potential due to the ion cores of the lattice

atoms. From this one-electron Hamiltonian, we obtain the energy bands and the wave functions for the infinite crystal. The potential is assumed to undergo a step function change from the bulk value to that of the vacuum (taken to be the zero reference) at the surface. The wave functions for the surface are obtained by a perturbation method. In this way, we have a wave mechanical description of a crystal with a surface.

The nature of chemical bonds in molecules depends largely on the orbitals of the interacting electrons, their energies and spatial distributions. Once the bonding is known, the structure corresponding to the most favorable configuration can be found. In chemical dynamics, reactions take place along minimum energy paths on the potential energy surfaces. In the gas phase, these energy surfaces are calculated by obtaining the energetically most favorable spatial distribution of the electrons at each configuration of the nuclei. Thus a knowledge of the spatial and energy distribution of the electrons is crucial in understanding both the structure and dynamics of molecules.

In solids, it is equally important to know the distribution of the electrons in momentum (\vec{k}) space assuming the one-electron picture. This corresponds to a knowledge of the band structure. For a crystal with a surface, both theory and experiment show a band structure that is different from that of the bulk. A knowledge of the electronic structure of the surface is crucial in understanding both the surface structure and dynamics.

It is believed that the two major factors affecting adsorption and chemical reactions on solid surfaces are the geometry of the atoms in the surface region and the electronic structure of the surface. Both are consistent with chemical bonding concepts in molecules, i.e., the role of the

spatial and energy distribution of the electrons. Therefore, before a clear understanding of adsorption and chemical reactions on solid surfaces can be obtained, we have to know first the electronic structure of the clean surface. The positions of the atoms in the surface region are inputs to the calculation. Although both the theoretical and experimental investigations are often carried out on well-characterized surfaces which are seldom realized in real situations, the importance of fundamental research cannot be overestimated. The ultimate goal of surface physics is to understand, control and improve catalytic reactions on surfaces, with the hope that the results obtained on well-characterized surfaces can be extrapolated to more realistic chemical reaction conditions.

Therefore, the first part of this project consists of a calculation of the electronic structure of the clean surface for a two-band crystal, appropriate for semiconductors or insulators. Experimentally, it is known that states localized on the surface can exist inside the band gap. These states are known to play an important role in semiconductor devices. Since they are localized on the surface, they might be important in the interaction with foreign gaseous molecules. Thus, it is desirable to know the conditions for their existence and their positions in momentum (\vec{k}) space. In addition, the presence of a surface can shift the energy levels in the bulk bands. Furthermore, the effect of the empty conduction band on the surface electronic structure can be studied.

The above calculation assumes that the positions of the surface atoms are the same as their equilibrium positions in the bulk. It is a well-known fact that on many surfaces, the atoms are shifted periodically from their bulk equilibrium positions. The positions of the atoms can be probed

by diffracting low-energy electrons ($\lesssim 500$ eV) from solid surfaces. The dimensions of the surface unit cells can be determined from the diffraction patterns. In some cases, they show a larger surface unit cell than if the atoms stay in their bulk equilibrium positions. In the second part of the project, we investigate a possible mechanism of surface reconstruction (rearrangement of atoms on the surface). The theory is based on the fact that the electronic energy must be lowered if the surface reconstructs.

After the properties of the clean surface are well-understood, we then proceed, in the third part of this project, to study the interaction of a foreign atom with the surface. This constitutes the most fundamental step in any surface reaction. We investigate the interaction of a discrete adatom state with an underlying continuum of states. The interaction leads to bonding and antibonding resonances which are familiar concepts in chemistry.

The above three parts of the project constitute a rather complete analysis of the fundamental properties of the clean surface and its interaction with a foreign atom. To summarize, the questions we want to answer in this project are the following:

1. What is the effect on the electronic structure when a surface is created?
2. Why do atoms on the surface rearrange into new periodic structures?
3. What is the effect on the electronic structure when a foreign atom interacts with the surface?

These three separate, but related, questions correspond to three different perturbations on a surface. The following three chapters explore fully their effects on the energy levels of the unperturbed systems.

CHAPTER II

ELECTRONIC STRUCTURE OF CLEAN SURFACES

Section A: An Overview of the Calculation and Results

[Published as an extended abstract in J. Vac.

Sci. Technol. 12, 351 (1975)].

Section B: Green's Function Calculation of the Surface

Properties of a Two-Band Crystal

[in press, Phys. Rev. B12 (1975)].

Abstract: Surface Properties of a Two-Band Semiconductor

W. Ho, S. L. Cunningham and W. H. Weinberg

Division of Chemistry and Chemical Engineering, California Institute of Technology, Pasadena, California 91125

L. Dobrzynski

Institut Max von Laue-Paul Langevin, B P 156 Centre de tri, 38042 Grenoble Cedex, France

It has been shown^{1,2,3} that very simple model calculations can give useful insight into the properties of solid surfaces. This is due largely to the fact that the calculations can be carried quite far analytically so that only simple numerical computations are needed. Previous work^{1,2,3} has been confined to the study of one-band crystals of various structure and has been used to simulate the surface properties of metals. In this work, we present results of a two-band calculation which are appropriate for the study of semiconductor surfaces.

Using the LCAO or the tight-binding formalism, we have calculated the band energies for a two-band semiconductor with a CsCl structure. One orbital is assumed for each atom in the crystal with the orbitals being different for the two basis atoms in the unit cell. With these bands, the free surface properties of the (001) surface are calculated using the Green's function and the phase shift techniques,^{1,2} which are similar to that used to study point defects in a crystal. The phase shift technique allows us to determine the change in the density of states due to the perturbation caused by creating the surface. A major advantage in the present calculation is that the Green's function is obtained analytically.

We have calculated the free surface properties for three different models. In the first, we consider only the nearest neighbor hopping integral (resonance integral), γ_1 . In the second calculation, we extend the first to include one

of the second neighbor interactions, γ_2 , the hopping integral between atoms of the same type in adjacent unit cells. In these two calculations, we do not consider the variation of the local potential in the vicinity of the surface. In the third calculation, we have added to the first model a change in the self-energies of the surface atoms, U_0 . With only γ_1 included in the calculation, no surface states are found. With γ_2 added, Shockley surface states appear inside the band gap. With U_0 added, Tamm surface states appear inside the band gap. In addition, surface states occur above the conduction band. The surface states appear for arbitrarily small γ_2 and U_0 , and their separation distance from the top of the valence band (and the top of the conduction band, in the case with U_0) is proportional to the magnitude of γ_2 and U_0 . Since the energy states below the band gap are completely filled for a semiconductor, Friedel's sum rule is satisfied, and all three of our calculations are self-consistent.

Within the nearest-neighbor-interaction framework, we have calculated the variation in the surface tension as a function of the filling of the band. We have also found the change, due to the surface, in the electronic specific heat and electronic surface entropy as a function of temperature. These properties are significantly different from those calculated with a filled one-band model,³ and are consistent with the known properties of a semiconductor. Thus, we show that the presence of the second unoccupied band is crucial in studying semiconductor surfaces.

The present calculations can be easily extended to the study of the free surface of the alkali metals with the b.c.c. crystal structure by setting the energy gap to zero. When this is done, our calculations agree with previous results.²

References

1. D. Kalkstein and P. Soven, Surface Sci., 26, 85 (1971).
2. G. Allan and P. Lengart, Surface Sci., 30, 641 (1972).
3. G. Allan and P. Lengart, Surface Sci., 15, 101 (1969).

Green's Function Calculation of the Surface
Properties of a Two-Band Crystal*

W. Ho[†], S. L. Cunningham[‡] and W. H. Weinberg
Division of Chemistry and Chemical Engineering
California Institute of Technology
Pasadena, California 91125

and

L. Dobrzynski
Laboratoire de Physique des Solides
Institut Supérieur d'Electronique du Nord
3, rue Francois Baës
59046 Lille Cedex
France

January, 1975

To Be Submitted to Physical Review B

* Work partially supported by NSF Grant GK-43433

† NSF Undergraduate Research Participant

‡ IBM Postdoctoral Research Fellow

ABSTRACT

We have calculated the electronic properties of the clean (001) surface of three model crystals with the CsCl structure. One model results in no surface states, the second model yields Shockley surface states, and the third model yields Tamm surface states. We derive analytic expressions for both the bulk crystal Green's function and the (001) surface Green's function. Using the resolvent technique, we present the surface state bands. Using the phase shift technique, we present the change in the total density of states (both inside and outside of the bands) due to the creation of the surface. From this we show the change in the specific heat due to the surface, and we find the surface entropy. Finally, we use the surface Green's function to determine the local densities of states for the layers near the surface and compare them with the local density of states in the bulk. Our results, which can be used to understand the properties of both semi-conductor and insulator surfaces, are contrasted with previous results for one-band crystal surfaces which are appropriate only for metals.

I. INTRODUCTION

Chemical and physical processes which occur at a solid surface depend critically upon the electronic structure of the surface layer of atoms. For example, adatoms which chemisorb to the surface interact with the first layer of atoms. In addition, the presence of surface states can cause the electronic energy bands to bend and thereby alter the electrical conductivity in the surface region. In order to understand these processes from a fundamental point of view, we must start with the study of the electronic structure of the clean surface. In a later paper,¹ we will build on the results of this paper and consider the problem of chemisorption and reconstruction.

In this paper we are concerned with the electronic properties of the clean (001) surface of a three-dimensional two-component crystal which has the CsCl structure (two interpenetrating simple cubic lattices). We use the Linear Combination of Atomic Orbitals (LCAO) formalism within the limits of the Tight Binding (TB) approximation. The Green's function (or resolvent) is determined for the bulk crystal as well as the perturbation required to create the surface. Then the phase shift function is calculated from which the change in the electronic density of states due to the perturbation can be found. In addition, we find the surface Green's function from which we obtain the density of states for each layer in the crystal. Each aspect of this calculation is reviewed briefly below.

There is a long history, reviewed by Koutecky² and by Davison and Levine,³ of the use of the LCAO and TB approximations for studying surface properties. In 1939 Goodwin⁴ first used the method to study a finite monatomic linear chain. He found that electronic surface states (where the wave function and charge density are localized near the chain ends) were present

only if the energy of the orbital on the end atoms was altered by more than a critical amount. Later, Hoffmann and Konya⁵ studied the same system without the restriction of the TB approximation.

Use of the LCAO method on mixed linear crystals started in 1951 with the work of Hoffmann.⁶ He considered the bulk properties of an infinite chain of the type $A_n B_m$ where n and m are arbitrary integers. Later, Amos and Davison⁷ examined the surface properties of the simpler AB type chain. For the infinite chain, there are two energy bands separated by an energy gap. As in the work of Goodwin,⁴ they found that the electron orbital energy on the surface atoms must be perturbed in order to get surface states. Their surface states (called outer states) fell either above the top band or below the bottom band. More general work by Davison and Koutecky⁸ found that surface states could also appear in the band gap (inner states) for certain types of perturbations.

Levine and Davison⁹ compared qualitatively the results from a one-dimensional LCAO chain calculation to real binary systems such as NaCl, CdS and GaAs. They assumed the chain to be made up of alternating s-like and p-like atoms. This model, unlike those previously considered, gives the band gap minimum at the center of the Brillouin zone rather than at the zone edge. They found that surface states appeared in the band gap even without perturbing the electron orbital energies of the end atoms. Thus the LCAO method can give rise to the two general types of surface states: namely, the Tamm state where a perturbation near the surface is required and the Shockley state where no perturbation is needed. In addition to the study of surface states, the LCAO formalism has been used to study more subtle properties of one-dimensional systems. As an example, Cunningham and Maradudin¹⁰ have recently used the LCAO approach to calculate the surface induced dynamic effective charge near the ends of a finite chain.

The LCAO-TB formalism has also been applied to three-dimensional systems using three different techniques. One important technique which was used by Koutecky and Tomasek¹¹ first solves for the bulk electronic energy levels as a function of the general complex wave vector. The allowed values of the wave vector are then determined by satisfying the appropriate boundary conditions; namely, the wave function in the crystal must match smoothly onto a decaying wave function in the vacuum. This technique of wave function matching has been used widely in studying surface states,¹² but since it does not generally use the LCAO formalism, we will not mention it further.

Another important technique which is used widely is based on the observation by Goodwin¹³ that for each wave vector component parallel to the surface, the three-dimensional problem takes on the same form as the one-dimensional problem. This has led to a series of papers dealing with slab systems in which the crystal is infinite in extent in two directions but finite (typically less than 20 layers) in the third direction. Then for each wave vector component, an eigenvalue matrix of manageable size (size is determined by the product of the number of orbitals per atom and the number of layers in the slab) is obtained. Work using this technique has appeared by Pugh,¹⁴ Hirabayashi,¹⁵ Alstrup,^{16,17} and more recently by Pandey and Phillips.^{18,19} With the exception of work by Joannopolous and Cohen²⁰ on GaAs, the use of the LCAO technique with slab calculations has been confined to single component crystals of the diamond structure. Many other slab calculations have been done,²¹ but they do not use the LCAO approach.

These two techniques give information about the energy and wave function of the surface states for various components of the two-dimensional wave vector parallel to the surface. They do not, however, allow one to determine the change in the bulk density of states upon creating the surface, nor do they

allow one to study the density of state changes which occur in chemisorption. This information is important in the study of photoemission and the study of heterogeneous catalysis, and it can be obtained by the third technique (the one we use in this paper).

The third technique for using the LCAO formalism for studying the surface of three-dimensional systems is known as the Green's function or resolvent technique. The details of this method will be discussed in Section III. Baldock²² used this approach (which is due to Lifshitz) to combine the Green's function method with the LCAO model. Then Koster and Slater²³ generalized the method and applied it to the study of impurity levels and end effects of simple one-dimensional systems. Koutecky and Davison²⁴ applied the technique to a general mixed one-dimensional crystal where the unit cell is composed of an arbitrary number of atoms of an arbitrary type. They demonstrated how both Tamm and Shockley surface states can arise. Thus, the situation now is that the surface electronic properties of one-dimensional systems are well understood.

Concerning three-dimensional systems, the resolvent method has been used by Koutecky,²⁵ Holland,²⁶ and Brown²⁷ to formally discuss the properties of surface states. Tomasek²⁸ applied the method to the study of the (111) surface of silicon and by using several simplifications performed the entire calculation analytically. Later, Freeman²⁹ showed how the resolvent method can be applied to more realistic systems by performing numerical calculations. Then Levine and Freeman³⁰ applied the technique to the surface of a crystal with the zinc blende structure. They examined the effect of changes in the positions of the surface atoms upon the energies of the surface states thereby illustrating the flexibility and power of the resolvent technique. Very recently, van der Avoird, et al.,³¹ have set up a numerical procedure based

on the resolvent technique applied to a finite slab geometry. This technique should be suitable for quantitative calculations on real systems, but results from this approach are yet to appear.

As we will see below, the resolvent technique requires knowledge of the bulk Green's function and the perturbation required to create the surface. The calculations presented above²²⁻³¹ result in a determination of the energy of the surface state as a function of wave vector parallel to the surface. The density of states is generally not obtained. A variation of the resolvent method was used by Kalkstein and Soven³² wherein they solve directly for the Green's function appropriate for the surface. This allows them to calculate directly the density of states for each layer in the crystal. Thus, the effect of the surface on the bulk electronic levels can be directly seen independent of whether surface states exist. Bose and Foo³³ have recently performed a similar calculation on a one-dimensional binary system simulating an ionic crystal.

The phase shift technique, coupled with the Green's function method, is a convenient way to study the effect of a perturbation upon the energy levels of a general Hamiltonian. DeWitt³⁴ presented the essential elements of the phase shift technique which has been formally applied to the problem of surfaces by Blandin³⁵ and Toulouse.³⁶ The method calculates the phase shift in the Bloch waves due to scattering from a perturbation (the surface). This phase shift gives the change in the energy levels due to the perturbation and thus can be related to the change in the density of states. This, in turn, can be related to several physical properties of interest regarding the surface.

This approach has been applied to several model systems. Allan,³⁷ and Allan and Lengart^{38,39} have extensively studied the clean surface properties of a one-electron-band crystal of various structures (sc, fcc, bcc). They

showed how the surface perturbation can give rise to surface states as well as how the bulk states are changed due to the surface, and, in addition, they found the change in the electronic specific heat due to the creation of the surface.

The phase shift approach can also be used to study chemisorption. Recently, Einstein⁴⁰ has expanded earlier work of Einstein and Schrieffer⁴¹ to study the changes in the density of states caused by chemisorption. This application of the phase shift technique complements the Green's function approach to chemisorption that has been discussed by Schrieffer⁴² and Grimley and Pisani.⁴³

The main advantage of the phase shift technique is that it gives directly the change in the density of states. This information is important since it is directly applicable to photoemission and chemisorption. No other method gives this same information in such a straightforward manner. The main disadvantage to the phase shift technique is its dependence on knowledge of the crystal Green's function. Usually, one must use numerical techniques for even the simplest of model cases. As a consequence, all of the work to date³⁷⁻⁴¹ has been confined to studying model one-band crystals. These results, then, have only been useful in understanding the surface properties of metals.

In this paper, we apply the phase shift technique for the first time to a model two-band crystal. An important point is that we have been able to obtain the Green's function for the bulk in an analytic form. Thus, whereas some numerical work is required, the complete calculation is no more difficult than the previously considered one-band crystals. The results of this calculation, then, are useful in understanding the surface properties of semi-conductors and insulators.

In Section II we derive the bulk properties of our model. This includes the bulk band structure as well as the bulk crystal Green's functions. In Section III we discuss the phase shift technique and present the perturbations appropriate for the surface. Here we consider three distinct cases; i.e., one which yields no surface states, one which results in Shockley surface states, and finally one which produces Tamm surface states. We show the change in the density of states due to the creation of the surface and determine the surface contribution to the specific heat for each case. In Section IV we obtain the surface Green's function for the case in which there are no surface states. This allows us to find the local density of states for each layer in the crystal. In Section V we summarize our results.

II. BULK GREEN'S FUNCTIONS

The one-electron Hamiltonian for the bulk crystal is given by

$$H_0 = \frac{p^2}{2m_e} + \sum_{\ell} \sum_{\beta} U \left[\vec{r} - \vec{x} \begin{pmatrix} \ell \\ \beta \end{pmatrix} \right] , \quad (1)$$

where p is the electron momentum operator, m_e and \vec{r} are the mass and position, respectively, of the electron, and $\vec{x}(\ell\beta)$ is the position of the β th type basis atom in the ℓ th unit cell of the crystal. We consider a crystal with the CsCl structure so that the index β takes on two values, 1 or 2, for the two types of atoms in the unit cell. The term U is the electron-ion core potential which is centered on each atom site. As is common in the LCAO formalism, electron-electron interactions are neglected.

The solution of the Schrödinger equation is assumed to be of the form

$$\psi(\vec{r}) = \sum_{\ell} \sum_{\beta} c_{\ell\beta} \phi \left[\vec{r} - \vec{x} \begin{pmatrix} \ell \\ \beta \end{pmatrix} \right] , \quad (2)$$

where $\Phi(\vec{r} - \vec{x}(\ell\beta))$ is an atomic-like orbital for a free atom centered on site $(\ell\beta)$. For this calculation, we assume one orbital for each atom in the crystal, and, whereas the specific form of the orbital is never needed, the orbital is assumed to be spherically symmetric (s-like).

Substituting Eq. (2) into the Schrödinger equation and using the Tight Binding (TB) approximation we obtain the following matrix equation:

$$\sum_{\ell} \sum_{\beta} H_0 \begin{pmatrix} \ell & \ell \\ \beta & \beta \end{pmatrix} C_{\ell\beta} = EC_{\ell\beta}, \quad (3)$$

where

$$H_0 \begin{pmatrix} \ell & \ell \\ \beta & \beta \end{pmatrix} \equiv \langle \ell \beta | H_0 | \ell \beta \rangle, \quad (4)$$

$$\langle \ell \beta | H_0 | \ell \beta \rangle = \delta_{\ell\ell} \delta_{\beta\beta}, \quad (5)$$

and

$$| \ell \beta \rangle \equiv \Phi \left(\vec{r} - \vec{x} \begin{pmatrix} \ell \\ \beta \end{pmatrix} \right). \quad (6)$$

Within the limits of the TB approximation, the diagonal elements of the Hamiltonian matrix becomes the orbital energies of the free atoms, E_1 and E_2 .

Thus,

$$\langle \ell \beta | H_0 | \ell \beta \rangle = E_{\beta}, \quad \beta = 1, 2. \quad (7)$$

For the off-diagonal elements (also called hopping integrals), we have for nearest neighbors

$$\langle 1 | H_0 | 2 \rangle \equiv \gamma_1, \quad (8)$$

and for second neighbors

$$\langle \ell | H_0 | \ell+1 \rangle \equiv \gamma_2^{(1)} = 0 \quad , \quad (9)$$

$$\langle \ell | H_0 | \ell+2 \rangle \equiv \gamma_2^{(2)} \equiv \gamma_2 \quad . \quad (10)$$

There are two types of second neighbor hopping integrals indicated by the superscript in Eqs. (9) and (10) because there are two types of second neighbors. Later in the calculation we are forced to set one of these hopping integrals to zero so that the bulk Green's function can be expressed in analytic form. In ionic crystals, the two components generally have different radii which implies that the two second neighbor hopping integrals will have different values, and quite often one will be significantly greater than the other. This justifies our neglect of one of the second neighbor hopping integrals.

In our calculation, all energy terms are expressed in units of γ_1 . The parameters E_1 , E_2 and γ_2 are taken as adjustable. Although approximate values can be obtained for these parameters by assuming a particular form for the orbitals and the potential, we feel that more specific choices than the general ones we have made would by no means change the qualitative nature of our results. The geometry and parameters of the problem are shown in Fig. 1. In all the results presented in this paper, we have chosen $E_1 = 2.0$ and $E_2 = -2.0$ in units of γ_1 .

Using the standard approach,⁴⁴ we assume the wavefunction to be of the Bloch form by assuming the coefficients $C_{\ell\beta}$ to be

$$C_{\ell\beta} = N^{-1/2} w(\beta | \vec{k}j) e^{i\vec{k} \cdot \vec{x}(\ell)} \quad , \quad j = 1,2 \quad (11)$$

where \vec{k} is the wave vector, j is the band index and N is the number of unit cells in the crystal. By substituting Eq. (11) into Eq. (3), and using the matrix element defined in Eqs. (7) - (10), we obtain a (2x2) secular matrix equation which can be solved to obtain the bulk energy bands. We find

$$\begin{aligned}
 E_{\vec{k}j} &= \frac{1}{2}(E_1 + E_2) + (\gamma_2^{(1)} + \gamma_2^{(2)}) f_2(\vec{\phi}) \\
 &\pm \frac{1}{2} \left\{ [E_1 - E_2 + 2(\gamma_2^{(1)} - \gamma_2^{(2)}) f_2(\vec{\phi})]^2 \right. \\
 &\left. + 256 \gamma_1^2 f_1^2(\vec{\phi}) \right\}^{1/2}, \quad (12)
 \end{aligned}$$

where

$$f_1(\vec{\phi}) \equiv \cos \frac{\phi_x}{2} \cos \frac{\phi_y}{2} \cos \frac{\phi_z}{2}, \quad (13)$$

$$f_2(\vec{\phi}) \equiv \cos \phi_x + \cos \phi_y + \cos \phi_z, \quad (14)$$

$$\vec{\phi} \equiv a_0 \vec{k}, \quad (15)$$

and where a_0 is the crystal lattice spacing. In Eq. (12), the plus (minus) sign is associated with the branch index $j = 1(2)$.

In this paper we are concerned with the surface properties of the (001) surface (See Fig. 1). For this surface, the wave vector components parallel to the surface (k_x and k_y) are good quantum numbers, but the wave vector perpendicular to the surface (k_z) is not. The Brillouin zone for the bulk crystal is a cube with sides of length $2\pi/a_0$. The Brillouin zone for the surface is a square with sides of length $2\pi/a_0$. To get the projection of the bulk energy bands onto the surface Brillouin zone, we sweep the z -component of the wave vector, k_z , from the value 0 to π/a_0 (the energy expression is symmetric with respect to reflection of k_z so that only half of the k_z values are needed).

In Fig. 2 we present the results obtained for a segment of the surface Brillouin zone where we have chosen a particular value of k_y . The zero of energy is taken to be the average of the orbital energies of the free atoms. In Fig. 2a we show the energy bands for the case in which only the nearest neighbor hopping integral is included. In Figs. 2b and 2c, the second neighbor interactions $\gamma_2^{(1)}$ and $\gamma_2^{(2)}$, respectively, are added to the first neighbor calculation. We see that $\gamma_2^{(1)}$ affects the upper band and $\gamma_2^{(2)}$ affects the lower band. Since in a semiconductor only the lower band is filled, we have made the arbitrary choice of retaining $\gamma_2^{(2)} = \gamma_2$ in our calculations and setting $\gamma_2^{(1)} = 0$.

In order to determine the Green's function, we must know the eigenvector, $w(\beta|\vec{k}j)$, of the (2x2) Hamiltonian matrix. From Eqs. (3) and (12) we obtain

$$w(1|\vec{k}j) = -F e^{-i\frac{1}{2}(\phi_x + \phi_y + \phi_z)} / \Delta, \quad (16)$$

$$w(2|\vec{k}j) = (E_1 - E_{\vec{k}j}) / \Delta, \quad (17)$$

where

$$F \equiv 8\gamma_1 f_1(\vec{\phi}), \quad (18)$$

$$\Delta \equiv [F^2 + (E_1 - E_{\vec{k}j})^2]^{1/2}. \quad (19)$$

The retarded Green's function satisfies the following matrix equation⁴⁵

$$\sum_{\ell'} \sum_{\beta'} \left[H_0 \begin{pmatrix} \ell\ell' \\ \beta\beta' \end{pmatrix} - (E + i\epsilon) \delta_{\ell\ell'} \delta_{\beta\beta'} \right] G^{(0)} \begin{pmatrix} \ell'\ell'' \\ \beta'\beta'' \end{pmatrix}, E = -\delta_{\ell\ell''} \delta_{\beta\beta''}, \quad (20)$$

where the superscript zero denotes the Green's function for the bulk crystal. The term $i\epsilon$, which is appropriate for a retarded Green's function, is a positive imaginary infinitesimal which will be dropped in the subsequent discussion until needed in Eq. (37). The Green's function can be related to the eigenvalues and eigenvectors of the Hamiltonian matrix by⁴⁶

$$G^{(0)} \begin{pmatrix} \ell \ell' \\ \beta \beta' , E \end{pmatrix} = \frac{1}{N} \sum_{\vec{k}j} \frac{w(\beta | \vec{k}j) w^*(\beta' | \vec{k}j)}{E - E_{\vec{k}j}} e^{i\vec{k} \cdot \vec{x}(\ell \ell')} , \quad (21)$$

where

$$\vec{x}(\ell \ell') = \vec{x}(\ell) - \vec{x}(\ell') , \quad (22)$$

and the summation is over all wave vectors in the three-dimensional Brillouin zone and over the two branch indices. That Eq. (21) satisfies Eq. (20) can be seen by direct substitution. Performing explicitly the summation over j in Eq. (21) gives

$$G^{(0)} \begin{pmatrix} \ell \ell' \\ \beta \beta' , E \end{pmatrix} = \frac{1}{N} \sum_{\vec{k}} \left\{ \frac{w(\beta | \vec{k}1) w^*(\beta' | \vec{k}1)}{E - E_{\vec{k}1}} + \frac{w(\beta | \vec{k}2) w^*(\beta' | \vec{k}2)}{E - E_{\vec{k}2}} \right\} e^{i\vec{k} \cdot \vec{x}(\ell \ell')} . \quad (23)$$

Substituting Eqs. (12), (16) and (17) into Eq. (23) gives for the bulk Green's functions

$$G^{(0)} \begin{pmatrix} \ell \ell' \\ 11 , E \end{pmatrix} = \sum_{\vec{k}} (E - E_B) D_B(\ell \ell') , \quad (24)$$

$$G^{(0)} \begin{pmatrix} \ell \ell' \\ 22 , E \end{pmatrix} = \sum_{\vec{k}} (E - E_1) D_B(\ell \ell') , \quad (25)$$

$$G^{(0)} \begin{pmatrix} \ell \ell' \\ 12 , E \end{pmatrix} = \sum_{\vec{k}} F D_B(\ell \ell') e^{-i\frac{1}{2}(\phi_x + \phi_y + \phi_z)} , \quad (26)$$

$$G^{(0)} \begin{pmatrix} \ell' \ell \\ 2 1 , E \end{pmatrix} = G^{(0)} \begin{pmatrix} \ell \ell' \\ 12 , E \end{pmatrix}^* , \quad (27)$$

where

$$D_B(\ell \ell') \equiv \frac{e^{i\vec{k} \cdot \vec{x}(\ell \ell')}}{N[(E - E_1)(E - E_B) - F^2]} \quad (28)$$

and

$$E_B \equiv E_2 + 2\gamma_2 f_2(\vec{\phi}). \quad (29)$$

An important feature of this calculation is the fact that, whereas Eq. (23) appears to be cumbersome, the eigenvalues and eigenvectors combine in just the right way to make the needed bulk Green's functions in Eqs. (24) - (27) rather simple.

In order to study the surface properties, it is appropriate to express the bulk Green's functions in a mixed Bloch-Wannier representation.^{32,38,39} This effectively reduces the three-dimensional problem into a number of one-dimensional problems. As we will show below, each one-dimensional problem can be solved analytically. Thus, we exploit the translational symmetry parallel to the surface by expanding the bulk Green's functions in terms of $\vec{k}_s (\equiv \vec{\phi}_s/a_0)$, the wave vector parallel to the surface,

$$G^{(0)} \left(\begin{matrix} \ell \ell' \\ \beta \beta' \end{matrix}, E \right) = \frac{1}{N_s} \sum_{\vec{k}_s} G^{(0)} \left(\begin{matrix} \ell_z \ell_z' \\ \beta \beta' \end{matrix}, \vec{\phi}_s, E \right) e^{i\vec{k}_s \cdot \vec{x}(\ell \ell')} \quad (30)$$

where N_s is the number of two-dimensional unit cells in the surface and ℓ_z labels the unit cells in the direction perpendicular to the surface.

By comparing Eq. (30) with the results in Eqs. (24) - (27), the bulk Green's functions in the mixed representation become

$$G^{(0)} \left(\begin{matrix} \ell_z \ell_z' \\ 1 \ 1 \end{matrix}, \vec{\phi}_s, E \right) = \sum_{k_z} (E - E_B) D_s(\ell_z \ell_z') \quad (31)$$

$$G^{(0)} \left(\begin{matrix} \ell_z & \ell_z' \\ 2 & 2 \end{matrix}, \vec{\phi}_s, E \right) = \sum_{k_z} (E - E_1) D_s(\ell_z \ell_z'), \quad (32)$$

$$G^{(0)} \left(\begin{matrix} \ell_z & \ell_z' \\ 1 & 2 \end{matrix}, \vec{\phi}_s, E \right) = \sum_{k_z} FD_s(\ell_z \ell_z') e^{-i\frac{1}{2}(\phi_x + \phi_y + \phi_z)}, \quad (33)$$

$$G^{(0)} \left(\begin{matrix} \ell_z & \ell_z' \\ 2 & 1 \end{matrix}, \vec{\phi}_s, E \right) = G^{(0)} \left(\begin{matrix} \ell_z & \ell_z' \\ 1 & 2 \end{matrix}, \vec{\phi}_s, E \right)^*, \quad (34)$$

where

$$D_s(\ell_z \ell_z') \equiv \frac{e^{ik_z x(\ell_z \ell_z')}}{L_z [(E - E_1)(E - E_B) - F^2]}, \quad (35)$$

and where L_z is the number of unit cells in the z-direction ($L_z N_s = N$).

To obtain the Green's functions in closed analytic form, we convert the sums to integrals through the transformation

$$\sum_{k_z} f(k_z) \longrightarrow \frac{L_z}{2\pi} \int_{-\pi}^{\pi} d\phi_z f(\phi_z/a_0). \quad (36)$$

All of the resulting integrals are of the general form⁴⁷

$$\int_{-\pi}^{\pi} d\phi_z \frac{\cos(\ell_z \phi_z)}{\cos \phi_z - \xi + i\epsilon} = \frac{4\pi t^{1+|\ell_z|}}{t^2 - 1}, \quad (37)$$

where

$$t = \begin{cases} \xi - (\xi^2 - 1)^{\frac{1}{2}}, & \xi > 1 \\ \xi + i(1 - \xi^2)^{\frac{1}{2}}, & |\xi| < 1 \\ \xi + (\xi^2 - 1)^{\frac{1}{2}}, & \xi < -1 \end{cases}. \quad (38)$$

It might be noted in passing that obtaining the integrals in the form of Eq. (37) is the step that forces us to set one of the second neighbor hopping integrals to zero.⁴⁸

The final results for the bulk Green's functions are

$$G^{(0)} \begin{pmatrix} \ell_z & \ell_z' \\ 1 & 1 \end{pmatrix}, \vec{\phi}_s, E = 2aPt \left| \ell_z - \ell_z' \right| + 1 - 2\gamma_2 Pt \left[t \left| \ell_z - \ell_z' + 1 \right| + t \left| \ell_z - \ell_z' - 1 \right| \right], \quad (39)$$

$$G^{(0)} \begin{pmatrix} \ell_z & \ell_z' \\ 2 & 2 \end{pmatrix}, \vec{\phi}_s, E = 2dPt \left| \ell_z - \ell_z' \right| + 1, \quad (40)$$

$$G^{(0)} \begin{pmatrix} \ell_z & \ell_z' \\ 1 & 2 \end{pmatrix}, \vec{\phi}_s, E = 2fPt \left[t \left| \ell_z - \ell_z' \right| + t \left| \ell_z - \ell_z' - 1 \right| \right] e^{-i\frac{1}{2}(\phi_x + \phi_y)}, \quad (41)$$

$$G^{(0)} \begin{pmatrix} \ell_z & \ell_z' \\ 2 & 1 \end{pmatrix}, \vec{\phi}_s, E = 2fPt \left[t \left| \ell_z - \ell_z' \right| + t \left| \ell_z - \ell_z' + 1 \right| \right] e^{i\frac{1}{2}(\phi_x + \phi_y)}, \quad (42)$$

where

$$a \equiv E - E_2 - 2\gamma_2 (\cos \phi_x + \cos \phi_y), \quad (43)$$

$$P \equiv 1/B(t^2 - 1), \quad (44)$$

$$d \equiv E - E_1, \quad (45)$$

$$f \equiv 4\gamma_1 \cos(\frac{1}{2}\phi_x) \cos(\frac{1}{2}\phi_y), \quad (46)$$

$$\xi \equiv -A/B, \quad (47)$$

$$A \equiv ad - 2f^2, \quad (48)$$

$$B \equiv -2\gamma_2 d - 2f^2. \quad (49)$$

Two important properties of the Green's functions are apparent from these equations. First, in the bulk, the Green's functions depend only upon the separation distance between layers, $l_z - l'_z$, and not on the value of l_z and l'_z separately. Second, the two Green's functions in Eqs. (39) and (40) are complex only when the magnitude of the parameter ξ is less than unity (see Eq. (38)). This occurs only when the energy E falls within one of the two bands (see Eqs. (43) - (49)).

Except for an ambiguity in sign which is fully discussed in both Section IV and in the Appendix, the set of equations from Eq. (38) through Eq. (49) completely defines the bulk Green's functions. It requires only a simple numerical program to obtain any of the bulk Green's functions for arbitrary energy E and two-dimensional wave vector $\vec{\phi}_s$.

III. PHASE SHIFT CALCULATIONS

We form the (001) surface by passing an imaginary plane between atoms of type 2 in the $l_z=0$ plane and atoms of type 1 in the $l_z=1$ plane as shown in Fig. 1. Each surface formed consists of only one type of atom. The effects of the surface formation can be introduced into the Hamiltonian by adding a perturbation term which exactly cancels all interactions which occur across the imaginary plane. Thus, in matrix notation analogous to Eq. (4), we write for the perturbed system

$$H \begin{pmatrix} ll' \\ \beta\beta' \end{pmatrix} = H_0 \begin{pmatrix} ll' \\ \beta\beta' \end{pmatrix} + V \begin{pmatrix} ll' \\ \beta\beta' \end{pmatrix}, \quad (50)$$

where V is the surface perturbation term. If, for example, we consider the bulk crystal to have only nearest neighbor interactions (i.e., $\gamma_2=0$), then the perturbation term is

$$\begin{aligned}
V \begin{pmatrix} \ell \ell' \\ \beta \beta' \end{pmatrix} = & -\gamma_1 \left(\delta_{\ell_z 1} \delta_{\beta 1} \delta_{\ell'_z 0} \delta_{\beta' 2} + \delta_{\ell_z 0} \delta_{\beta 2} \delta_{\ell'_z 1} \delta_{\beta' 1} \right) \\
& \times \left[\delta_{\ell_x \ell'_x} \delta_{\ell_y \ell'_y} + \delta_{\ell_x \ell'_x} \delta_{\ell_y \ell'_y + 1} + \delta_{\ell_x \ell'_x + 1} \delta_{\ell_y \ell'_y} + \delta_{\ell_x \ell'_x + 1} \delta_{\ell_y \ell'_y + 1} \right] \quad (51)
\end{aligned}$$

In the resolvent technique,²⁵⁻²⁷ the energy of the surface state is obtained from the determinant equation

$$\det \left[\delta_{\ell \ell'} \delta_{\beta \beta'} - \sum_{\ell''} \sum_{\beta''} V \begin{pmatrix} \ell \ell'' \\ \beta \beta'' \end{pmatrix} G^{(0)} \begin{pmatrix} \ell'' \ell' \\ \beta'' \beta' \end{pmatrix}, E \right] = 0 \quad (52)$$

The value of E for which this equation is satisfied is the surface state energy. The equation is valid only for energies outside the bands where the Green's functions are real. For energies inside the band, the real part of Eq. (52) gives resonances inside the bulk bands. The matrices appearing in Eq. (52) are infinite in size. Since the translational symmetry in the direction parallel to the surface is preserved in the cleaved crystal, each matrix in Eq. (52) can be expressed in the mixed Bloch-Wannier representation. For the Green's function, this is done in Eq. (30). For the perturbation matrix, we have

$$V \begin{pmatrix} \ell \ell' \\ \beta \beta' \end{pmatrix} \begin{pmatrix} z \ell' \\ z \ell' \\ \vec{\phi}_s \end{pmatrix} = \sum_{\substack{\ell_x, \ell_y \\ x, y}} V \begin{pmatrix} \ell \ell' \ell'' \\ x \ y \ z \\ \beta \beta' z \end{pmatrix} e^{-i\vec{k}_s \cdot \vec{x}(\ell \ell')} \quad (53)$$

In contrast to the matrix in Eq. (51), the non-zero elements in Eq. (53) form a matrix which is finite in size; in fact, it is quite small, either (2x2) or (3x3) in this paper.

In analogy with the resolvent technique, the phase shift technique³⁷⁻³⁹ defines the determinant function (Fredholm determinant)

$$D(\vec{\phi}_s, E) = \det \left[\delta_{\ell_z \ell'_z} \delta_{\beta \beta'} - \sum_{\ell''} \sum_{\beta''} V \begin{pmatrix} \ell \ell'' \\ \beta \beta'' \end{pmatrix} \begin{pmatrix} z \ell'' \\ z \ell'' \\ \vec{\phi}_s \end{pmatrix} G^{(0)} \begin{pmatrix} \ell'' \ell' \\ \beta'' \beta' \end{pmatrix} \begin{pmatrix} z \ell' \\ z \ell' \\ \vec{\phi}_s \end{pmatrix}, E \right] \quad (54)$$

For energies E outside the bands, the condition

$$D(\vec{\phi}_s, E) = 0 \quad (55)$$

gives the energy of the surface state for each value of $\vec{\phi}_s$. For energies inside the bands, the function $D(\vec{\phi}_s, E)$ is complex. For this case, we define the partial phase shift function

$$\eta(\vec{\phi}_s, E) = - \arg D(\vec{\phi}_s, E) \quad (56)$$

The total phase shift per surface unit cell is obtained by summing the partial phase shift over the surface Brillouin zone, i.e.,

$$\eta(E) = \frac{1}{N_s} \sum_{\vec{\phi}_s} \eta(\vec{\phi}_s, E). \quad (57)$$

It is related in a simple way to the change in the density of states. We have^{35,36}

$$\Delta n(E) = \frac{1}{\pi} \frac{d\eta(E)}{dE}, \quad (58)$$

where $\Delta n(E)$ is the shift in the number of energy states per unit energy per surface unit cell. This change in the density of states is the desired result of this portion of the calculation. From it, several physical properties of the surface can be determined.

To proceed with this calculation, then, we must define the explicit form of the perturbation matrix which creates the surface. In this paper we consider three different model cases. For Model I, we consider the bulk crystal to have only nearest neighbor interactions. To create the surface we cancel the effect of the transfer integrals across the imaginary plane. Thus, the perturbation for Model I is given in Eq. (51). Upon substitution into Eq. (53), we obtain a matrix whose non-zero elements can be put into (2x2) form,

$$V \begin{pmatrix} \ell_z & \ell_z \\ \beta & \beta \end{pmatrix}, \vec{\phi}_s = \begin{bmatrix} 0 & -f\chi(\vec{\phi}_s) \\ -f\chi^*(\vec{\phi}_s) & 0 \end{bmatrix}, \quad (59)$$

where

$$\chi(\vec{\phi}_s) = e^{i\frac{1}{2}(\phi_x + \phi_y)}, \quad (60)$$

and where f is given in Eq. (46). The rows and columns of this matrix are labelled by the rows of atoms in Fig. 1 that participate in the perturbation. For this case, the first row indicates a value of $(\ell_z \beta) = (02)$ while the second row is for $(\ell_z \beta) = (11)$. For all other values of $(\ell_z \beta)$, the matrix elements of V are identically zero. Thus, whereas matrix V is technically infinite in size, there are only two non-zero terms. As we will see below, there are no surface states for Model I.

For Model II we consider the bulk crystal to have both first and second neighbor interactions as shown in Fig. 1 and discussed in Section II. For this case the perturbation needed to create the surface extends to the second layer from the surface, and the resulting perturbation matrix is (3x3). We have

$$V \begin{pmatrix} \ell_z & \ell_z \\ \beta & \beta \end{pmatrix}, \vec{\phi}_s = \begin{bmatrix} 0 & -f\chi(\vec{\phi}_s) & -\gamma_2 \\ -f\chi^*(\vec{\phi}_s) & 0 & 0 \\ -\gamma_2 & 0 & 0 \end{bmatrix}. \quad (61)$$

For this matrix, the third row and column are labelled by the atomic row $(\ell_z \beta) = (12)$. As we will see below, Model II gives rise to Shockley surface states.

For Model III we again consider the situation in Model I where only first neighbor interactions are assumed. However, upon creating the surface we assume that the orbital energy on the first layer of atoms on each surface is changed by an amount U_0 . The physical basis for this perturbation is that the crystal potential at the surface is different from its value in the bulk. The perturbation matrix for this case is

$$V \begin{pmatrix} \ell & \ell & z & z \\ \beta & \beta & \beta & \beta \end{pmatrix}, \vec{\phi}_s = \begin{pmatrix} U_0 & -f\chi(\vec{\phi}_s) \\ -f\chi^*(\vec{\phi}_s) & U_0 \end{pmatrix}, \quad (62)$$

where the labels of the rows and columns are the same as in Model I. The reason for considering this model is that it results in Tamm surface states.

The surface states which fall outside of the bands can now be easily determined by the resolvent technique. We have numerically calculated the Fredholm determinant (Eq. (54)) for each of the three models as a function of energy E for various choices of wave vector, $\vec{\phi}_s$. When the determinant goes through zero as we vary E , we have a surface state. For Model I, this never occurs which means there are no surface states within the context of this model.

For Model II, Shockley surface states occur in the band gap. In Fig. 3 we show a three-dimensional view of the energy band structure for one-quarter of the surface Brillouin zone. The shaded region just above the valence band is the Shockley surface state band. In Fig. 4 we show a detail of this surface state band as a function of ϕ_x for a particular choice of ϕ_y . The energy between the crossing point in the bulk band and the surface state curve is exactly equal to the magnitude of γ_2 , which for the calculations in

this paper has been chosen to be 0.2, in units of γ_1 . Note that the surface state band merges with the bulk band and stops at a point in the Brillouin zone slightly beyond the position where the top and bottom of the valence band cross. This property of the surface state band is shown fully in Fig. 5 where we plot the boundary of the surface state inside the two-dimensional surface Brillouin zone.

Finally, in Fig. 6 we show the Tamm surface states which arise from Model III. Here, surface states exist above both the valence band and the conduction band (note break in energy axis). The surface state above the conduction band merges with the bulk band near the Brillouin zone boundary. At the Brillouin zone boundary, the energy difference between the band edges and the surface states is equal to the perturbation U_0 which for these calculations has been chosen to be 0.2 in units of γ_1 .

It is important to note a significant difference in the existence conditions for the surface states in the present calculation compared with previous results. In this work, Shockley surface states appear in Model II for arbitrarily small values of γ_2 and Tamm surface states appear in Model III for arbitrarily small values of U_0 . In the one-band model calculations of Allan and Lengart^{38,39} only Tamm states appear and only when the surface perturbation U_0 exceeds a certain critical value (for the (001) surface of simple cubic crystals, the existence condition is that $U_0 > \gamma_1$). It is also generally true for one-dimensional systems (as discussed in Section I) that a perturbation exceeding a critical value is needed before surface states appear.

States in the bulk bands are localized on one of the two types of atoms in the crystal. States with energies in the upper (conduction) band are localized on atoms of type 1, whereas states with energies in the lower (valence) band are localized on atoms of type 2. This is because we chose E_1 to be

positive and E_2 to be negative. Concerning surface states, then, those which originate from the upper band (the upper surface state for Model III) are localized on the surface where the first layer consists of atoms of type 1 (upper surface in Fig. 1). On the other hand, surface states originating from the lower band (Model II and lower state in Model III) are localized on the surface where the first layer of atoms is of type 2 (lower surface in Fig. 1).

For arbitrary wave vector, $\vec{\phi}_s$, the Fredholm determinant (Eq. (54)) can also be evaluated for energies inside the bands for each of the three models. In this case the determinant is complex, and by using Eq. (56) the partial phase shift can be calculated. By way of illustration, in Fig. 7 we have plotted the partial phase shift for a particular point in the surface Brillouin zone. In Fig. 7a we show the partial phase shift for Model I at the point $\phi_x = \phi_y = \pi/2$. Since there are no surface states in this model, the phase shift is non-zero only for energies inside the bands (compare with Fig. 2a). The phase shift function is antisymmetric with respect to the energy zero due to the sign of the Green's function as is fully discussed in Section IV and the Appendix.

In Fig. 7b we show the partial phase shift for Model II. In this figure the surface state which exists just above the valence band is indicated by the step in the partial phase shift from the value $-\pi$ to 0. As we move down in energy from the energy zero, the phase shift jumps from 0 to $-\pi$ at the zero of the Fredholm determinant.^{34,49} It stays constant at $-\pi$ until the top of the valence band is reached at which point it jumps to $-\pi/2$. The results for Model III are presented in Fig. 7c. Again we see the effect of the surface state just above the valence band. In Fig. 7d we show the partial phase shift for Model III, but this time for a different wave vector point which is closer to the zone boundary where the bands are more narrow (notice the change in scale).

Here we see the effect of the two surface states, one above the valence band and one above the conduction band.

Superficially, there seem to be discrepancies between our partial phase shifts and those obtained previously for one-band crystals by Allen and Lengart.³⁹ They find a jump of $\pm 2\pi$ at the surface state energies rather than $-\pi$ as in our case. The difference is explained by realizing that when a crystal is cleaved, two surfaces are formed. The properties derived from the phase shift technique are the combined contributions from both surfaces. In the model of Allan and Lengart,³⁹ the two created surfaces are identical since their model contains only one type of atom. Thus, if surface states exist (in their model only Tamm surface states are possible), they exist on both surfaces resulting in a phase shift of $\pm 2\pi$. (The plus or minus sign distinguishes between states appearing below or above the single energy band, respectively.) In our calculation, however, the type surfaces formed are not identical (see Fig. 1). The surface states are localized on either one or the other of the surfaces. Therefore, our phase shift changes by $-\pi$, with the minus sign due to the fact the surface state appears above the band from which it originates. If we had cleaved the CsCl crystal along the (110) plane, the two surfaces formed would be identical and the phase shift would then jump by $\pm 2\pi$ at the surface state energy.

To obtain the total phase shift function, the partial phase shift function for each wave vector must be summed over the surface Brillouin zone as shown in Eq. (57). We have done this numerically by choosing a uniform displaced mesh of points in the irreducible segment of the Brillouin zone. The method of deriving this mesh, which is the optimum set of points of a given size for accurately determining averages over the Brillouin zone, has been fully described recently by Cunningham.⁵⁰ If the number of points chosen is

too small, the results of the summation will fluctuate as the number of points is changed. We have increased the number of points in the sample until the fluctuations in the results have become small. Typically, this means that we used samples containing 400 points.

The total phase shifts for the three models are shown in Fig. 8. For Model I we obtain the simple antisymmetric curve shown in Fig. 8a. The curves start and stop at the bulk crystal band edges since there are no surface states. In Fig. 8b we show the total phase shift for Model II. Since the inclusion of γ_2 does not change the shape of the conduction band and does not introduce surface states near that band, the total phase shift in the energy range $E > 0$ is very nearly the same as in Fig. 8a. The results in the region of the valence band, however, are quite different due to the difference in the band shape and the presence of the surface state. Even though the partial phase shifts equal $-\pi$ between the bulk and surface states, the total phase shift does not reach the value of $-\pi$. This is due to the fact that there is not a single value of energy E which lies between the bulk and surface state for every point in the Brillouin zone (see Figs. 3 and 4). The total phase shift for Model III is shown in Fig. 8c. Here, the total phase shift does reach a value of $-\pi$ since energies just above the valence band edge are always between the bulk and surface states for all points in the Brillouin zone (see Fig. 6). In addition, the presence of the surface state associated with the valence band changes the total phase shift in the region of positive energies.

The interest in the total phase shift is due to the simple relation between it and the change in the density of states due to the creation of the surface (see Eq. (58)). Upon taking the derivative of the curves in Fig. 8, we obtain the change in the density of states for each model, and these results are shown in Fig. 9. In Fig. 9a we show the results for Model I. We see that the creation

of the surface has shifted the bulk states toward the band gap by increasing the number of states near the gap and depleting the number of states far from the gap. The magnitude of the sharp peaks at the band edges is only approximate since the differentiation is done numerically, and small uncertainties in the phase shift values lead to large uncertainties in the derivative when the derivative is large.

In Fig. 9b we present the results for Model II. The conduction band results are similar to the results in Fig. 9a. The presence of the Shockley surface states, however, greatly changes the valence band results. The complexity of the changes in the density of states is a result of the band structure. The increase in the density of states at $E=-2.0$ is due to the presence of surface states. The increase in the density of states at $E=-3.2$ is analogous to the shift of bulk states toward the band gap in Fig. 9a. The minimum in the density of states at $E=-2.8$ is due to the fact that more bulk states are removed in this region than there are surface states added.

In Fig. 9c we present the change in the density of states for Model III. Here the interpretation is a little easier since the band structure is simpler. For the valence band, there is a sharp depletion of bulk states right at the band edge with all of the states being put into the surface states just inside the band gap. For the conduction band, again the bulk states are depleted right at the band edge, but this time the surface states have energies that overlap those of the bulk bands.

Once the change in the density of states is known, changes in the thermodynamic properties of the crystal due to the surface can be obtained. For example, the change in the electronic specific heat, $\Delta C_V(T)$, is given by

$$\Delta C_V(T) = \int_{-\infty}^{\infty} dE E \Delta n(E) \frac{\partial f(E,T)}{\partial T} , \quad (63)$$

where $f(E,T)$ is the Fermi-Dirac function, given by

$$f(E,T) = \left[e^{(E-\mu)/k_B T} + 1 \right]^{-1} , \quad (64)$$

and where μ is the Fermi energy. We assume the Fermi energy to be exactly in the middle of the band gap ($\mu=0$) and to be independent of temperature T . Another thermodynamic property, the surface entropy, is given by an integration of Eq. (63),

$$S_e(T) = \int_0^T \Delta C_V(T') \frac{dT'}{T'} . \quad (65)$$

In Fig. 10 we present the change in the electronic specific heat due to the surface for each of the three models. Three features are worth noting. First, the results for the three models are quite similar. This is expected since the addition of a weak second neighbor interaction ($\gamma_2=0.2\gamma_1$) or a weak surface atom perturbation ($U_0=0.2\gamma_1$) should not greatly change the thermodynamic properties. This is true even though two of the models have surface states, while one does not. Second, at low temperatures we find that the change in the specific heat approaches zero exponentially with temperature. This is consistent with the fact that the models have a forbidden energy gap in the change in the density of states. In contrast to this, we have also plotted in Fig. 10 the results obtained by Allan and Lenglar³⁸ for the (001) surface of a half-filled one-band simple cubic crystal. In this case, the change in the electronic specific heat at low temperature approaches zero linearly with temperature. Third, at high temperatures (possibly above the melting temperature of real crystals), the change in the specific heat becomes

negative. This occurs because at high temperatures the levels far from the Fermi energy are more strongly weighted in the integral (Eq. (63)) than those close to the Fermi energy, and the change in the density of states for these levels (see Fig. 9) is negative.

In Fig. 11 we show the electronic surface entropy obtained from Eq. (65) for each of the three models. Again we see the exponential behavior at low temperatures. In addition, we see that the electronic surface entropy is positive for all temperatures as it should be.

A comment should be made regarding the positioning of the Fermi level. Since our method of creating the surface does not change the total number of electrons in the crystal, then the integral up to the Fermi level of the change in the density of states must vanish. From Eq. (58), this integral is proportional to the phase shift function at the Fermi level. Thus, to insure that we conserve the number of electrons in the crystal, we have the condition

$$\begin{aligned} \eta(\mu) &= \pi \int_{-\infty}^{\mu} \Delta n(E) dE \\ &= 0 \end{aligned} \tag{66}$$

This is one of the ways to express the Friedel⁵¹ sum rule for perturbed systems. By examining Fig. 8, we see that without further changes, this condition forces us to place the Fermi level either inside the band gap or outside of the bands for all three models (for Model III, we can also chose the Fermi level to be just above the conduction band edge). Thus our model calculations are particularly suited for discussion of semiconductor or insulator properties. In order to apply our model to two-band metals, we would need to add a "self-consistency" term to the perturbation matrix in the same manner as Allan.³⁷

IV. SURFACE GREEN'S FUNCTIONS

In this section we derive the Green's functions appropriate for the surface. There are two main reasons for doing this. First, the layer density of states can be calculated in the manner shown by Kalkstein and Soven.³² This allows us to see directly how the effect on the electronic levels due to the surface perturbation is localized within the first few layers of the solid. From this we can make contact with photoemission experiments since it is the density of states near the surface that is measured, and this need not be the same as the density of states in the bulk. Second, the surface Green's functions can be used as a starting point in studying further changes in the crystal surface. Specifically, the surface Green's function can be used to study the effects of reconstruction^{1,52} and chemisorption^{1,40-43}.

In analogy with Eq. (20), the retarded surface Green's function satisfies the equation

$$\sum_{\ell'} \sum_{\beta'} \left[H \begin{pmatrix} \ell \ell' \\ \beta \beta' \end{pmatrix} - (E + i\epsilon) \delta_{\ell \ell'} \delta_{\beta \beta'} \right] G \begin{pmatrix} \ell' \ell'' \\ \beta' \beta'' \end{pmatrix}, E = -\delta_{\ell \ell''} \delta_{\beta \beta''} \quad , \quad (67)$$

where H is given by Eq. (50), and where we have dropped the superscript (0) to represent the surface Green's function. By multiplying Eq. (67) by the bulk Green's function $G^{(0)}(\ell''' \beta''', \ell \beta)$ and by summing over indices ℓ and β , we obtain

$$G \begin{pmatrix} \ell'''' \ell'''' \\ \beta'''' \beta'''' \end{pmatrix}, E = G^{(0)} \begin{pmatrix} \ell'''' \ell'''' \\ \beta'''' \beta'''' \end{pmatrix}, E + \sum_{\ell, \beta} \sum_{\ell', \beta'} G^{(0)} \begin{pmatrix} \ell'''' \ell \\ \beta'''' \beta \end{pmatrix}, E V \begin{pmatrix} \ell \ell' \\ \beta \beta' \end{pmatrix} G \begin{pmatrix} \ell' \ell'' \\ \beta' \beta'' \end{pmatrix}, E \quad , \quad (68)$$

where V is the perturbation matrix given by Eq. (51). As in Eq. (30) and Eq. (53), we convert the surface Green's function to the mixed Bloch-Wannier representation,

$$G \begin{pmatrix} \lambda \lambda' \\ \beta \beta' \end{pmatrix}, E = \frac{1}{N_s} \sum_{\vec{k}_s} G \begin{pmatrix} \lambda_z \lambda'_z \\ \beta \beta' \end{pmatrix}, \vec{\phi}_s, E e^{i\vec{k}_s \cdot \vec{x}(\lambda \lambda')} . \quad (69)$$

In this representation, Eq. (68) becomes

$$G \begin{pmatrix} \lambda_z \lambda'_z \\ \beta \beta' \end{pmatrix}, \vec{\phi}_s = G^{(0)} \begin{pmatrix} \lambda_z \lambda'_z \\ \beta \beta' \end{pmatrix}, \vec{\phi}_s + \sum_{\lambda_z \beta} \sum_{\lambda'_z \beta'} G^{(0)} \begin{pmatrix} \lambda_z \lambda'_z \\ \beta \beta' \end{pmatrix}, \vec{\phi}_s V \begin{pmatrix} \lambda_z \lambda'_z \\ \beta \beta' \end{pmatrix}, \vec{\phi}_s G \begin{pmatrix} \lambda_z \lambda'_z \\ \beta \beta' \end{pmatrix}, \vec{\phi}_s , \quad (70)$$

where we have dropped the explicit dependence on E for convenience.

In this portion of the problem, we chose (for convenience) to consider only Model I. Because of the particularly simple form of the perturbation matrix, Eq. (59), we can explicitly carry out the matrix multiplication in Eq. (70). In addition, we use the fact that $G(\lambda_z \beta, \lambda'_z \beta')$ is nonzero only if λ_z and λ'_z are on the same side of the surface. Thus, if we consider first the upper surface in Fig. 1 we obtain

$$G \begin{pmatrix} \lambda_z \lambda'_z \\ \beta \beta' \end{pmatrix} = G^{(0)} \begin{pmatrix} \lambda_z \lambda'_z \\ \beta \beta' \end{pmatrix} + G^{(0)} \begin{pmatrix} \lambda_z \lambda'_z \\ \beta \beta' \end{pmatrix} V \begin{pmatrix} 01 \\ 21 \end{pmatrix} G \begin{pmatrix} 1 \lambda_z \\ 1 \beta \end{pmatrix} , \quad (71)$$

where we have suppressed the dependence on $\vec{\phi}_s$. By setting $\lambda_z \lambda'_z = 1$ and $\beta \beta' = 1$, we solve Eq. (71) for the surface Green's function to get

$$G \begin{pmatrix} 1 \lambda_z \\ 1 \beta \end{pmatrix} = G^{(0)} \begin{pmatrix} 1 \lambda_z \\ 1 \beta \end{pmatrix} / \left[1 - G^{(0)} \begin{pmatrix} 10 \\ 12 \end{pmatrix} V \begin{pmatrix} 01 \\ 21 \end{pmatrix} \right] . \quad (72)$$

Finally, this expression can be substituted back into Eq. (71) to give the

general surface Green's functions. By substituting the explicit expressions in Eqs. (39)-(42) for the bulk Green's functions and after considerable algebraic manipulation, the surface Green's functions can be written as (remember that λ_z and $\lambda_z' \geq 1$)

$$G \begin{pmatrix} \lambda_z & \lambda_z' \\ \beta & 1 \end{pmatrix} = G(0) \begin{pmatrix} \lambda_z & \lambda_z' \\ \beta & 1 \end{pmatrix} - G(0) \begin{pmatrix} \lambda_z + \lambda_z' - 1 \\ \beta & 1 \end{pmatrix}, \quad (73)$$

$$G \begin{pmatrix} \lambda_z & \lambda_z' \\ \beta & 2 \end{pmatrix} = G(0) \begin{pmatrix} \lambda_z & \lambda_z' \\ \beta & 2 \end{pmatrix} - G(0) \begin{pmatrix} \lambda_z + \lambda_z' - 0 \\ \beta & 2 \end{pmatrix}, \quad (74)$$

where $\beta=1,2$. Similarly, for the lower surface in Fig. 1 (λ_z and $\lambda_z' \leq 0$) we obtain

$$G \begin{pmatrix} \lambda_z & \lambda_z' \\ \beta & 1 \end{pmatrix} = G(0) \begin{pmatrix} \lambda_z & \lambda_z' \\ \beta & 1 \end{pmatrix} - G(0) \begin{pmatrix} \lambda_z + \lambda_z' - 1 & 1 \\ \beta & 1 \end{pmatrix}, \quad (75)$$

$$G \begin{pmatrix} \lambda_z & \lambda_z' \\ \beta & 2 \end{pmatrix} = G(0) \begin{pmatrix} \lambda_z & \lambda_z' \\ \beta & 2 \end{pmatrix} - G(0) \begin{pmatrix} \lambda_z + \lambda_z' - 1 & 0 \\ \beta & 2 \end{pmatrix}, \quad (76)$$

where $\beta=1,2$. The fact that the surface Green's function can be expressed as the difference of two bulk Green's functions is a significant simplification in our problem. This fact was recognized to be true for the one-band crystal surfaces by Dobrzynski and Mills,⁵² and it is also true for a finite diatomic chain.⁵³

The density of states on the layer labelled by λ_z and β is related to the imaginary part of the surface Green's function by³²

$$\rho \begin{pmatrix} \lambda_z \\ \beta \end{pmatrix}, E = \frac{-1}{\pi N_s} \text{Im} \sum_{\vec{\phi}_s} G \begin{pmatrix} \lambda_z & \lambda_z \\ \beta & \beta, \vec{\phi}_s \end{pmatrix}, E. \quad (77)$$

Only the diagonal elements of the Green's function matrix are needed. By substituting the analytic expressions for the bulk Green's functions into Eqs. (73) - (76), we obtain the simple expressions

$$G \begin{pmatrix} \ell_z & \ell_z \\ 1 & 1 \end{pmatrix} = J d(1-t^{2\ell_z-1}) \quad , \quad \ell_z \geq 1 \quad , \quad (78)$$

$$G \begin{pmatrix} \ell_z & \ell_z \\ 2 & 2 \end{pmatrix} = J a(1-t^{2\ell_z}) \quad , \quad \ell_z \geq 1 \quad , \quad (79)$$

$$G \begin{pmatrix} \ell_z & \ell_z \\ 1 & 1 \end{pmatrix} = J d(1-t^{-2\ell_z+2}) \quad , \quad \ell_z \leq 0 \quad , \quad (80)$$

$$G \begin{pmatrix} \ell_z & \ell_z \\ 2 & 2 \end{pmatrix} = J a(1-t^{-2\ell_z+1}) \quad , \quad \ell_z \leq 0 \quad , \quad (81)$$

where

$$J = 2t/B(t^2-1) \quad , \quad (82)$$

and $\text{Im } t$ is to be interpreted as $-\text{sgn}(E)\text{Im } t$, where $\text{sgn}(E)$ is the sign of E .

The term $\text{sgn}(E)$ is added because of an ambiguity in sign in taking the square root of a square. This ambiguity arises in all aspects of the use of this Green's function. The ambiguity is removed by comparing the results of the calculation in the limit of zero band gap (when the two atoms in the unit cell become identical) with a separate calculation for a body-centered cubic (bcc) crystal. There is no ambiguity in sign for the bcc case. The sign which is given in Eq. (82), then, is based on the assumption that there is a continuous change in the Green's functions in going from the zero band gap case to the case with finite band gap. In the Appendix we show explicitly how this is done for the calculation of the partial phase shift discussed in Sec. III.

In Fig. 12 we show the layer density of states (LDS) calculated numerically by sampling the surface Brillouin zone and evaluating Eq. (77). From the form

of the surface Green's functions in Eqs. (78) - (81), the LDS for the upper surface in Fig. 1 is the mirror image of the LDS for the lower surface. This means, for example, that the LDS for the layer $\lambda_z=1$, $\beta=1$ is the same as the LDS for the layer $\lambda_z=0$, $\beta=2$ when the energy axis E is changed to $-E$. For this reason we only show the LDS for layers in the lower surface.

In Fig. 12a we show the LDS for atoms of type 2 representing the first, third and fifth layer of atoms from the surface and for a layer in the bulk. In Fig. 12b we show the LDS for atoms of type 1 corresponding to the second, fourth, and sixth layer of atoms along with the LDS for a layer in the bulk. From these curves we see that the density of states at the surface is considerably more narrow in energy than the bulk density of states. This feature of band narrowing has been demonstrated theoretically for metals^{32,54} and has been observed using photoemission.⁵⁵ Here we have demonstrated that band narrowing also occurs for semiconductors. Experimentally, the observed photoemission bandwidths for a large number of semiconductors are more narrow for UPS than for XPS.⁵⁶ This trend can be interpreted as being due to band narrowing at the surface since the escape depth of electrons in UPS is smaller than for XPS.

In addition, from Fig. 12 we see that the density of states for the surface layers rapidly approaches the bulk density of states as we move into the crystal from the surface. By the fifth layer, the LDS is very similar to the bulk density of states.

V. CONCLUSIONS

We have obtained, for the first time, analytic expressions for both the bulk Green's function and the (001) surface Green's function of a two-band model crystal of the CsCl structure. These Green's functions are significant

because, in addition to studying the properties presented in this paper, they can serve as a starting point for calculations of both surface reconstruction and chemisorption on semiconductors and insulators. These two vital problems have not yet been examined from the Green's function point of view. The fact that the Green's functions are analytic is important because it is then possible to study the surface using only simple numerical calculations, and consequently, it is much easier to understand how the results depend on the model parameters. This feature is often missing from more elaborate numerical calculations.

We have calculated the change in the density of electronic states caused by the creation of the surface for three separate models. The three models were chosen because one results in no surface states, one results in Shockley surface states, and one results in Tamm surface states. The existence conditions for these surface states is significantly different from those obtained previously, both in one-dimensional models and in one-band three-dimensional models. The change in the density of states shows both the addition of the derived surface states and, equally important, the concomitant perturbation of the infinite crystal density of states. In addition, we have used the change in the density of states to calculate various thermodynamic properties of the semiconductor or insulator surface, namely, the electronic specific heat and the surface electronic entropy. We have found, in contrast to one-band metals, that the surface specific heat falls to zero exponentially at low temperatures.

We have presented the local densities of states for a few layers of atoms in the surface region for the case when there are no surface states. We expect the results to be qualitatively the same for the other two models. We have shown, as is true for one-band crystals, that the band widths of the densities of states on the surface layers are more narrow than for the bulk layers. This fact can explain some of the discrepancies which have appeared between the results

of UPS and XPS studies on semiconductor surfaces.

Finally, whereas the work in this paper is concerned with a specific surface of a specific structure of a two-band crystal, we believe that the qualitative features of the results are quite general and are common to all semiconductor and insulator surfaces. This belief is supported by analogy to the fact that for one-band metals, the model results for three faces of a simple cubic crystal, two faces of a body-centered cubic crystal, and one face of a face-centered cubic crystal are all qualitatively the same. Thus we believe that the results in this paper can serve as a general basis for the way in which one views both semiconductor and insulator surfaces.

ACKNOWLEDGMENT

We acknowledge, with gratitude, support of this research by the National Science Foundation (Grant No. GK-43433), the IBM Corporation via a postdoctoral research fellowship (SLC), and the NSF via an undergraduate research participation (WH).

APPENDIX

We present here the calculation of the partial phase shift for the case of zero band gap by two different methods. For the first method, we set $E_1 = E_2 = 0$ in the derivation of the bulk Green's function of Sec. II to get the Green's function appropriate for a body-centered cubic (bcc) crystal. We then obtain an analytic expression for the partial phase shift which contains no sign ambiguity. For the second method, we use the partial phase shift expression given in Sec. III and evaluate them in the limit $E_1 \rightarrow E_2 \rightarrow 0$. By comparing the two results, the sign ambiguity is removed for Model I. The same method has been used for Model II and III, and for the surface Green's function in Sec. IV.

Setting $E_1 = E_2 = \gamma_2 = 0$ in Eqs. (31) - (35), we find that each of the Green's functions, when written in integral form (using Eq. (36)), contains the factor $E/(E^2 - F^2)$. This factor can be split into partial fractions as

$$\frac{2E}{E^2 - F^2} = \frac{1}{E+F} + \frac{1}{E-F} \quad . \quad (\text{A.1})$$

Using this identity and the integral from Eq. (37), we obtain for the bcc bulk crystal Green's functions

$$G^{(0)} \left(\begin{array}{cc} \lambda_z & \lambda_z' \\ \beta & \beta \end{array} , \vec{\phi}_s, E \right) = P^{-1} \tau^{-2} |\lambda_z - \lambda_z'| + 1, \quad \beta=1,2, \quad (\text{A.2})$$

$$G^{(0)} \left(\begin{array}{cc} \lambda_z & \lambda_z' \\ 1 & 2 \end{array} , \vec{\phi}_s, E \right) = -P^{-1} \tau^{-2} |2(\lambda_z - \lambda_z') - 1| + 1 \chi^*(\vec{\phi}_s), \quad (\text{A.3})$$

$$G^{(0)} \left(\begin{array}{cc} \lambda_z & \lambda_z' \\ 2 & 1 \end{array} , \vec{\phi}_s, E \right) = -P^{-1} \tau^{-2} |2(\lambda_z - \lambda_z') + 1| + 1 \chi(\vec{\phi}_s), \quad (\text{A.4})$$

where

$$P' = 1/f(\tau^2-1) \quad , \quad (A.5)$$

$$\tau = \begin{cases} s - (s^2-1)^{\frac{1}{2}} \quad , & s > 1 \\ s + i(1-s^2)^{\frac{1}{2}} \quad , & -1 < s < 1 \\ s + (s^2-1)^{\frac{1}{2}} \quad , & s < -1 \end{cases} \quad , \quad (A.6)$$

$$s = -E/2f \quad , \quad (A.7)$$

and where f is given by Eq. (46) and $\chi(\vec{\phi}_s)$ is given by Eq. (60).

Using the perturbation matrix for Model I, Eq. (59), the Fredholm determinant in Eq. (54) reduces to the simple expression

$$D(\vec{\phi}_s, E) = -1/(\tau^2-1) \quad . \quad (A.8)$$

Inside the band, the magnitude of s (Eq. (A.7)) is less than unity. Thus, using Eq. (A.6) in Eq. (A.8) and calculating the partial phase shift in Eq. (56) we obtain

$$\eta(\vec{\phi}_s, E) = -\arg \left[\frac{s}{(1-s^2)^{\frac{1}{2}}} \right] \quad . \quad (A.9)$$

There is no ambiguity in the sign of the square root in this expression since the sign of the square root in Eq. (A.6) is fixed.

In the second approach, we use the expressions for the bulk Green's functions given in Eqs. (39) - (42) and take the limit as $E_1 = E_2 = \gamma_2 = 0$. Again, the Fredholm determinant in Eq. (54) can be written analytically with the result

$$D(\vec{\phi}_s, E) = -1/(t-1) \quad , \quad (A.10)$$

where t is given by Eq. (38). Inside the bands, we have

$$t = \xi + i(1-\xi^2)^{\frac{1}{2}}, \quad (\text{A.11})$$

and the parameter ξ (from Eq. (47)) can be related to s (Eq. (A.7)) by

$$\xi = 2s^2 - 1. \quad (\text{A.12})$$

Substituting for t in Eq. (A.10) we obtain

$$D(\vec{\phi}_s, E) = \frac{1}{2} \left[1 + i \frac{(1-\xi^2)^{\frac{1}{2}}}{(1-\xi)} \right]. \quad (\text{A.13})$$

The partial phase shift thus becomes

$$\eta(\vec{\phi}_s, E) = -\arg \left[\frac{(s^2)^{\frac{1}{2}}}{(1-s^2)^{\frac{1}{2}}} \right]. \quad (\text{A.14})$$

The ambiguity in sign lies in the numerator of the argument since s can be negative. By comparison with Eq. (A.9) we see that the positive root is the correct root. Thus, the numerator always has the sign opposite in sign to the energy E (note f is always positive in Eq. (A.7)). We assume from continuity that this sign convention is valid even when the band gap is not zero and when the partial phase shift cannot be obtained analytically.

REFERENCES:

1. W. Ho, S. L. Cunningham, W. H. Weinberg and L. Dobrzynski, to be published.
2. J. Koutecky, Adv. Chem. Phys. 9, 85 (1965).
3. S. G. Davison and J. D. Levine, Solid State Phys. 25, 1 (1970).
4. E. T. Goodwin, Proc. Cambridge Phil. Soc. 35, 221 (1939).
5. T. A. Hoffmann and A. Konya, Acta. Physica Hung. 1, 5 (1951).
6. T. A. Hoffmann, Acta Physica Hung. 1, 175 (1951).
7. A. T. Amos and S. G. Davison, Physica 30, 905 (1964).
8. S. G. Davison and J. Koutecky, Proc. Phys. Soc. (London) 89, 237 (1966).
9. J. D. Levine and S. G. Davison, Phys. Rev. 174, 911 (1968).
10. S. L. Cunningham and A. A. Maradudin, Phys. Rev. B7, 3870 (1973).
11. J. Koutecky and M. Tomasek, Phys. Rev. 120, 1212 (1960).
12. See, for example, R. O. Jones, J. Phys. C: Solid State Phys. 5, 1615 (1972);
F. Yndurain and M. Elices, Surface Sci. 29, 540 (1972).
13. E. T. Goodwin, Proc. Cambridge Phil. Soc. 35, 232 (1939).
14. D. Pugh, Phys. Rev. Lett. 12, 390 (1964).
15. K. Hirabayashi, J. Phys. Soc. Japan 27, 1475 (1969).
16. I. Alstrup, Surface Sci. 20, 335 (1970).
17. I. Alstrup, Phys. Stat. Solidi (b) 45, 209 (1971).
18. K. C. Pandey and J. C. Phillips, Solid State Commun. 14, 439 (1974).
19. K. C. Pandey and J. C. Phillips, Phys. Rev. Lett. 32, 1433 (1974).
20. J. D. Joannopoulos and M. L. Cohen, Phys. Lett. 49A, 391 (1974).
21. See, for example, E. Caruthers, L. Kleinman and G. P. Alldredge, Phys. Rev. B9, 3325, 3330 (1974).
22. G. R. Baldock, Proc. Cambridge Phil. Soc. 48, 457 (1952).
23. G. F. Koster and J. C. Slater, Phys. Rev. 95, 1167 (1954).
24. J. Koutecky and S. G. Davison, Int. J. Quant. Chem. 2, 73 (1968).

25. J. Koutecky, Phys. Rev. 108, 13 (1957).
26. B. W. Holland, Phil. Mag. 8, 87 (1963).
27. R. A. Brown, Phys. Rev. 156, 889 (1967).
28. M. Tomasek, in The Structure and Chemistry of Solid Surfaces, ed. by G. A. Somorjai (Wiley, New York, 1969).
29. S. Freeman, Phys. Rev. B2, 3272 (1970).
30. J. D. Levine and S. Freeman, Phys. Rev. B2, 3255 (1970). More recently, D. Lohez and M. Lannoo, J. Physique 35, 647 (1974), have studied the same system by means of the resolvent technique using a more complicated model. They obtain the bulk Green's functions in analytic form.
31. A. van der Avoird, S. P. Liebmann and D. J. M. Fassaert, Phys. Rev. B10, 1230 (1974).
32. D. Kalkstein and P. Soven, Surface Sci. 26, 85 (1971).
33. S. M. Bose and E-Ni Foo, Phys. Rev. B10, 3534 (1974).
34. B. S. DeWitt, Phys. Rev. 103, 1565 (1956).
35. A. Blandin, J. Phys. Rad. 22, 507 (1961).
36. G. Toulouse, Solid State Commun. 4, 593 (1966).
37. G. Allan, Ann. Phys. (Paris) 5, 169 (1970).
38. G. Allan and P. Lengart, Surface Sci. 15, 101 (1969).
39. G. Allan and P. Lengart, Surface Sci. 30, 641 (1972).
40. T. L. Einstein, Surface Sci. 45, 713 (1974).
41. T. L. Einstein and J. R. Schrieffer, Phys. Rev. B7, 3629 (1973).
42. J. R. Schrieffer, J. Vac. Sci. Technol. 9, 561 (1971).
43. T. B. Grimley and C. Pisani, J. Phys. C: Solid State Phys. 7, 2831 (1974).
44. J. M. Ziman, Principles of the Theory of Solids (Cambridge University Press, 1965) Chapter 5.
45. D. N. Zubarev, Soviet Physics Uspekhi 3, 320 (1960).
46. A. A. Maradudin, E. W. Montroll, G. H. Weiss and I. P. Ipatova, Theory of Lattice Dynamics in the Harmonic Approximation (Academic Press, 1971) Chapter 2, Solid State Phys., Supplement 3, 2nd Edition.

47. L. Dobrzynski, Ann. Phys. (Paris) 4, 637 (1969)
48. If we had included the other second neighbor interaction, $\gamma_2^{(1)}$, the denominator in the integral would be quadratic in $\cos \phi_z$ rather than linear.
49. The phase shift jumps to $-\pi$ rather than $+\pi$ because we use the retarded Green's functions. The factor $i\epsilon$ tells us we must circle the singularity in the upper half of the complex plane resulting in a change of phase of π . However, the phase shift is the negative of the change of phase; therefore we get a jump of $-\pi$.
50. S. L. Cunningham, Phys. Rev. B10, 4988 (1974).
51. J. Friedel, Nuovo Cimento Supp. 7, 287 (1958).
52. L. Dobrzynski and D. L. Mills, Phys. Rev. B7, 2367 (1973).
53. S. L. Cunningham, unpublished, has been able to show that the "surface" Green's function for a finite diatomic chain where each atom has one orbital (two orbitals per unit cell) can also be expressed as a simple linear combination of "bulk" Green's functions.
54. R. Haydock and M. J. Kelly, Surface Sci. 38, 139 (1973).
55. See, for example, N. E. Christensen and B. Feuerbacher, Phys. Rev. B10, 2349, 2373 (1974).
56. See, for example, D. E. Eastman, W. D. Grobman, J. L. Freeouf and M. Erbudak, Phys. Rev. B9, 3473 (1974).

FIGURE CAPTIONS:

- Figure 1: The geometry of the (001) surface of a crystal with the CsCl structure. The plane of atoms of type 2 is a distance $a_0/2$ behind the plane of atoms of type 1. The first-neighbor interaction is γ_1 and the second-neighbor interaction between atoms of type 2 is γ_2 .
- Figure 2: The projection of the infinite crystal energy bands onto a segment of the surface Brillouin zone showing the quasi-continuum of states for each value of wave vector. Results are for the cases when (a) only nearest-neighbor interactions are included, (b) second-neighbor interactions between atoms of type 1 are included, and (c) second-neighbor interactions between atoms of type 2 are included. For all results we use $E_1 = 2.0$ and $E_2 = -2.0$.
- Figure 3: The energy bands for one-quarter of the surface Brillouin zone for Model II showing the Shockley surface states (shaded area) lying just above the valence band.
- Figure 4: Detail of the surface states for Model II for a particular segment, $k_y = \pi/2a_0$, of the surface Brillouin zone.
- Figure 5: The shaded region shows the region in the surface Brillouin zone for which Shockley surface states exist in Model II.

- Figure 6: Position of the Tamm surface states for Model III for a particular segment, $k_y = \pi/2a_0$, of the surface Brillouin zone. Note the break in the vertical scale.
- Figure 7: The partial phase shift as a function of energy for a particular point, $k_x = k_y = \pi/2a_0$, in the surface Brillouin zone for (a) Model I, (b) Model II, and (c) Model III. (d) The partial phase shift at a point near the zone edge, $k_x = 9\pi/10a_0$ and $k_y = \pi/2a_0$, for Model III. Note the break in scale.
- Figure 8: Total phase shift as a function of energy for (a) Model I, (b) Model II, and (c) Model III.
- Figure 9: The change due to the creation of the surface in the total density of states (per unit energy) per surface unit cell as a function of energy for (a) Model I, (b) Model II, and (c) Model III.
- Figure 10: The change due to the creation of the surface in the electronic specific heat as a function of temperature for each of the three models. The results for the half-filled one-band crystal (ref. 38) are plotted for comparison.
- Figure 11: Electronic contribution to the surface entropy as a function of temperature for each of the three models. The results for the half-filled one-band crystal (ref. 38) are plotted for comparison.

Figure 12: The local density of states (per unit energy) per surface atom for the first six layers of atoms in the lower surface of Figure 1. (a) Results for atoms of type 2 and (b) results for atoms of type 1. The local density of states for layers in the bulk are shown for comparison.

(a)

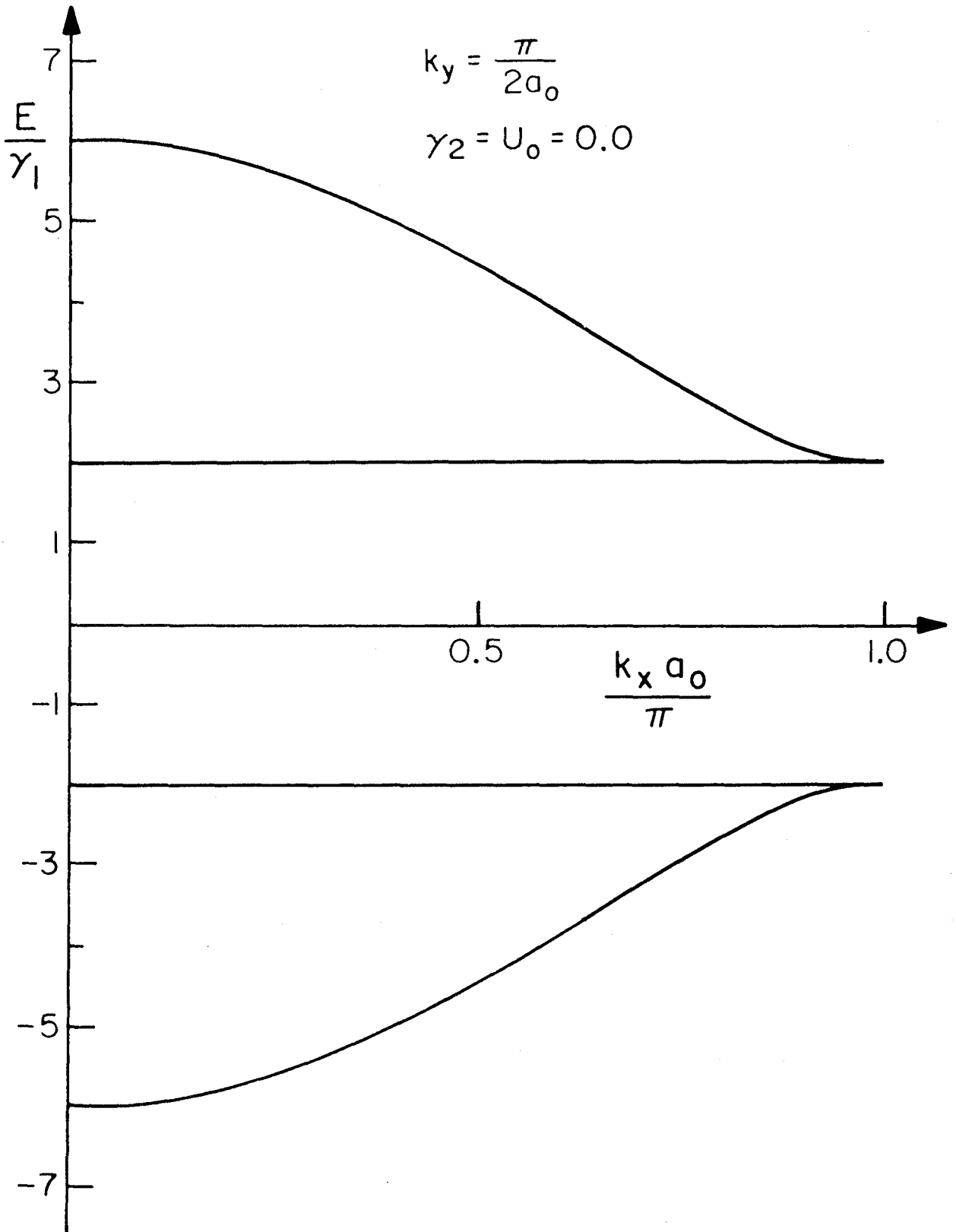


Figure 2(a)

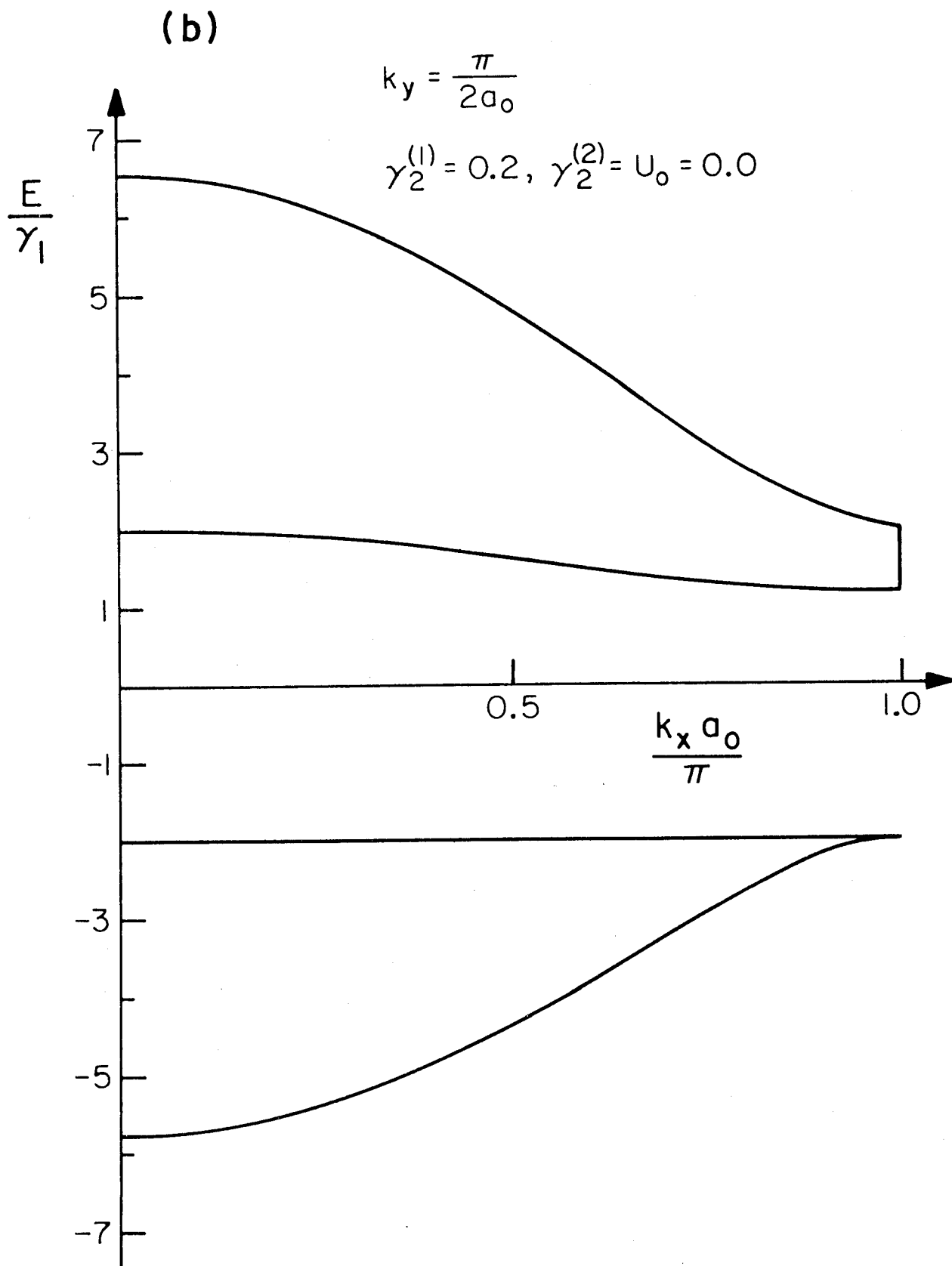


Figure 2(b)

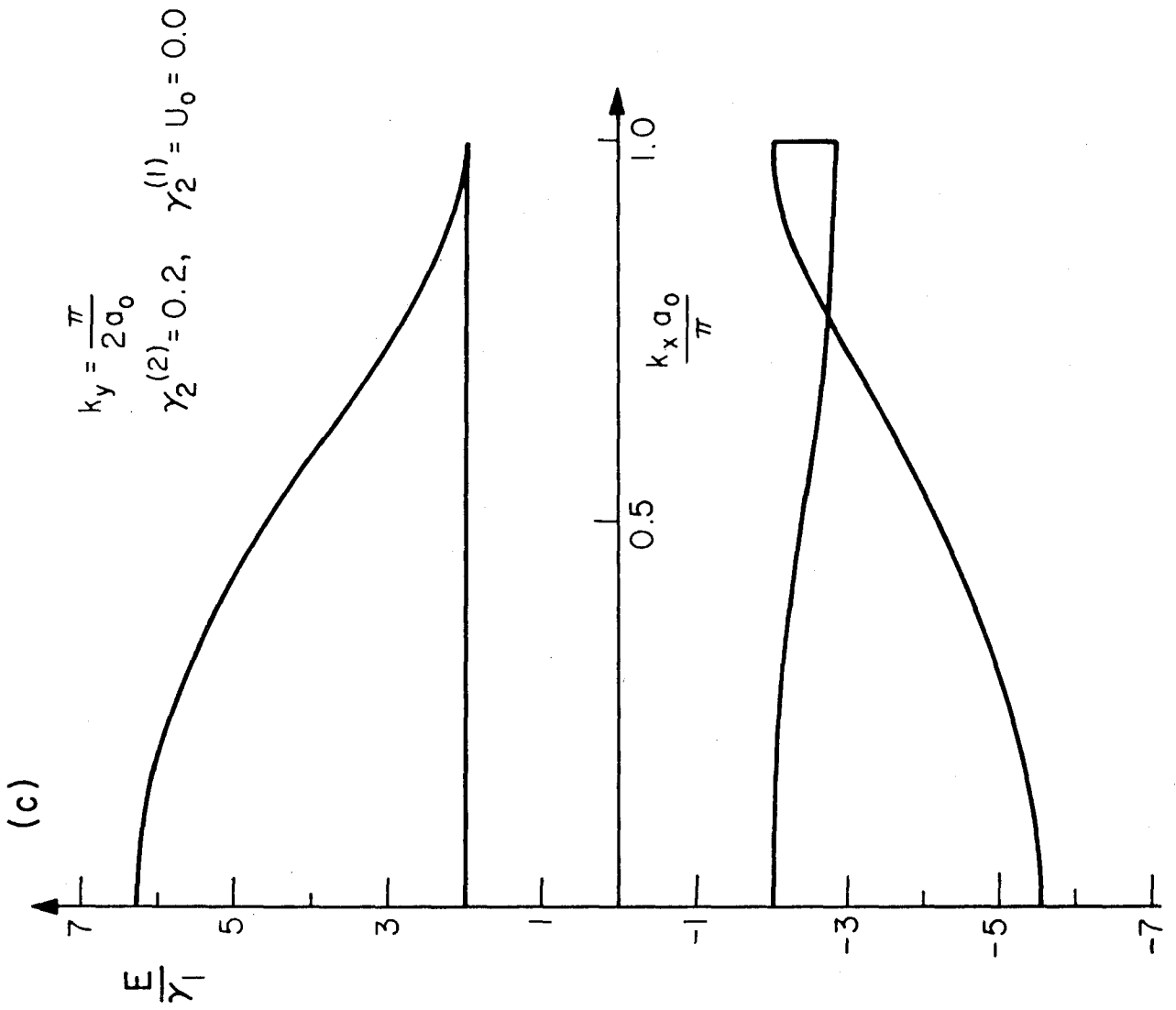


Figure 2(c)

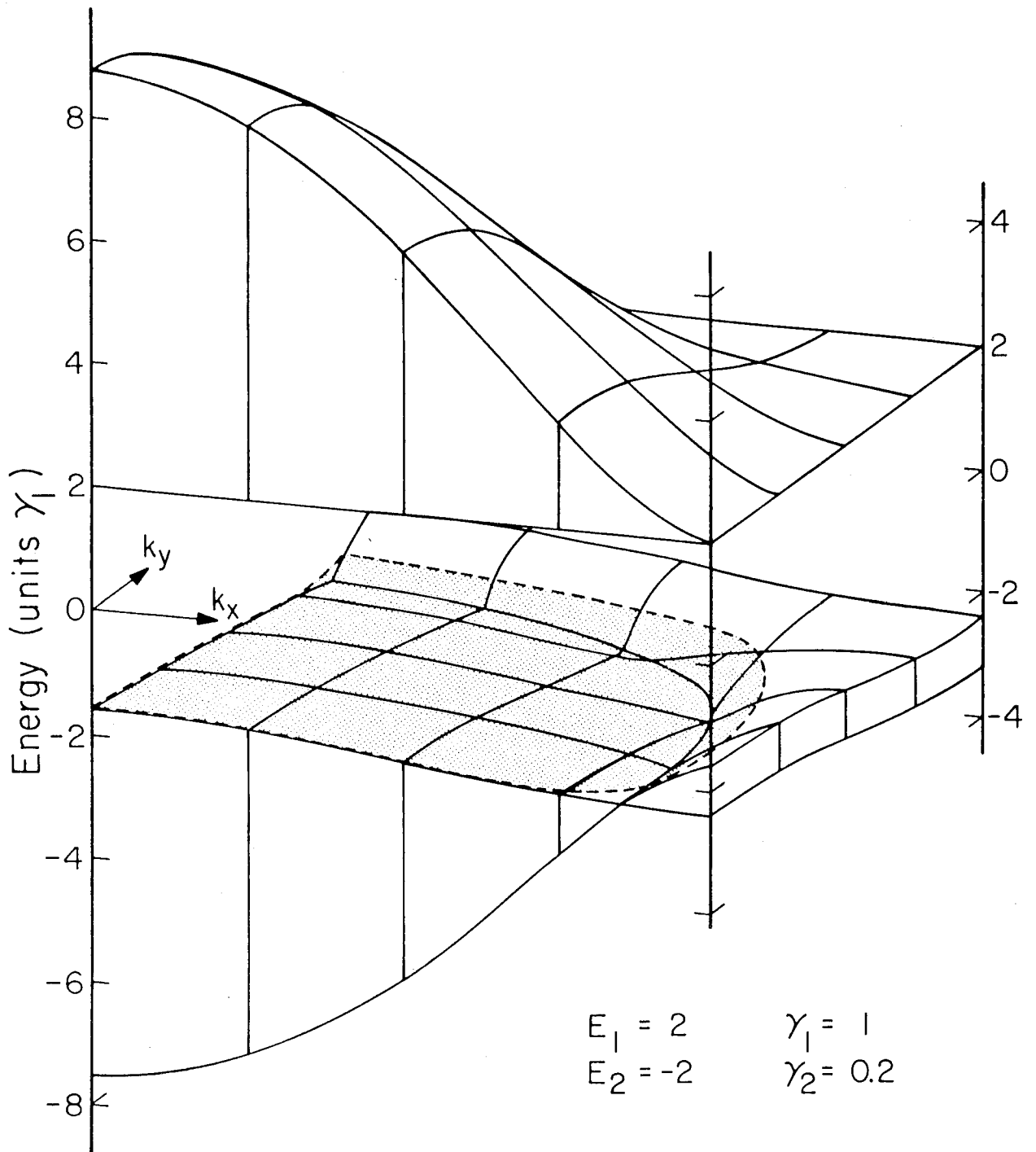


Figure 3

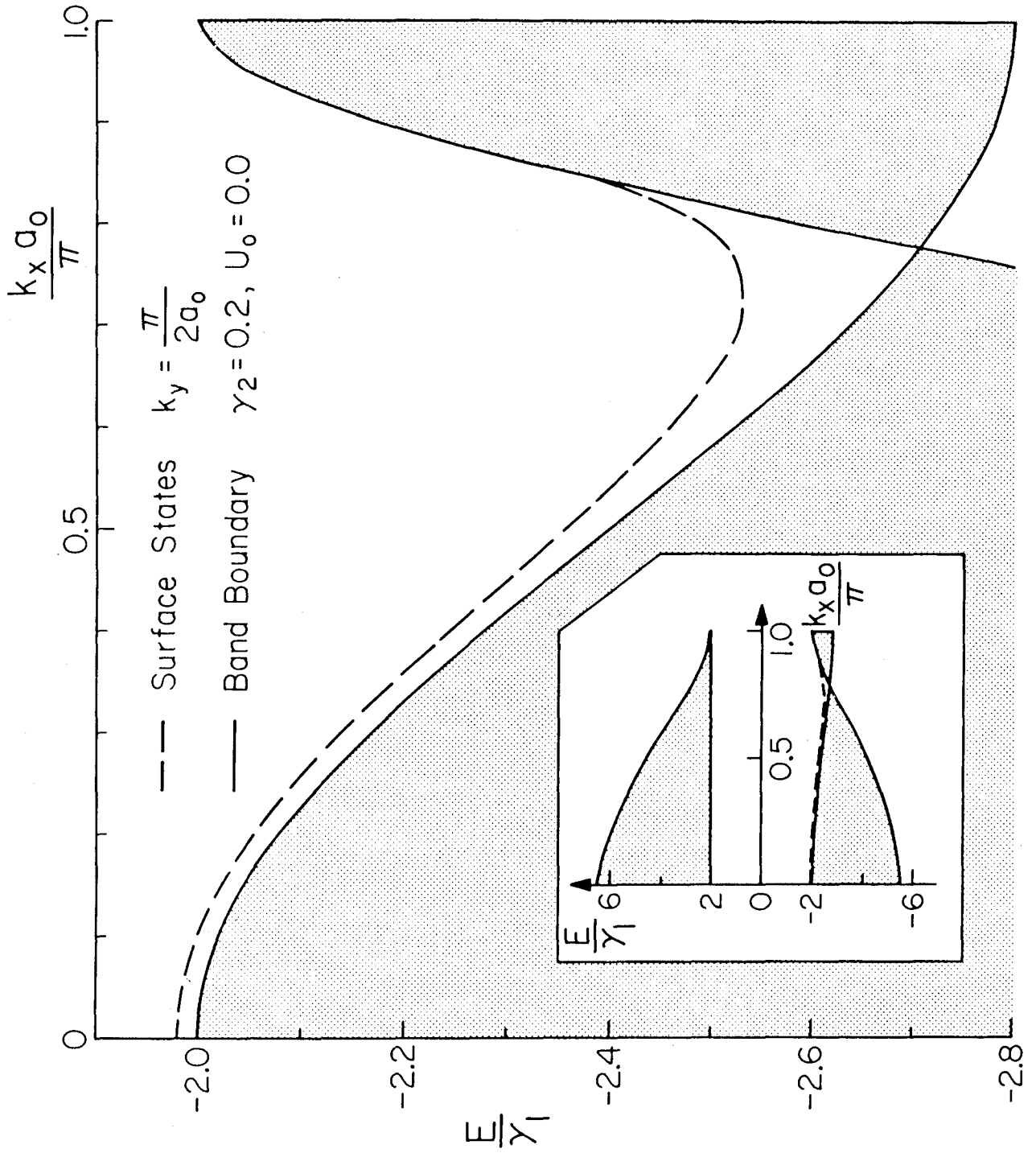


Figure 4

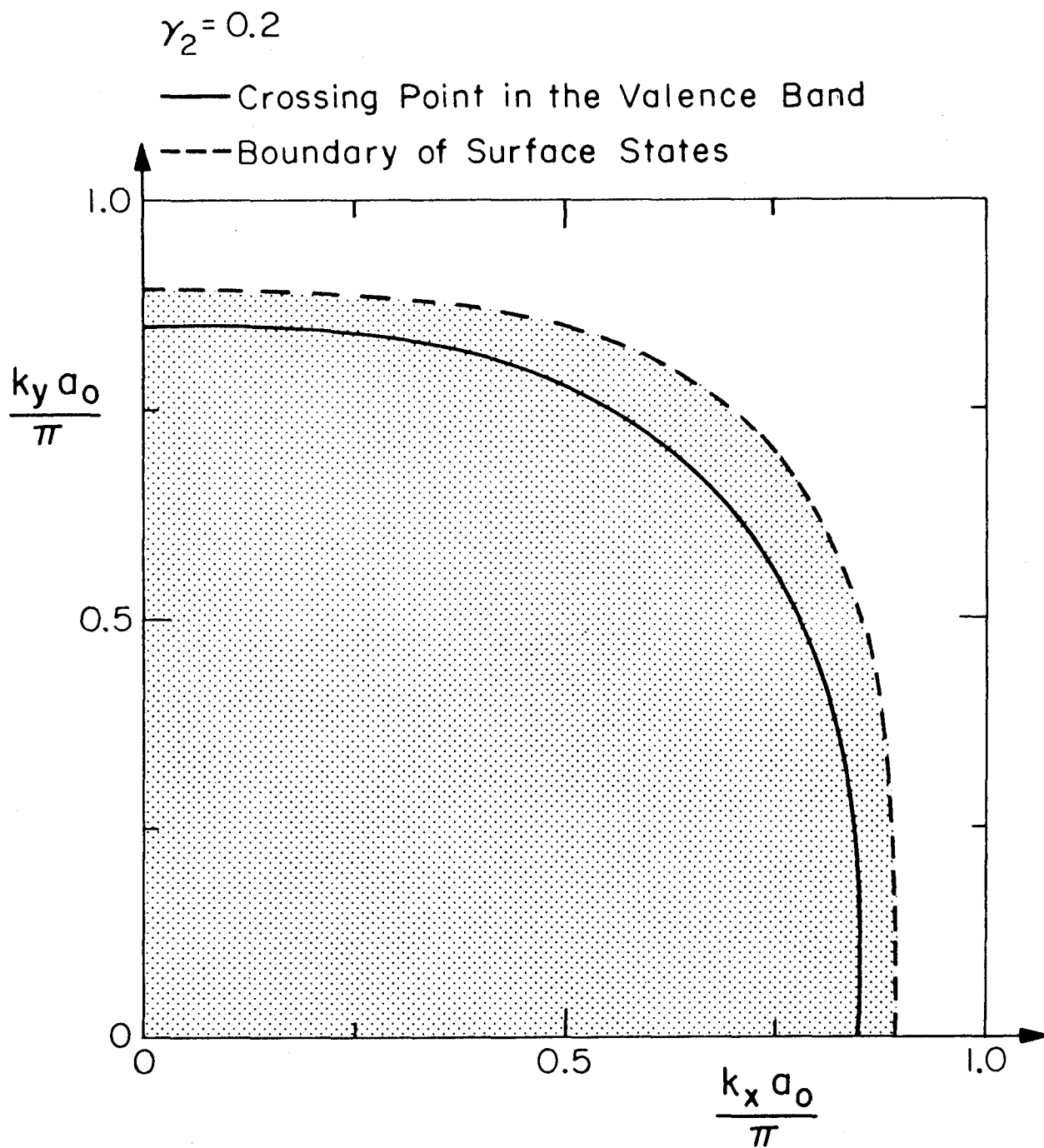


Figure 5

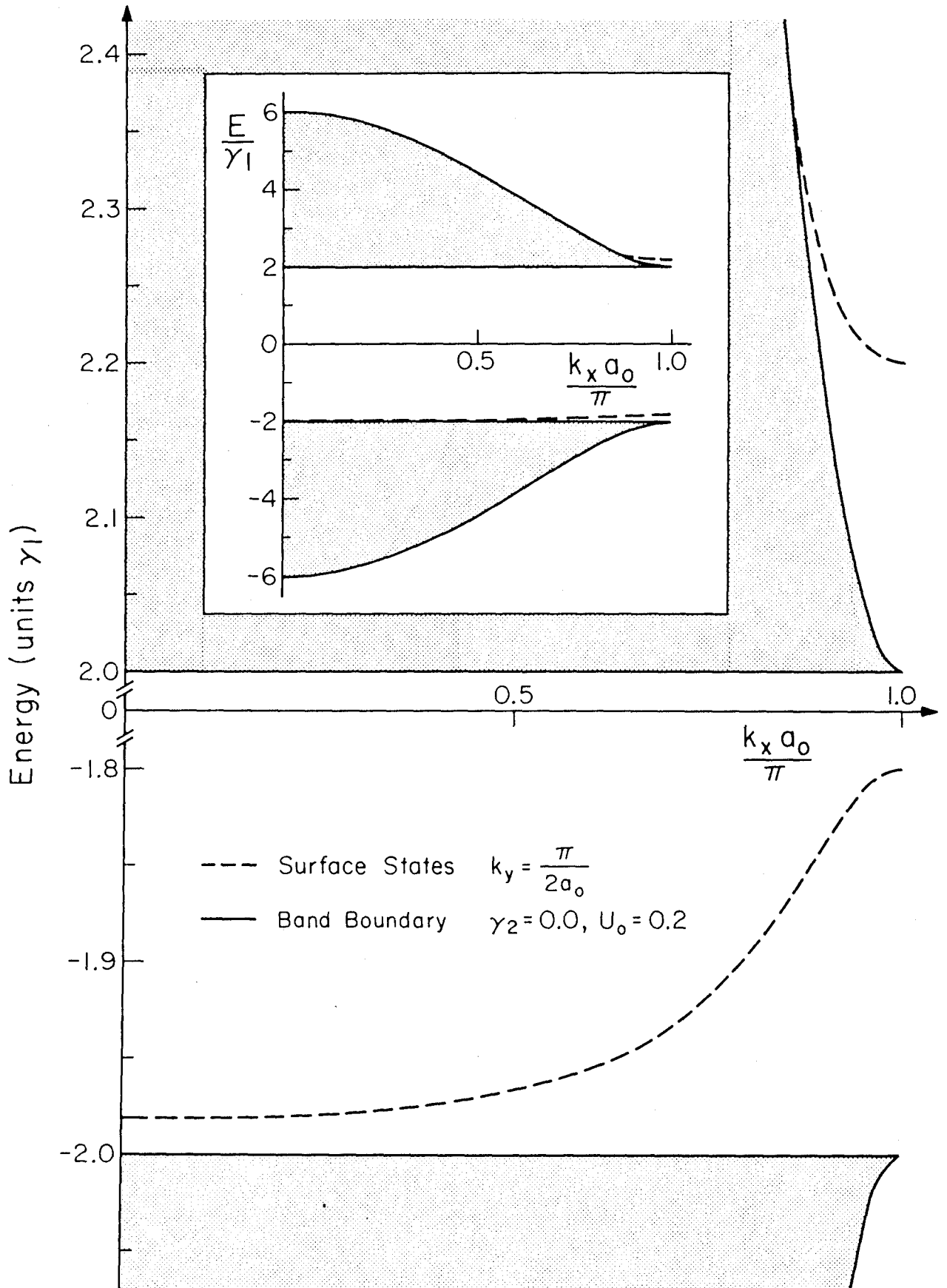


Figure 6

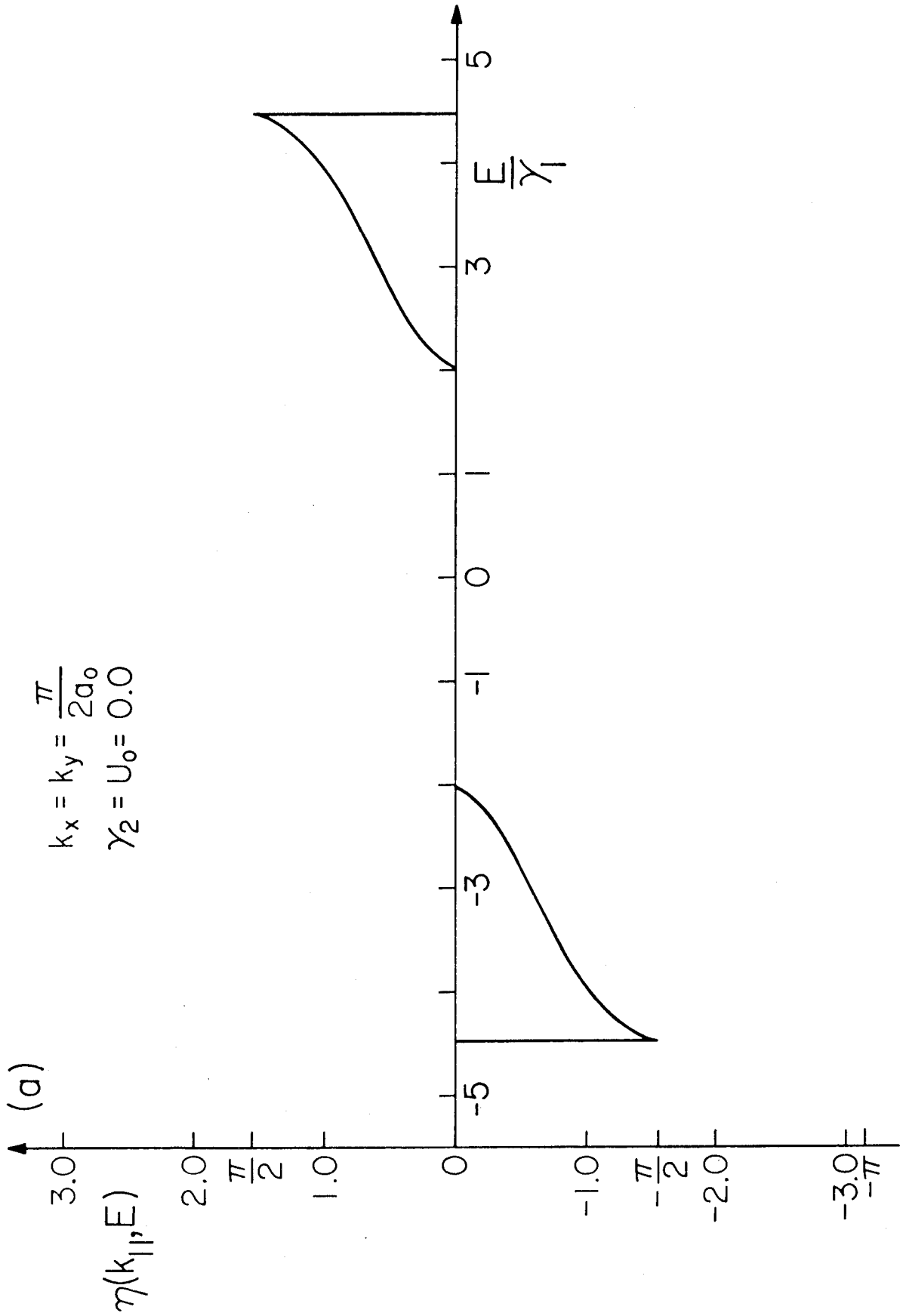


Figure 7(a)

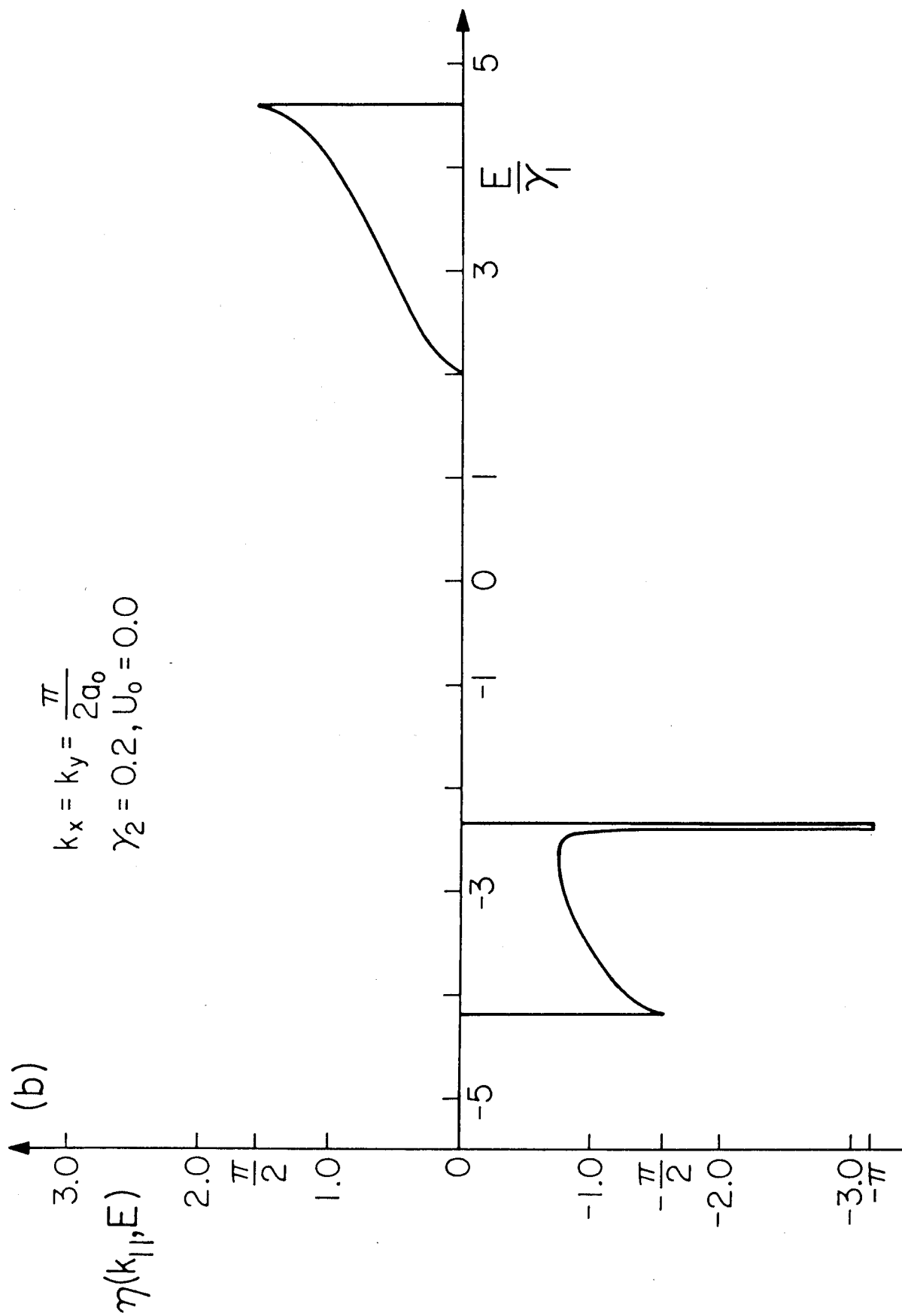


Figure 7(b)

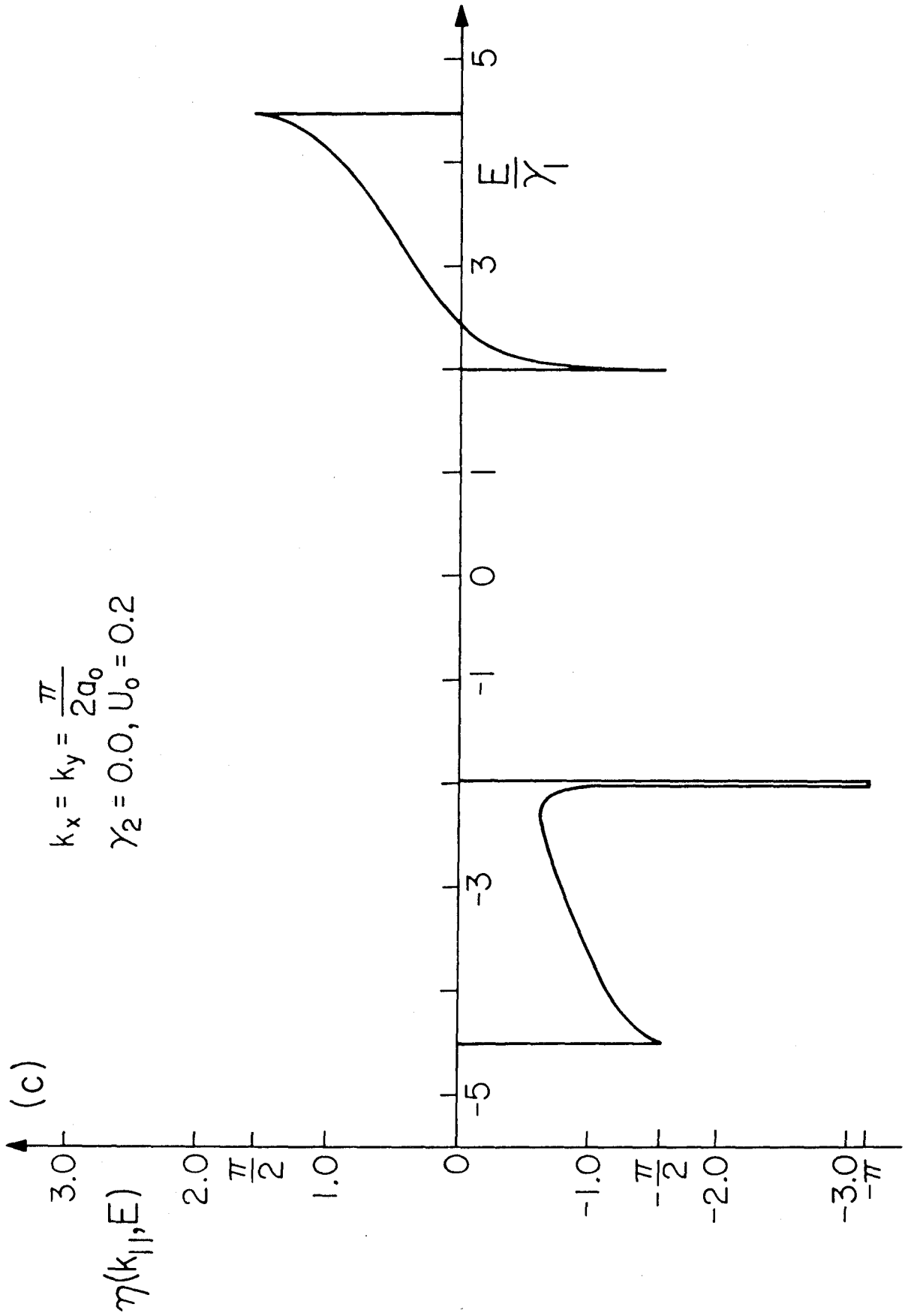


Figure 7(c)

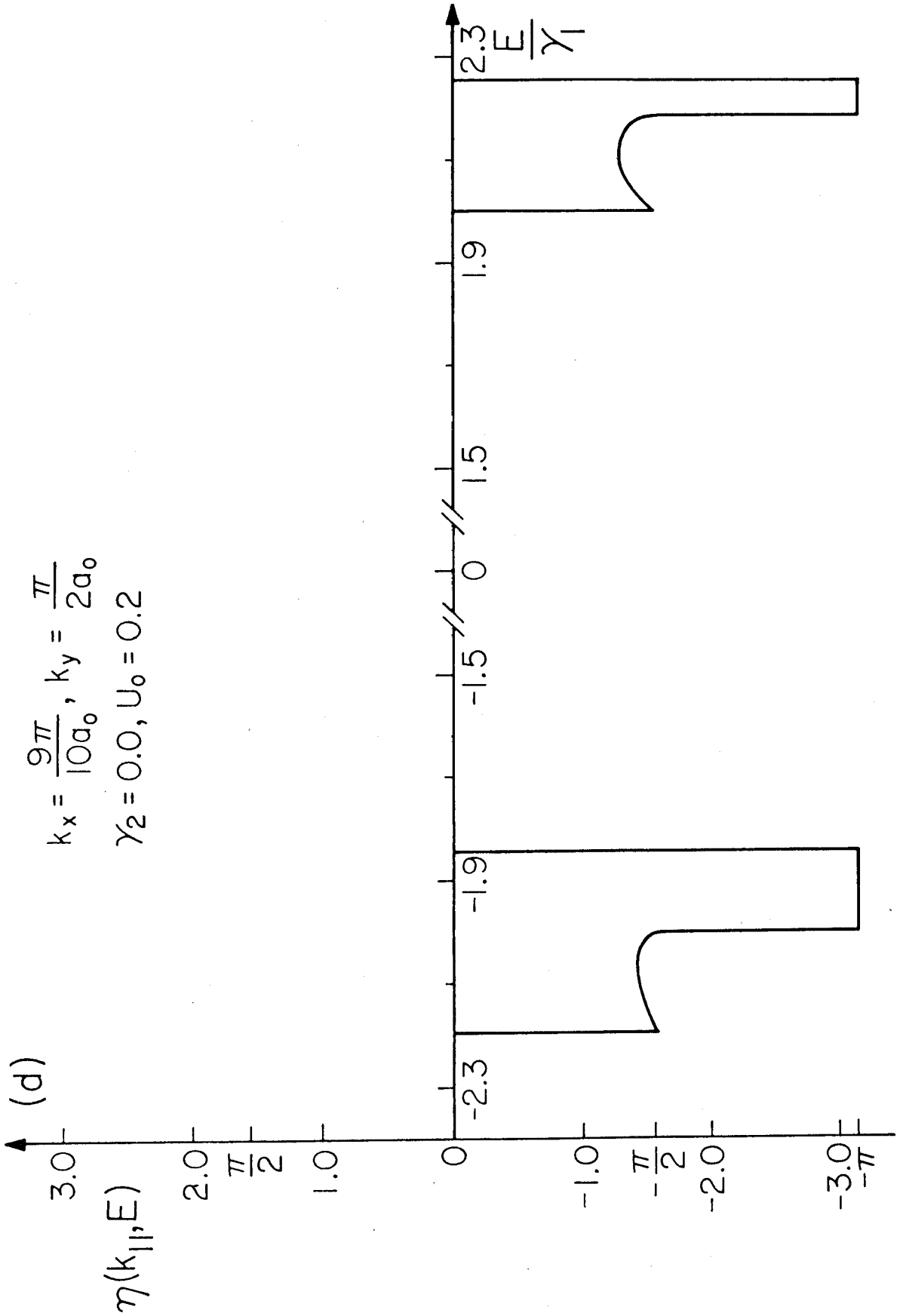


Figure 7(d)

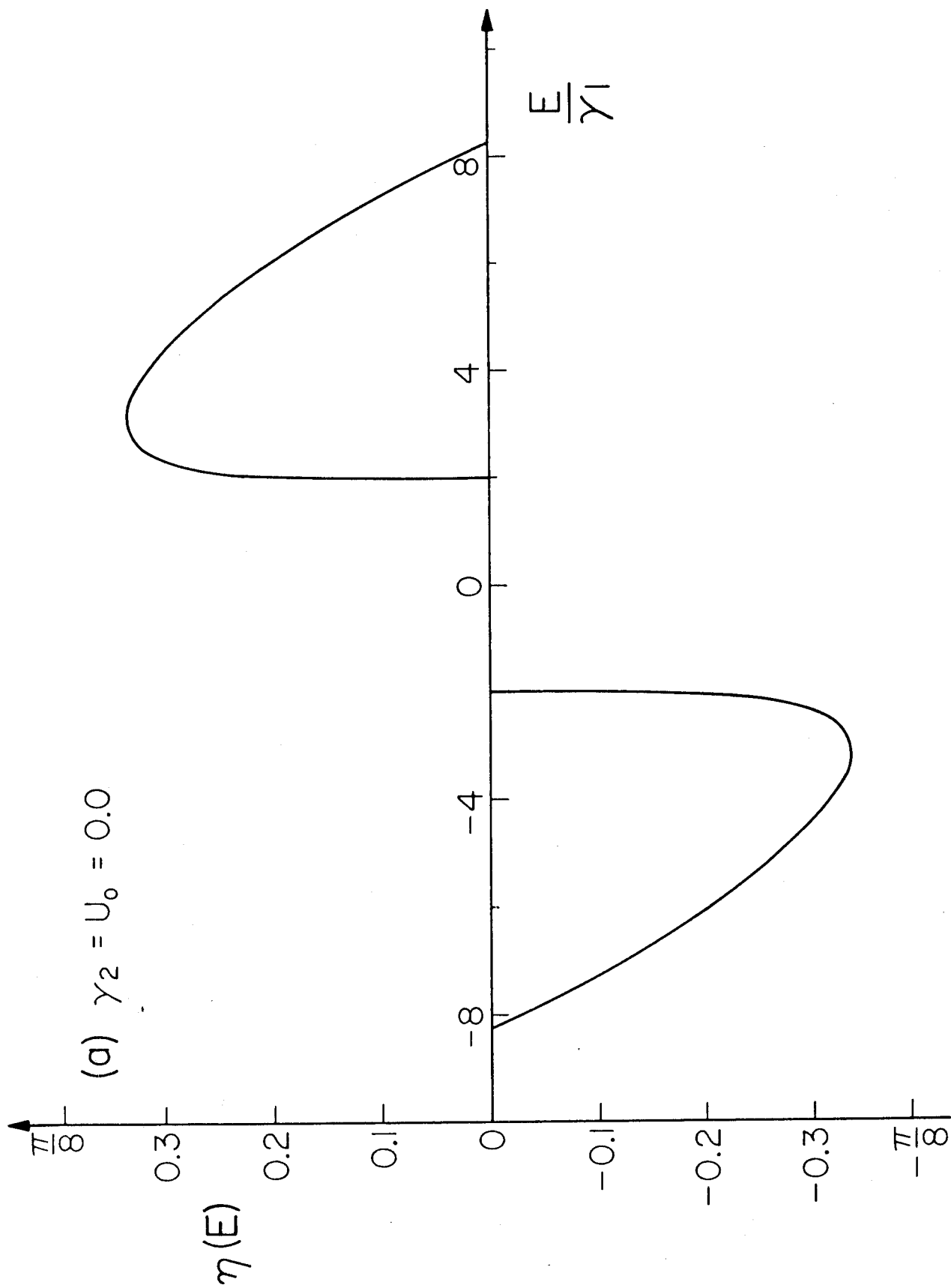


Figure 8(a)

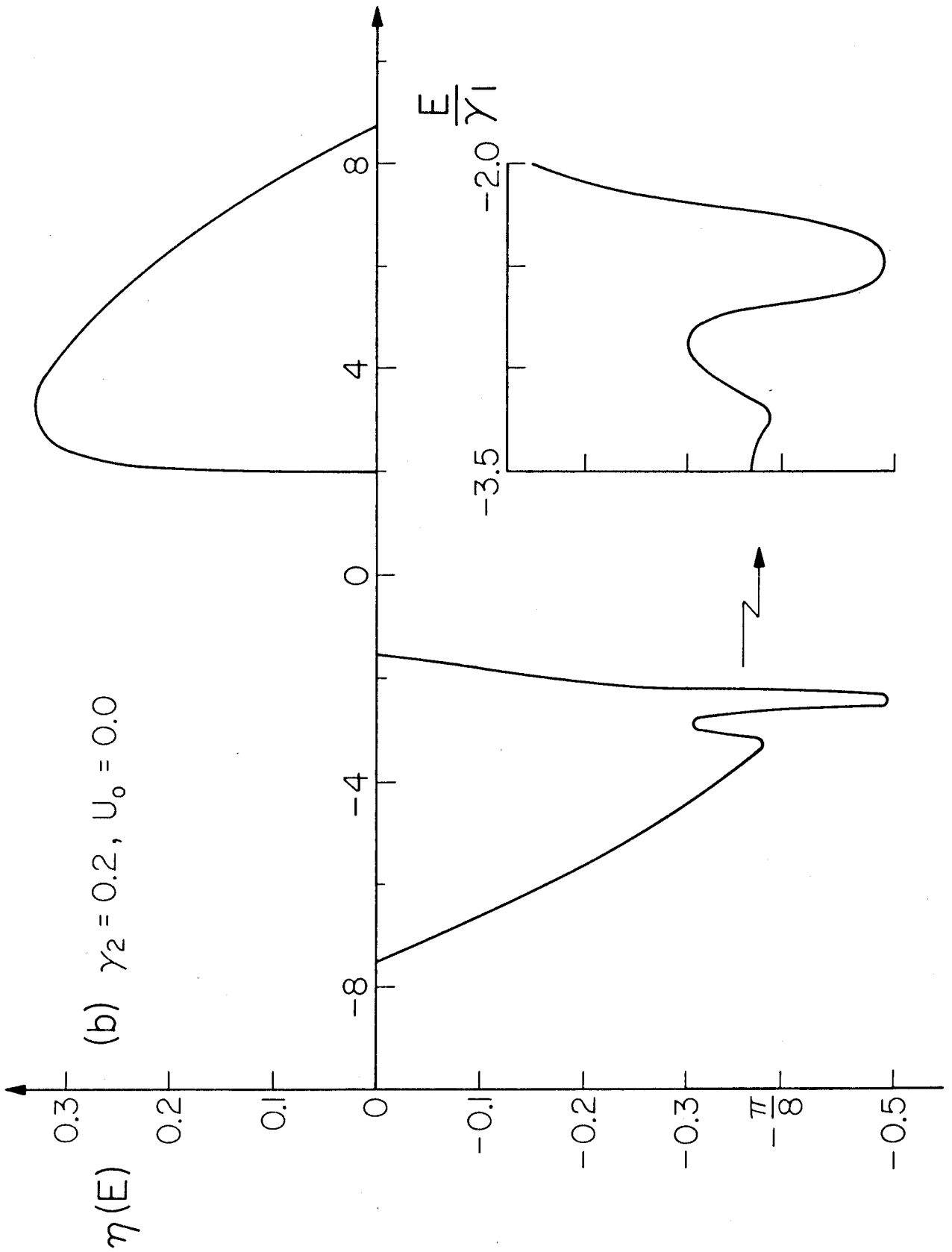


Figure 8(b)

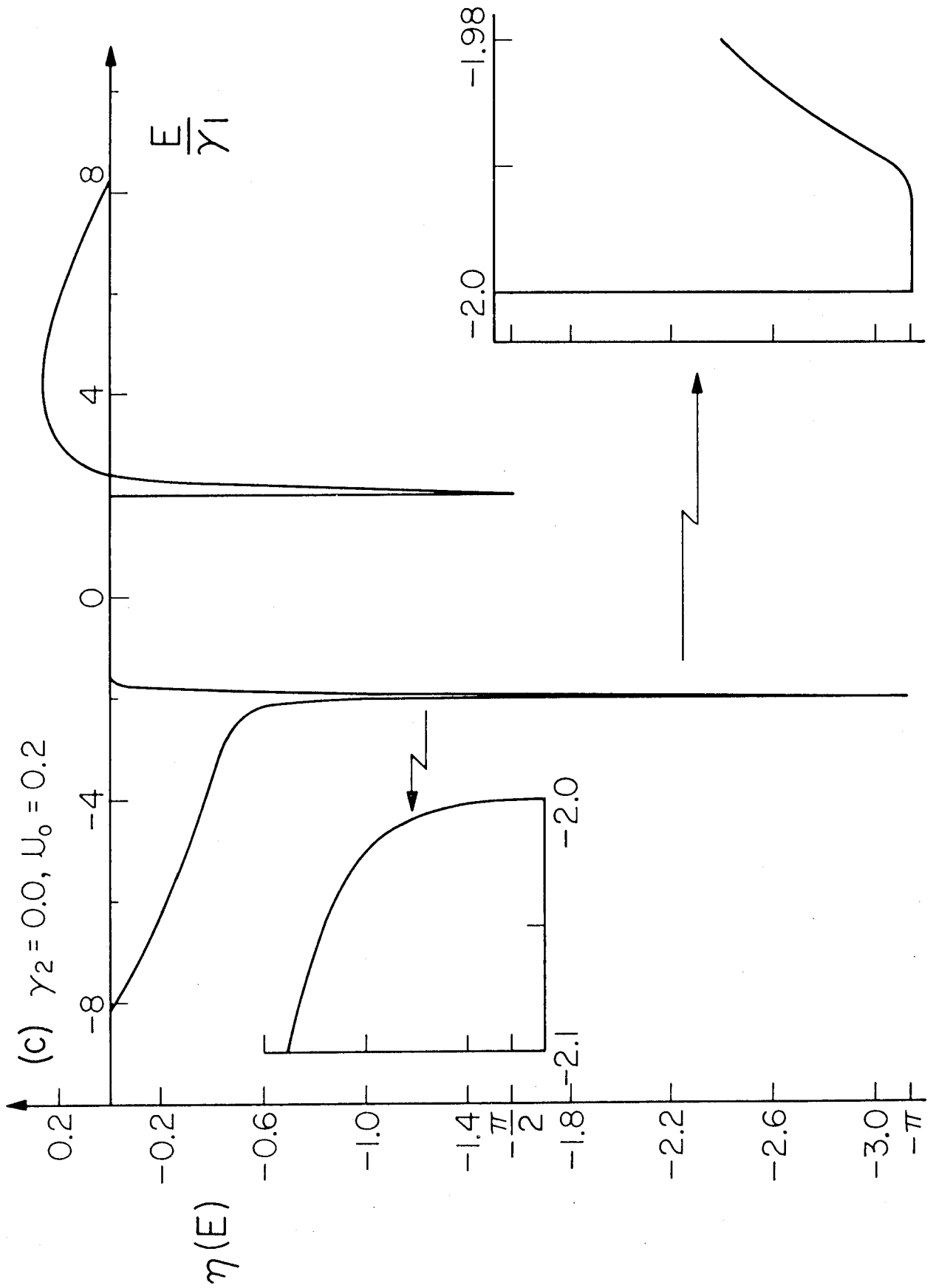


Figure 8(c)

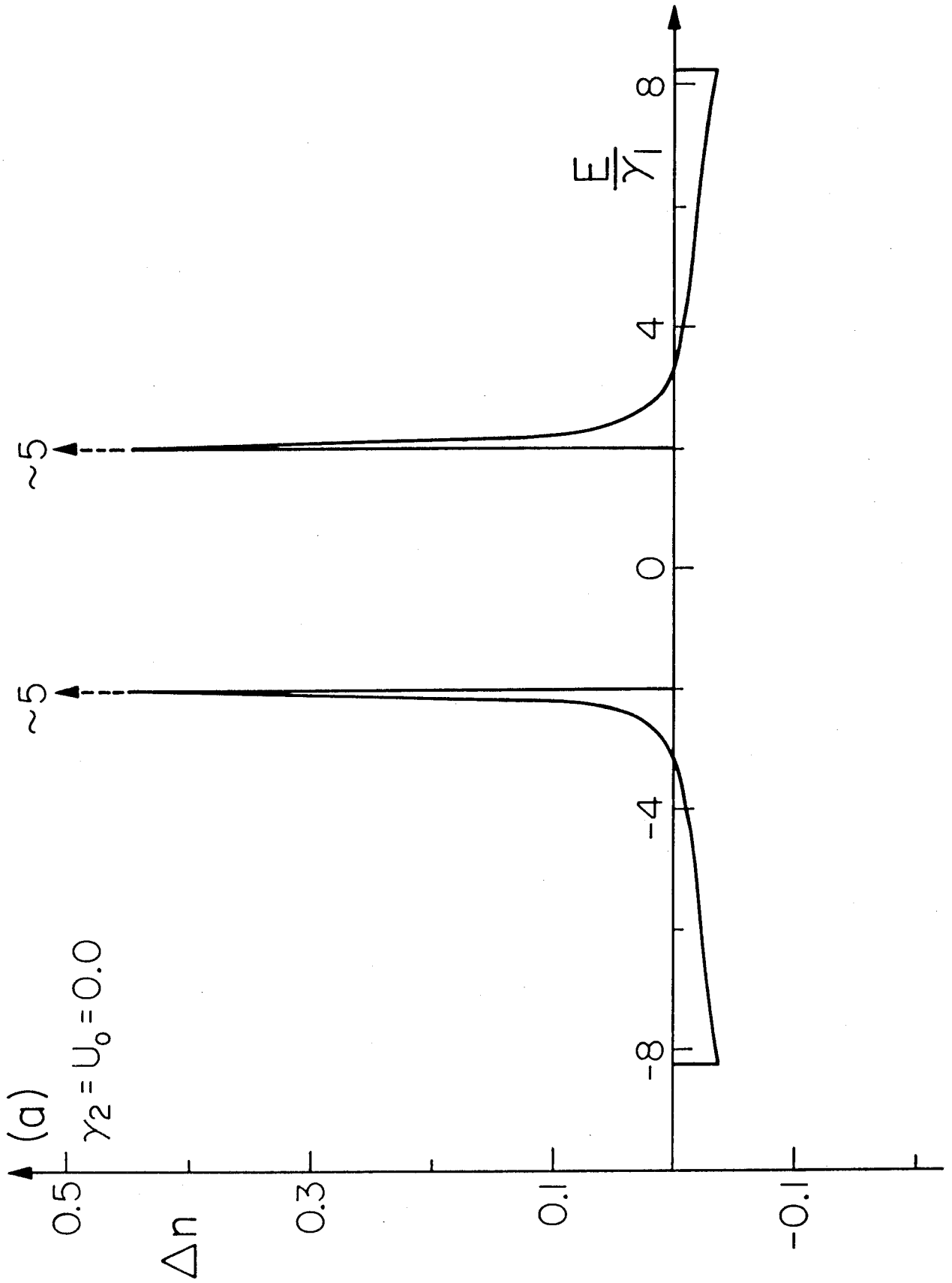


Figure 9(a)

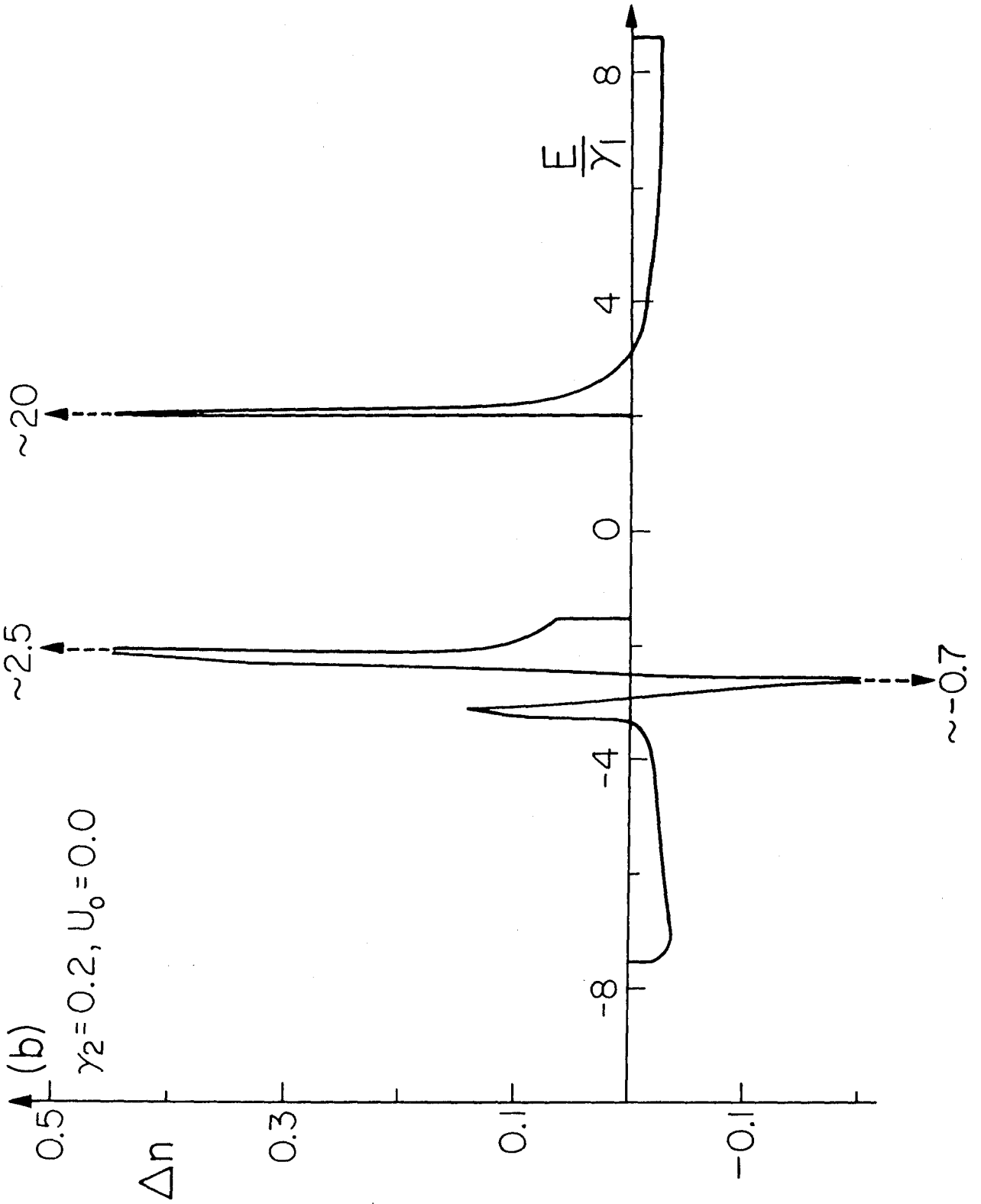


Figure 9(b)

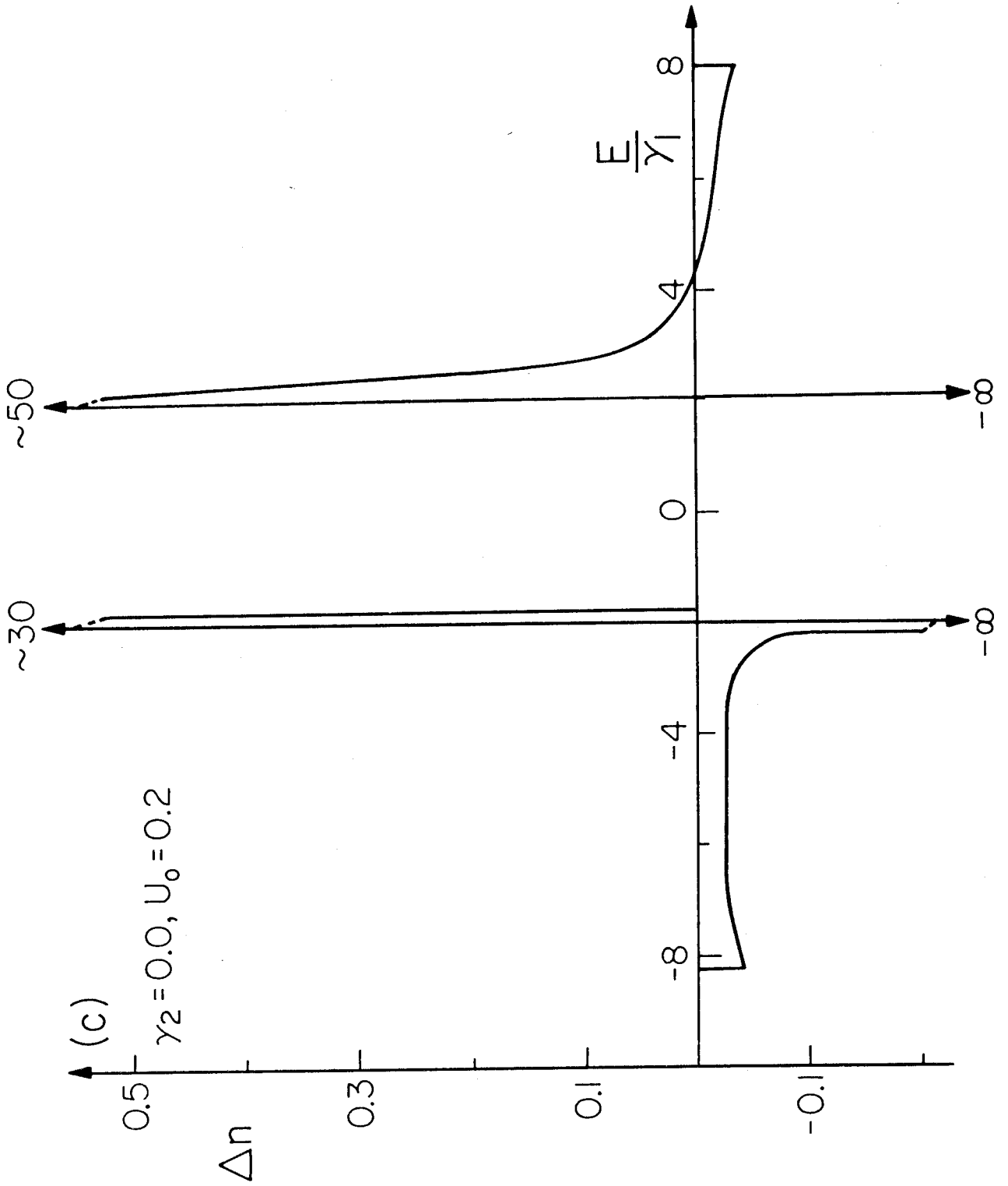


Figure 9(c)

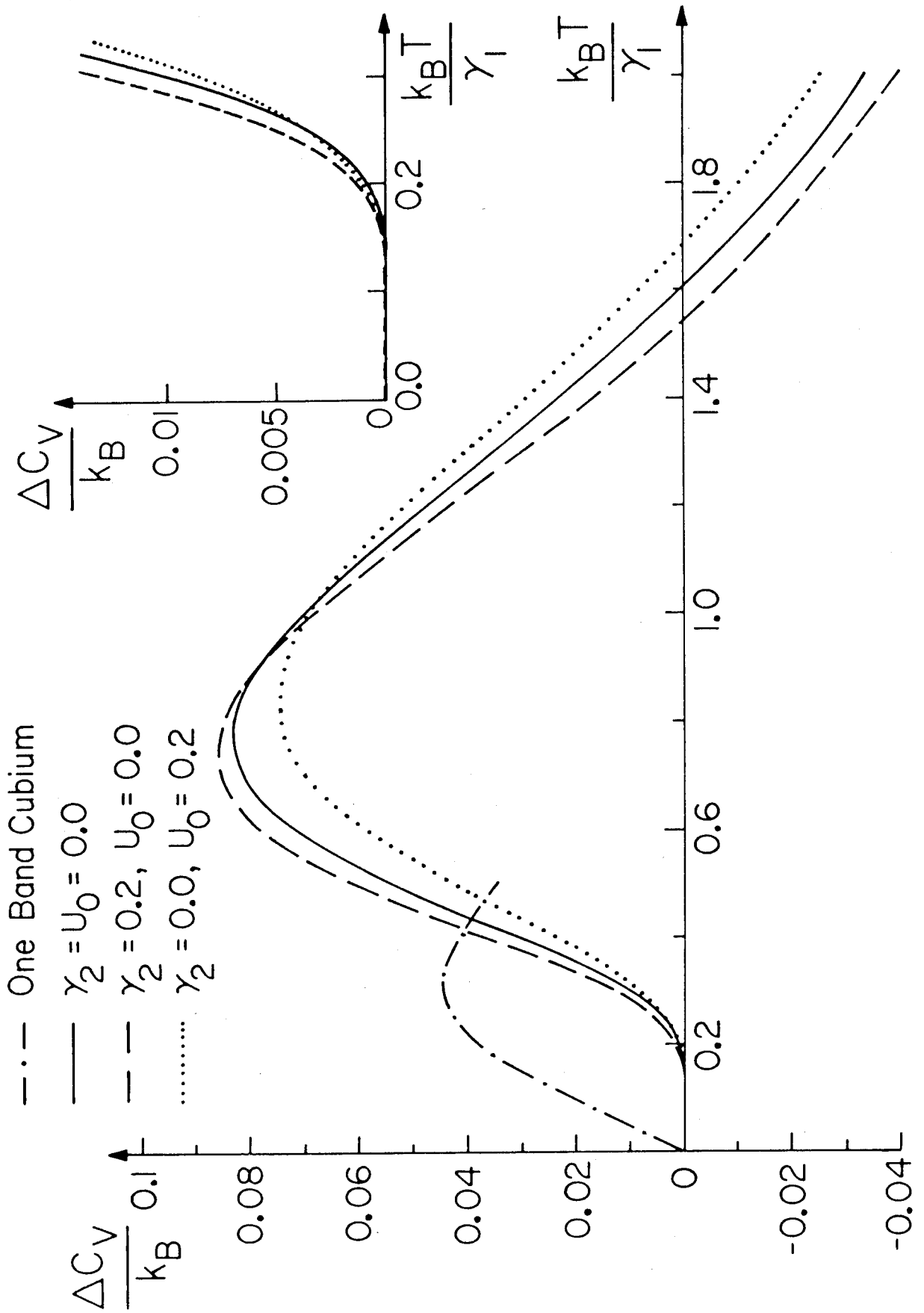


Figure 10

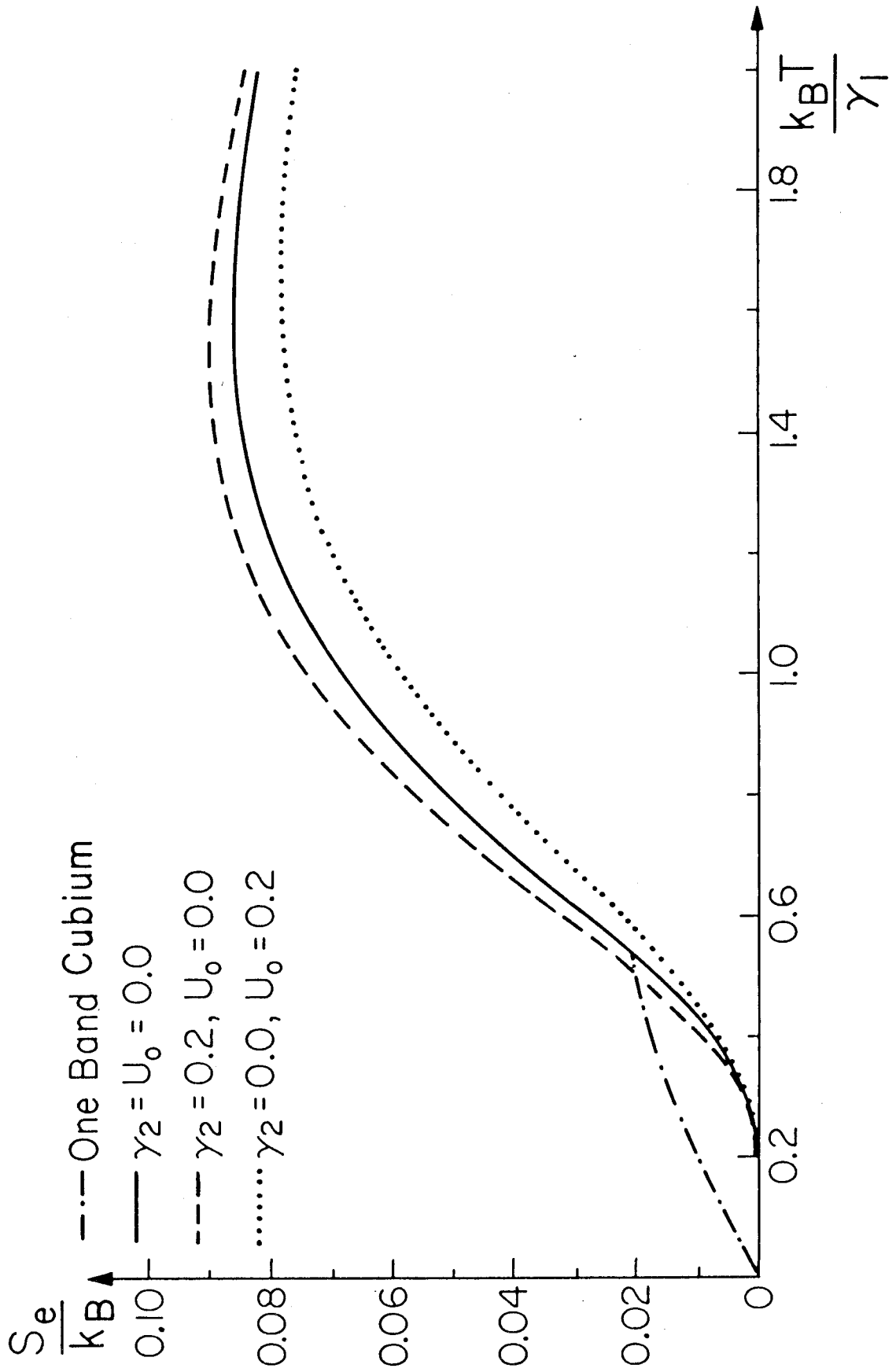


Figure 11

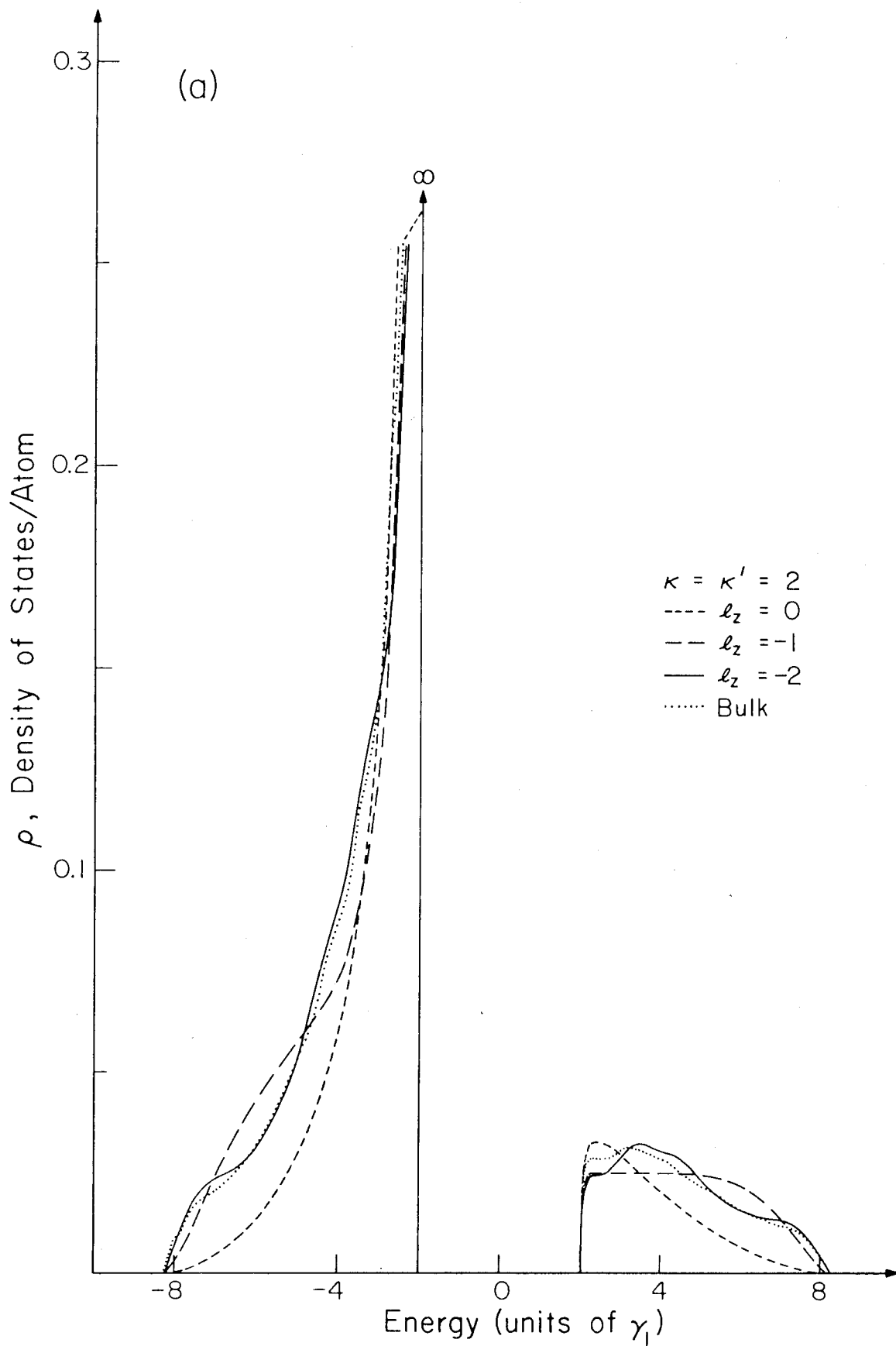


Figure 12(a)

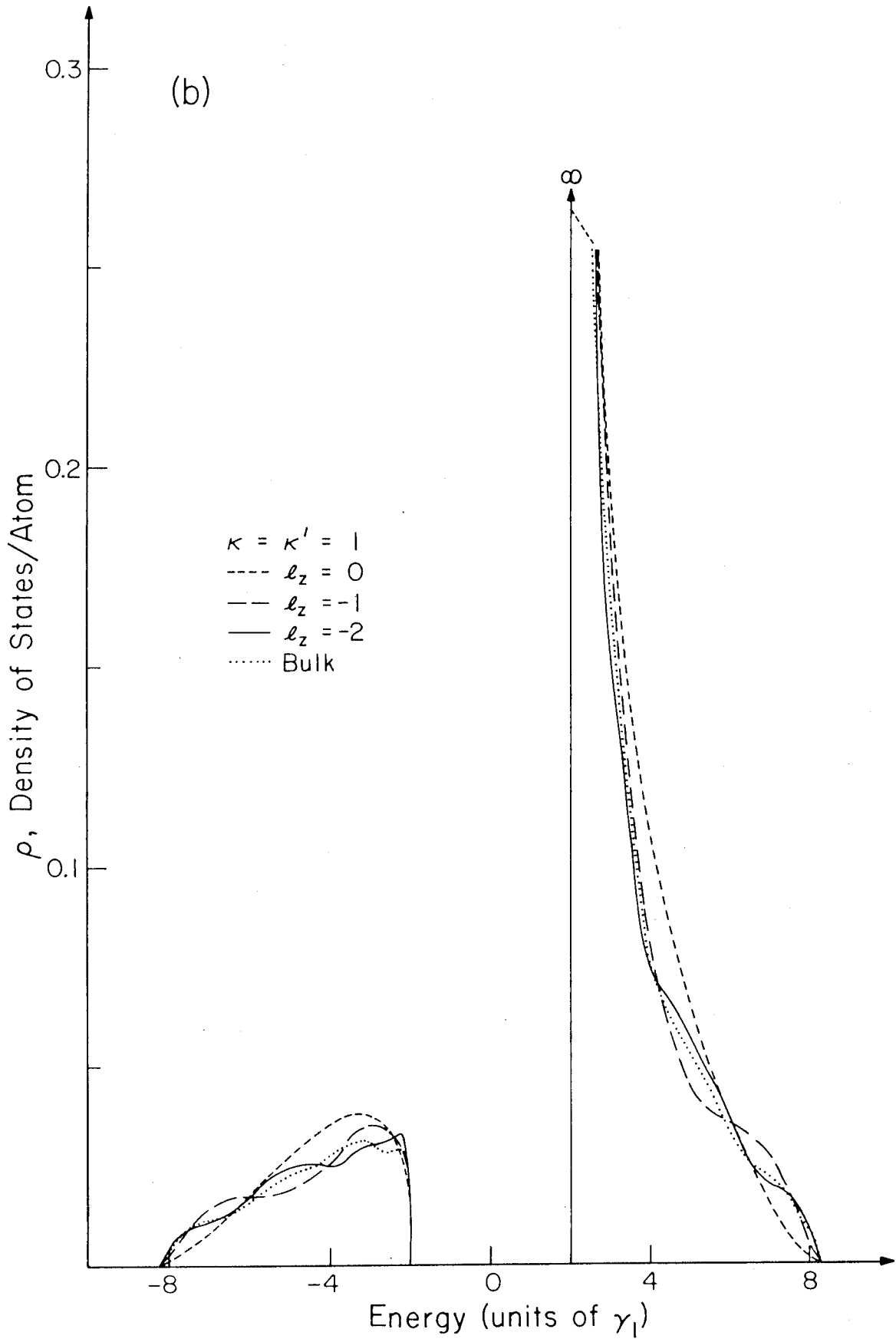


Figure 12(b)

CHAPTER III

ATOMIC REARRANGEMENT ON CLEAN CRYSTAL SURFACES

Section A: Lowering of the Electronic Energy Due to
Surface Reconstruction

[submitted as a Letter to the Editor to
Surface Science (1975)].

Section B: Effect of Surface Reconstruction on the
Electronic Energy of a Two-Band Crystal

[submitted to Phys. Rev. B (1975)].

ON THE LOWERING OF THE ELECTRONIC ENERGY IN SEMICONDUCTORS
DUE TO SURFACE RECONSTRUCTION*

W. Ho, S. L. Cunningham,[†] and W. H. Weinberg
Division of Chemistry and Chemical Engineering
California Institute of Technology
Pasadena, California 91125 USA

and

L. Dobrzynski
Laboratoire de Physique des Solides
Institute Supérieur d' Electronique du Nord
3, rue Francois Baës
59046 Lille Cedex
France

May, 1975

To be submitted as a Letter to the Editor to Surface Science.

* Work partially supported by NSF Grant GK-43433.

[†] IBM Post-doctoral Research Fellow.

When atoms spontaneously rearrange on the surface of a crystal due to any of a variety of possible mechanisms, then the total surface electronic energy (or the Gibbs energy) must be lower for the reconstructed surface than for the unreconstructed surface. This fact may make it possible in the future to predict, and thereby fully understand, the structures due to surface reconstruction on arbitrary crystal surfaces. At present, however, calculations are limited to model systems with the aim at understanding the general physical principles involved.

The first calculation of the change in the total electronic energy due to reconstruction was recently performed by Dobrzynski and Mills.¹ They considered a simple cubic monatomic crystal with one orbital (s-type) per atom (sometimes called s-band cubium). They used the Linear Combination of Atomic Orbitals (LCAO) formalism and assumed only nearest neighbor hopping integrals. This model gives a single cosine-like energy band. The unreconstructed surface unit cell and surface Brillouin zone (SBZ) for the (001) surface is a square.

Dobrzynski and Mills¹ then imposed a (2x1) reconstruction pattern on the (001) surface by arbitrarily displacing every other row of atoms in the surface in the y-direction (parallel to the surface). This had the several effects of (1) perturbing the overlap integrals in a regular manner between the atoms in the first plane, (2) making the surface unit cell twice as long in the y-direction, and (3) reducing the size of the SBZ in the k_y direction by a factor of two. This "folding" of the SBZ allows two states which formerly had the wave vector values of k_y and $-k_y + \text{sgn}(k_y)\pi/a$ (a is the unreconstructed unit cell dimension and $\text{sgn}(k_y)$ is the sign of k_y) to interact, thereby reducing the energy of the low energy state and increasing the

energy of the high energy state. The overall effect throughout the zone is for the lower energy states in the band to move down in energy, and for the higher energy states to move up.

At $T = 0^{\circ}\text{K}$, the Gibbs energy and the total electronic energy are equivalent. To calculate the total electronic energy, the energies of the occupied states are summed from the bottom of the band up to the Fermi level. Dobrzynski and Mills¹ showed, and it should be clear from the above discussion, that if the Fermi level is located anywhere in the band, there is a decrease in the total electronic energy for the reconstructed surface when compared to the unreconstructed surface. However, if the band is completely filled (or completely empty), Dobrzynski and Mills found that the total electronic energy is unchanged upon reconstruction.

Semiconductors and insulators are known to reconstruct. Therefore, it is of interest to consider what happens when the bulk crystal has more than one band and to see if reconstruction on semiconductors and insulators can be described in this same language.

In this paper, we report results on an investigation parallel to that of Dobrzynski and Mills wherein the crystal model has two bulk bands. We consider a simple cubic crystal with a two atom basis in the CsCl structure. In Fig. 1(a) we show the (001) unreconstructed surface in which the open circles represent basis atoms of type 1 in the surface plane, the filled circles represent basis atoms of type 2 in a plane located $a/2$ below the surface plane. The SBZ is a square, as shown in Fig. 1(b), with the boundaries at wave vector values of $\pm \pi/a$. We use the LCAO formalism, the tight binding approximation, and assume only nearest neighbor hopping integrals. The projection of the bulk energy bands onto the SBZ is shown

in Fig. 1(c) where we have varied k_y for a fixed value of k_x . The cross-hatch indicates that there is a continuum of energy states in that region. The explicit values of the energies of these bands depends upon the following: (1) the choice of orbital energies E_1 and E_2 for the two basis atoms; (2) the choice of the size of γ , the nearest neighbor hopping integral; and (3) the choice of k_x . However, the shape of the bands is independent of these choices. Note also that if the orbital energies $E_1 = E_2$, i.e., the two basis atoms become identical, then the model becomes a body-centered-cubic metal and the band gap goes to zero.

Upon this surface, we impose the atomic motions shown in Fig. 2(a) which represent a (2x1) reconstruction of the surface. Alternate rows of atoms of type 1 in the first plane are moved in the positive or negative y-direction. This has the effect of increasing some of the nearest neighbor hopping integrals by an amount ϵ , and decreasing others. The new unit cell is twice as long in the y-direction as in the unreconstructed surface, and therefore the new SBZ is half as large in the k_y direction, as shown in Fig. 2(b). In Fig. 2(c) we show a schematic of the "folding" of bands in the k_y direction. Where the cross-hatch is double, there are two continua of electronic states overlapping. These overlapping states interact in exactly the same fashion as for the one-band situation.¹

The method for finding the effect of reconstruction on the electronic density of states, and hence on the electronic energy is tedious and will only be outlined here. The formalism we follow is the same as that of Dobrzynski and Mills,¹ and the details will be presented elsewhere.² The steps are as follows: (1) Determine the Green's functions for the bulk crystal as a function of energy, E , and k_x and k_y . (2) Perturb the system

by cutting bonds across a plane to create a surface. (3) From a Dyson equation formalism, use the bulk Green's functions and the perturbation to determine a new Green's functions appropriate for a crystal with a surface. To perform these first three steps, there is considerable advantage in having analytic expressions for the Green's functions. The model we have chosen has this important advantage. These first three steps have been fully discussed elsewhere³ (including the analytic expressions for the surface Green's functions) in a study of the properties of the clean surface of this model.

(4) Determine the perturbation which creates the reconstructed surface. This is shown in Fig. 2(a). (5) Manipulate the surface Green's functions from step (3) into a form appropriate for the enlarged unit cell and the reduced Brillouin zone. (6) Use the reconstruction perturbation and these new Green's functions to calculate the partial phase shift functional. This quantity is given by $-\arg \det (I - VG)$ (I is the unit matrix, V is the perturbation matrix, and G is the Green's function matrix) as is fully described in refs. (1) and (3) and references therein. (7) The total phase shift functional is a sum of the partial phase shifts over the two-dimensional Brillouin zone⁴ appropriate for the reconstructed surface. (8) Finally, from the total phase shift we determine the change in the density of electronic states due to the surface reconstruction perturbation and hence, by a simple integration, the change in the electronic energy. This above procedure is well established¹⁻³ as a general prescription for analyzing the effects of perturbations on systems with a large number of particles.

It is possible, as in the work of Dobrzynski and Mills,¹ that the perturbation which gives rise to the reconstruction can also create new

surface states. In our model and for this (2x1) structure, there are no new surface states created. However, we have found new surface states when the surface is reconstructed into a c(2x2) structure as is fully discussed elsewhere.²

In Fig. 3, we present the results of this work. Here we show the decrease in the total electronic energy, ΔU , as a function the size of the perturbation, ϵ , where both are expressed in units of the hopping integral γ . We show three cases, ranging from a large band gap (curve a) to a zero band gap or bcc metal (curve c). (Band gaps, E_g , are expressed in units of γ .) The Fermi level is assumed to be in the middle of the band gap. (For the case where the band gap is zero, the Fermi level is put exactly at the middle of the band.) Based on this graph, we may make the following three conclusions:

(1) The decreases in the total energy for the case of a metal with a half-filled band (curve c) and for a large gap semiconductor (curve a) are of the same order of magnitude. This result proves, as was impossible with the Dobrzynski and Mills¹ model, that when a band becomes nearly full, the presence or absence of other empty bands nearby fundamentally affects the behavior of the system upon reconstruction. Contrary to the previous result,¹ we have shown that the phenomenology presented here is capable of explaining reconstruction on semiconductor surfaces.

(2) The decrease in the electronic energy is a quadratic function of the perturbation for small values of ϵ . This was previously shown to be true for metals,¹ and we have shown that it is also true for semiconductors and insulators. This is a general result for small perturbations.

(3) The decrease in the electronic energy is inversely related to the band gap. As the band gap gets larger, all other model parameters being

held constant, the magnitude of the decrease in the electronic energy gets smaller (compare curves a, b, and c). This implies that metals and narrow gap semiconductors will have a greater tendency to reconstruct than will large gap insulators. The tendency for the metals and narrow gap semiconductors is nearly the same (as seen by the closeness of curves b and c).

Other structures due to reconstruction of this surface give similar, but not identical, results. A complete discussion of this behavior will be presented elsewhere.²

ACKNOWLEDGMENT

We acknowledge, with gratitude, the support of this research by the National Science Foundation (Grant No. GK-43433) and the IBM Corporation via a post-doctoral fellowship (SLC).

References

1. L. Dobrzynski and D. L. Mills, Phys. Rev. B7, 2367 (1973).
2. W. Ho, S. L. Cunningham, W. H. Weinberg, and L. Dobrzynski, to be published.
3. W. Ho, S. L. Cunningham, W. H. Weinberg, and L. Dobrzynski, to appear, Phys. Rev. B12 (1975).
4. S. L. Cunningham, Phys. Rev. B10, 4988 (1974).

Figure Captions

Figure 1(a) Atomic geometry of the unreconstructed (001) surface of a crystal with the CsCl structure. Open circles are surface atoms of type 1; filled circles are second plane atoms of type 2.

(b) Square surface Brillouin zone (SBZ).

(c) Schematic of the projection of the bulk energy bands onto the SBZ as a function of k_y for a fixed value of k_x . The cross-hatch in each band represents a continuum of states.

Figure 2(a) Imposed displacement pattern for the (2x1) reconstructed surface.

(b) Reduced surface Brillouin zone appropriate for the reconstructed surface.

(c) Schematic of the folded energy bands.

The double cross-hatched area in each band is where two continua of states exist and interact.

Figure 3 Decrease in the total electronic energy as a function of the perturbation parameter ϵ for three different values of the band gap. All quantities are in units of γ .

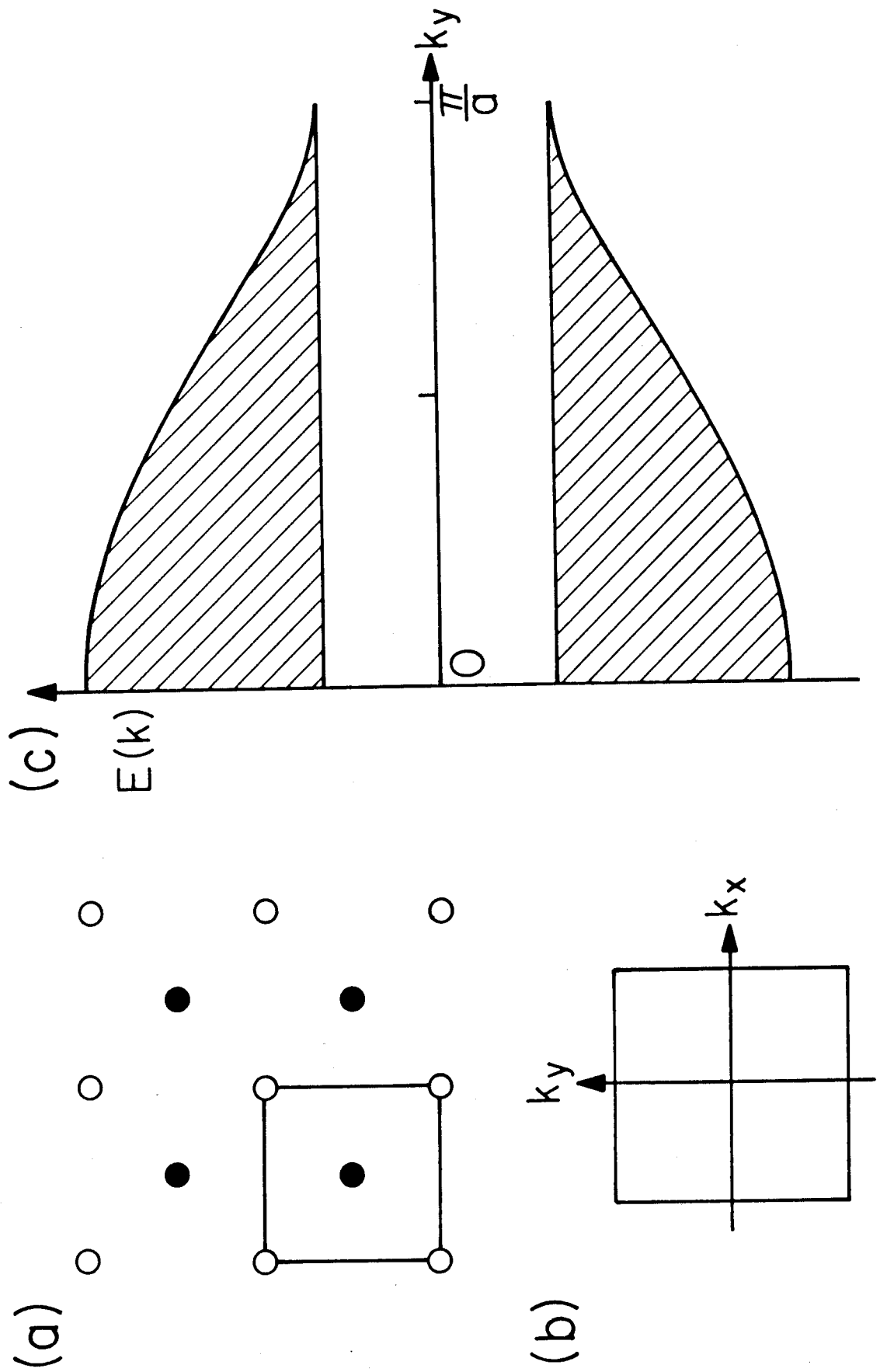


Figure 1

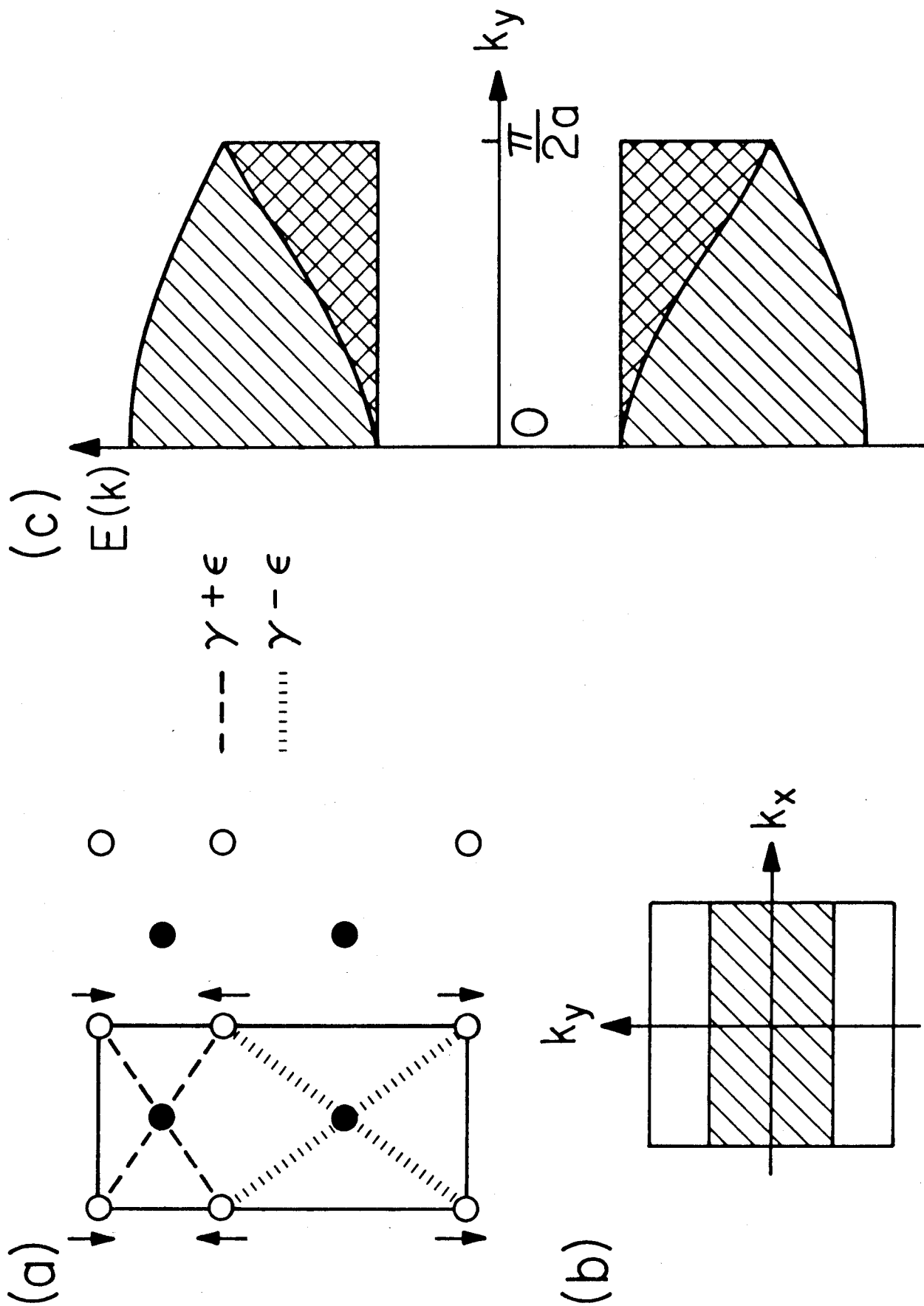


Figure 2

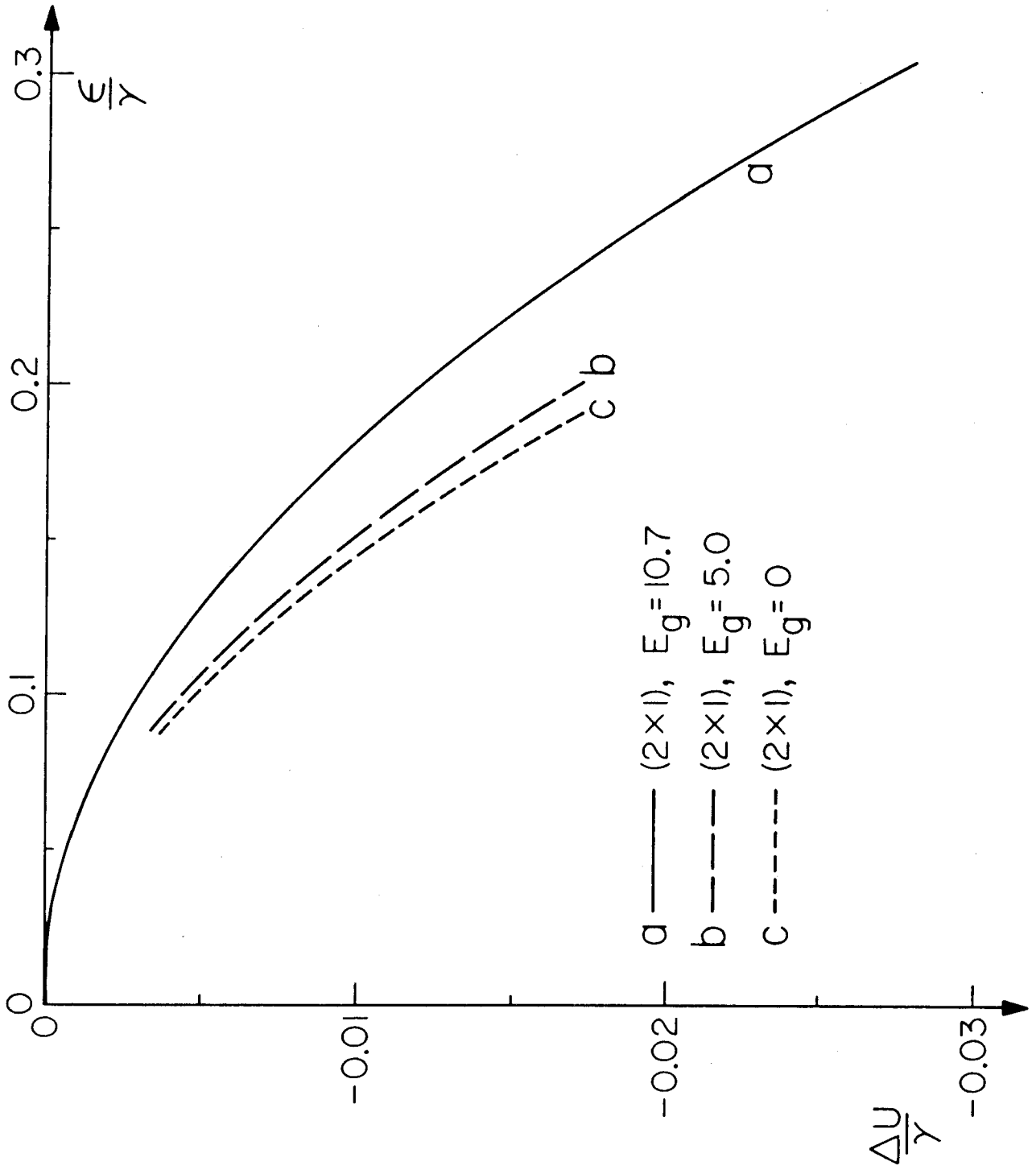


Figure 3

Effect of Surface Reconstruction on the Electronic Energy
of a Two-Band Crystal*

W. Ho, S. L. Cunningham[†] and W. H. Weinberg
Division of Chemistry and Chemical Engineering
California Institute of Technology
Pasadena, California 91125

and

L. Dobrzynski
Laboratoire de Physique des Solides
Institut Supérieur d'Electronique du Nord
3, rue François Baès
59046 Lille Cedex
France

May, 1975

To be Submitted to Physical Review B

* Work partially supported by NSF Grant GK-43433

† IRM Postdoctoral Research Fellow

ABSTRACT

We present the change in the total electronic energy which occurs when the surface atoms of a crystal reconstruct in a periodic manner. We study the (001) face of a model two-band crystal with the CsCl structure. The energy changes due to uniform relaxation of the surface, as well as a (2x1) and a c(2x2) reconstruction, are considered. The results are obtained by a Green's function perturbation technique where a resolvent is used to determine the presence of surface states, and a phase shift function is calculated to determine the change in the density of states. The Green's functions appropriate for the reconstructed surfaces are analytic. We find that relaxation inward lowers the electronic free energy, and, in addition, we show that reconstruction always lowers the electronic free energy. The method is quite general and can be used to study arbitrary reconstructed structures.

I. Introduction

Currently there exist several different theories¹⁻⁶ which attempt to explain the origin of the fractional order beams⁷ obtained by low-energy electron diffraction (LEED) experiments from solid surfaces. The appearance of these fractional order beams is due to a different arrangement of the atoms near the surface than in the ideal bulk crystal. These theories can be divided into four categories in which it is suggested that reconstruction is due to the following: (1) missing atoms, (2) hybridized surface orbitals, (3) vibrational instabilities, and/or (4) a lowering of the total electronic energy. In this paper, we will consider the fourth category. First, however, we will briefly discuss each of the other three approaches.

A model first used by Lander and Morrison¹ to explain the various equilibrium positions of the surface atoms is based on the presence of vacancies periodically arranged on the surface. By choosing carefully the different sites where the vacancies occur, different structures are obtained due to surface reconstruction on the (100) and (111) crystallographic orientations of Ge and Si. More recently, Phillips¹ has extended this idea and obtained the fraction of vacancies for the (100), (110), and (111) faces of Ge and Si. He asserts that the presence of vacancies reduces the strain energy caused by the dangling bonds. The fraction of vacancies is correlated to the degree of covalency by examining the covalent contribution to the Gibbs energy. Thus, the covalent forces are taken to be responsible for rearranging and removing atoms from the surface. What remains to be shown in this theory is the reason why the vacancies arrange themselves in certain structures and not others, and whether the theory

is applicable to metal surfaces.

A second type of model proposed by Haneman and co-workers² deals with hybridization of the surface dangling bond. In their model, the reconstruction is achieved through a "rumpling" of the surface atoms. By increasing the s-character in the dangling bonds of the raised atoms and the p-character in the lowered surface atoms, they have been able to use chemical bonding ideas to explain the (2x1) structure. This scheme indicates that the fractional order diffraction beams can be explained by relatively small changes in the positions of the atoms near the surface. What remains to be shown in this theory is how the ideas are applicable to other semiconductor surfaces, whether the theory can distinguish between different reconstructed surface structures, and whether the ideas are applicable to metal surfaces.

A third possible mechanism for surface reconstruction is that the surface may be unstable to a surface vibration.³ In some cases this instability may be due merely to the lower coordination number for the atoms at the surface.⁴ On the other hand, the interatomic force constants are quite likely different near the surface compared to those in the bulk. This difference may be due to either the fact that the normal bulk force constants are altered near the surface or to the fact that additional forces may be present at the surface which are symmetry forbidden in the bulk.³ Alternatively, it has been suggested⁵ that the instability could be due to the coupling of the surface phonon to a charge density wave. Several variations of this same basic idea have appeared using the labels Peirel's transition, giant Kohn anomaly, or Jahn-Teller distortion.⁵ This approach has the two advantages that it is applicable in some form to all surfaces

and that the reconstructed surface structure does not need to be known in advance. However, what remains to be shown is how the surface force constants quantitatively change near the surface by whatever mechanism and whether reasonable changes in the force constants on real systems lead to the observed structures (this has been done only for the Si(111) surface^{3,5}).

The fourth type of approach to the question of surface reconstruction is to determine the lowering of the electronic energy which might occur due to the reconstruction. Since this is the approach used in this paper, we will discuss this idea fully below.

Recently, Ibach and Rowe⁸ have been able to infer indirectly the structure of the reconstructed clean surfaces of Si(100) and (111) by studying the adsorption of hydrogen on these surfaces with Energy Loss Spectroscopy (ELS), Ultraviolet Photoemission Spectroscopy (UPS) and LEED. Upon hydrogen adsorption, the LEED patterns do not change for the (7x7) structure on the clean (111) surface and the (2x1) structure on the (100) clean surface. However, in the case of the (2x1) structure on the cleaved (111) surface, the LEED pattern returns to that of the unreconstructed surface. For the models which don't assume missing atoms, the fractional order spots would disappear upon adsorption. With the missing atom model, one might expect the LEED pattern to remain the same before and after adsorption. From these considerations, Ibach and Rowe suggested that different mechanisms are responsible for the different reconstructed structures on the various surfaces. Therefore, at present it appears that each of the above theories should be pursued, for it is not yet clear which approach will ultimately prove to be most useful.

It is clear that if atoms rearrange on surfaces, it is because the

reconstructed surface has a lower Gibbs energy. This is true no matter which of the first three approaches is used. Recently, ideas concerning the lowering of the Gibbs energy (also called the total electronic energy) have begun to be put on a quantitative basis, in particular by the work of Dobrzynski and Mills.⁶ They have studied the (001) surface of a model one-band simple cubic crystal, simulating the properties of transition metals. The particular surface rearrangement they considered resulted in a (2x1) structure. They found that the greatest decrease in the total electronic energy occurred when the single band was half-filled and that the decrease diminished to zero as the band became either empty or completely filled.

In this paper, we use the same scheme as Dobrzynski and Mills to calculate the decrease in the electronic energy of a two-band crystal upon reconstruction of the surface. It was found in our previous study⁹ of this two-band crystal that the presence of an empty second (conduction) band greatly changes the surface electronic and thermodynamic properties compared to the results one obtains with a filled one-band calculation. Therefore, the present study was undertaken to see whether, contrary to the results of Dobrzynski and Mills, there is a decrease in the electronic energy upon reconstruction when the crystal has one filled band and a second empty band, i.e., the model studied is to be applicable to insulator or semiconductor crystals.

The physical basis of our theory can be briefly stated as follows. When the surface unit cell becomes larger upon reconstruction, there are two immediate consequences. The surface Brillion zone (SBZ) becomes smaller in size, and the energy bands fold over. In the region where the bands overlap, the states are degenerate. The perturbation which causes the

folding of the energy bands removes the degeneracies and changes the density of states of the unperturbed (1x1) surface. The net result of this change is to push states away from the energy band gap region toward the bottom (top) of the valence (conduction) band. For a filled valence band, this leads to a net lowering of the total electronic energy.

In a previous paper,⁹ we studied the ideal unreconstructed (001) surface of a crystal having the CsCl structure. We used the LCAO formalism, assumed the Tight Binding approximation, and derived analytic expressions for both the bulk and the surface Green's functions. In this paper, we use the previously derived surface Green's functions as the wavefunction describing the unreconstructed surface. The change in the density of states due to the reconstruction is determined conveniently by the phase shift technique. The change in the electronic energy is then obtained by a simple integration. In the few cases where they occur, we find the surface states by the resolvent technique.

Two different reconstructed structures are considered here. The surface atoms are arbitrarily rearranged in two different ways forming the (2x1) and the c(2x2) structures. In the (2x1) case, we have studied separately motions parallel and perpendicular to the surface. In addition, we have studied the change in the electronic energy as a function of the band gap. In all cases considered, we have found a decrease in the total electronic energy for a filled band. Depending upon the relative strength of this energy compared to the unfavorable strain energy created by moving the surface atoms out of their bulk equilibrium positions, reconstruction can occur.

In Section II, we present the general Green's function formalism for

an arbitrary structure of a reconstructed surface, and this is then used to obtain the change in the electronic energy due to the reconstruction. We also present the geometry of the different cases considered, which includes in addition to the (2x1) and c(2x2) structures, a uniform surface relaxation as well. In Section III, we present and discuss the results. These include the phase shift functions, the changes in the density of states, and the change in the electronic energy for each of the cases considered. In addition, a simple lattice dynamical calculation is carried out to get an estimate of the elastic strain energy associated with the reconstruction deformation. Comparing these results, we obtain the conditions necessary to obtain a decrease in the total energy of the system. We summarize our results in Section IV.

II. Formalism

The surface we study in this paper is the (001) surface of a crystal with the CsCl structure. The (001) surface consists of atoms of the same type. Although second neighbor interaction was taken into account in our previous paper,⁹ for simplicity we will include only the first neighbor interaction here. Due to this limitation, there are no surface states on the unreconstructed surface. In Fig. 1,¹⁰ we present the geometries for the reconstructed surface structures considered. In Fig. 1(a) we show a (2x1) structure with the rows of atoms in the first plane displaced alternately in opposite [010] directions. The hopping integral decreases (increases) in magnitude as the distance between the atoms in the first and second planes increases (decreases). The effect of the reconstruction is described by ϵ , which is the change in the nearest neighbor hopping integral γ . The unit cell has become twice as long in the y-direction and the number of basis atoms in the first two planes has increased from two to four. In Fig. 1(b), the (2x1) structure is obtained with atoms in the first plane displaced alternately in opposite directions perpendicular to the surface. The reconstructed unit cell and the basis atoms are the same as in Fig. 1(a). In Fig. 1(c), the atoms are displaced in yet a third manner in order to produce the c(2x2) structure. The unit cell has again become twice as large, but in this case it is square and rotated by 45° . The number of basis atoms is again four.

The sizes and shapes of the SBZ change as the unit cells become larger and assume different shapes. In Fig. 2(a) the SBZ is seen to decrease to half its former dimension in the y-direction for the (2x1) structure. In Fig. 2(b) the SBZ for the c(2x2) structure is rotated by 45° and is again

half the original size. These changes in the SBZ's affect the band structure and thus the density of states because the energy bands fold along the new SBZ boundaries.

In the following, we will derive a general scheme upon which the calculations for the various reconstructed structures are based. We will not repeat the arguments given in our previous paper⁹ since the models are the same in both places.

Since the translational symmetry in the directions parallel to the surface are still present in both the unreconstructed and the reconstructed semi-infinite crystals, the problem is simplified by expressing the surface Green's functions in a mixed Bloch-Wannier representation. Expanding the surface Green's functions for the (1x1) surface in terms of the two-dimensional wave vector parallel to the surface,

$$G(\ell\beta, \ell'\beta', E) = \frac{1}{N_s} \sum_{\vec{k}_s} \hat{G}(\ell_z\beta, \ell'_z\beta', \vec{k}_s, E) e^{i\vec{k}_s \cdot \vec{x}(\ell\ell')}, \quad (1)$$

where N_s is the number of unit cells on the (1x1) surface, β and β' take on the values 1 or 2 (the labels for the two basis atoms), $(\ell\beta)$ denotes the β th type basis atom in the ℓ th unit cell, the notation

$$\vec{x}(\ell\ell') = \vec{x}(\ell) - \vec{x}(\ell') \quad (2)$$

is the vector difference of the positions of the ℓ th and ℓ' th unit cells, ℓ_z labels the unit cell in the direction perpendicular to the surface, and the letter s above the summation sign indicates that the sum is over the wave vectors in the "standard" (1x1) SBZ. For the reconstructed surface, a similar expansion is obtained,

$$G(LA, L'A', E) = \frac{1}{N_N} \sum_{\vec{k}_s} \hat{G}(L_zA, L'_zA', \vec{k}_s, E) e^{i\vec{k}_s \cdot \vec{x}(LL')}, \quad (3)$$

where $N_N (= \frac{1}{2} N_S$ for our cases) is the number of unit cells in the reconstructed surface, A and A' index the new basis atoms (A and A' take on the values 1, 2, 3 or 4 in the case of (2x1) and c(2x2) reconstruction), (LA) denotes the Ath basis atom in the Lth unit cell, and the letter N above the summation sign indicates that the sum is over the wave vectors in the "new" reconstructed SBZ. Notice the caret over the Green's function.

If we refer to the same pair of atoms in both the (1x1) and the reconstructed cases, i.e., if we set

$$(\ell\beta, \ell'\beta') = (LA, L'A') \quad (4)$$

we have

$$G(\ell\beta, \ell'\beta', E) = G(LA, L'A', E) \quad (5)$$

We can then equate the right hand side of Eqs. (1) and (3) and obtain

$\hat{G}(L_z A, L'_z A', \vec{k}_s, E)$ as a linear combination of $G(\ell_z \beta, \ell'_z \beta', \vec{k}_s, E)$ where \vec{k}_s will now only refer to the reconstructed SBZ. Effectively $\hat{G}(L_z A, L'_z A', \vec{k}_s, E)$ is the wavefunction describing the reconstructed layers. Since the perturbation is confined to the surface layer, L_z and L'_z take on the value of the surface layer (note that the two planes of atoms of type 1 and 2 make up one layer). The details of this calculation are illustrated for both the (2x1) and the c(2x2) reconstruction in the next section.

The effects of surface reconstruction can be studied by the phase shift technique which is basically a perturbation method. Of major interest is the change in the density of states due to the perturbation. This scheme is quite general and has been applied to a wide variety of problems.¹¹ In our previous paper,⁹ the method is applied to study the effects of creating a clean surface. The method can equally well be applied to the study of

chemisorption.¹²

Due to the translational symmetry, the perturbation matrix can also be expressed in the mixed Bloch-Wannier representation. In our present case, the perturbation matrix is given by

$$\hat{V}(L_z A, L_z' A', \vec{k}_s) = \sum_{L_x, L_y} V(LA, L'A') e^{-i\vec{k}_s \cdot \vec{x}(LL')} , \quad (6)$$

where the sum is over the unit cells in the reconstructed surface and where $V(LA, L'A')$ is the change in the interaction between atoms (LA) and (L'A').

We then obtain the Fredholm determinant,

$$D(\vec{k}_s, E) = \det(I - \hat{V}\hat{G}) . \quad (7)$$

The surface states which arise from surface reconstruction are located at energies E outside the energy bands such that

$$D(\vec{k}_s, E) = 0 . \quad (8)$$

Within the bands, the partial phase shift function is given by ("partial" implies that the function is found for only a single value of \vec{k}_s)

$$\eta(\vec{k}_s, E) = - \arg D(\vec{k}_s, E) , \quad (9)$$

and the total phase shift per surface unit cell is obtained by summing over the reconstructed SBZ,

$$\eta(E) = \frac{1}{N} \sum_{\vec{k}_s} \eta(\vec{k}_s, E) . \quad (10)$$

The change in the density of states is obtained directly from

$$\Delta n(E) = \frac{1}{\pi} \frac{d\eta(E)}{dE} . \quad (11)$$

With a simple integration we then obtain the change in the Gibbs energy at absolute zero temperature (ground state energy),⁶

$$U = - \frac{1}{\pi} \int^{E_F} dE \eta(E) \quad , \quad (12)$$

where E_F is the Fermi energy. Dobrzynski and Mills⁶ have investigated the temperature dependence of the Gibbs energy. From their analysis, the first order correction is zero in our case since the Fermi level lies in the middle of the band gap and Δn vanishes there. Thus, the change in the Gibbs energy at absolute zero is a good approximation for all temperatures. In the next section, we apply the formalism presented here to two different reconstructed surface structures.

III. Results and Discussion

The band structure for the bulk crystal referenced to the unreconstructed SBZ, within the tight-binding approximation and assuming only first neighbor interactions, is given by⁹

$$E_{\vec{k}j} = \pm \frac{1}{2} \left(E_g^2 + 256\gamma^2 \cos^2 \frac{\phi_x}{2} \cos^2 \frac{\phi_y}{2} \cos^2 \frac{\phi_z}{2} \right)^{1/2}, \quad (13)$$

where

$$\vec{\phi} = a_0 \vec{k}, \quad (14)$$

a_0 is the crystal lattice constant indicated in Fig. 1(a), and E_g is the band gap which for this structure is equal to the magnitude of the difference in orbital energies, E_1 and E_2 , between the two types of atoms. There are two branches and j takes on the values 1 and 2. The zero of the energy is arbitrarily chosen to be the average of E_1 and E_2 .

For purposes of illustration, the parameters γ and E_g are fitted to the photoemission data for CsI obtained by DiStefano and Spicer.¹³ They found the width of the valence band to be 2.5 ± 0.3 eV and the band gap at 300°K to be 6.2 eV. Using these values, we find

$$\gamma = 0.58 \text{ eV}, \quad (15)$$

and

$$\frac{E_g}{\gamma} = 10.7. \quad (16)$$

The Green's functions for crystals with the (001) unreconstructed surface obtained in our previous paper⁹ are given as the difference of two bulk Green's functions. They take on a rather simple form for the surface layer, $\ell_z = \ell'_z = 1$; namely,

$$G(11,11,\vec{\phi}_s) = \frac{dt}{f^2(t+1)}, \quad (17)$$

$$G(12,12,\vec{\phi}_S) = \frac{at}{f^2} , \quad (18)$$

$$G(11,12,\vec{\phi}_S) = \frac{t}{f} e^{-i\frac{1}{2}(\phi_x + \phi_y)} , \quad (19)$$

$$G(12,11,\vec{\phi}_S) = \frac{t}{f} e^{i\frac{1}{2}(\phi_x + \phi_y)} , \quad (20)$$

where

$$a = E - E_1 , \quad (21)$$

$$d = E - E_2 , \quad (22)$$

$$f = 4\gamma \cos \frac{\phi_x}{2} \cos \frac{\phi_y}{2} , \quad (23)$$

$$\xi = (ad - 2f^2)/2f^2 , \quad (24)$$

$$t = \begin{cases} \xi - (\xi^2 - 1)^{1/2} & \xi > 1 \\ \xi + i(1 - \xi^2)^{1/2} & |\xi| < 1 \\ \xi + (\xi^2 - 1)^{1/2} & \xi < -1 \end{cases} , \quad (25)$$

A. Static Relaxation Without Reconstruction

For uniform relaxation, the surface unit cell is (1x1), and the perturbation matrix is a simple (2x2) matrix given by

$$V(\ell_Z\beta, \ell'_Z\beta', \vec{\phi}_S) = \begin{pmatrix} 0 & g^* \\ g & 0 \end{pmatrix} , \quad (26)$$

where the rows (and columns) of the matrix are labeled by the sites $(\ell_Z\beta) = (11)$ and (12) , and where

$$g = 4\Delta \cos \frac{\phi_x}{2} \cos \frac{\phi_y}{2} e^{i\frac{1}{2}(\phi_x + \phi_y)} . \quad (27)$$

In Eq. (27), Δ , expressed in units of γ , is the change in γ as the surface plane of atoms of type 1 is displaced in the direction perpendicular to the surface. The Green's function matrix is reduced to a (2x2), and its elements are given in Eqs. (17) - (20). The Fredholm determinant in Eq. (7) is obtained analytically and is given by

$$D(\vec{k}_s, E) = (1 - \Delta t)^2 - \frac{ad\Delta^2 t^2}{f^2(t + 1)} \quad (28)$$

From the argument of this determinant, the total phase shift is obtained numerically by summing the partial phase shift over the SBZ (by sampling values at a set of special points as described in ref. 14). The result obtained is shown in Fig. 3. In Fig. 4, we show the change in the density of states calculated from Eq. (11). The singularities at $E = \pm 5.35$ are due to the flat nature of the bands.¹⁵ We see that states are pushed away from the band gap region and toward the bottom (top) of the valence (conduction) band. *Thus, for a filled valence band and positive values of Δ , the electronic energy of the system is necessarily decreased.* The actual decrease is calculated from Eq. (12). In Table I, we summarize the results for two values of Δ . Positive values of Δ , i.e., an increase in γ , are chosen for the following reason. In the gas phase, the bond distance in CsI is 3.32 \AA ¹⁶, and increases to 3.96 \AA ¹⁷ in the crystal. One might expect the nearest neighbor distance on the surface to approach the value in the gas phase since one end of the surface layer is free. Therefore, the surface atoms seek a new minimum in potential energy at a shorter nearest neighbor distance. We assume that the whole surface layer relaxes inward, and this relaxation increases γ . From the results for two different values of Δ , an approximate linear relation is obtained between Δ and ΔU . There is an appreciable decrease in the

electronic energy due to the contraction of the first layer.

Relaxation on a one-band metal was treated by Allan and Lannoo¹⁸ within the tight-binding approximation. Our approach here is very similar to theirs. In addition, they included a Born-Mayer type of repulsive energy between nearest neighbor atoms. They found that the surface layers relax inward with a maximum decrease in the separation between the first and second planes of atoms occurring for a half-filled band. For empty or filled bands, no relaxation was found. Thus, the results we present here show the importance of the second empty band in the study of semiconductor and insulator surfaces.

Benson and co-workers¹⁹ have investigated extensively surface relaxation and surface energies of the neutral (100) and ionic (110) faces of alkali halides with the NaCl structure and the neutral (110) face for those with the CsCl structure. In general, the atoms in the surface layer relax inward with different amounts of displacement for the anions and cations on the neutral surfaces. For the ionic (110) face of the alkali halides with the NaCl structure, the decrease in surface energy due to relaxation is two to three times greater than the corresponding decrease for the neutral (100) face. The values we obtain for ΔU have the same order of magnitude as the values they have for the (110) face of the cesium halides.¹⁹ In our calculation, we include neither the polarization of the ions nor the van der Waals interactions. The inclusion of these effects would decrease further the surface energies.¹⁹ Thus, our results are the lower limits to the "actual" values.

Laramore and Switendick²⁰ studied the relaxation of the neutral (100) surface of LiF by analyzing LEED intensity profiles. They found the best

fit to the experimental data occurred when the lithium ions relax inward by 0.35 \AA and the fluorine ions by 0.1 \AA .

Contraction of the surface layer of atoms is also found for semiconductors. Appelbaum and Hamann²¹ have studied the effects of relaxation on the electronic energy states of the Si(111) surface by numerically integrating the Schrödinger equation. By assuming that the surface atoms contract by 0.33 \AA , new surface states appear which can be associated with the S_2 and S_3 states observed experimentally by Rowe and Ibach.²²

For metal surfaces, Alldredge and Kleinman²³ also found a large inward contraction for the Li(001) surface. Their calculation, which is a fully self-consistent treatment of the electrons, is probably the best first principles calculation performed to date.

However, not all the surface layers of crystals contract. The surfaces of fcc crystals tend to expand. Benson and Claxton²⁴ studied the (110), (100) and (111) faces of rare-gas crystals and found an outward expansion of 3.6, 2.6 and 1.2% of the bulk interlayer spacings, respectively. The (100), (110) and (111) faces of fcc metals (including transition metals) were studied by Burton and Jura.²⁵ The interlayer spacings were found to increase in all cases, and the distortions decreased away from the surface region. The close-packness of the fcc structure tends to discourage any closer approach of the atoms compared to their bulk separations. We do not believe that our simple model is capable of explaining outward relaxations.

B. (2x1) Reconstruction, z-Displacement

The assumed displacement geometry for this problem is shown in Fig. 1(b), and the corresponding SBZ is shown in Fig. 2(a). To proceed, we must first derive the unperturbed surface Green's functions appropriate for the (2x1) reconstruction. There are two possible approaches. The first method is

to equate the coefficients in the Fourier transforms in Eqs. (1) and (3) after converting the sum in Eq. (1) to a sum over the reconstructed SBZ. This method was mentioned previously in Sec. II. The second approach is to find the transformation matrix between the basis functions for the reconstructed and the unreconstructed surfaces. Then a similarity transformation can be performed on the Green's function matrix. The two methods give the same results, but we will present only the first due to its relative simplicity.

There are four basis atoms in the (2x1) reconstructed surface. Thus, the bulk band structure referenced to the new SBZ consists of four branches and is given by⁹

$$E_{\vec{k}j} = \pm \frac{1}{2} \left[E_g^2 + 256\gamma^2 \cos^2 \frac{\phi_x}{2} \cos^2 \frac{\phi_y}{2} \cos^2 \frac{\phi_z}{2} \right]^{1/2}, \quad (29)$$

where we have chosen the plus (minus) sign for $j = 1(2)$, and

$$E_{\vec{k}j} = \pm \frac{1}{2} \left[E_g^2 + 256\gamma^2 \cos^2 \frac{\phi_x}{2} \sin^2 \frac{\phi_y}{2} \cos^2 \frac{\phi_z}{2} \right]^{1/2}, \quad (30)$$

for $j = 3(+)$ and $4(-)$. These equations result naturally from simply folding the bulk bands appropriate to the unreconstructed surface in Eq. (13).

To derive the surface Green's functions, we observe that the sum in Eq. (1) can be converted to a sum over the (2x1) SBZ as follows

$$G(\ell\beta, \ell'\beta', E) = \frac{1}{N_s} \sum_{\vec{\phi}_s} \left\{ G(\ell_z\beta, \ell'_z\beta', \vec{\phi}_s, E) e^{i \frac{\vec{\phi}_s}{a_0} \cdot \vec{x}(\ell\ell')} + G\left(\ell_z\beta, \ell'_z\beta', \vec{\phi}_s - \text{sgn}(\phi_y)\pi\vec{e}_y, E\right) e^{i \frac{[\vec{\phi}_s - \text{sgn}(\phi_y)\pi\vec{e}_y]}{a_0} \cdot \vec{x}(\ell\ell')} \right\}, \quad (31)$$

where $\text{sgn}(\phi_y)$ denotes the sign of the y-component of $\vec{\phi}$, and \vec{e}_y is the unit vector in the y-direction. The sum in Eq. (31) still includes the same terms in the SBZ as in Eq. (1). Since we have chosen to distort the surface in the y-direction, the unit distance in the x-direction remains the same as the $(1x1)$ surface, while that in the y-direction becomes twice as long. When referring to the same pair of atoms, we have simply

$$X_x(\ell\ell') = X_x(LL') \quad (32)$$

for the x-component of $\vec{X}(\ell\ell')$ and $\vec{X}(LL')$. However, the corresponding equality for the y-component does not always hold. From Eq. (5) we then equate the coefficients of the sums in Eqs. (3) and (31) and obtain immediately

$$\hat{G}(L_Z A, L'_Z A', \vec{\phi}_S, E) = \frac{1}{2} e^{i \frac{\phi_y}{a_0} [x_y(\ell\ell') - x_y(LL')]} \left\{ \begin{aligned} &G(\ell_Z \beta, \ell'_Z \beta', \vec{\phi}_S, E) \\ &+ G(\ell_Z \beta, \ell'_Z \beta', \vec{\phi}_S - \text{sgn}(\phi_y) \pi \vec{e}_y, E) e^{-i \text{sgn}(\phi_y) \frac{\pi}{a_0} x_y(\ell\ell')} \end{aligned} \right\}, \quad (33)$$

where we have used the fact that

$$N_N = \frac{1}{2} N_S. \quad (34)$$

We can further simplify Eq. (33) by evaluating the exponentials. Eq. (33) may then be dissected into the following

$$\hat{G}(L_Z \beta, L'_Z \beta', \vec{\phi}_S, E) = \frac{1}{2} \left\{ G(\ell_Z \beta, \ell'_Z \beta', \vec{\phi}_S, E) + G(\ell_Z \beta, \ell'_Z \beta', \vec{\phi}_S - \text{sgn}(\phi_y) \pi \vec{e}_y, E) \right\}, \quad (35)$$

$$= \hat{G}(L_Z \beta + 2, L'_Z \beta' + 2, \vec{\phi}_S, E), \quad (36)$$

$$\hat{G}(L_Z\beta, L_Z'\beta' + 2, \vec{\phi}_S, E) = \frac{1}{2} e^{-i\phi_y} \left\{ G(\ell_Z\beta, \ell_Z'\beta', \vec{\phi}_S, E) - G(\ell_Z\beta, \ell_Z'\beta', \vec{\phi}_S - \text{sgn}(\phi_y)\pi\vec{e}_y, E) \right\}, \quad (37)$$

$$\hat{G}(L_Z\beta + 2, L_Z'\beta', \vec{\phi}_S, E) = \frac{1}{2} e^{i\phi_y} \left\{ G(\ell_Z\beta, \ell_Z'\beta', \vec{\phi}_S, E) - G(\ell_Z\beta, \ell_Z'\beta', \vec{\phi}_S - \text{sgn}(\phi_y)\pi\vec{e}_y, E) \right\}, \quad (38)$$

where $\beta, \beta' = 1, 2$, and

$$X_y(LL') = 0, \quad (39)$$

since all the atoms are in the same enlarged unit cell. Thus, we see that the layer-by-layer reconstructed surface Green's functions are obtained as a sum or difference of two known (1×1) surface Green's functions.

The perturbation matrix is obtained from Eq. (6). The periodic change in the nearest neighbor hopping integrals is shown in Fig. 1(b). The perturbation is confined to the first and second planes both of which are in the first layer and is given by

$$\hat{V}(1A, 1A', \vec{\phi}_S) = 2\varepsilon \cos \frac{\phi_x}{2} \begin{pmatrix} 0 & v^* & 0 & v^* e^{-i2\phi_y} \\ v & 0 & -v & 0 \\ 0 & -v^* & 0 & -v^* \\ v e^{i2\phi_y} & 0 & -v & 0 \end{pmatrix}, \quad (40)$$

where the rows (and columns) are labeled by the index $L_Z = 1$ and $A = 1, 2, 3$, and 4, and

$$v = e^{i\frac{\phi_x}{2}}. \quad (41)$$

We recall that ϵ , in units of γ , is the change in γ due to reconstruction. The Green's function \hat{G} that is needed is therefore reduced to a (4x4) matrix with $\ell_z = \ell'_z = L_z = L'_z = 1$ in Eqs. (35) - (38). Once \hat{V} and \hat{G} are known, the effects of reconstruction on the electronic structure of the surface can be studied within the formalism developed in Section II.

There are no surface states for this reconstructed surface structure. In Fig. 5, we present the total phase shift and in Fig. 6, the corresponding change in the density of states. Again, states are shifted toward the bottom (top) of the valence (conduction) band, leading to a decrease in the electronic energy. States are also pushed toward the band gap region in a very small energy range. These singularities in the density of states are always present in our calculation since the band edges are flat.¹⁵ To insure conservation of states, the integral of Δn up to the Fermi level must be zero. This is one way of stating the Friedel sum rule,⁹ and it is satisfied at the zeros of the total phase shift. From Fig. 5, we see that there are two new zeros inside the bands which are absent in the case of static relaxation (Fig. 3). This would allow us to place the Fermi level inside the bands if we so desired. However, *in all cases* the sum rule is satisfied with the Fermi level in the middle of the band gap.

C. (2x1) Reconstruction, y-Displacement

The unperturbed energy bands and Green's function for the y-displacement reconstructed surface are the same as those for the z-displacement. The displacements of the atoms and their effects on γ are shown in Fig. 1(a). Since the structures are different for y- and z-displacements, the perturbation matrices are different. For the y-displacement, the perturbation matrix becomes

$$\hat{V}(1A, 1A', \vec{\phi}_S) = 2\epsilon \cos \frac{\phi_x}{2} \begin{pmatrix} 0 & -v^* & 0 & v^* e^{-i2\phi_y} \\ -v & 0 & -v & 0 \\ 0 & -v^* & 0 & v^* \\ v e^{i2\phi_y} & 0 & v & 0 \end{pmatrix}. \quad (42)$$

The matrix elements are between the same basis vectors as Eq. (40).

Again, no surface states due to this type of reconstruction are found. The changes in the electronic structure with 0, 5.0 and 10.7 γ band gaps are considered. In Fig. 7, we present the total phase shifts for the three cases. An obvious effect is the narrowing of the bands as the band gap becomes larger. The phase shift changes continuously from the zero band gap case to one with a finite gap, and its shape is preserved. The derivatives of the phase shifts become larger at larger band gaps. This means that the change in the density of states is more pronounced at larger band gaps. However, the change in the electronic energy is an integrated effect weighted by the energy. According to Eq. (12), the decrease in the electronic energy should be the greatest for the case of zero band gap.

In Fig. 7(c), scale expansion is shown of the sharp change in the phase shift at the band edge. Within each band, the phase shift and its derivative are continuous except at the band edges where there are singularities in the derivative. All the other phase shifts show similar behavior.

In Fig. 8, we show the change in the density of states for Fig. 7(c). Qualitatively, it is very similar to the one for z-displacement shown previously in Fig. 6. However, the exact structure is different and will result in a different gain in electronic energy for the same set of model parameters.

D. c(2x2) Reconstruction

The geometry for this problem is shown in Fig. 1(c), and the corresponding SBZ is shown in Fig. 2(b). The bulk band structure corresponding to this SBZ is given by

$$E_{\vec{k}j} = \pm \frac{1}{2} \left(E_g^2 + 256\gamma^2 \cos^2 \frac{\phi_x}{2} \cos^2 \frac{\phi_y}{2} \cos^2 \frac{\phi_z}{2} \right)^{1/2}, \quad (43)$$

for $j = 1(+)$ and $2(-)$, but in contrast with Eq. (30), we have

$$E_{\vec{k}j} = \pm \frac{1}{2} \left(E_g^2 + 256\gamma^2 \sin^2 \frac{\phi_x}{2} \sin^2 \frac{\phi_y}{2} \cos^2 \frac{\phi_z}{2} \right)^{1/2}, \quad (44)$$

for $j = 3(+)$ and $4(-)$.

The surface Green's functions are derived in the same way as for the (2x1) case. We first convert the sum in Eq. (1) to a sum over the c(2x2) SBZ,

$$G(\ell\beta, \ell'\beta', E) = \frac{1}{N_s} \sum_{\vec{\phi}_s} \left\{ G(\ell_z\beta, \ell'_z\beta', \vec{\phi}_s, E) e^{i \frac{\vec{\phi}_s}{a_0} \cdot \mathbf{x}(\ell\ell')} + G(\ell_z\beta, \ell'_z\beta', \vec{\phi}_s - \text{sgn}(\phi_x)\vec{e}_x - \text{sgn}(\phi_y)\vec{e}_y, E) e^{i \frac{[\vec{\phi}_s - \text{sgn}(\phi_x)\vec{e}_x - \text{sgn}(\phi_y)\vec{e}_y]}{a_0} \cdot \mathbf{x}(\ell\ell')} \right\}. \quad (45)$$

Equating the coefficients of the sums in Eqs. (3) and (45), we obtain

$$\hat{G}(L_z A, L'_z A', \vec{\phi}_s, E) = \frac{1}{2} e^{i \frac{\vec{\phi}_s}{a_0} \cdot \mathbf{x}(\ell\ell')} \left\{ G(\ell_z\beta, \ell'_z\beta', \vec{\phi}_s, E) + G(\ell_z\beta, \ell'_z\beta', \vec{\phi}_s - \text{sgn}(\phi_x)\vec{e}_x - \text{sgn}(\phi_y)\vec{e}_y, E) e^{-i \text{sgn}(\phi_x) \frac{\pi}{a_0} x_x(\ell\ell') - i \text{sgn}(\phi_y) \frac{\pi}{a_0} x_y(\ell\ell')} \right\}, \quad (46)$$

where, again,

$$N_N = \frac{1}{2} N_s, \quad (47)$$

and

$$\vec{X}(LL') = 0, \quad (48)$$

since all the atoms are in the same enlarged $c(2 \times 2)$ unit cell. Eq. (46) can similarly be dissected as was done in the (2×1) z-displacement case. However, the result is more lengthy and will not be given.

The perturbation matrix, referring to the geometry in Fig. 1(c), is given by

$$\hat{V}(1A, 1A', \vec{\phi}_S) = \epsilon \begin{pmatrix} 0 & -1 + e^{-i(\phi_x + \phi_y)} & 0 & -e^{-i(\phi_x + \phi_y)} + e^{-i2\phi_y} \\ -1 + e^{i(\phi_x + \phi_y)} & 0 & -1 + e^{i(\phi_x - \phi_y)} & 0 \\ 0 & -1 + e^{-i(\phi_x - \phi_y)} & 0 & 1 - e^{-i(\phi_x + \phi_y)} \\ -e^{i(\phi_x + \phi_y)} + e^{i2\phi_y} & 0 & 1 - e^{i(\phi_x + \phi_y)} & 0 \end{pmatrix}, \quad (49)$$

where, again, the rows (and columns) are labeled by $L_z = 1$ and $A = 1, 2, 3,$ and 4 .

For this case, surface states are found to lie both below the valence band and above the conduction band for arbitrarily small ϵ . In Fig. 9, we show the regions in the SBZ where the surface states exist for three different values of ϵ . The portions of the SBZ where the surface states exist become larger for larger values of ϵ . The fact that reconstruction can create new surface states is not new. For the one-band model, simulating the transition metals, Dobrzynski and Mills⁶ found that reconstruction created surface states lying symmetrically below and above the energy band but only when the perturbation exceeded a certain critical value. Thus, reconstruction can add new features to surface electronic spectra.

In Fig. 10, we show the positions of the surface states in relation to the surface energy bands. In each case the energy bands are cross sections along a particular segment in the SBZ. These segments are labeled in Fig. 2(b).

In Fig. 10, the single cross-hatched areas denote a continuum of single bulk states, whereas the double cross-hatched area shows where two continua of bulk states overlap due to the folding back of the SBZ. In Fig. 10(a), the surface states are located near the zone boundary and merge into the energy bands for smaller wave vectors. At a higher value of k_y , shown in Fig. 10(b), surface states exist for all values of k_x . Surface states, when they exist, lie close to the band edges, but no surface states are found inside the band gap.

In Fig. 11, we present the total phase shift with the contribution from the surface states included. For surface states lying below (above) an energy band, the partial phase shift jumps from 0 to $\pi(-\pi)$.⁹ This introduces two additional spikes in the total phase shift. As before, the total phase shift and its derivative are continuous except for the singularities at the band edges. In Fig. 12, we show the change in the density of states. The extra spikes in Fig. 11 lead to the oscillations near the band edges which are shown with an expanded energy scale. The positive peak below the band edge shows an increase in the density of states due to the presence of the surface states. As before, the net effect of reconstruction is to push states toward the bottom (top) of the valence (conduction) band. In comparison with Fig. 8, we see that the changes in the density of states for the (2x1) and the c(2x2) reconstruction are quite different.

E. Decrease in the Ground State Electronic Energy, Strain Energy and Change in the Total Energy

The change in the ground state electronic energy is given by Eq. (12). The integration is carried out numerically for all the cases considered with the Fermi level pinned at the middle of the band gap ($E_F = 0$).

The results are summarized in Table II and plotted in Fig. 13. There are four features to notice. First, the values of ΔU are considerably smaller than those obtained for the static relaxation. Second, for the values of ϵ considered, our numerical results show a quadratic dependence of ΔU on ϵ . This was also found to be true for small values of ϵ with the one-band model.⁶ Third, for the (2x1) reconstruction, the results show that for all values of ϵ and for a band gap of 10.7γ , the lowering in the electronic energy is greater for an in-plane displacement than for a displacement perpendicular to the surface. For the same gap, the lowering is greater still for the in-plane motion of the c(2x2) reconstruction. Fourth, with all other parameters equal, the results show an inverse relation between the decrease in the electronic energy and the band gap.

In Fig. 14, we show the explicit dependence of ΔU on the band gap for two values of ϵ . The decrease in the electronic energy is largest in the case of zero band gap (bcc metal). This can be understood in terms of the interaction between states with the same \vec{k} but different in energy, i.e., the smaller the energy difference, the stronger the interaction. Therefore, the interaction between states in different bands increases as the band gap decreases and is the strongest in the zero band gap case. As a result, states are pushed more toward the bottom (top) of the valence (conduction) band with decreasing energy gap, and the decrease in electronic energy is largest at zero band gap. In addition, as the gap increases the bands become more narrow, while the absolute maximum of the phase shift remains approximately constant (see Fig. 7). In the limit of infinite gap, the bands approach zero width, and ΔU also goes to zero.

From Fig. 13, we see that reconstruction using our simple model *always* lowers the electronic energy of the system, and the decrease becomes larger

at increasing values of ϵ (and hence, by assumption, for increasing values of atomic displacements). This is because the present calculation does not include many of the electron interactions in the system. In particular, there are no repulsive interactions between the atoms in the crystal. When such terms are included, the change in the total energy, rather than continuing negative indefinitely, must eventually rise for displacements greater than some critical value.

One method of modeling this behavior is to include an elastic strain energy term in the total energy expression.⁶ The total energy becomes, then, a sum of the electronic energy in Fig. 13 (which is negative) plus a strain energy term (which is positive). In what follows, we will first relate, in a simple way, the strain energy to the displacement of the atoms. Second, we will relate the parameter ϵ to the displacement of the atoms. Finally, we will show the necessary conditions under which reconstruction can occur.

First, we consider the elastic strain energy associated with the relative displacement of the atoms in the first and second planes. We do this by assuming that these atoms interact with their nearest neighbors via a harmonic potential. The force constant of these oscillators, λ , can be determined by considering the phonon dispersion curves. We will consider only the (2x1) structure with in-plane displacements. The other cases can be treated similarly. From Fig. 1(a) we see that the displacement is similar to the displacement structure one obtains for a longitudinal phonon propagating in the y-direction with wavelength $2a_0$. This corresponds to a wave vector of π/a_0 which is at the bulk Brillouin zone boundary. The frequency of this phonon is given by²⁶

$$\omega_{LO}^2 = \frac{8\sqrt{3}}{3} \frac{\lambda}{M} , \quad (50)$$

where M is the mass of the atom which is moving and ω_{LO} is the frequency of the longitudinal optic phonon of interest. Continuing with our example of CsI, the phonon dispersion curves have been calculated by Karo and Hardy²⁷ with the result that ω_{LO} at the X point in the bulk Brillouin zone is found to be $1.3 \times 10^{13} \text{ sec}^{-1}$. If we assume that the force constant at the surface is reduced by a factor of α , then we obtain for the strain energy per unit cell

$$\begin{aligned} Q &= 8 \frac{\alpha\lambda}{2} \left(\frac{\sqrt{3}}{3} \delta y \right)^2 \\ &= \frac{\sqrt{3}}{6} M \omega_{LO}^2 \alpha (\delta y)^2 , \end{aligned} \quad (51)$$

where $\sqrt{3} \delta y/3$ is equal to the effective displacement, δr , in the direction of the nearest neighbors, and the factor 8 arises from the fact that there are 8 nearest neighbor bonds per reconstructed unit cell.

In order to relate the strain energy Q to the electronic energy ΔU , it is necessary to relate δr to ϵ . For small displacements, we can expand the hopping integral γ as follows:

$$\gamma = \gamma_0 + \left. \frac{d\gamma}{dr} \right|_{r=r_0} \delta r , \quad (52)$$

where r_0 is the nearest neighbor distance in the bulk and γ_0 is the bulk nearest neighbor hopping integral. From the definition of ϵ , we have

$$\frac{\epsilon}{\gamma} = \frac{1}{\gamma} \left. \frac{d\gamma}{dr} \right|_{r=r_0} \delta r . \quad (53)$$

We now define a new positive constant c such that

$$\frac{\epsilon}{\gamma} = -\frac{c}{a} \delta r \quad , \quad (54)$$

where a is the Bohr radius (used merely to make c a dimensionless constant).

Since we have already related ΔU to ϵ (in Fig. 13), we use Eq. (54) in Eq. (51) to express Q in terms of ϵ . This gives

$$Q = \frac{\sqrt{3}}{2} M \omega_{LO}^2 a^2 \frac{\alpha}{c^2} \left(\frac{\epsilon}{\gamma} \right)^2 . \quad (55)$$

Inserting the values of the constants and using the mass of the iodine atom for M , we obtain

$$\frac{Q}{\gamma} = 0.93 \frac{\alpha}{c^2} \left(\frac{\epsilon}{\gamma} \right)^2 . \quad (56)$$

We see that this simple model results in Q (as well as ΔU) being quadratic in ϵ . Consequently, whether the total energy ΔE_t is positive or negative is determined entirely by the choice of constants α and c .

In Fig. 15 we present the two cases where $Q < \Delta U$ and $Q > \Delta U$. For this figure, ΔU can be given approximately by²⁸

$$\frac{\Delta U}{\gamma} = -0.30 \left(\frac{\epsilon}{\gamma} \right)^2 . \quad (57)$$

Thus, we see in comparison with Eq. (56), that if $\alpha/c^2 < 0.32$, then the total energy ΔE_t will be negative as in Fig. 15(a). This situation leads to reconstruction. On the other hand, if $\alpha/c^2 > 0.32$, the total energy ΔE_t will be positive as in Fig. 15(b), and no reconstruction will occur.

IV. Conclusions

We have found that the presence of an empty conduction band is of fundamental importance in understanding reconstruction on semiconductor or insulator surfaces. Contrary to the results of Dobrzynski and Mills⁶ which showed that surface reconstruction has no effect on a one-band crystal when the band is filled, we find that if a second band is present, the magnitude of the decrease in the electronic energy upon reconstruction is comparable to that obtained on a bcc metal with a half-filled band. In other words, the fact that the electronic band structure may contain gaps is not of fundamental importance as far as the change in electronic energy due to reconstruction is concerned. What is important, however, is that the calculation of this energy change includes the effect of these empty conduction bands.

The process of reconstruction discussed in this paper is not like those discussed elsewhere⁵ and which carry the labels Peirel's transition, giant Kohn anomaly, or Jahn-Teller distortion. The difference is that the process discussed in this paper (and also by Dobrzynski and Mills⁶) does not require the system to open any new gaps in the density of states, or undergo a metal-insulator transition. Rather, in our mechanism, if the system is initially a metal (or an insulator), it remains a metal (or an insulator) after reconstruction.

We have found that the gain in the electronic energy is inversely proportional to the band gap, i.e., the smaller the band gap, the larger the effect of reconstruction. Thus, this mechanism will have its greatest effect on metals and narrow gap semiconductors and its least effect on large gap insulators.

We have found that different reconstructed structures result in

different changes in the electronic energy in spite of the fact that all of the model parameter values are identical and the fact that the model is very simple. Thus, it is, in principle, possible to use this method to predict the reconstructed structures on systems that have not yet been investigated experimentally. This feature of being able to make predictions is not shared by all the other theoretical approaches to reconstruction.

Most important, we have found that our simple model *always* gives a decrease in the electronic energy. This statement is true no matter how many bands (2 or more) are included and no matter what the reconstructed structures may be. This is because the process of reconstruction always allows new states to interact which didn't interact before the reconstruction. This new interaction always pushes the states apart in energy. Thus, the lower energy states which are filled are always pushed down, and the higher energy states which are empty are pushed up. This always leads to a gain in the electronic energy. The reason this conclusion is important is that it now adds a burden to the theorist in future calculations. It will not be sufficient, as in the past,² to show that any particular chosen reconstructed surface structure lowers the electronic energy. It will also be necessary both to prove that the model used is sufficiently accurate to distinguish between various structures and that other structures do not have a lower electronic energy than the chosen structure. Meeting all these necessary criteria will not be easy.

Acknowledgment

We acknowledge, with gratitude, support of this research by the

National Science Foundation (Grant No. GK-43433) and the IBM Corporation via a postdoctoral research fellowship (SLC).

References

1. J. J. Lander and J. Morrison, J. Appl. Phys. 34, 1403 (1963); J. C. Phillips, Surface Sci. 40, 459 (1973), and 44, 290 (1974).
2. D. Haneman, Phys. Rev. 121, 1093 (1961); N. R. Hansen and D. Haneman, Surface Sci. 2, 566 (1964); D. Haneman and D. L. Heron, in The Structure and Chemistry of Solid Surfaces, G. A. Somorjai, Ed., (Wiley, New York, 1969); D. L. Heron and D. Haneman, Surface Sci. 21, 12 (1970).
3. S. E. Trullinger and S. L. Cunningham, Phys. Rev. Lett. 30, 913 (1973), and Phys. Rev. B8, 2622 (1973). The results on Si(111) are to be published.
4. A. Blandin, D. Castiel and L. Dobrzynski, Solid State Comm. 13, 1175 (1973); R. Srinivasan and G. Lakshmi, J. Phys. Chem. Solids 34, 2149 (1973); 35, 1453 (1974), and Surface Sci. 43, 617 (1974).
5. E. Tosatti and P. W. Anderson, Solid State Commun. 14, 773 (1974), and Japan. J. Appl. Phys. Suppl. 2, Pt. 2, 381 (1974).
6. L. Dobrzynski and D. L. Mills, Phys. Rev. B7, 2367 (1973).
7. See, for example, R. E. Schlier and H. E. Farnsworth, J. Chem. Phys. 30, 917 (1959); P. W. Palmberg and T. N. Rhodin, Phys. Rev. 161, 586 (1967); A. E. Morgan and G. A. Somorjai, Surface Sci. 12, 405 (1968); C. M. Comrie, Ph.D. Thesis (1973), and unpublished results; J. E. Rowe and J. C. Phillips, Phys. Rev. Lett. 32, 1315 (1974).
8. H. Ibach and J. E. Rowe, Surface Sci. 43, 481 (1974).
9. W. Ho, S. L. Cunningham, W. H. Weinberg and L. Dobrzynski, Phys. Rev. B, in press (1975).

10. In this paper the orbital energy of atoms of type one, E_1 , is lower than that of atoms of type two, E_2 . In our previous paper⁹ the opposite was assumed. This does not affect our results; the two types are just labels. This may easily be demonstrated by interchanging the two values in our derived expressions.
11. See, for example, L. Dobrzynski, *Ann. Phys.* 4, 637 (1969); G. Allan and P. Lenglard, *Surface Sci.* 15, 101 (1969); 30, 641 (1972).
12. G. Allan, *Ann. Phys.* 5, 169 (1970); T. L. Einstein and J. R. Schrieffer, *Phys. Rev.* B7, 3629 (1973); A van der Avoird, S. P. Liebmann and D. J. M. Fassaert, *Phys. Rev.* B10, 1230 (1974).
13. T. H. DiStefano and W. E. Spicer, *Phys. Rev.* B7, 1554 (1973).
14. S. L. Cunningham, *Phys. Rev.* B10, 4988 (1974).
15. L. van Hove, *Phys. Rev.* 89, 1189 (1953).
16. R. T. Sanderson, *Chemical Bonds and Bond Energy*, Academic Press, 1971, p. 176.
17. R. W. G. Wyckoff, *Crystal Structures*, Interscience, 2nd Edition, Vol. I, 1963, p. 104.
18. G. Allan and M. Lannoo, *Surface Sci.* 40, 375 (1973).
19. G. C. Benson, *J. Chem. Phys.* 35, 2113 (1961); G. C. Benson and K. S. Yun, in *The Solid-Gas Interface*, Vol. 1, Ch. 8, Marcel Dekker, E. A. Flood, Ed., 1967.
20. G. E. Laramore and A. C. Switendick, *Phys. Rev.* B7, 3615 (1973).
21. J. A. Appelbaum and D. R. Hamann, *Phys. Rev. Lett.* 31, 106 (1973); *Phys. Rev.* B6, 2166 (1972).
22. J. E. Rowe and H. Ibach, *Phys. Rev. Lett.* 31, 102 (1973).
23. G. P. Alldredge and L. Kleinman, *Phys. Lett.* 48A, 337 (1974); *J. Phys. F: Metal Phys.* 4, L207 (1974).

24. G. C. Benson and T. A. Claxton, J. Phys. Chem. Solids 25, 367 (1964).
25. J. J. Burton and G. Jura, J. Phys. Chem. 71, 1937 (1967).
26. This expression was obtained using standard techniques (see, for example, C. Kittel, Introduction to Solid State Physics, 4th ed., Ch. 5, Wiley, 1971) where we assume central forces between nearest neighbors and where only the second derivative of the potential is nonzero. At the X point, the calculation is particularly simple.
27. A. M. Karo and J. R. Hardy, J. Chem. Phys. 48, 3173 (1968).
28. A second degree polynomial fit to the six data points in Table II was used to derive Eq. (57). The constant term is zero and the linear term is negligible compared to the quadratic term for these values of ϵ .

Table Captions

Table I: Decrease in the electronic energy due to a uniform contraction of the surface layer of atoms. The band gap is appropriate for CsI. We assume $\gamma = 0.58$ eV for all cases.

Table II: Decrease in the electronic energy due to the (2x1) and c(2x2) reconstruction. Three different band gaps are considered for the (2x1) in-plane displacement. The displacements δr , in the direction of the nearest neighbors, (in units of the lattice constant $a_0 = 4.57 \text{ \AA}$) are obtained with $c = \sqrt{3}$ [see Eq. (54) and Fig. 15(a)]. Note the quadratic dependence of ΔU on ϵ . We assume $\gamma = 0.58$ eV for all cases.

Table I

$\frac{E_g}{\gamma}$	$\frac{\Delta}{\gamma}$	$\frac{\Delta U}{\gamma}$	$\frac{\Delta U}{\text{ergs/cm}^2}$
	0.10	-0.0626	-27.9
10.7			
	0.20	-0.130	-57.9

Table II

Reconstructed Structures	$\frac{E_g}{\gamma}$	$\frac{\epsilon}{\gamma}$	$\frac{ \delta r }{a_0}$ ($c = \sqrt{3}$)	$\frac{\Delta U}{\gamma}$ ($\times 10^2$)	ΔU ergs/cm ²
		0.0	0.0	0.0	0.0
		0.05	0.0033	-0.0753	-0.168
(2x1) y- Displacement	10.7	0.10	0.0067	-0.301	-0.671
		0.15	0.010	-0.677	-1.51
		0.20	0.013	-1.21	-2.70
		0.30	0.020	-2.70	-6.02
		0.10	0.0067	-0.427	-0.951
	5.0	0.20	0.013	-1.71	-3.81
		0.10	0.0067	-0.459	-1.02
	0.0	0.20	0.013	-1.86	-4.14
(2x1) z- Displacement	10.7	0.20	0.013	-1.12	-2.50
c(2x2) y- Displacement	10.7	0.10	0.0067	-0.347	-0.773
		0.20	0.013	-1.35	-3.01

Figure Captions

- Figure 1: Geometries of the reconstructed surfaces. Type 1 atoms are on the (001) surface. Type 2 atoms are beneath the plane and in the body-centered positions. ϵ is the change in the nearest neighbor hopping integral γ . Solid lines represent the new unit cells. Arrows point in the directions of displacements.
- (a) (2x1) in-plane displacement,
 (b) (2x1) normal displacement. Dots (crosses) represent atoms moving out (into) the surface plane,
 (c) c(2x2) in-plane displacement.
- Figure 2: Surface Brillouin Zone (SBZ) for the reconstructed surface.
- (a) (2x1), (b) c(2x2), and a and b refer to the segments in the SBZ where the cross sections in the energy bands are taken for Figs. 10(a) and 10(b), respectively. Large square represents SBZ for (1x1) surface.
- Figure 3: Total phase shift per surface unit cell for the uniform contraction of the surface layer. No reconstruction is included.
- Figure 4: Change in the density of states per surface unit cell for the uniform contraction of the surface layer. This is proportional to the derivative of Fig. 3.
- Figure 5: Total phase shift per (2x1) reconstructed surface unit cell for displacements of atoms normal to the surface.
- Figure 6: Change in the density of states per (2x1) reconstructed surface unit cell for displacements of atoms normal to the surface. Singularities at the band edges are due to the flatness of the bands.

Figure 7: Total phase shift per (2x1) reconstructed surface unit cell as a function of the band gap, E_g , for in-plane displacement of the atoms, (a) $E_g = 0$, bcc crystal, (b) $E_g = 5.0$, (c) $E_g = 10.7$, appropriate for CsI. An expansion is included of the sharp change in $\eta(E)$ for (c). Note for larger band gaps the bands get more narrow, but the shape and the absolute magnitude of $\eta(E)$ remain approximately the same.

Figure 8: Change in density of states per (2x1) reconstructed surface unit cell for Fig. 7(c). It is qualitatively the same as Fig. 6.

Figure 9: Region of the SBZ where surface states exist for in-plane displacement of the c(2x2) reconstruction. Area in dots is for $\epsilon = 0.2$. Area in double cross-hatches is for $\epsilon = 0.3$. Area in single cross-hatches is for $\epsilon = 0.4$. Surface states spread through the SBZ as the value of ϵ is increased.

Figure 10: Relation of surface states to energy bands of the c(2x2) reconstruction along two segments in the SBZ [labelled a and b in Fig. 2(b)]. Surface states appear symmetrically below and above the valence and the conduction bands, respectively. Double cross-hatched areas denote overlap due to folding of the bands. (a) Along a in Fig. 2(b) surface states merge into the energy bands. (b) Along b in Fig. 2(b) surface states exist for all values of k_x . No surface states are found inside the band gap.

Figure 11: Total phase shift per c(2x2) reconstructed unit cell. Two new spikes at $E/\gamma = \pm 5.45$ are due to the presence of surface states.

Figure 12: Change in the density of states per $c(2 \times 2)$ surface unit cell. Rapid oscillations are due to the surface states which lie close to the band edges. In the expanded scale the positive finite peak in Δn is due to the surface states.

Figure 13: Change in the electronic ground state energy, ΔU , as a function of the change ϵ in the nearest neighbor hopping integral, γ . Subscript z in case d denotes displacement normal to the surface. In cases without subscripts, displacements are taken to be in the plane of the surface. The decrease in U is quadratic in ϵ .

Figure 14: Change in the electronic ground state energy, ΔU , as a function of the energy gap, E_g , for two values of ϵ . Surface is reconstructed into a (2×1) structure with displacement in the plane of the surface.

Figure 15: Change in the total electronic energy, ΔE_t , as a function of ϵ for the (2×1) reconstruction. Strain energy Q depends quadratically on ϵ . The surface force constant is taken to be $1/2$ the bulk value. Displacement is in the plane of the surface. (a) $c = \sqrt{3}$ in Eq. (54), (b) $c = \sqrt{3}/2$.

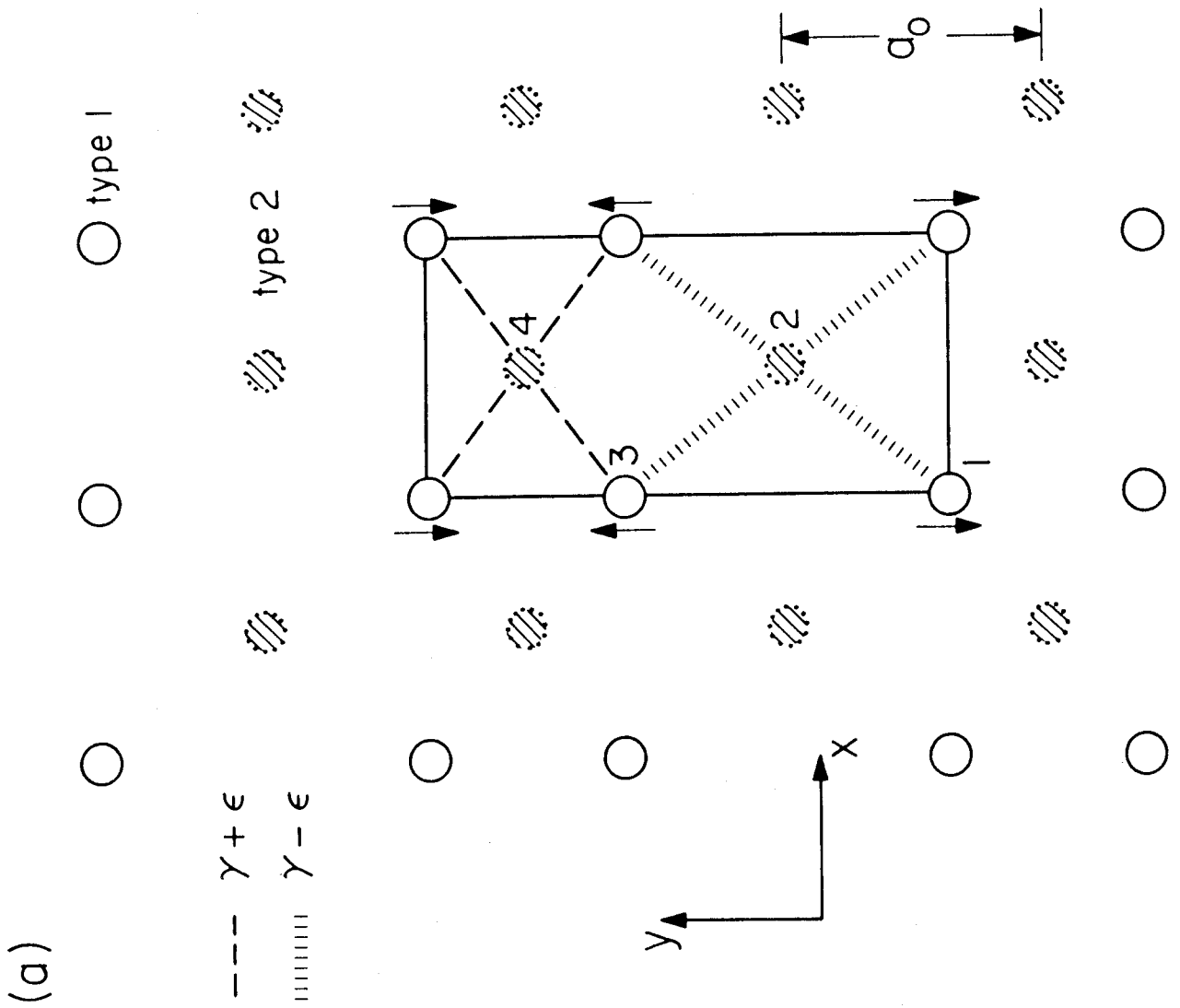
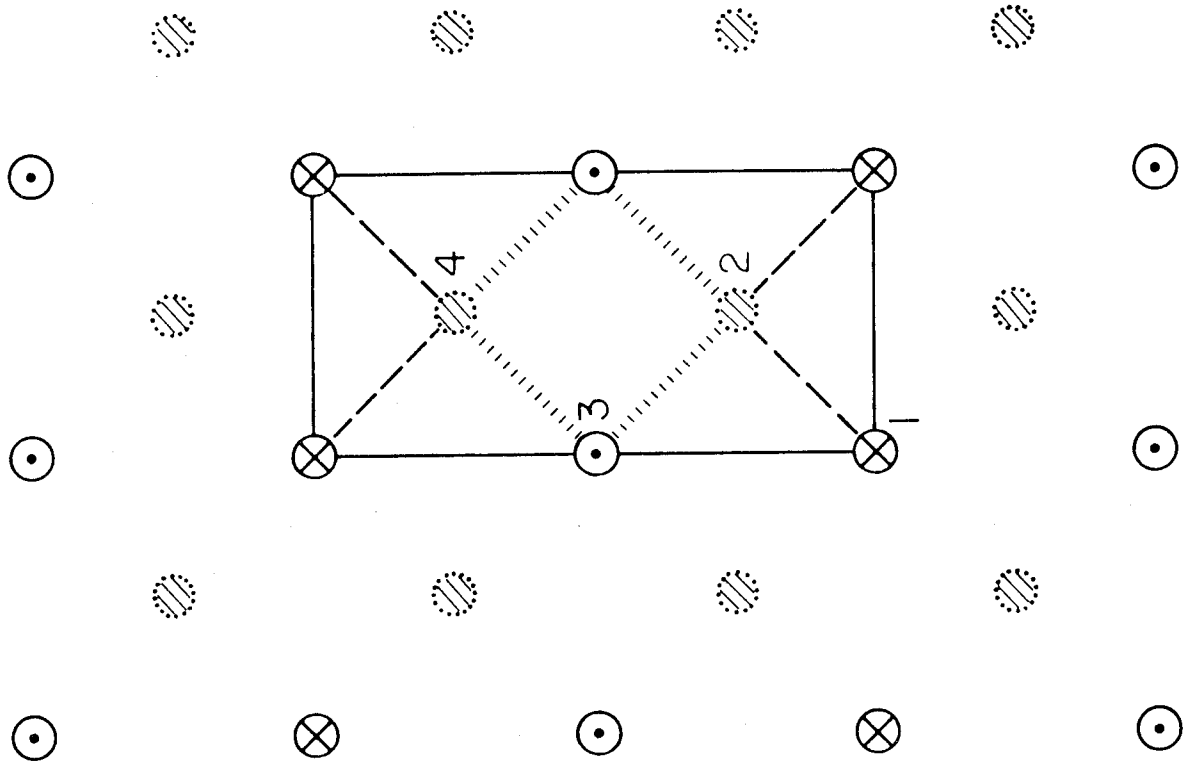


Figure 1 (a)



(b)

Figure 1 (b)

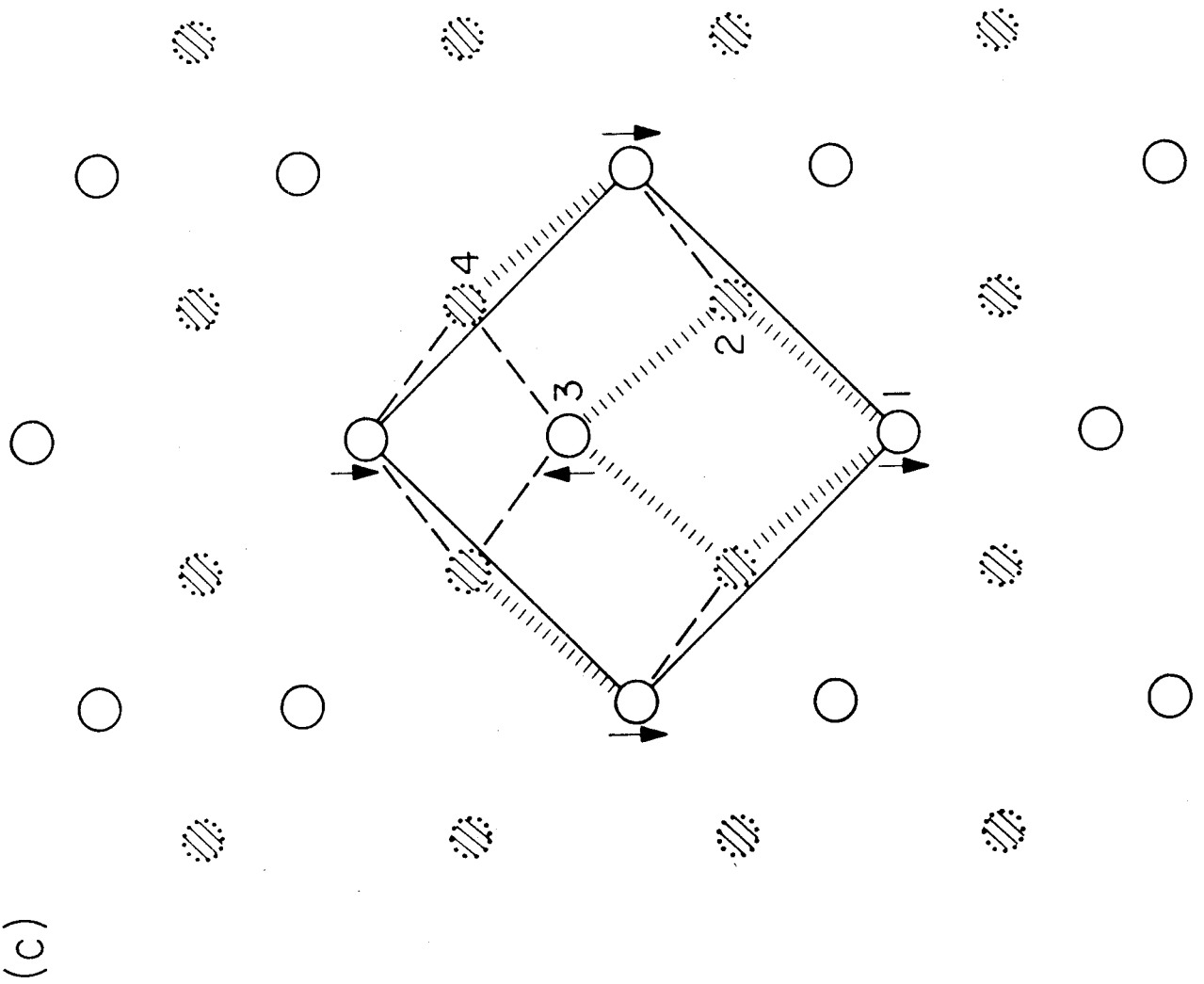


Figure 1 (c)

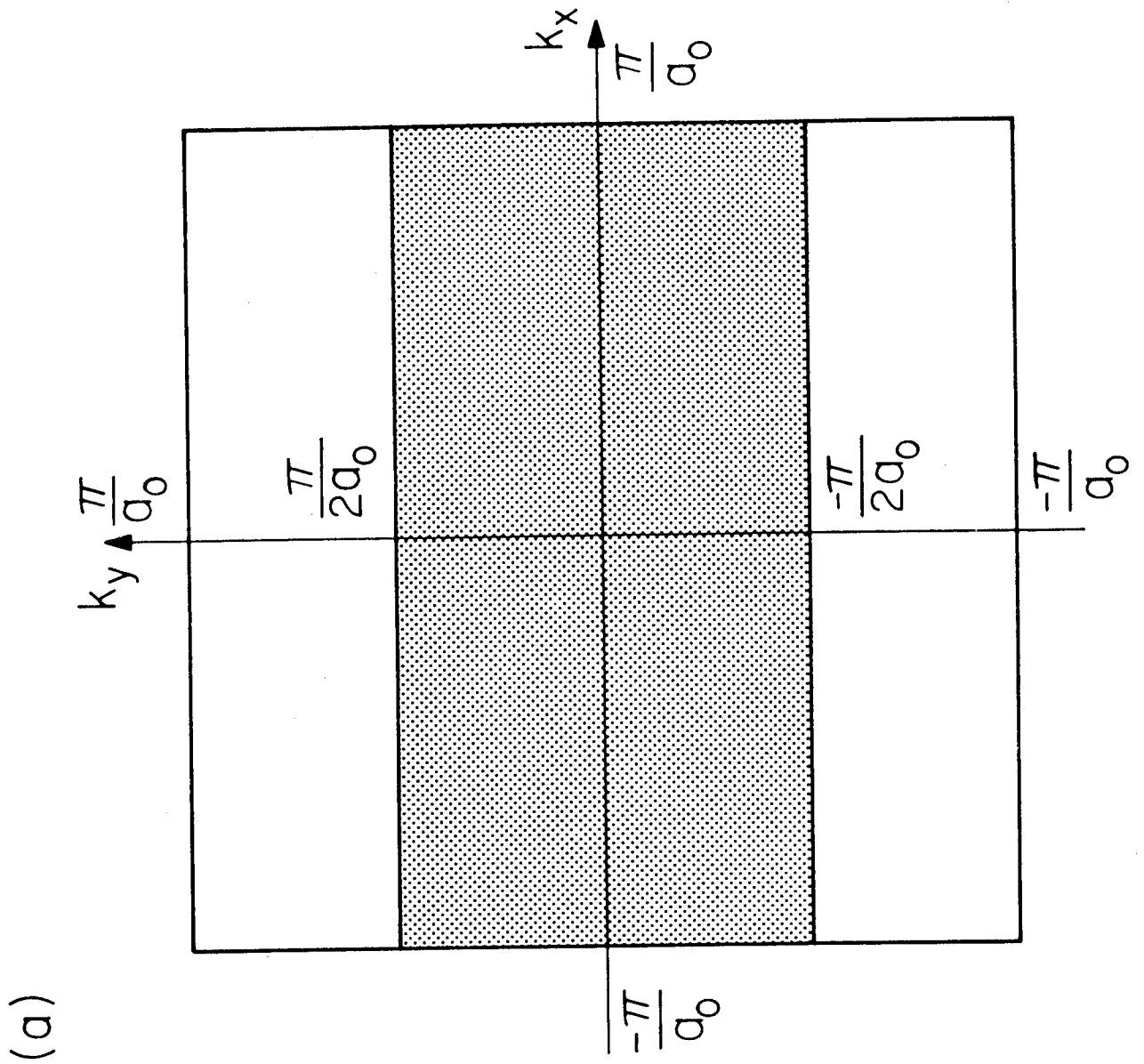


Figure 2 (a)

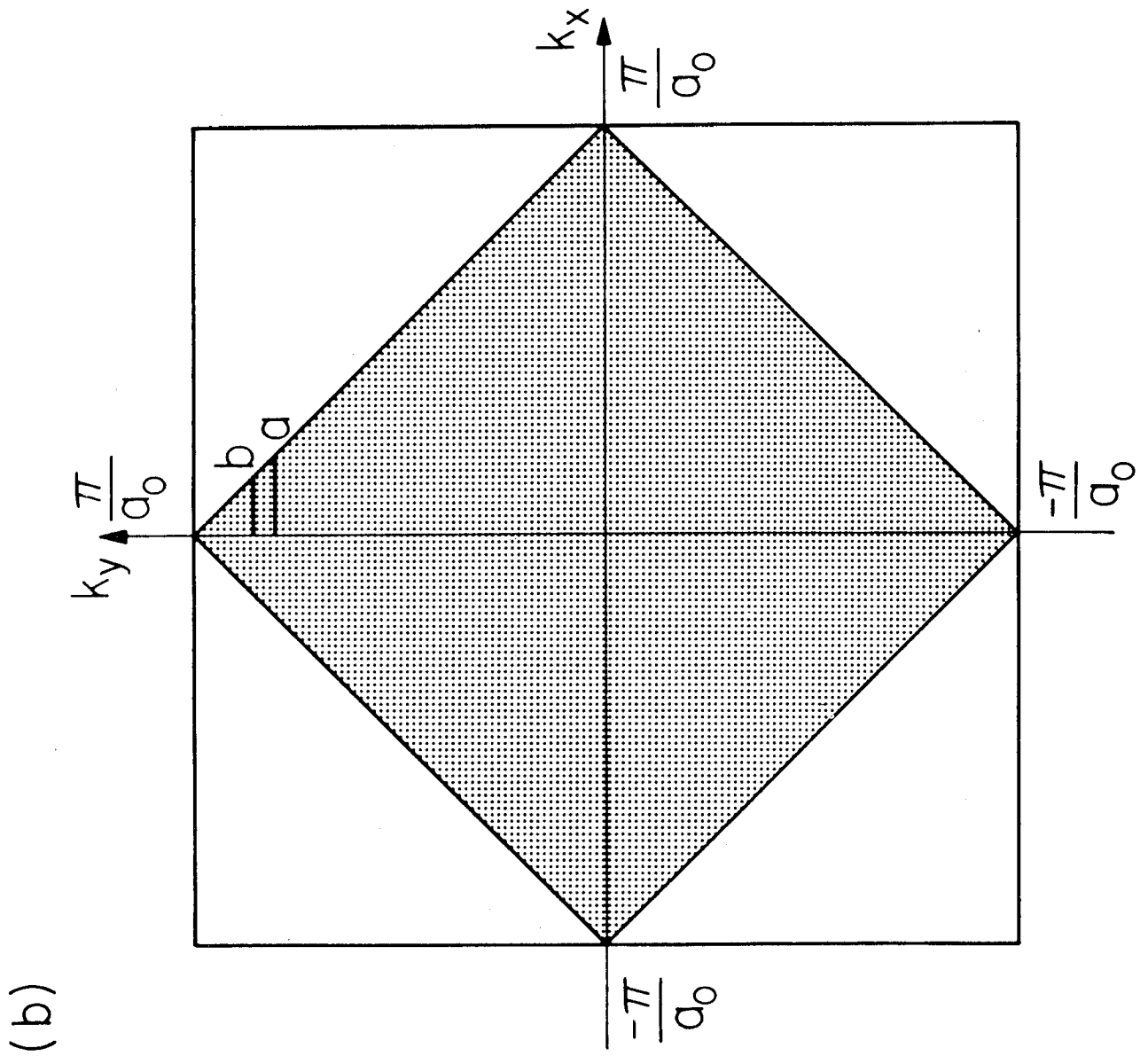


Figure 2 (b)

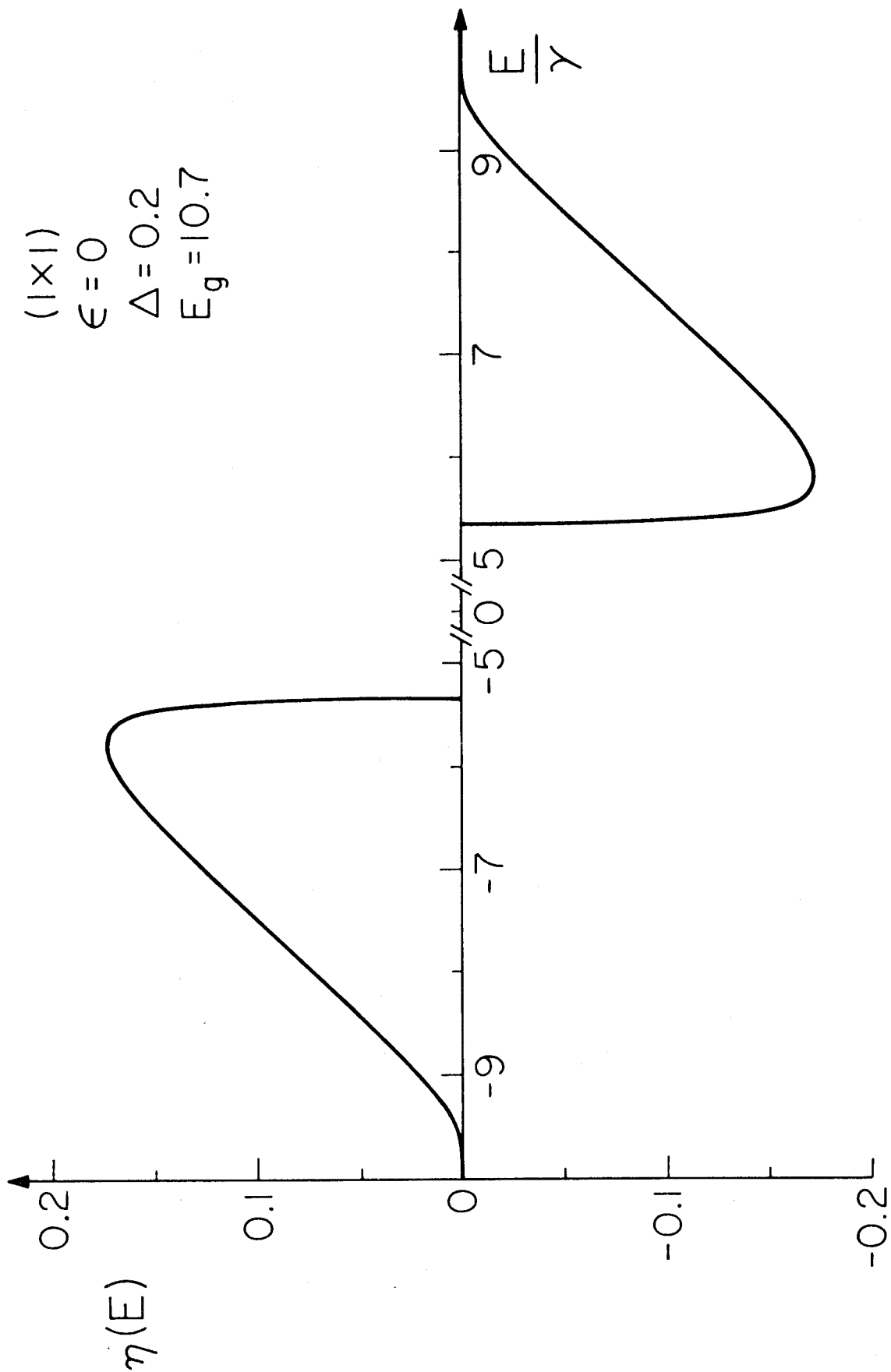


Figure 3

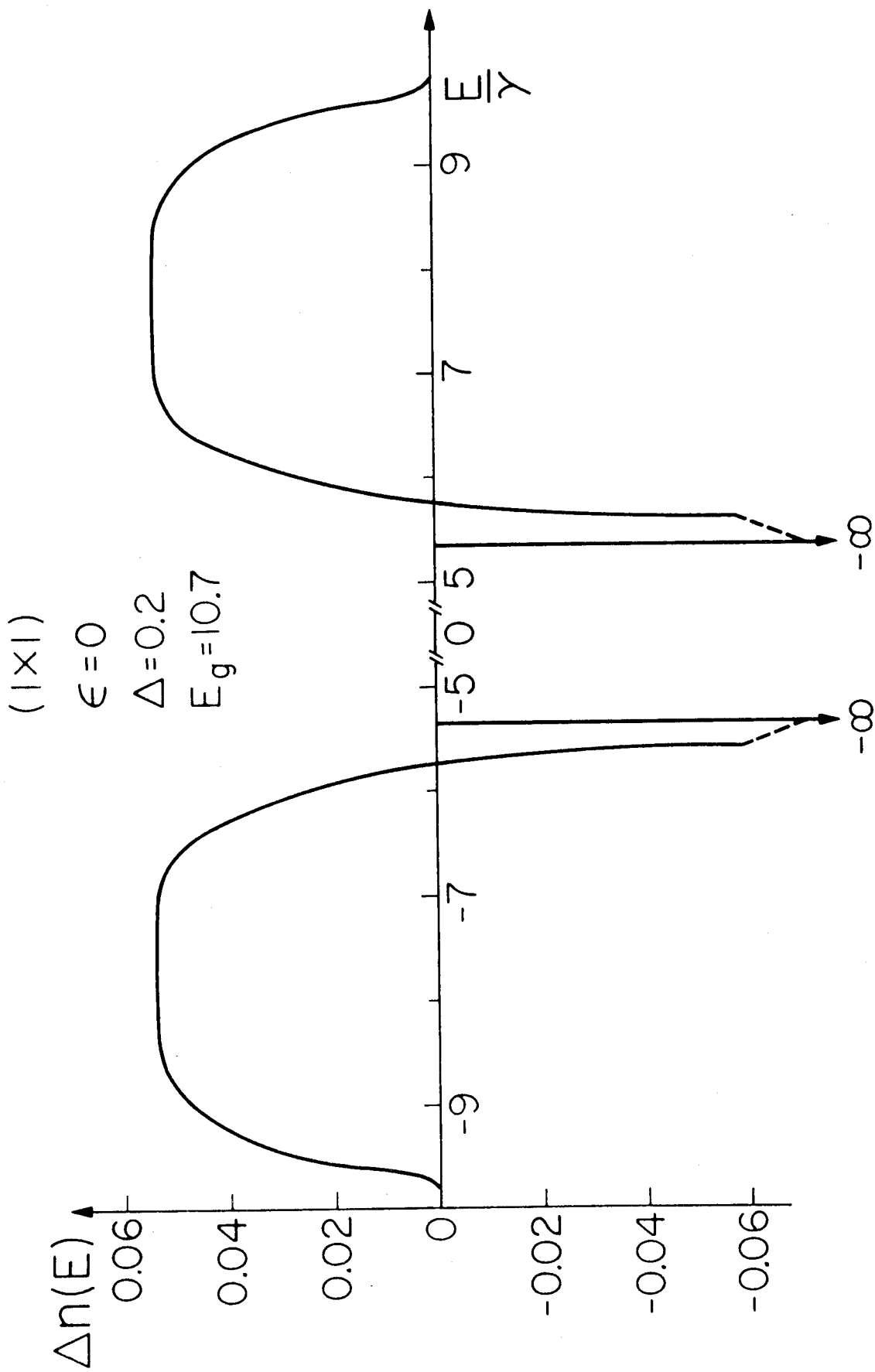


Figure 4

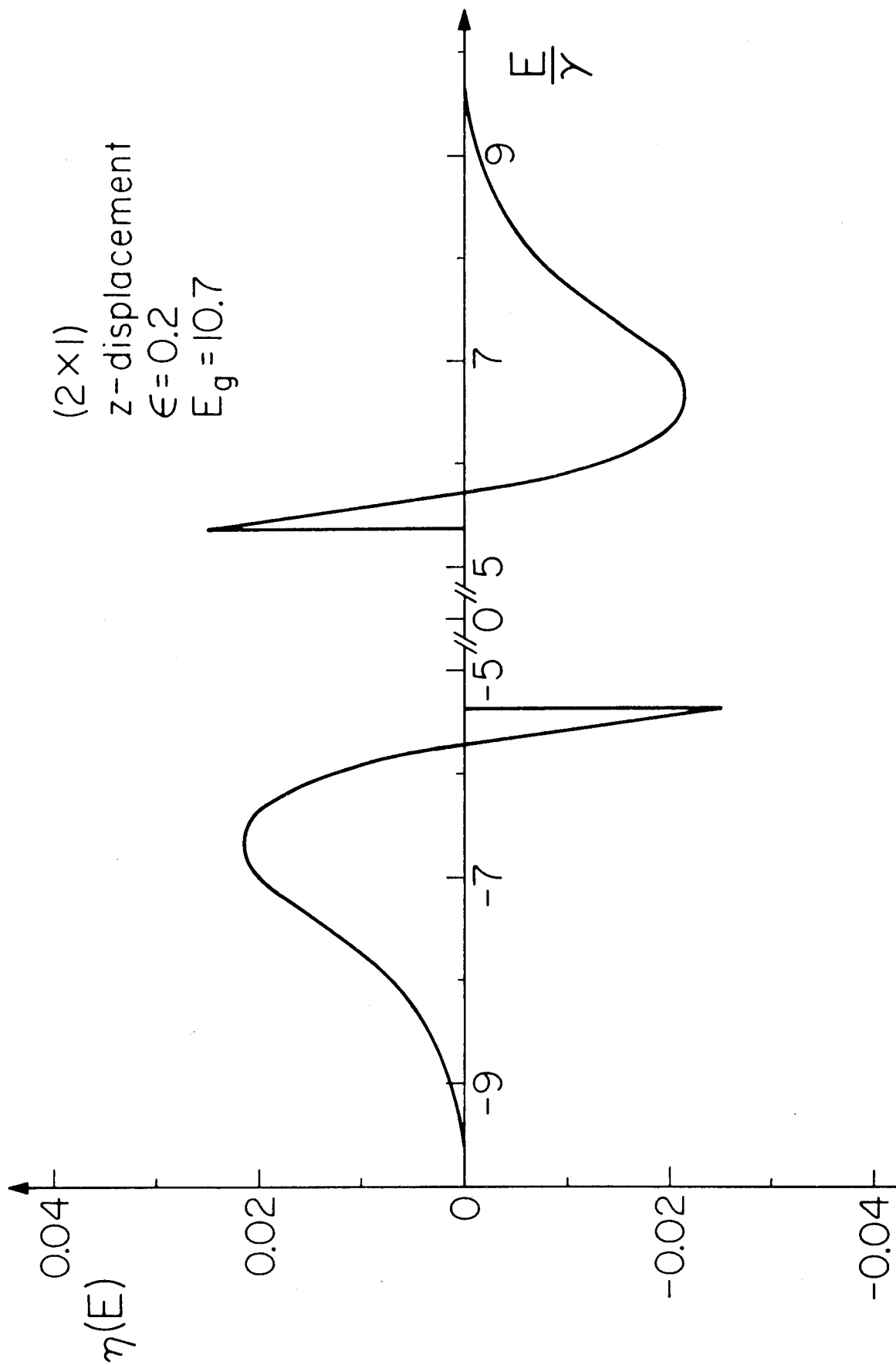


Figure 5

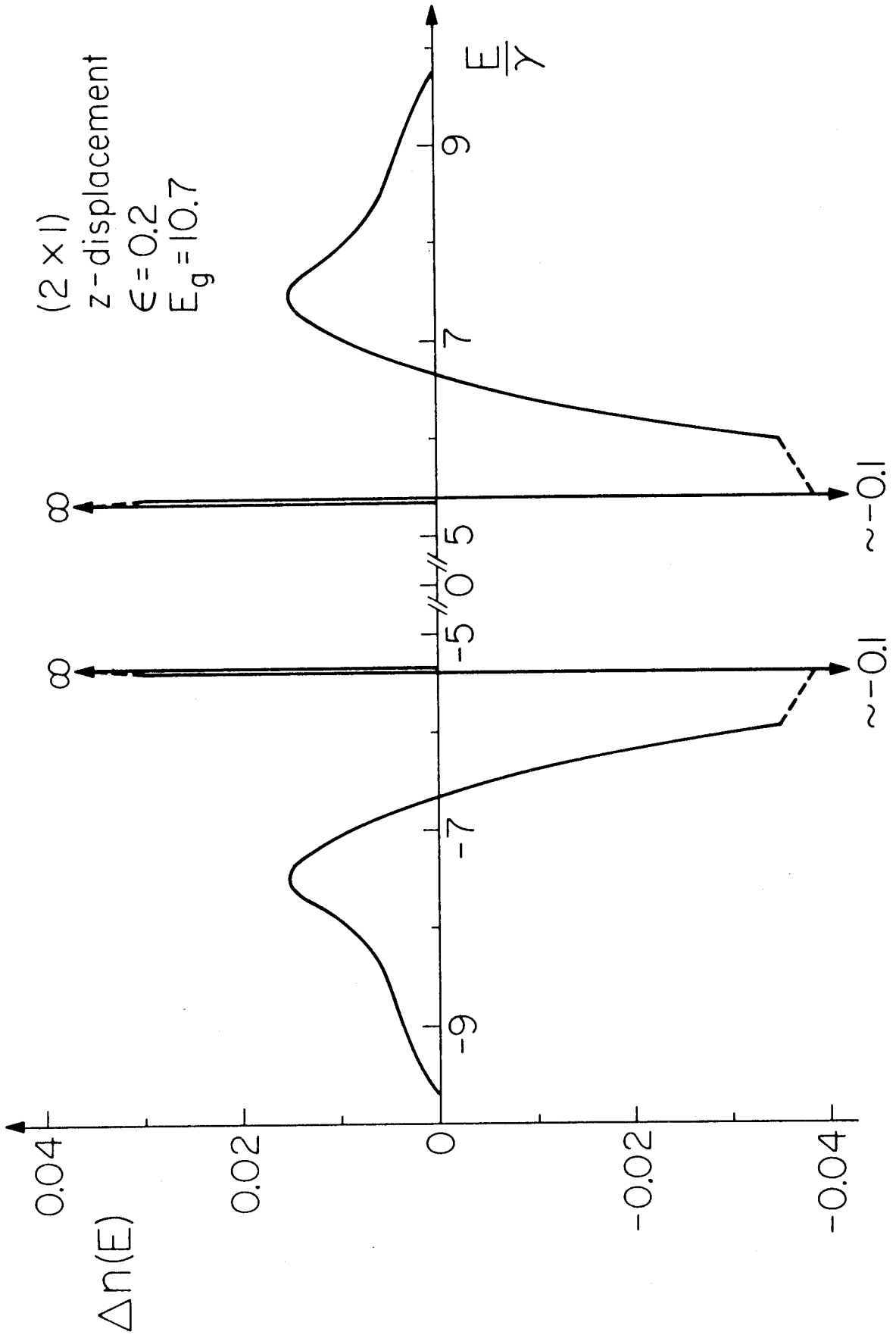


Figure 6

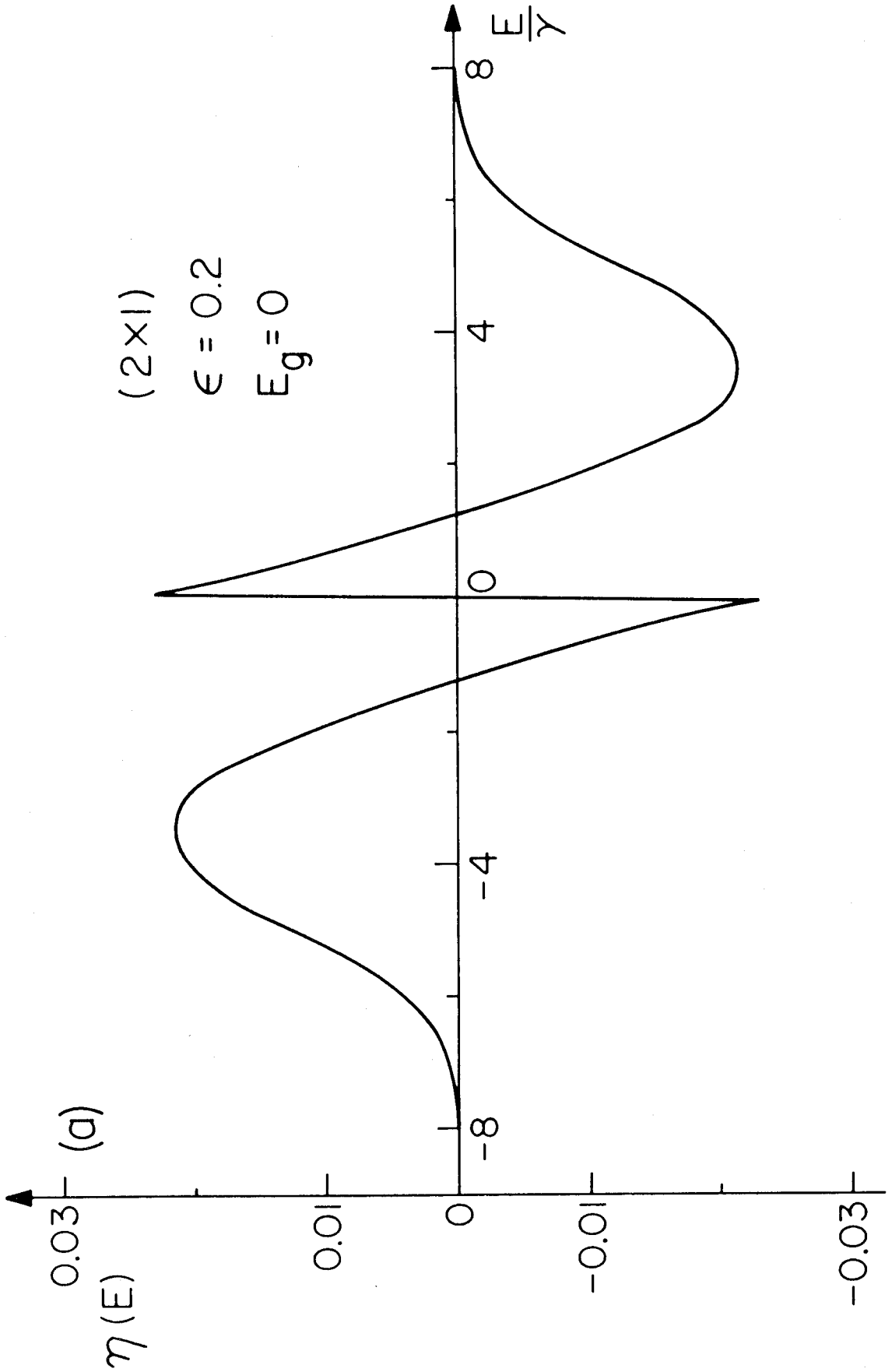


Figure 7 (a)

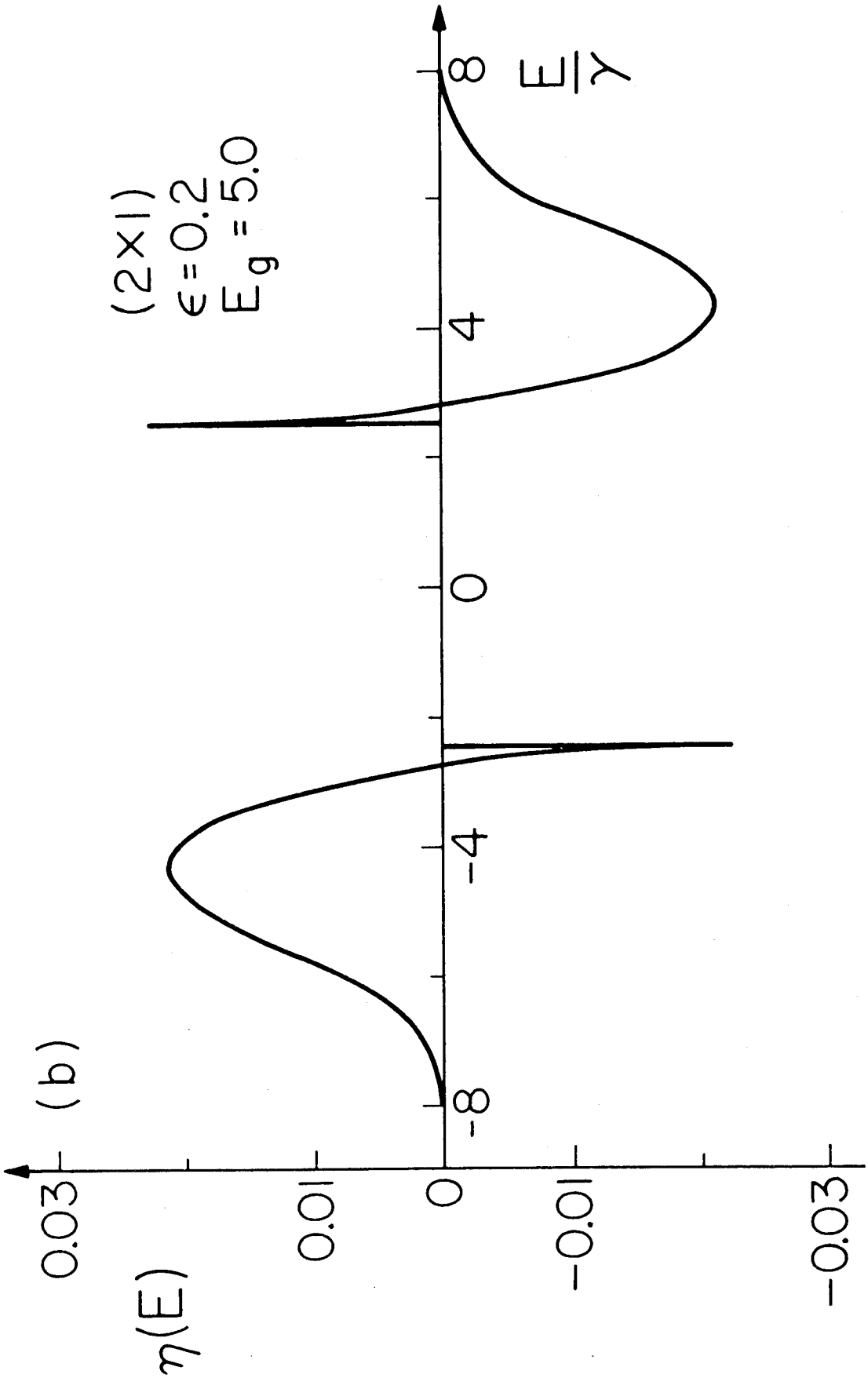


Figure 7 (b)

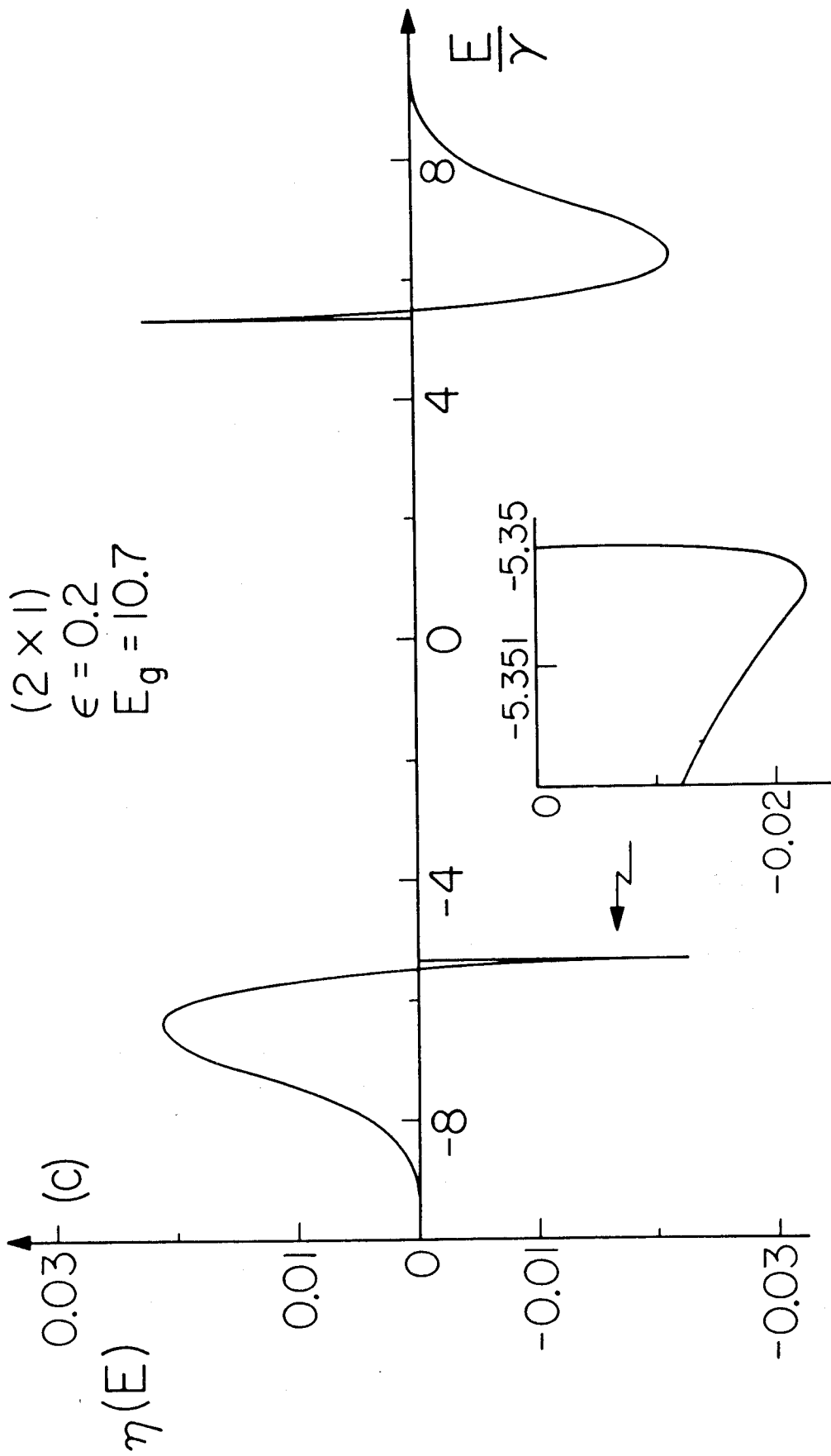


Figure 7 (c)

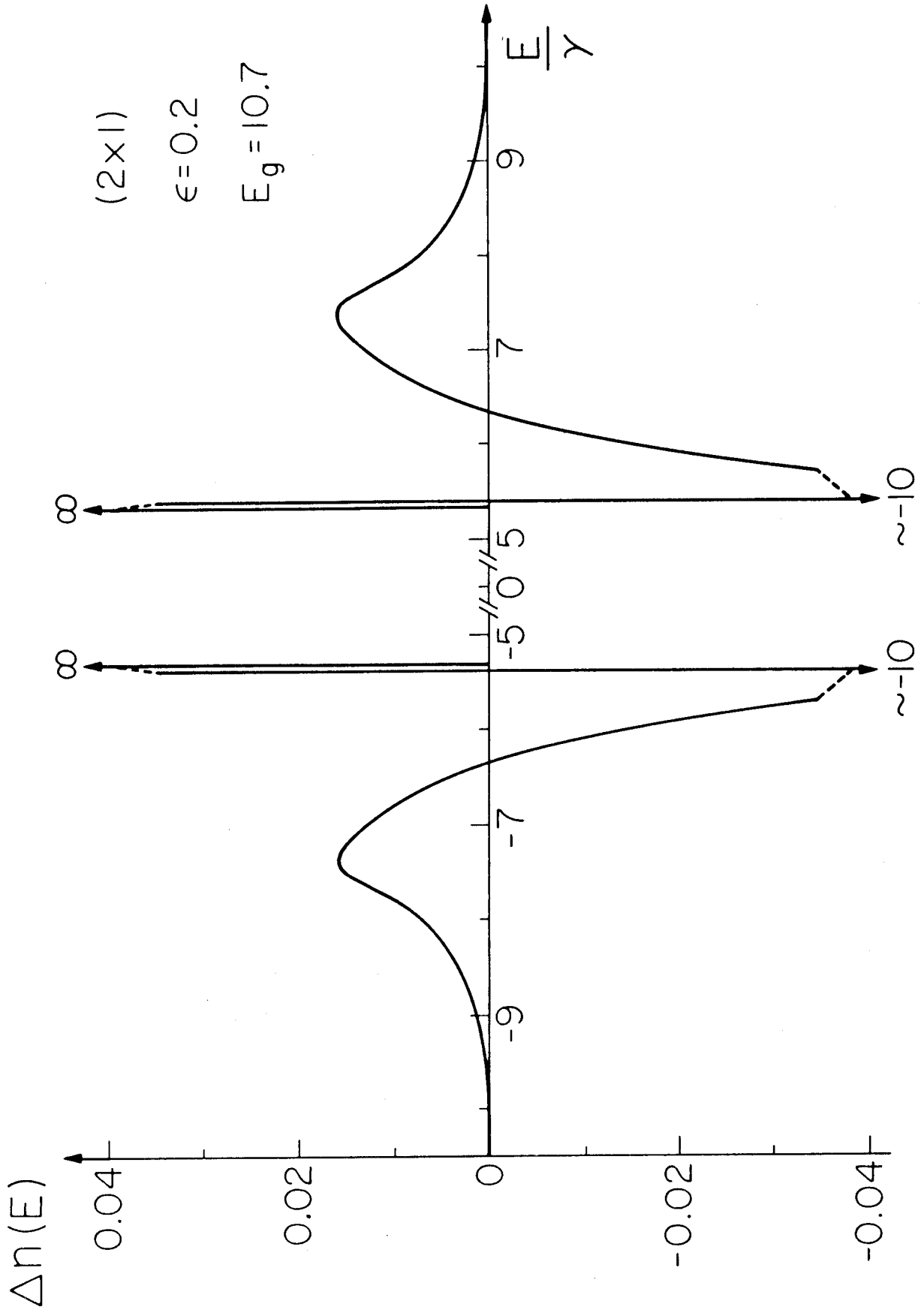


Figure 8

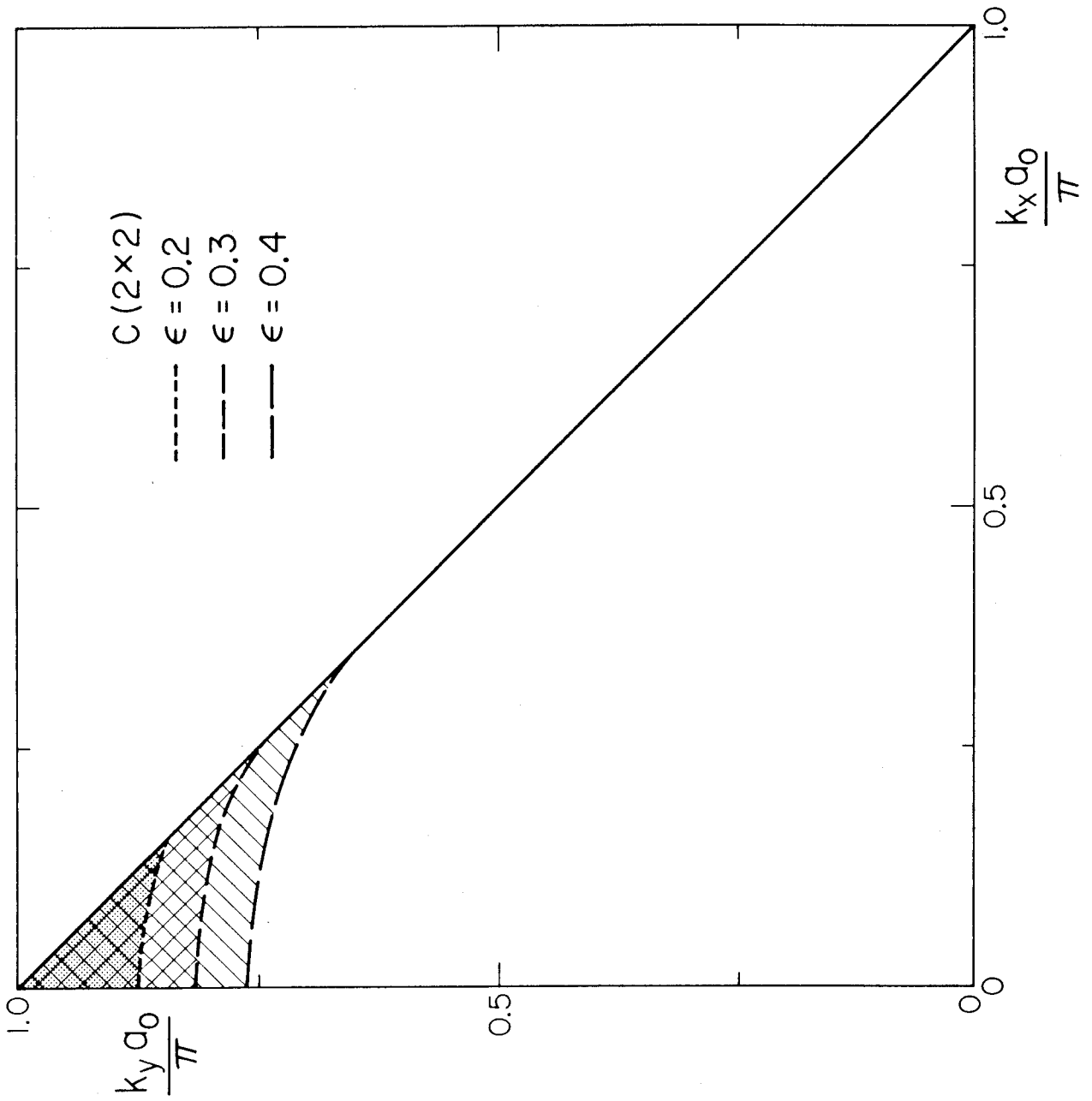


Figure 9

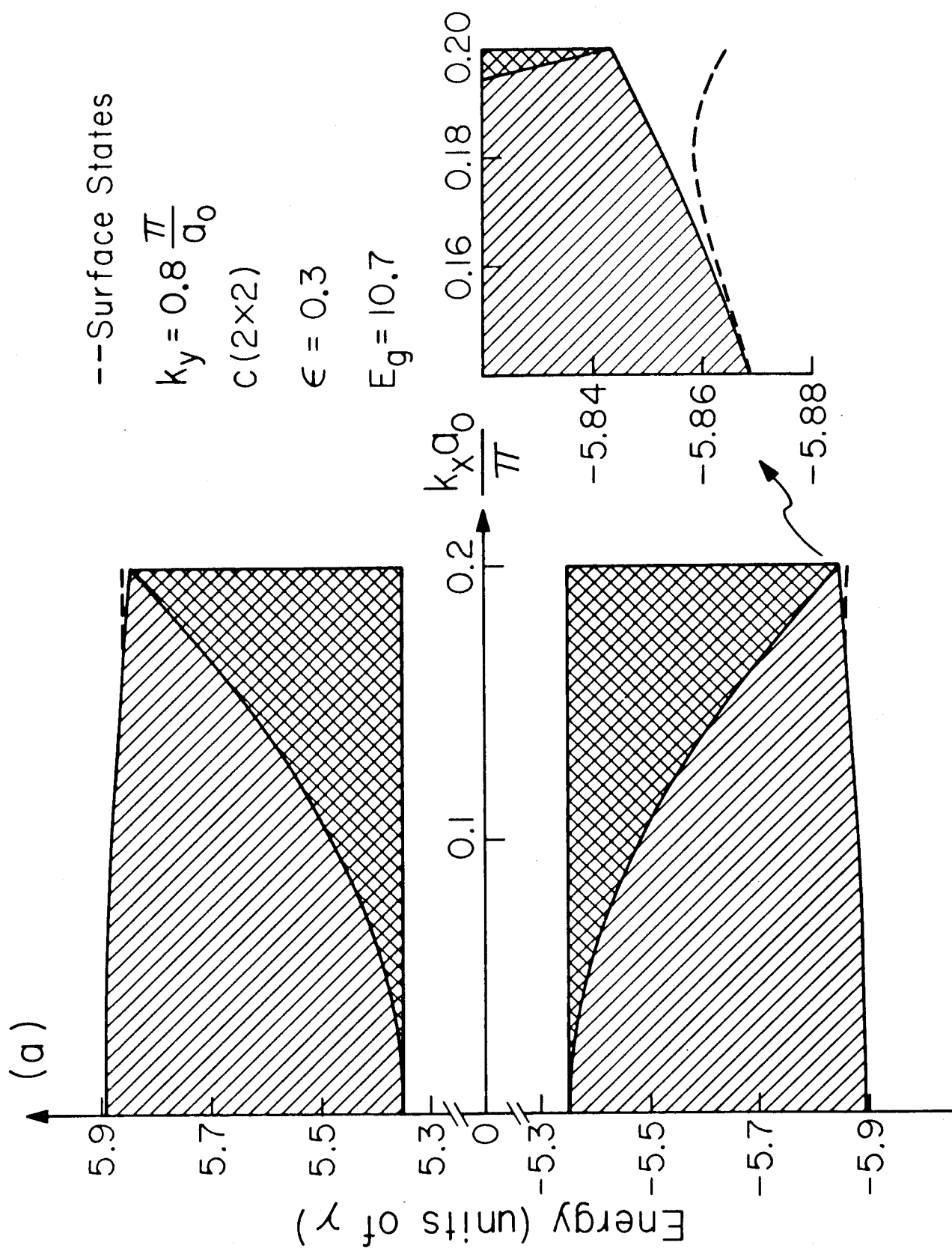


Figure 10 (a)

(b)

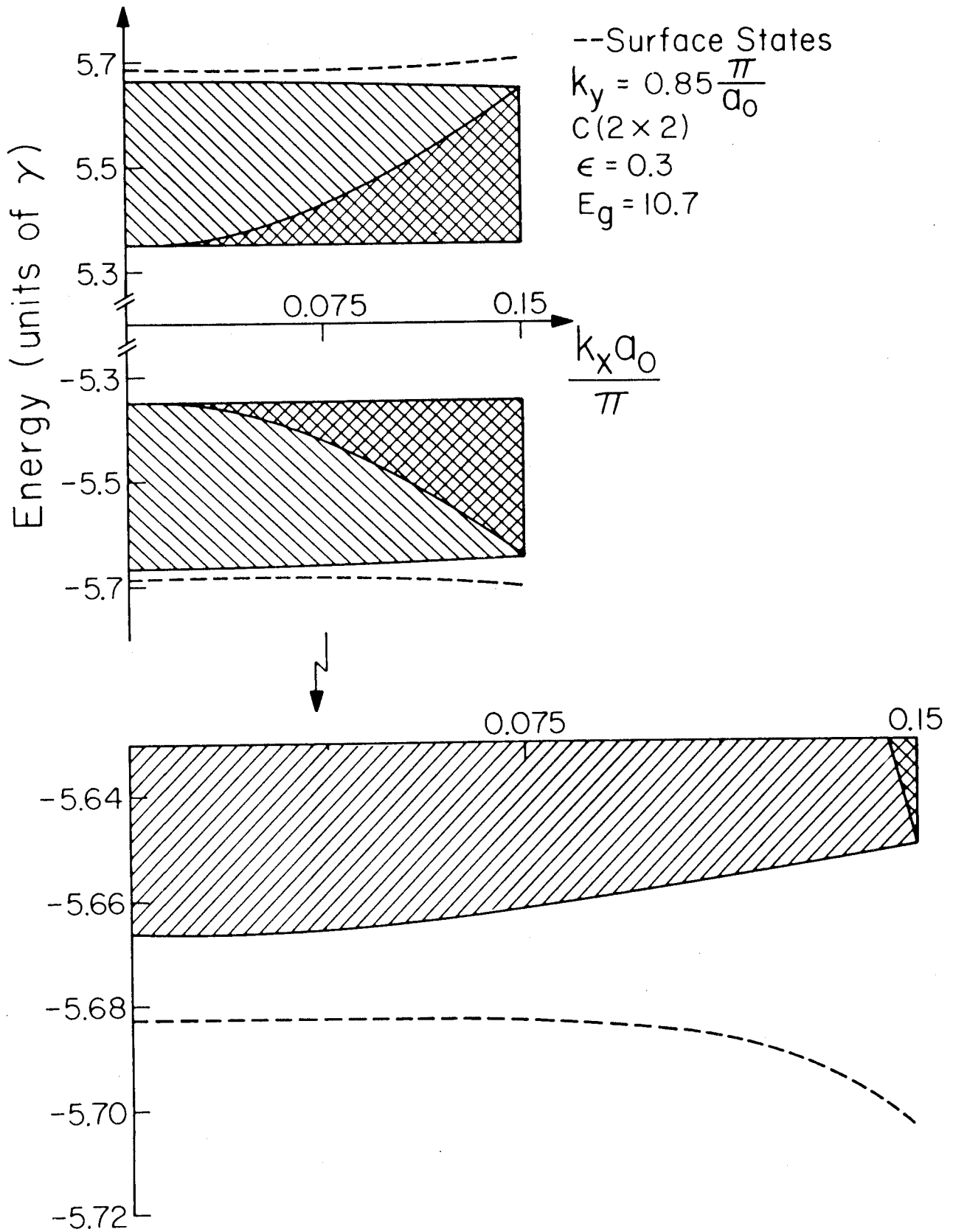


Figure 10 (b)

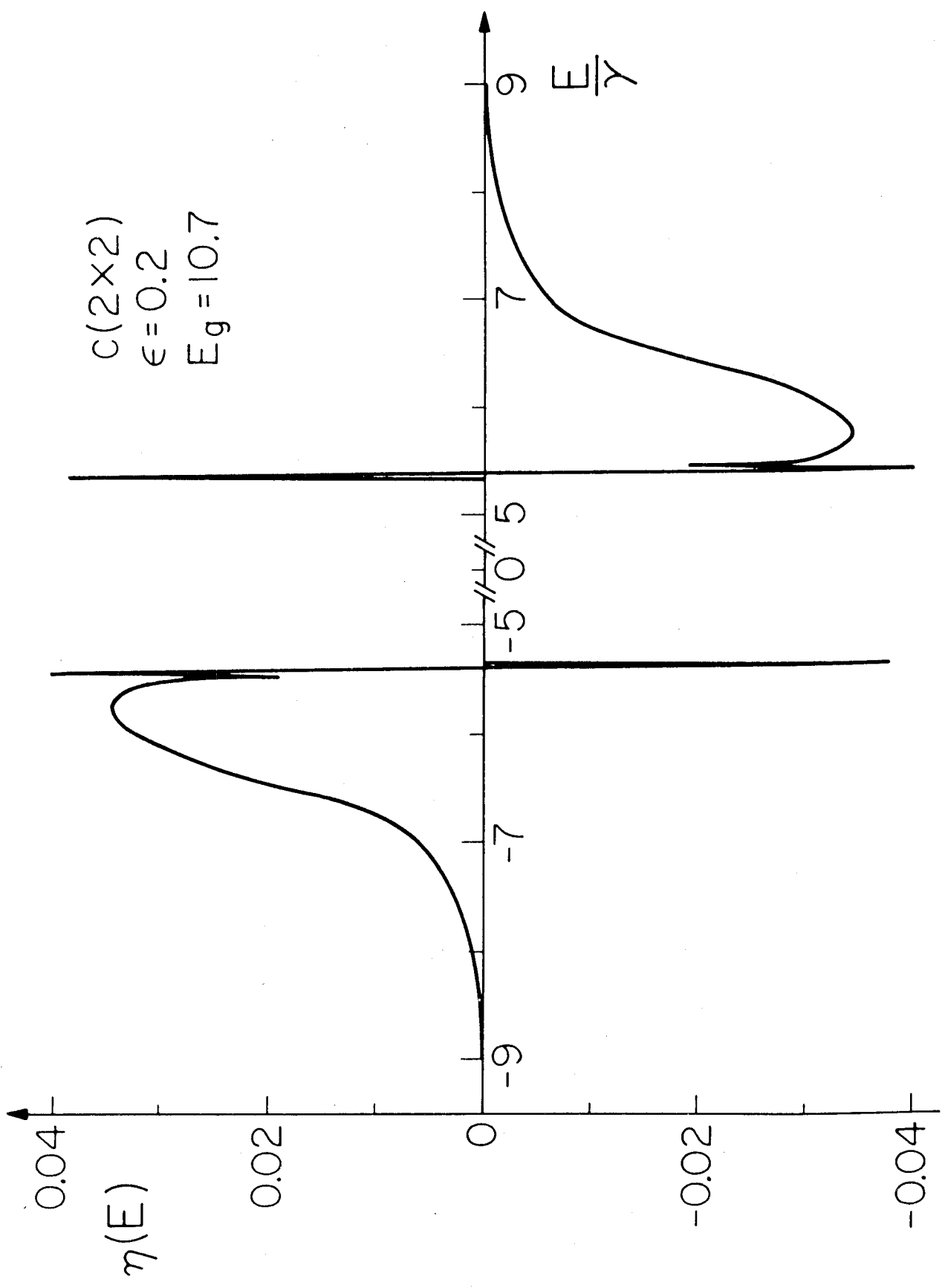


Figure 11

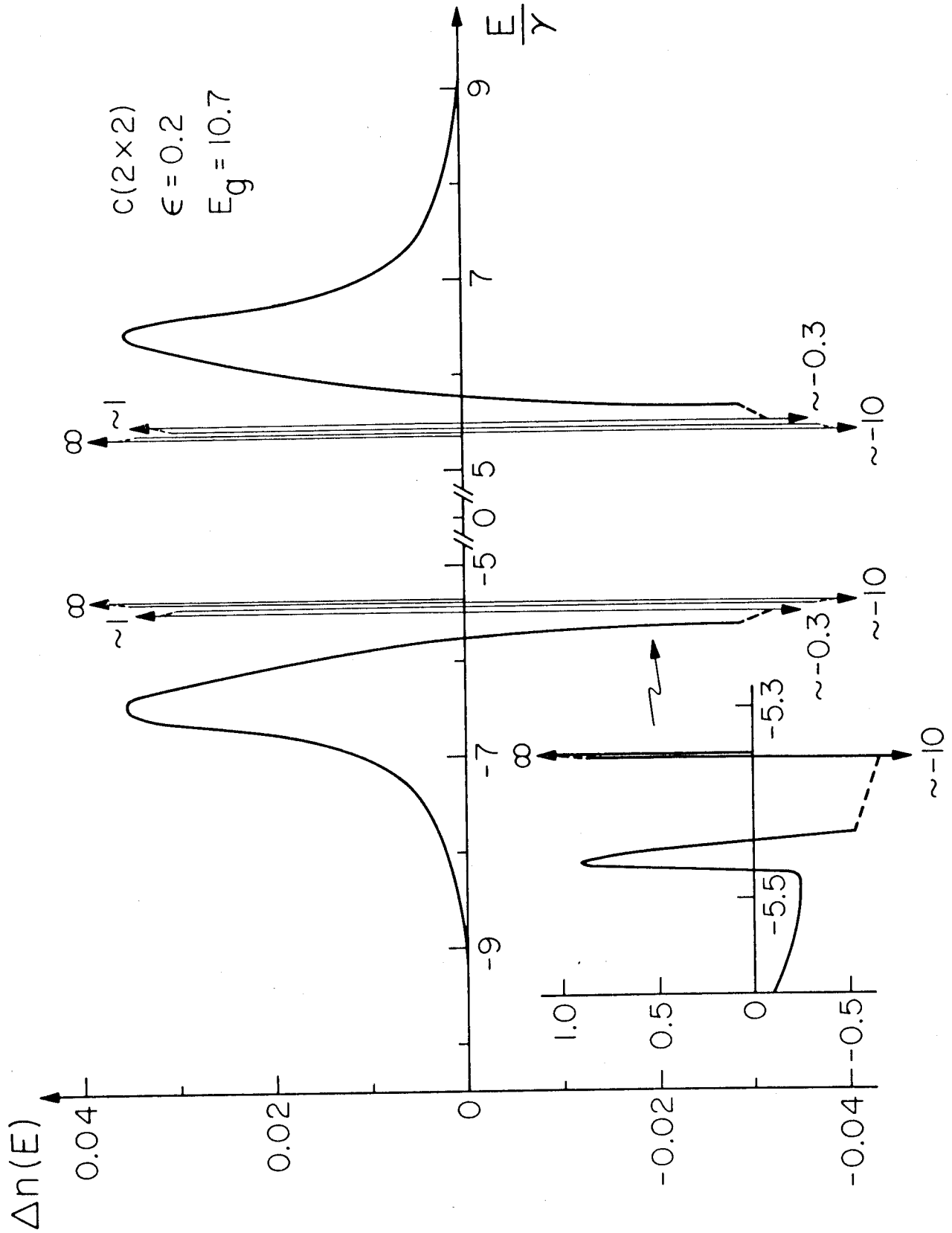


Figure 12

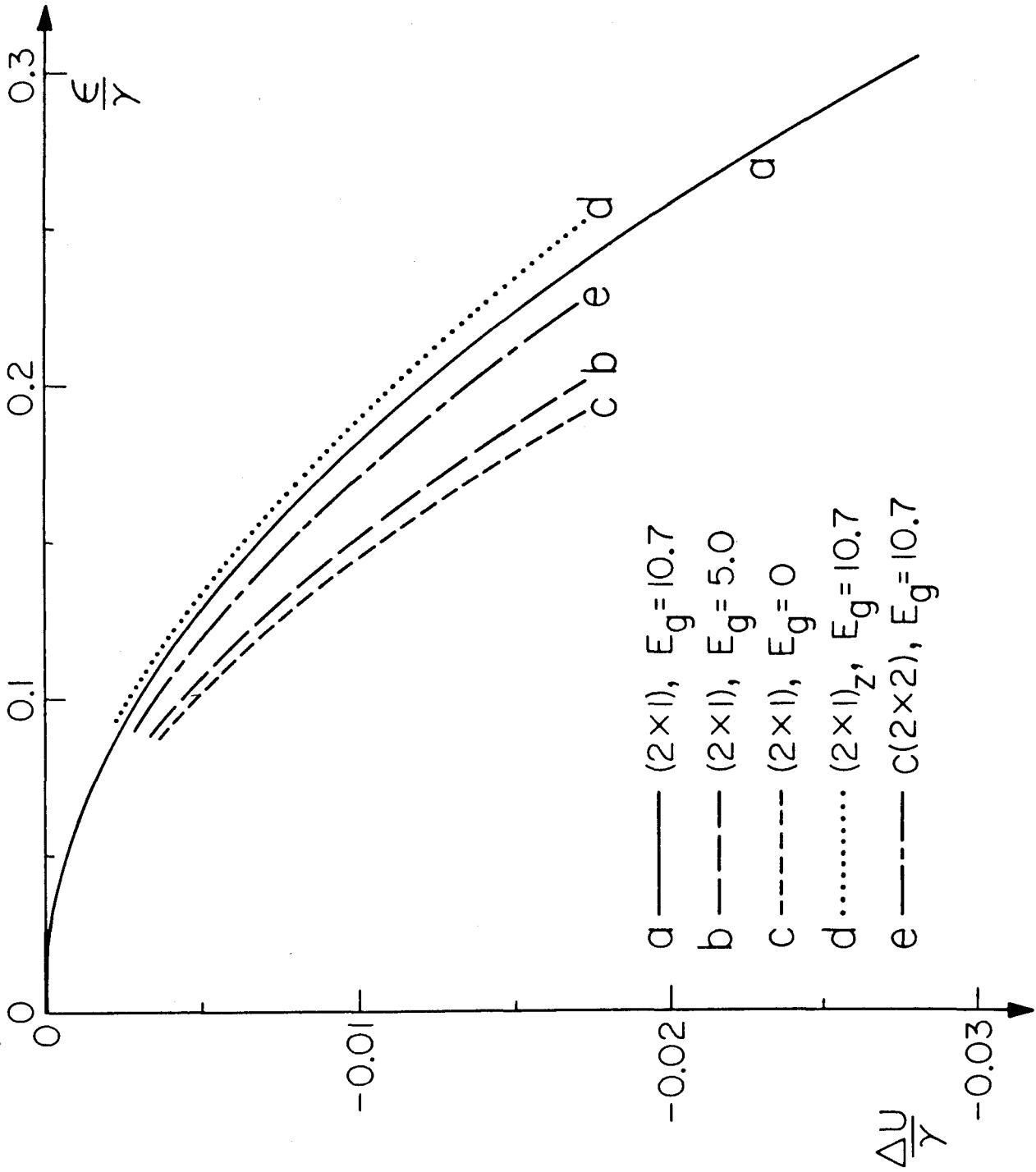


Figure 13

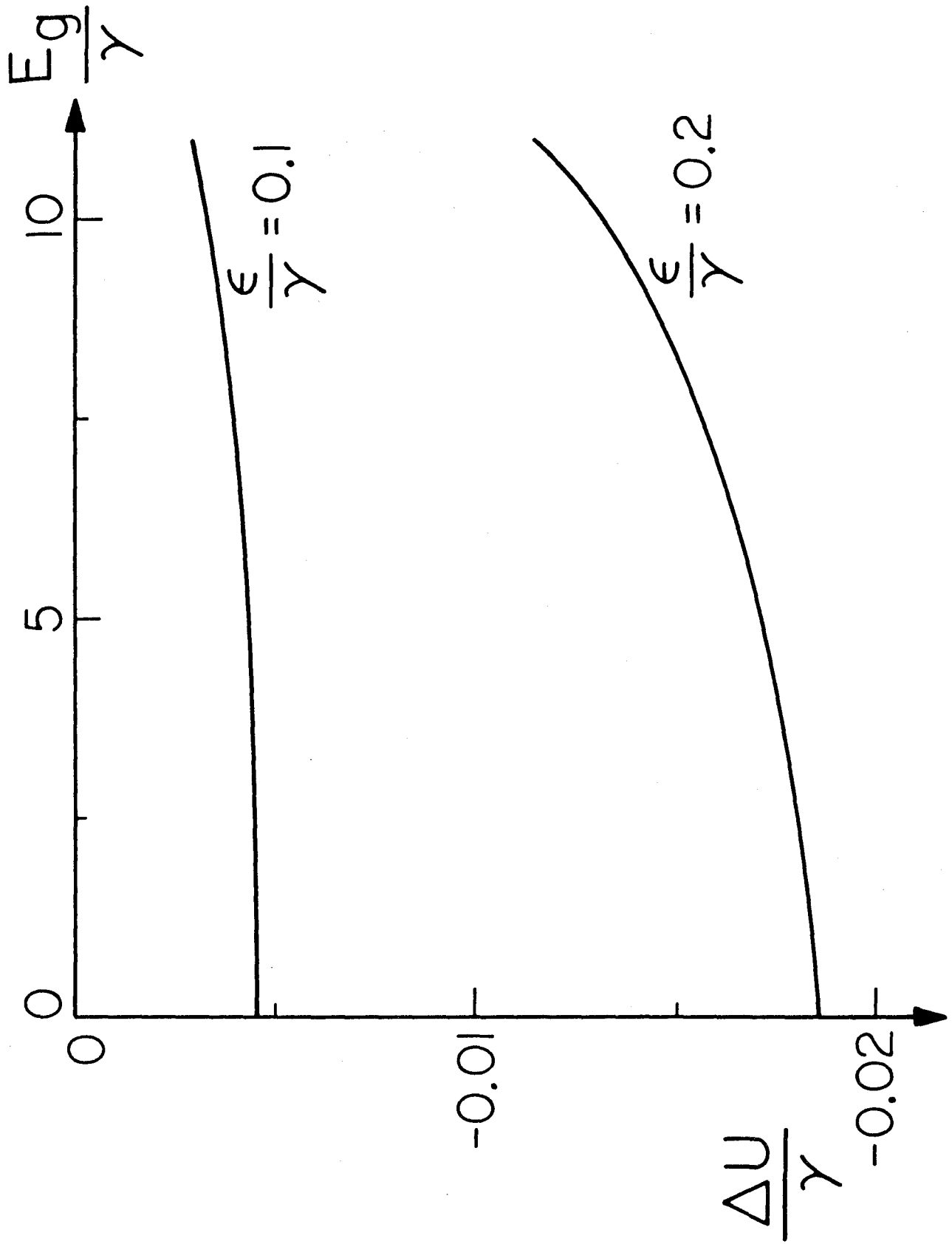


Figure 14

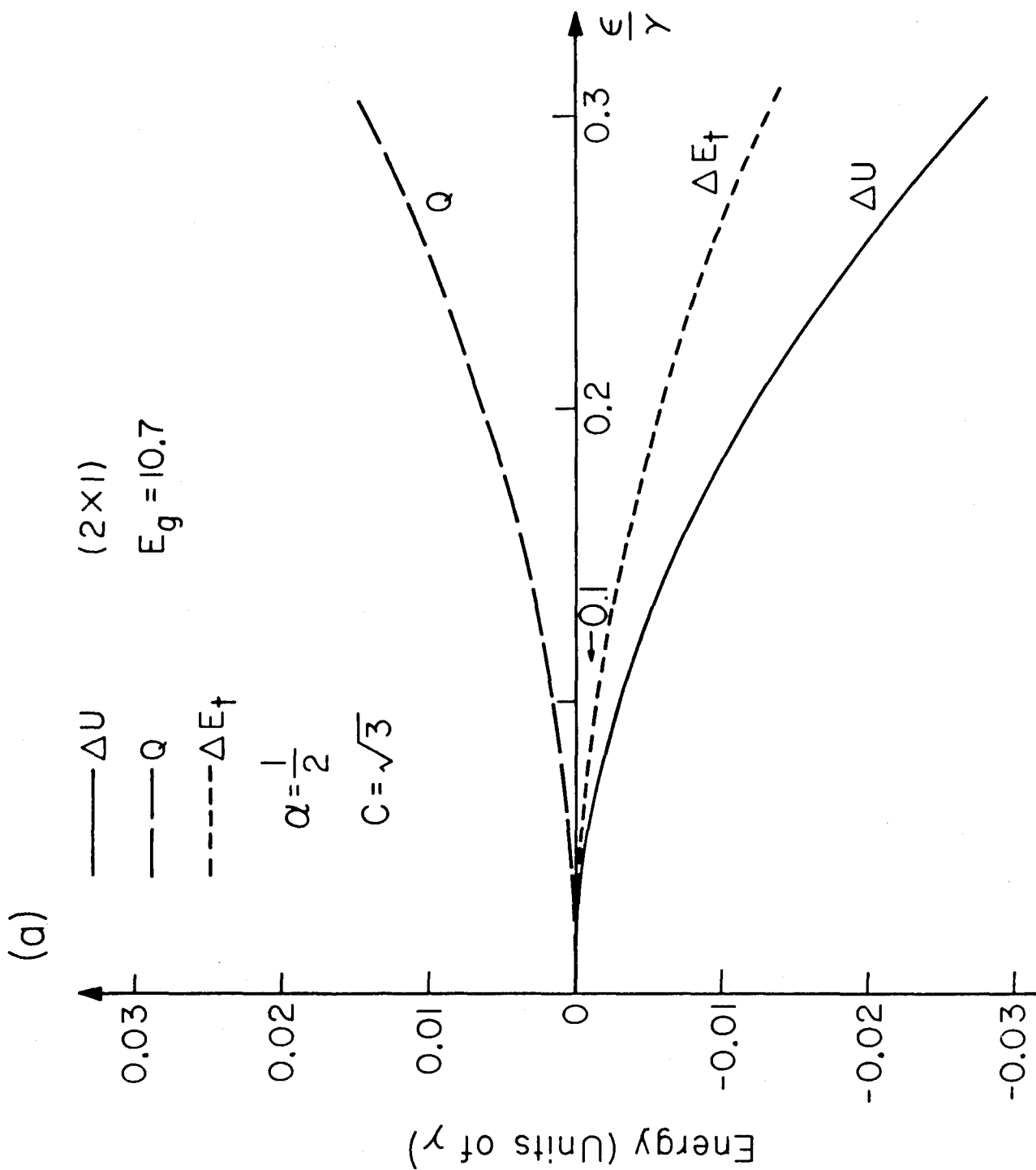


Figure 15 (a)

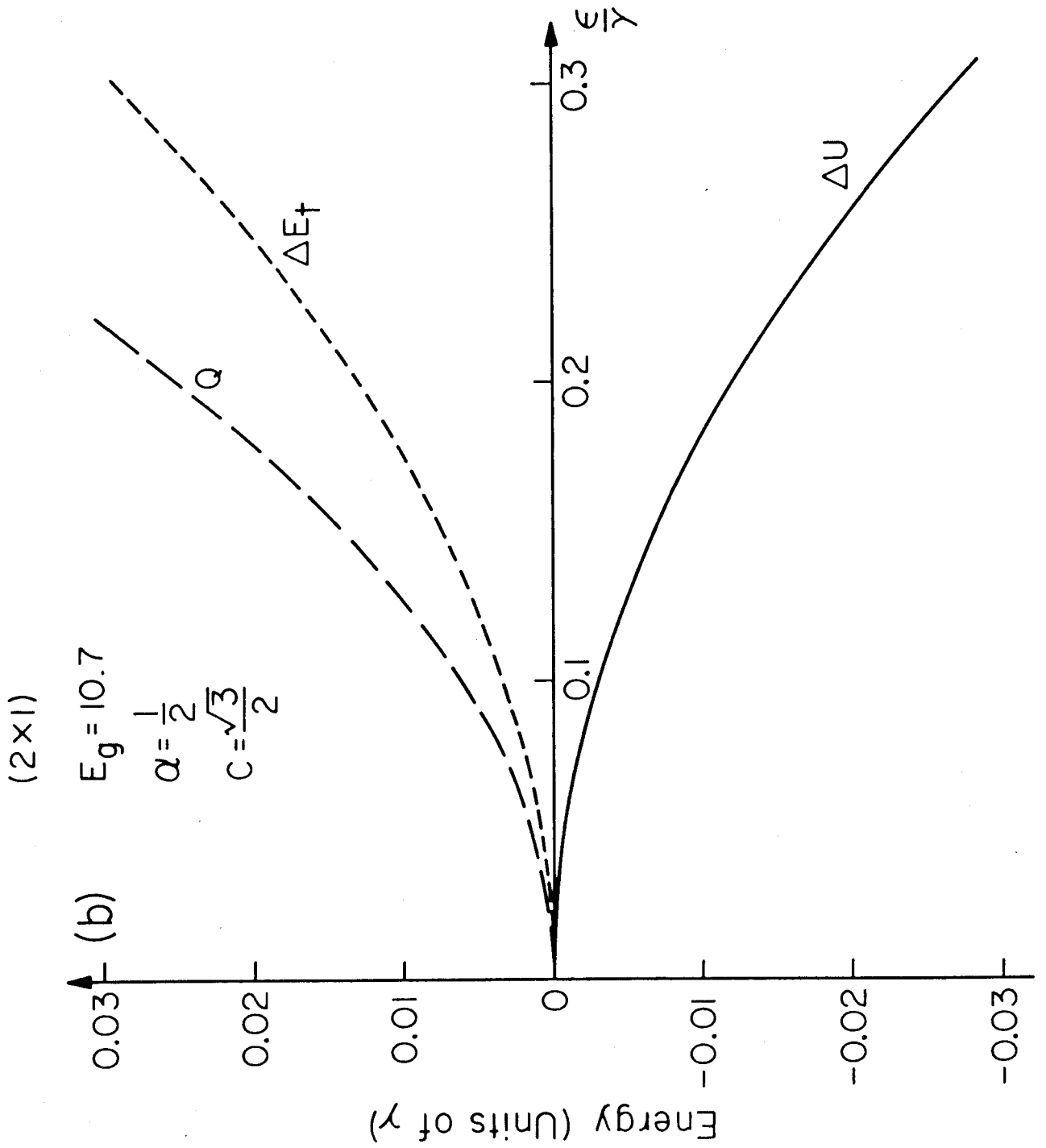


Figure 15 (b)

CHAPTER IV

SINGLE ATOM CHEMISORPTION ON A BCC METAL

SINGLE ATOM CHEMISORPTION ON A BCC METAL[†]

W. Ho, S. L. Cunningham* and W. H. Weinberg

Division of Chemistry and Chemical Engineering
California Institute of Technology
Pasadena, California 91125

June, 1975

To be Submitted to Surface Science

[†] Work partially supported by NSF Grant GK-43433

* IBM Postdoctoral Research Fellow

ABSTRACT

The effect of chemisorption of a single atom on the (001) surface of a bcc metal is investigated via the Green's function and the phase shift techniques using the LCAO method and the tight-binding approximation. In particular, we obtain the change in the electronic density of states $\Delta\tilde{n}$ due to two different binding sites, the on-site and the centered fourfold-site. For each site, the adatom energy level E_a is set both inside and outside the band and several adatom-substrate interaction strengths σ are considered. By varying these parameters we obtain a qualitative understanding of the effects on $\Delta\tilde{n}$ due to either the adsorption of different atoms or a readjustment of E_a arising from a flow of charge onto or away from the adsorbed atom. We compare our results to previous studies of chemisorption on the (001) surface of an s-band simple cubic crystal and find that the overall qualitative features are similar.

I. Introduction

The theory of chemisorption constitutes a formidable many-body problem. A fundamental understanding of the process would require an extensive treatment of the interaction of the electrons in the semi-infinite crystal and those in the adsorbed molecules. Lacking such a theory, much insight and understanding can be gained through simpler model calculations. In this paper, we use the Linear Combination of Atomic Orbitals (LCAO) method and the tight-binding approximation to study the effect of single atom chemisorption on the electronic structure of a semi-infinite crystal. We obtain, via the Green's function technique, the change in the density of states due to the interaction of the adatom with the surface. Such properties have been observed experimentally by photoemission.⁽¹⁾

In our model, the semi-infinite crystal is described by a one-electron Hamiltonian, and the adatom interacts with the nearest-neighbor surface atoms with a strength σ . We do not include explicitly the coulomb interaction between the electrons in the solid and on the adatom. Any redistribution of the electrons due to a change in potential energy around the adatom can be partially accounted for by a readjustment of the orbital energy E_a of the adatom in its free state. The amount of change can be solved for self-consistency to satisfy Friedel's sum rule.⁽²⁾ In the Anderson model,⁽³⁾ the occupancy of the adatom orbital is solved for self-consistency, and the resulting coulomb interaction redefines E_a . This shift in the orbital energy does not affect qualitatively our results since we place E_a in several different locations, both inside and outside the energy band. This will become clearer in section III. For a complete account of the current theories in chemisorption, there exist several recent reviews on the subject.⁽⁴⁾

In order to study chemisorption, the electronic wave function of a solid with a surface must be known. Assuming the tight-binding approximation, we generate the energy levels and the associated wave functions using the LCAO formalism for the (001) surface of a bcc metal. A complete description of this surface has been given elsewhere.⁽⁵⁾ There, we obtained the Green's functions appropriate for the (001) surface with only the nearest neighbor interaction γ in the solid being considered. In this present work, the adatom energy level is assumed to be a nondegenerate delta function at energy E_a . The adatom is coupled to the surface atoms with a binding strength σ . The interaction is treated by a perturbation method.

The approach taken here has been used by Allan⁽²⁾ in obtaining the binding energy of single transition metals adsorbed on the (001) surface of tungsten, simulated by a fivefold degenerate s-band simple cubic crystal. Self-consistency is treated both in the adatom and the surface atom directly bonded to it in order to satisfy Friedel's sum rule. More recently, Einstein and Schrieffer⁽⁶⁾ have extended the method to study the indirect interaction between two adatoms on the (100) surface of a simple cubic metal. The adatom energy is fixed just below the center of the band. Three different binding positions, the on-site, the bridge-site, and the centered fourfold-site, are considered. The binding energies for single atom adsorption are obtained as a function of the filling of the energy band for different interaction strengths of the adatom with the surface atoms. Similar calculations are carried out to obtain the indirect interaction between two adatoms. The change in the electronic density of states due to chemisorption on the (100) s-band simple cubic crystal has been studied both by Davenport, Einstein and Schrieffer⁽⁷⁾ and by Einstein.⁽⁸⁾ Only the on-site adsorption is considered.

The perturbation of the density of states is found to diminish rapidly away from the adatom-surface atom complex and oscillates rapidly, as it should for an indirect interaction through the substrate electrons.

There are four reasons for carrying out the present calculation on the change in the density of states due to chemisorption on the (001) bcc crystal. First, it constitutes a test of the sensitivity of the results to the different substrate crystal structures. Second, it investigates the effect of different binding sites on the change in the density of states. Third, within the same model, the calculation can be easily extended to a single atom adsorbate on the (001) surface of a two-band crystal with the CsCl structure. The interaction of the adatom level with the second (conduction) band can be studied, and its importance can be assessed. The adatom level can now be fixed inside the band gap, in addition to being inside the bands or above or below the conduction and the valence bands, respectively. Finally, a simple modification of the present theory can be made to study the adsorption of a monolayer of atoms on the same surface with or without a band gap. Even if there is no direct interaction between the adatoms, the indirect interaction through the substrate electrons is present. Other effects can arise in addition to the sum of the individual adatom effects. The present calculation will then be important as a basis for comparison. Such calculations are in progress.

Two binding sites, the on-site and the centered fourfold-site, are considered in the present calculation. For each binding site, the adatom energy level is set at three different values, one just below the middle of the band, one near the bottom of the band and one below and outside the band. For each position of the adatom level, the change in the density of states

is calculated for several different adatom-substrate interaction strengths. The same interaction strengths are used for both binding sites, allowing us to compare the two results with the same parameters. Since the adatom-substrate interaction σ depends on the distance of the adatom from the surface, by varying σ , we have in fact studied the change in the density of states as the adatom position varies in the direction perpendicular to the surface.

In section II, we present briefly the perturbation method used in the calculation. The method is quite general and can be used to study a variety of surface problems, such as the electronic structure of the clean surface⁽⁵⁾ and surface reconstruction.⁽⁹⁾ The practicality of the method depends on knowing the Green's functions analytically. As such, it has been limited to date to simple model systems. In section III, we present the calculations and results for the on-site adsorption, and in section IV, those for the centered fourfold-site adsorption. We summarize our results in section V.

II. General Formalism

In order to derive the Green's functions appropriate for the (001) surface of a bcc metal, we need to know first the infinite crystal (bulk) Green's functions. Assuming only nearest-neighbor interactions, the energy band calculated within the LCAO formalism and the tight-binding approximation is given by

$$E_{\vec{k}} = \pm 8\gamma \cos \frac{\phi_x}{2} \cos \frac{\phi_y}{2} \cos \frac{\phi_z}{2} , \quad (1)$$

where

$$\vec{\phi} = \vec{k} a_0 , \quad (2)$$

γ is the nearest-neighbor hopping integral and a_0 is the crystal lattice spacing. The energy band appropriate for the surface is obtained by sweeping ϕ_z over its possible values in the first Brillouin zone. In Fig. 1, we show the energy band along a particular segment at a constant value of k_y in the surface Brillouin zone (SBZ). The zero of energy is chosen to be at the orbital energy of the substrate atoms in their free states, and all energies are expressed in units of the nearest-neighbor hopping integral γ . There is a continuum of states inside the band. From the eigenvalues and eigenfunctions, the bulk Green's functions $G^{(0)}$ are generated within this one-electron picture as has been done previously.⁽⁵⁾

We then create the (001) surface by passing an imaginary plane perpendicular to the z-axis. The Hamiltonian of the system becomes

$$H = H_0 + V \quad , \quad (3)$$

where H_0 is the infinite crystal Hamiltonian and V is the perturbation associated with the creation of the surface, i.e., breaking the bond γ . The (001) surface Green's functions have been obtained⁽⁵⁾ from the bulk Green's functions through the perturbation V by

$$G = G^{(0)} + G^{(0)}VG \quad . \quad (4)$$

Once the Green's functions are known,⁽⁵⁾ the shift in the energy levels caused by the perturbation can be studied by the phase shift technique.⁽¹⁰⁾ To understand the effect of surface formation,⁽⁵⁾ the phase shift function is given by

$$\eta = -\arg \det(I - VG^{(0)}) \quad , \quad (5)$$

where I is the identity matrix. In the case of chemisorption, the perturbation is associated with the formation of chemical bonds between the adatom and the substrate. Thus, we can define a phase shift function for chemisorption by

$$\eta = -\arg \det(I - \bar{V}\bar{G}) \quad , \quad (6)$$

where \bar{V} is the interaction matrix and \bar{G} is the Green's function appropriate for the adatom and substrate. As shown later, \bar{G} is composed of G and the adatom Green's function G_a given by

$$\begin{aligned} G_a(E) &= \langle \phi_a \left| \frac{1}{E - H_a + i\epsilon} \right| \phi_a \rangle \\ &= \frac{1}{E - E_a + i\epsilon} \quad , \end{aligned} \quad (7)$$

where ϕ_a and H_a are the adatom orbital and Hamiltonian, respectively, in the free state, and ϵ is a positive infinitesimal. Once the phase shift functions are known, the change in the density of states is given by a simple differentiation,

$$\Delta n = \frac{1}{\pi} \frac{d\eta}{dE} \quad . \quad (8)$$

The surface Green's functions for a two-band crystal with the CsCl structure are derived in a previous paper⁽⁵⁾ on the study of the electronic structure of the clean surface. By setting the band gap equal to zero in that work, we obtain the (001) surface Green's functions for a bcc metal. These functions are given by

$$G(\ell_z) = JE(1 - t^{\frac{2\ell_z - 1}{z}}) \quad , \quad \ell_z \geq 1 \quad (9)$$

for odd numbered planes with the surface plane chosen arbitrarily to be the first plane, and $l_z \geq 1$ for the semi-infinite crystal. For even numbered planes, the Green's functions for a crystal with a surface are given by

$$G(l_z) = JE(1 - t^{2l_z}), \quad l_z \geq 1. \quad (10)$$

The symbols in Eqs. (9) and (10) are defined by

$$J = \frac{2t}{B(t^2 - 1)}, \quad (11)$$

$$t = \begin{cases} \xi - (\xi^2 - 1)^{1/2} & , \quad \xi > 1 \\ \xi + i(1 - \xi^2)^{1/2} & , \quad |\xi| < 1 \\ \xi + (\xi^2 - 1)^{1/2} & , \quad \xi < -1 \end{cases}, \quad (12)$$

where

$$\xi = \frac{E^2 - 2f^2}{2f^2}, \quad (13)$$

$$f = 4\gamma \cos \frac{\phi_x}{2} \cos \frac{\phi_y}{2}, \quad (14)$$

$$B = -2f^2, \quad (15)$$

and where $\text{Im } t$ is to be interpreted as $-\text{sign}(E) \text{Im } t$, and l_z labels the unit cells in the z -direction (perpendicular to the surface).

For the surface plane of atoms, the Green's function takes on a simple form,

$$G_S(\vec{\phi}_S, E) = \frac{Et}{f^2(t + 1)}, \quad (16)$$

where $\vec{\phi}_S$ is the component of the vector $\vec{\phi}$ parallel to the surface. In the case of single atom adsorption, the appropriate Green's function to use is the total Green's function defined by^(2,6)

$$G^{ij}(E) = \frac{1}{N_s} \sum_{\vec{\phi}_s} G_s(\vec{\phi}_s, E) e^{i \frac{\vec{\phi}_s}{a_0} \cdot \vec{R}_{ij}} , \quad (17)$$

where N_s is the number of surface unit cells, and

$$\vec{R}_{ij} = i a_0 \vec{e}_x + j a_0 \vec{e}_y , \quad (18)$$

where \vec{e}_x and \vec{e}_y are unit vectors in the x and y directions, respectively.

An origin is chosen at an arbitrary surface atom. In actual calculations, the sum in Eq. (17) is converted into an integral

$$G^{ij}(E) = \frac{1}{(2\pi)^2} \int_{-\pi}^{\pi} d\phi_y \int_{-\pi}^{\pi} d\phi_x G_s(\vec{\phi}_s, E) e^{i \frac{\vec{\phi}_s}{a_0} \cdot \vec{R}_{ij}} . \quad (19)$$

With this background, the single atom chemisorption can be easily formulated.

We first present the on-site adsorption.

III. On-Site Adsorption

The geometry for the on-site adsorption is shown in Fig. 2. The adatom is assumed to interact directly only with the single substrate atom located beneath it. The on-site Green's function is given by

$$G_T(E) = \frac{1}{(2\pi)^2} \int_{-\pi}^{\pi} d\phi_y \int_{-\pi}^{\pi} d\phi_x G_s(\vec{\phi}_s, E) , \quad (20)$$

This integral is evaluated by summing over a set of special points in the

SBZ.⁽¹¹⁾ The real and imaginary parts of G_T are shown in Fig. 3. The

imaginary part is related to the local density of states for the first plane of atoms through

$$\rho(E) = -\frac{1}{\pi} \text{Im } G_T(E) . \quad (21)$$

The Green's function matrix for the adatom-substrate system is given by

$$\bar{G}_T(E) = \begin{pmatrix} G_T(E) & 0 \\ 0 & G_a(E) \end{pmatrix}. \quad (22)$$

Since we include only the direct interaction σ of the adatom with the substrate atom beneath it, the perturbation matrix is (2x2) and becomes

$$\bar{V}_T(E) = \begin{pmatrix} 0 & \sigma \\ \sigma & \delta V_a \end{pmatrix}, \quad (23)$$

where δV_a takes into account the change in the adatom orbital energy. In the Anderson model,⁽³⁾ this shift in energy is due to a coulomb interaction term where the occupation number of the electrons in each spin direction is solved self-consistently for the adatom orbital. In a separate approach, δV_a is solved self-consistently in order to satisfy Friedel's sum rule.⁽²⁾ Both methods simulate the response of the adatom to its coupling to the substrate.

The phase shift function is given by

$$\begin{aligned} \eta_T(E) &= -\arg \left[1 - \delta V_a G_a(E) - \sigma^2 G_a(E) G_T(E) \right] \\ &= -\tan^{-1} \left[\frac{-\sigma^2 \text{Im} G_T(E)}{E - (E_a + \delta V_a) - \sigma^2 \text{Re} G_T(E)} \right]. \end{aligned} \quad (24)$$

From Eq. (24), we can redefine E_a by

$$E'_a = E_a + \delta V_a. \quad (25)$$

Hence, by setting E_a at different places, inside and outside the bands, we

do in fact obtain the effect of δV_a on the qualitative results. In our calculations, δV_a is set equal to zero.

Then change in the density of states is given by Eqs. (8) and (24). It is the difference in the density of states of the adatom-substrate system from that of the clean semi-infinite crystal plus the free atom. Instead, following Davenport, Einstein and Schrieffer,^(6,7) we plot the difference in the density of states between the adatom-substrate system and the clean substrate, i.e.,

$$\Delta\tilde{n}(E) = \Delta n(E) + \delta(E - E_a) \quad . \quad (26)$$

In Fig. 4, we present the results with E_a set at $-\gamma$ for three values of σ . The overall qualitative features are similar to the s-band simple cubic crystal results. For $\sigma = \gamma$, the adatom energy level interacts with the substrate band resulting in bonding and antibonding resonances below E_a and above $E = 0$, respectively. For $\sigma = 6\gamma$, these two peaks approach the band edges. For a still larger interaction ($\sigma = 9\gamma$), these peaks split off the bands and become delta functions at energies given by

$$E - E_a - \sigma^2 \text{Re}G_T(E) = 0 \quad (27)$$

All these results are qualitatively obtained with the s-band simple cubic model. However, there is one essential difference which is due to the difference in the underlying substrate crystal band structure. For the bcc crystal, there is a divergence in the bulk density of states at $E = 0$. As a result, a decrease in the density of states near $E = 0$ is always present for arbitrarily small σ . For large values of σ , rather than a smooth energy independent $\Delta\tilde{n}$ inside the band, there are sharp dips near $E = 0$. Such dips

do not occur in the simple cubic crystal results.

In Fig. 5, we show the results with $E_a = -6\gamma$. For $\sigma = \gamma$, we obtain the bonding and antibonding resonances with the dip below $E = 0$. As σ increases, the bonding resonance splits off first, while the antibonding resonance approaches the top band edge and eventually splits off. At $\sigma = 9\gamma$, the antibonding resonance assumes a sharp peak just below the top band edge. Again, we see the large dips near $E = 0$. In Fig. 6, we place E_a below the band at -10γ . In this case, the bonding state is always below the band. The antibonding peak first broadens and then sharpens as it approaches the top band edge for increasing values of σ .

For the cases we have considered, $\Delta_{n_T}^{\sim}$ has a quite smooth and predictable behavior. The positions of the split off states, when they exist, are given by Eq. (27) and are presented in Table I.

IV. Centered Fourfold-Site Adsorption

The geometry for this type of adsorption is given in Fig. 7. The adatom is situated above the center of the surface unit cell and interacts directly with the four substrate atoms with a total strength of σ . The binding strength is assumed to be the same as in the case of on-site adsorption. The four substrate atoms can be considered collectively when the adatom binds to the surface. The orbitals localized on the substrate atoms which directly interact with the adatom can be combined symmetrically to represent the ground state wavefunction of the substrate.^(2,6) The centered Green's function G_c is then a sum of four total surface Green's functions and is given by

$$G_c(E) = G^{00}(E) + G^{10}(E) + G^{01}(E) + G^{11}(E) \quad , \quad (28)$$

where the superscripts indicate the coordinates of each atom. From Eq.

(17), we obtain

$$G_c(E) = \frac{1}{N_s} \sum_{\vec{\phi}_s} G_s(\vec{\phi}_s, E) \left[1 + e^{i\phi_x} + e^{i\phi_y} + e^{i(\phi_x + \phi_y)} \right] . \quad (29)$$

Since $G_s(\vec{\phi}_s, E)$ is an even function in ϕ_x and ϕ_y , the phase factors in Eq.

(29) reduce to a sum of cosines and Eq. (29) becomes

$$G_c(E) = \frac{4}{N_s} \sum_{\phi_x, \phi_y > 0} G_s(\vec{\phi}_s, E) [1 + 2 \cos \phi_x + \cos \phi_x \cos \phi_y] . \quad (30)$$

In Fig. 8, we present the imaginary and the real parts of G_c . In contrast to G_T , both $\text{Im}G_c$ and $\text{Re}G_c$ are continuous. This result has also been noted for the simple cubic crystal.^(2,12) On this basis, we would expect our results to be quite similar to those for the simple cubic crystal.

The Green's function matrix is given by

$$\bar{G}_c(E) = \begin{pmatrix} G_c(E) & 0 \\ 0 & G_a(E) \end{pmatrix} . \quad (31)$$

In order to evaluate the perturbation matrix, we assume that the total direct interaction of the adatom with the four immediate substrate atoms is σ . We then obtain

$$\bar{V}_c(E) = \begin{pmatrix} 0 & \sigma \\ \sigma & \delta V_a \end{pmatrix} . \quad (32)$$

Since \bar{G}_c and \bar{V}_c have the same form as \bar{G}_T and \bar{V}_T , we obtain the phase shift function $\eta_c(E)$ and the change in the density of states $\Delta\tilde{n}_c(E)$ by simply replacing the subscript T by c in Eqs. (24) and (26), respectively.

In Fig. 9, we present the results for $E_a = -\gamma$ and four different values of σ . The results are quite similar to those for the simple cubic crystal. For a relatively weak interaction, the delta function of the adatom energy level broadens into a Lorentzian peak. This is expected since the atomic state with energy E_a is no longer a stationary state when it binds to the surface. As σ is increased, the single Lorentzian peak splits into a bonding and an antibonding resonance. The peaks become more narrow as they approach the band edges. For $\sigma = 9\gamma$, the peaks split off both below and above the band. For larger values of σ , $\Delta\tilde{n}_c$ is quite smooth inside the band. In Fig. 10, we show the results for $E_a = -6\gamma$. For $\sigma = \gamma$, the peak is sharper. The bonding state is split off the band for both $\sigma = 6\gamma$ and 9γ . In Fig. 11, E_a is placed below the band at -10γ . In this case, the bonding state has split off the band for all values of σ . The antibonding resonance behaves similar to the on-site case. Again, positions of the split off states, when they exist from Eq. (27) by replacing the subscript T with c, are given in Table I.

V. Conclusions

We have obtained the change in the density of states Δn for a single atom adsorption on the (001) face of a bcc metal. While the overall qualitative behavior is similar to that of the simple cubic crystal for the same binding site, the details of the change are sensitive to the band structure of the substrate. For the on-site adsorption, a sharp decrease in the density of states is obtained near $E = 0$ where degeneracies in energy levels occur for the bcc metal. These are absent in the simple cubic crystal. As a consequence of this singularity in the bulk density of states, there are always bonding and antibonding resonances for an arbitrary small adatom-substrate interaction.

The details in $\tilde{\Delta n}$ also depend on the binding site. For the centered fourfold adsite, the above mentioned singularities are absent. For large values of σ , $\tilde{\Delta n}$ is negative and smooth throughout the band. For small σ , a Lorentzian peak is obtained. For an adatom near the center of the band ($E_a = -\gamma$), the results are very similar to the on-site adsorption on the simple cubic crystal. The reasons for this behavior lie in our choice of a symmetric combination of the four substrate wavefunctions nearest to the adatom. As can be seen from the imaginary part of G_c in Fig. 8, the singularity in the local density of states for the surface plane of atoms is removed in the symmetric combination. [The local density of states is related to $\text{Im}G_c$ by Eq. (21).] The smoothness in this symmetrically combined wavefunction prevents any sharp decrease in the density of states near the center of the band.

As a function of the position of E_a , the effect due to chemisorption is most pronounced for E_a near the center of the band. For E_a near the bottom of the band, the antibonding resonances become prominent only after the bonding resonances have split off below the band. For E_a below the band, only the antibonding resonances appear since the bonding resonances lie below E_a .

The present results will serve as the basis for comparison to a similar calculation which will be carried out for a substrate having a gap in its energy band.⁽¹³⁾ They can further lead to a qualitative assessment of the effect and importance of other adatoms when a monolayer of atoms is adsorbed on the surface. These simple model calculations can only give us a qualitative understanding of the interaction of a discrete energy level with a continuum of energy states. However, they have allowed us to formulate a very complicated many-body problem in terms of much simpler

one-electron concepts. A quantitative or semi-quantitative understanding of chemisorption must await a much more sophisticated theory.

REFERENCES

1. See, for example, W. F. Egelhoff and D. L. Perry, *Phys. Rev. Lett.* 34, 93 (1975); E. W. Plummer, B. J. Waclawski and T. V. Vorburger, *Chem. Phys. Lett.* 28, 510 (1974); A. M. Bradshaw, D. Menzel and M. Steinkilberg, *Chem. Phys. Lett.* 28, 516 (1974); B. Feuerbacher and M. R. Adriaens, *Surface Sci.* 45, 553 (1974); J. E. Demuth and D. E. Eastman, *Phys. Rev. Lett.* 32, 1123 (1974); D. E. Eastman and M. I. Nathan, *Physics Today* 28, 44 (1975).
2. G. Allan, *Ann. Phys.* 5, 12 (1970).
3. P. W. Anderson, *Phys. Rev.* 124, 41 (1961).
4. J. R. Schrieffer, *J. Vac. Sci. Technol.* 9, 561 (1972); R. Gomer, *Adv. Chem. Phys.* 27, 211 (1974); T. B. Grimley, *Structure and Properties of Metal Surfaces*, Ed., S. Shimodaira, Maruzen, Tokyo, 1, 72 (1973); *Progress in Surface and Membrane Science*, Eds., D. A. Cadenhead, J. F. Danielli and M. D. Rosenberg, Academic Press, 9, 71 (1975).
5. W. Ho, S. L. Cunningham, W. H. Weinberg and L. Dobrzynski, in press, *Phys. Rev.* B12 (1975). The results given here are for a two-band crystal with the CsCl structure. By setting the band gap equal to zero, we obtain results appropriate for a bcc metal.
6. T. L. Einstein and J. R. Schrieffer, *Phys. Rev.* B7, 3629 (1973).
7. J. W. Davenport, T. L. Einstein and J. R. Schrieffer, *Proc. 2nd Internl. Conf. on Solid Surfaces*, 1974, Japan. *J. Appl. Phys. Suppl.* 2, Pt. 2, p. 691 (1974).
8. T. L. Einstein, *Surface Sci.* 45, 713 (1974).
9. W. Ho, S. L. Cunningham, W. H. Weinberg and L. Dobrzynski, submitted to *Phys. Rev. B* (1975).

10. G. Toulouse, Solid State Commun. 4, 593 (1966).
11. S. L. Cunningham, Phys. Rev. B10, 4988 (1974).
12. T. Horiguchi, J. Phys. Soc. Japan 30, 1261 (1971).
13. W. Ho, S. L. Cunningham and W. H. Weinberg (in preparation, 1975).

TABLE CAPTION

Table I: Energies of the split off states (SOS) for the on-site and the centered fourfold-site adsorption. All energies are expressed in units of the nearest neighbor hopping integral γ .

TABLE I

E_a	σ	E_T^{SOS}	E_C^{SOS}
-1	9	- 9.75	-10.04
		8.83	9.19
-6	6	- 9.85	-10.02
	9	-12.61	-12.76
-10	1	-10.10	-10.11
	3	-10.87	-10.91
	6	-12.88	-12.96
	9	-15.37	-15.46

FIGURE CAPTIONS

- Figure 1: Energy band along a particular segment in the square surface Brillouin zone (SBZ) for the (001) surface of a bcc metal. A continuum of states exists inside the band.
- Figure 2: Geometry for the on-site adsorption. The adatom, circle with cross-hatch, bonds directly to a single surface atom. Dotted circles denote atoms located beneath the y-z plane and in the body-centered positions. λ_z labels the unit cells in the z-direction. a_0 is the crystal lattice spacing.
- Figure 3: Real and imaginary parts of the Green's function appropriate for on-site adsorption. The imaginary part is related to the local density of states for the surface plane of atoms through Eq. (21).
- Figure 4: Change in the density of states $\Delta\tilde{n}$ for on-site adsorption. The arrow points to the position of the adatom energy level, $E_a = -\gamma$, in its free state.
- Figure 5: Change in the density of states $\Delta\tilde{n}$ for on-site adsorption. The arrow points to the position of the adatom energy level, $E_a = -6\gamma$, in its free state.
- Figure 6: Change in the density of states $\Delta\tilde{n}$ for on-site adsorption. The arrow points to the position of the adatom energy level, $E_a = -10\gamma$, in its free state. E_a is below the band.
- Figure 7: Geometry for the centered fourfold adsorption site. The adatom, circle with cross-hatch, bonds directly to four adjacent surface atoms.
- Figure 8: Real and imaginary parts of the Green's function appropriate for the centered fourfold adsorption site. Both curves are continuous

in contrast to the discontinuities at $E = 0$ for the case of on-site adsorption in Fig. 3.

Figure 9: Change in the density of states $\Delta\tilde{n}$ for the centered fourfold adsorption site. The arrow points to the position of the adatom energy level, $E_a = -\gamma$, in its free state.

Figure 10: Change in the density of states $\Delta\tilde{n}$ for the centered fourfold adsorption site. The arrow points to the position of the adatom energy level, $E_a = -6\gamma$, in its free state.

Figure 11: Change in the density of states $\Delta\tilde{n}$ for the centered fourfold adsorption site. The arrow points to the position of the adatom energy level, $E_a = -10\gamma$, in its free state. E_a is below the band. The graph with an expanded vertical scale is also given.

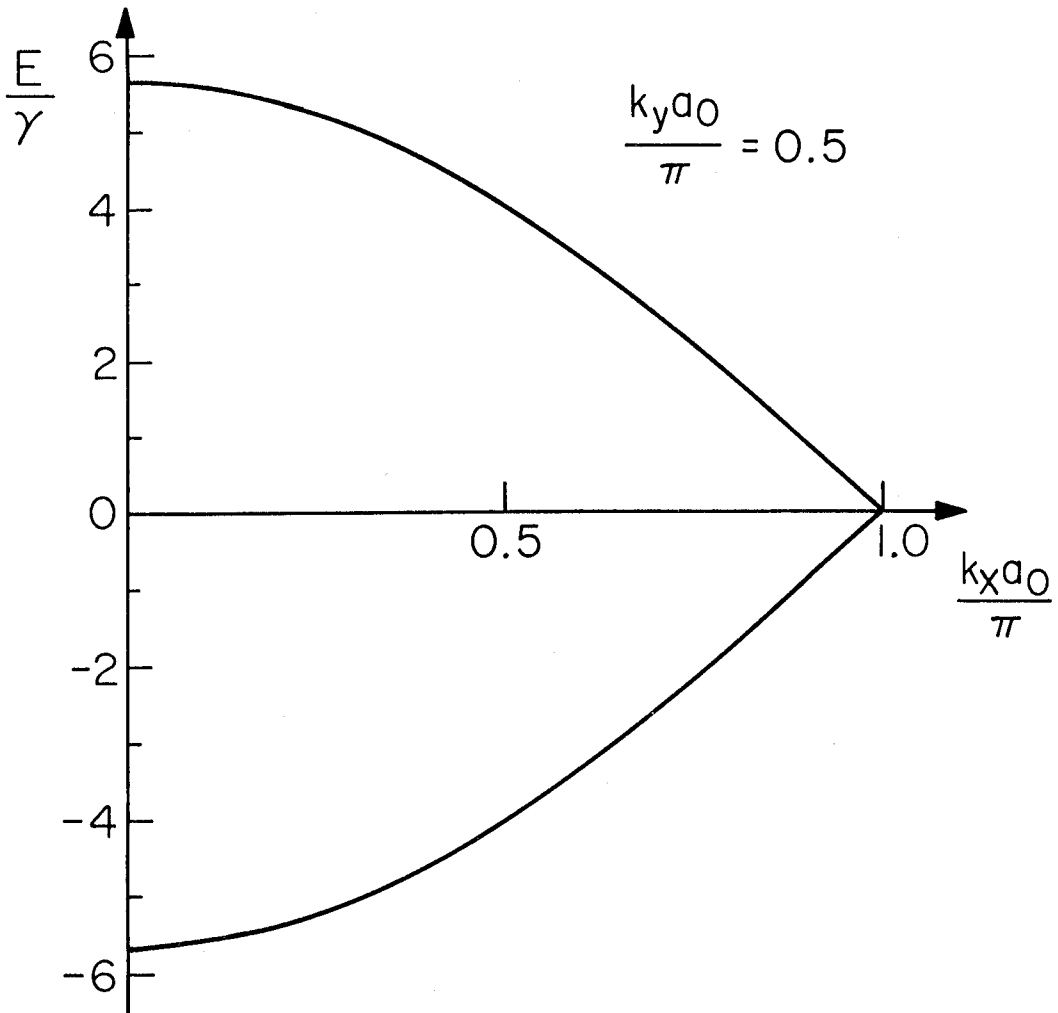


Figure 1

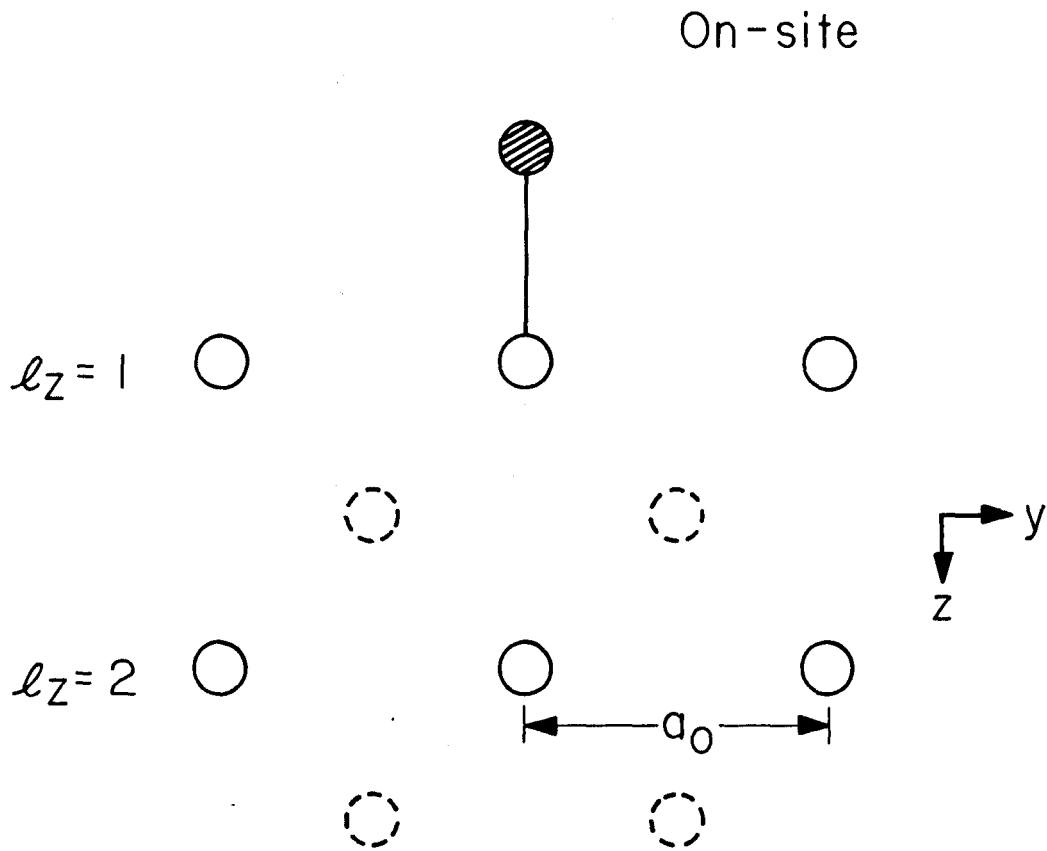


Figure 2

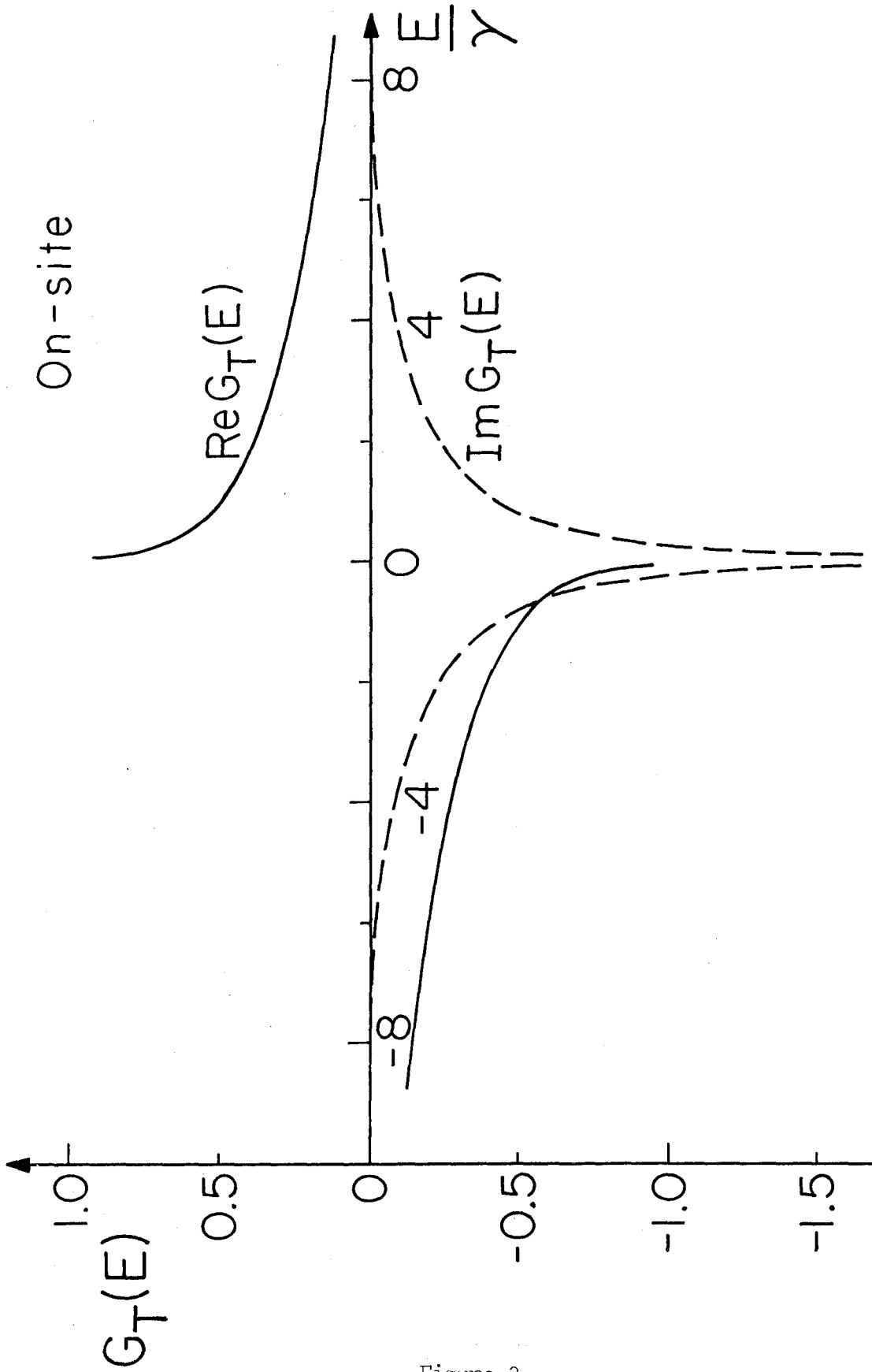


Figure 3

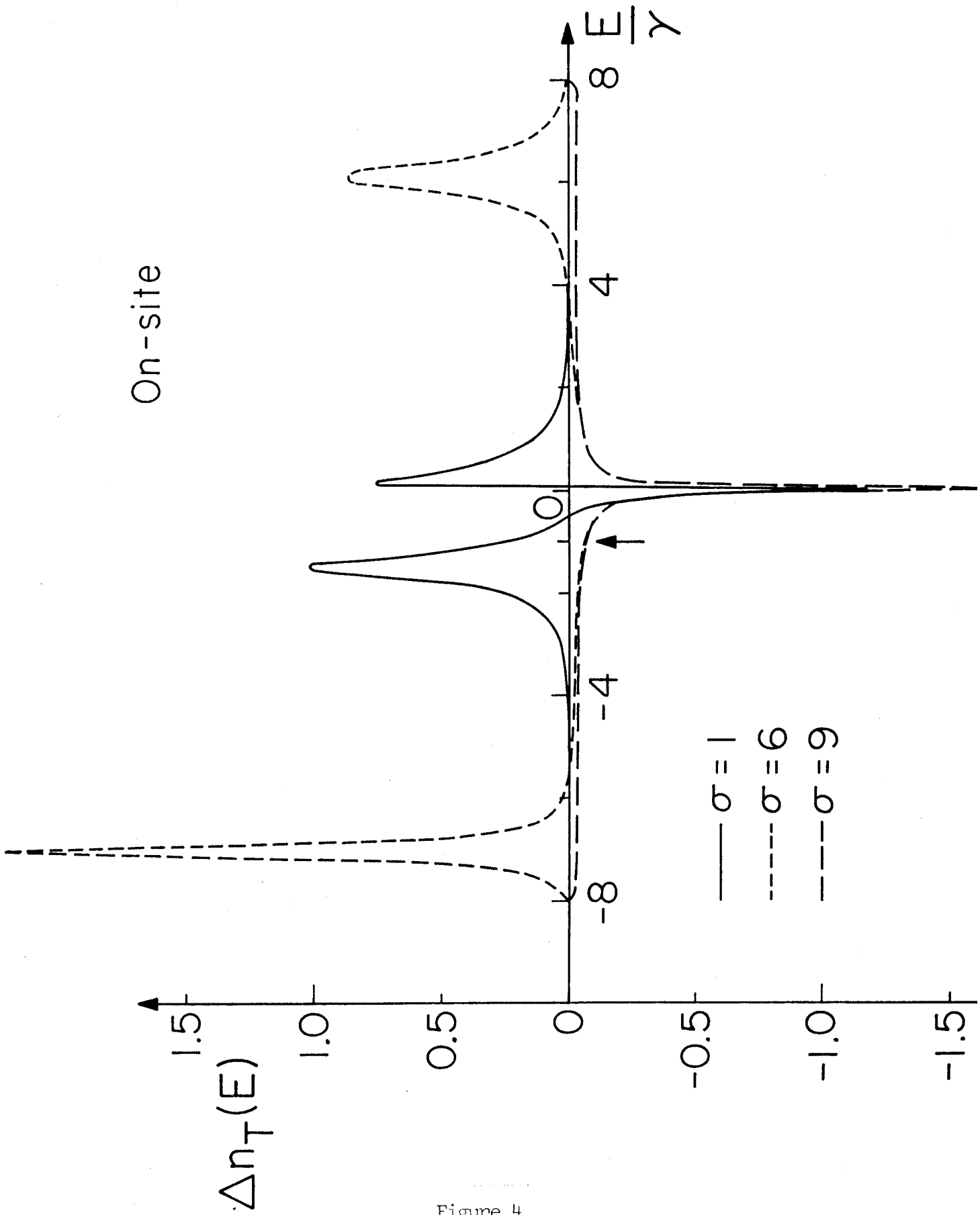


Figure 4

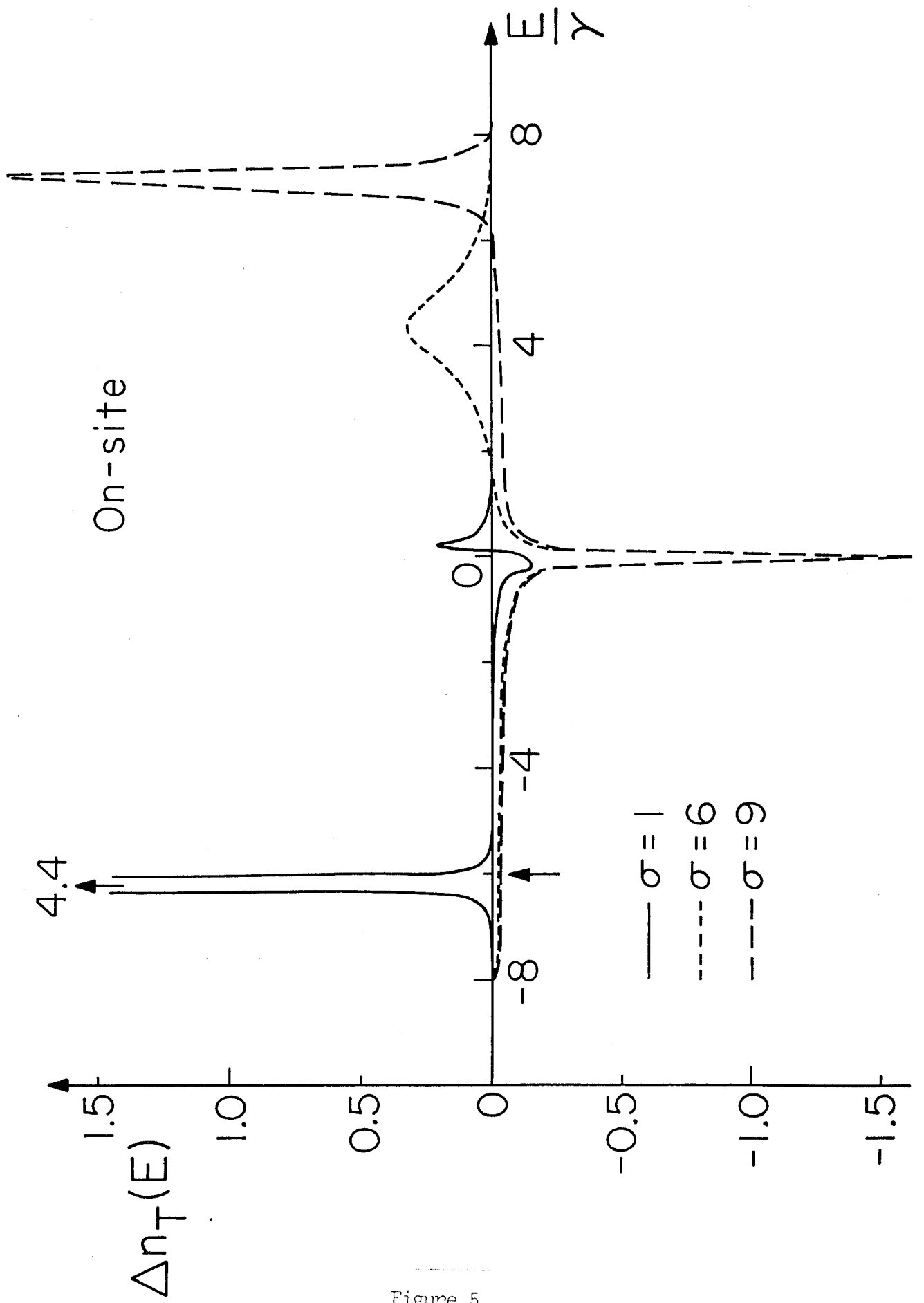


Figure 5

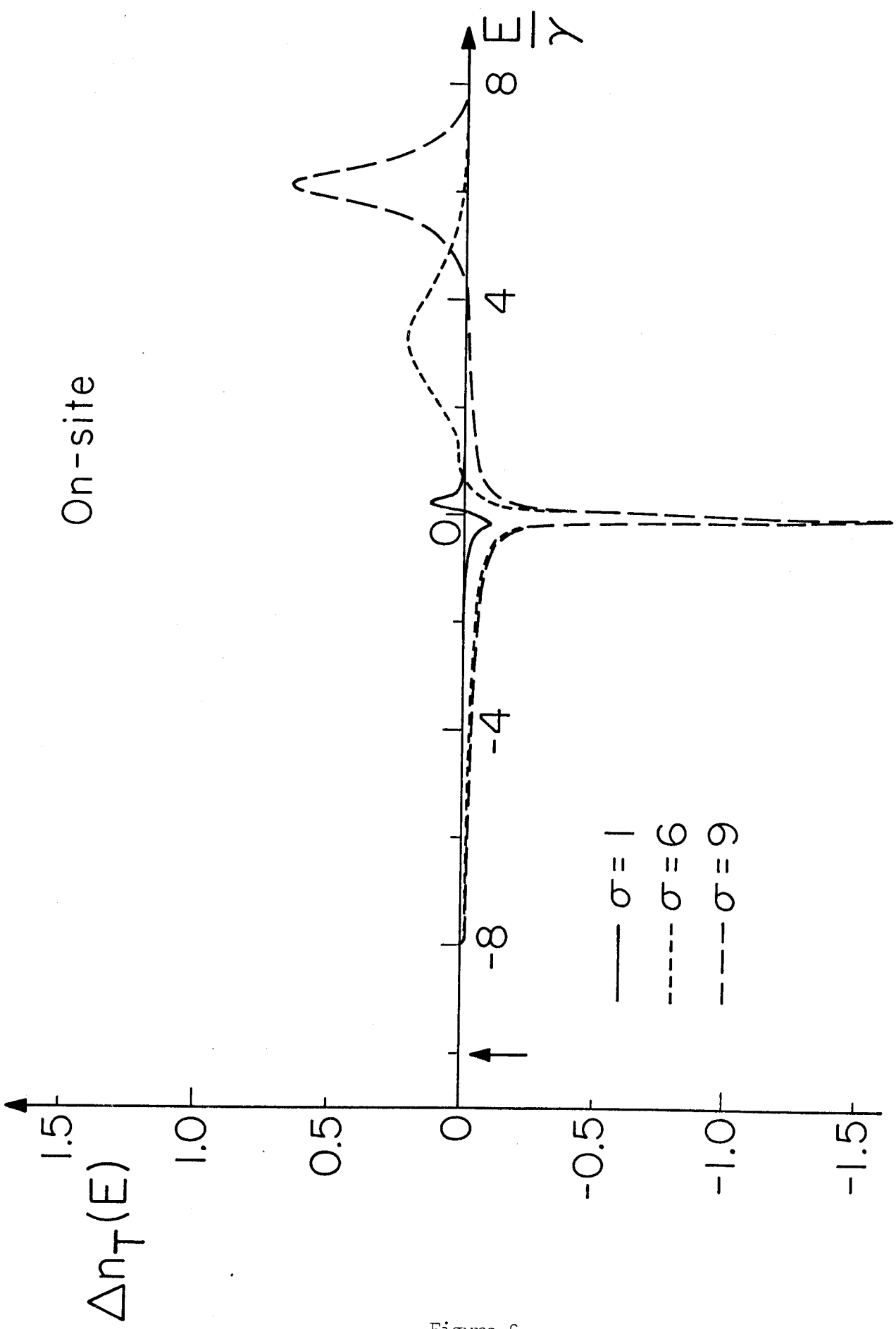


Figure 6

Centered

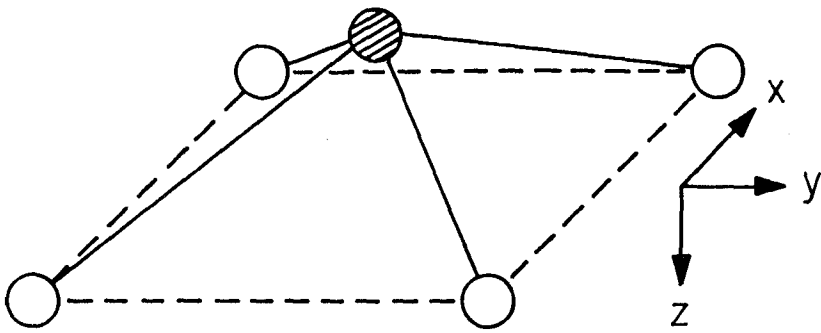


Figure 7

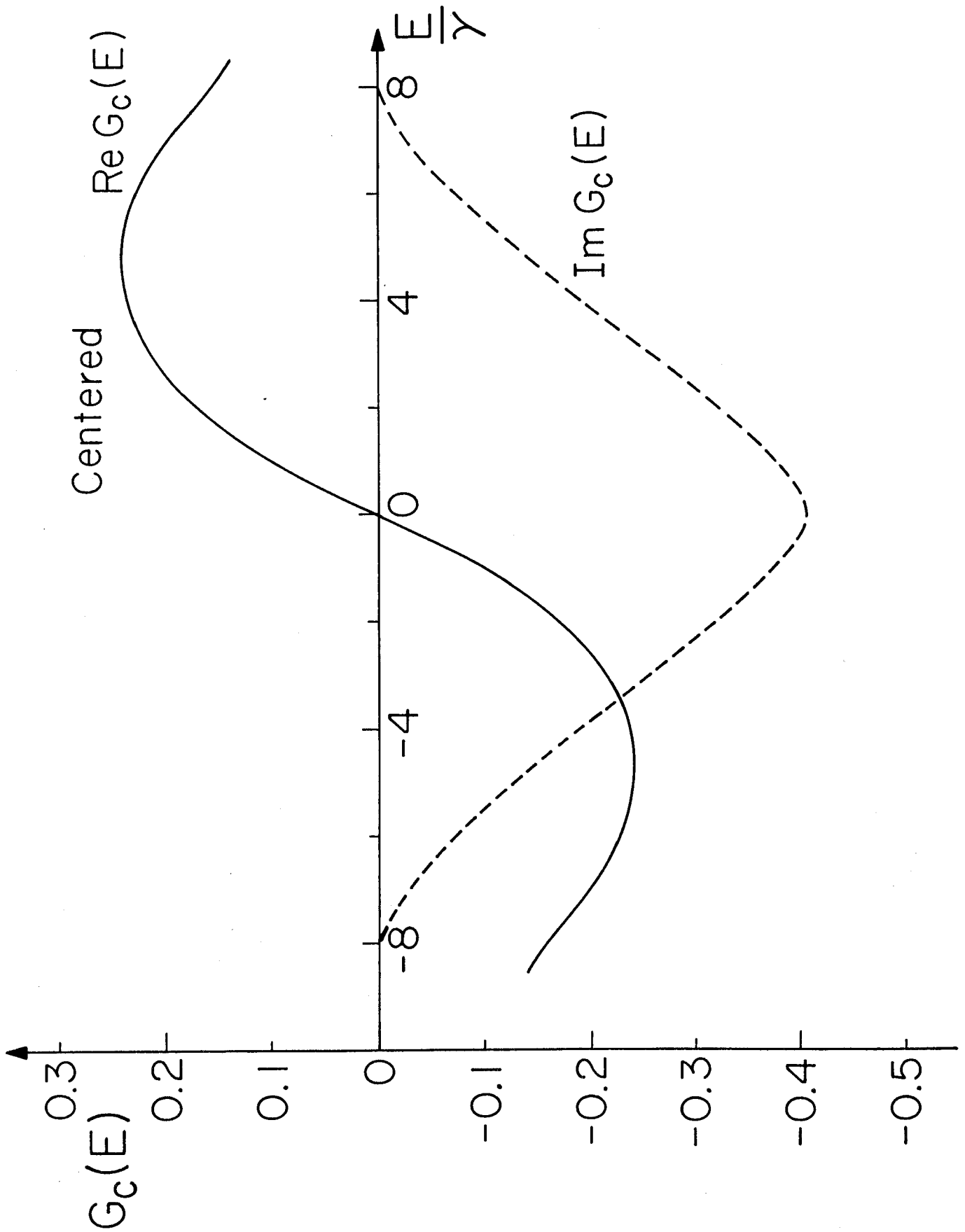


Figure 8

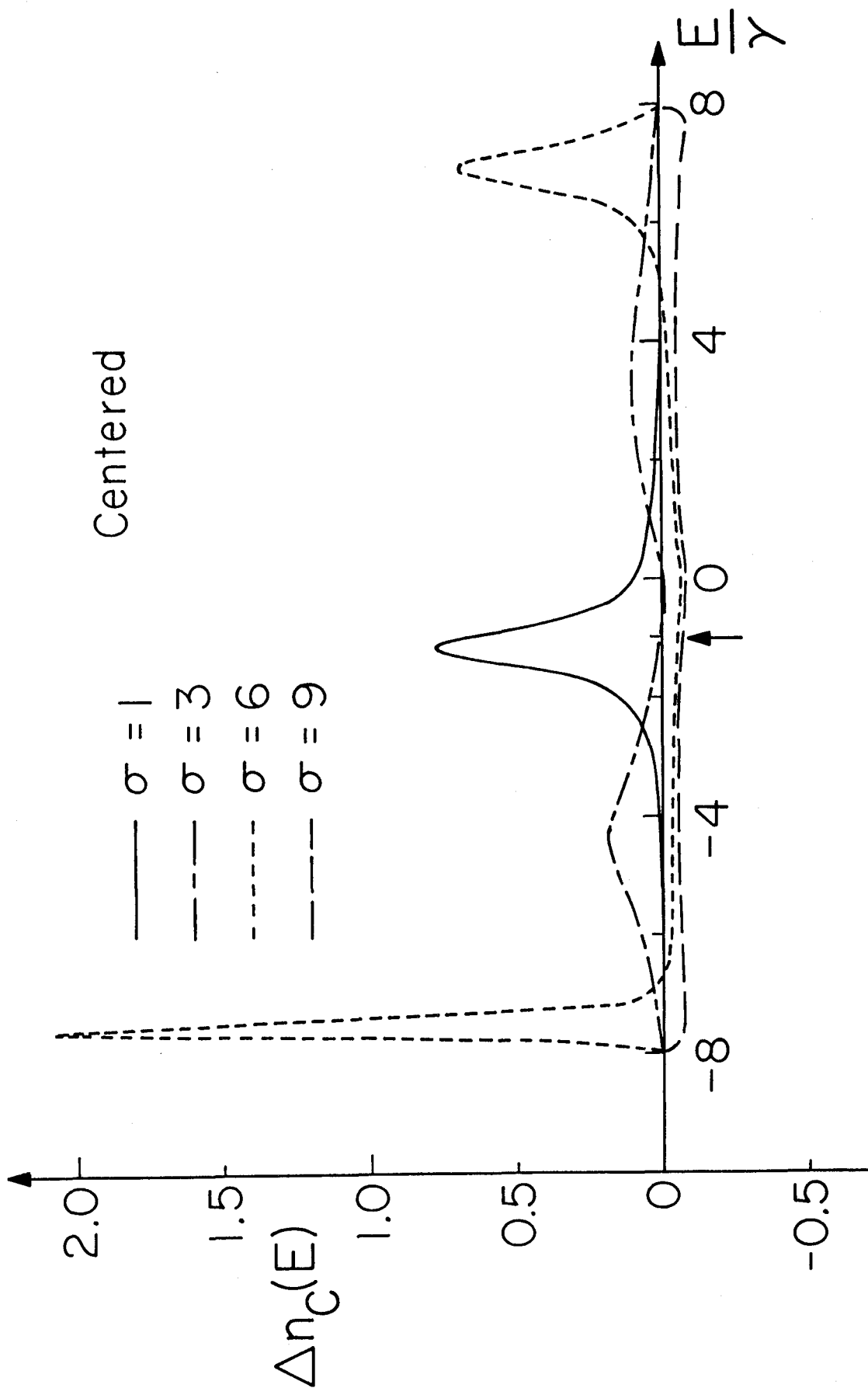


Figure 9

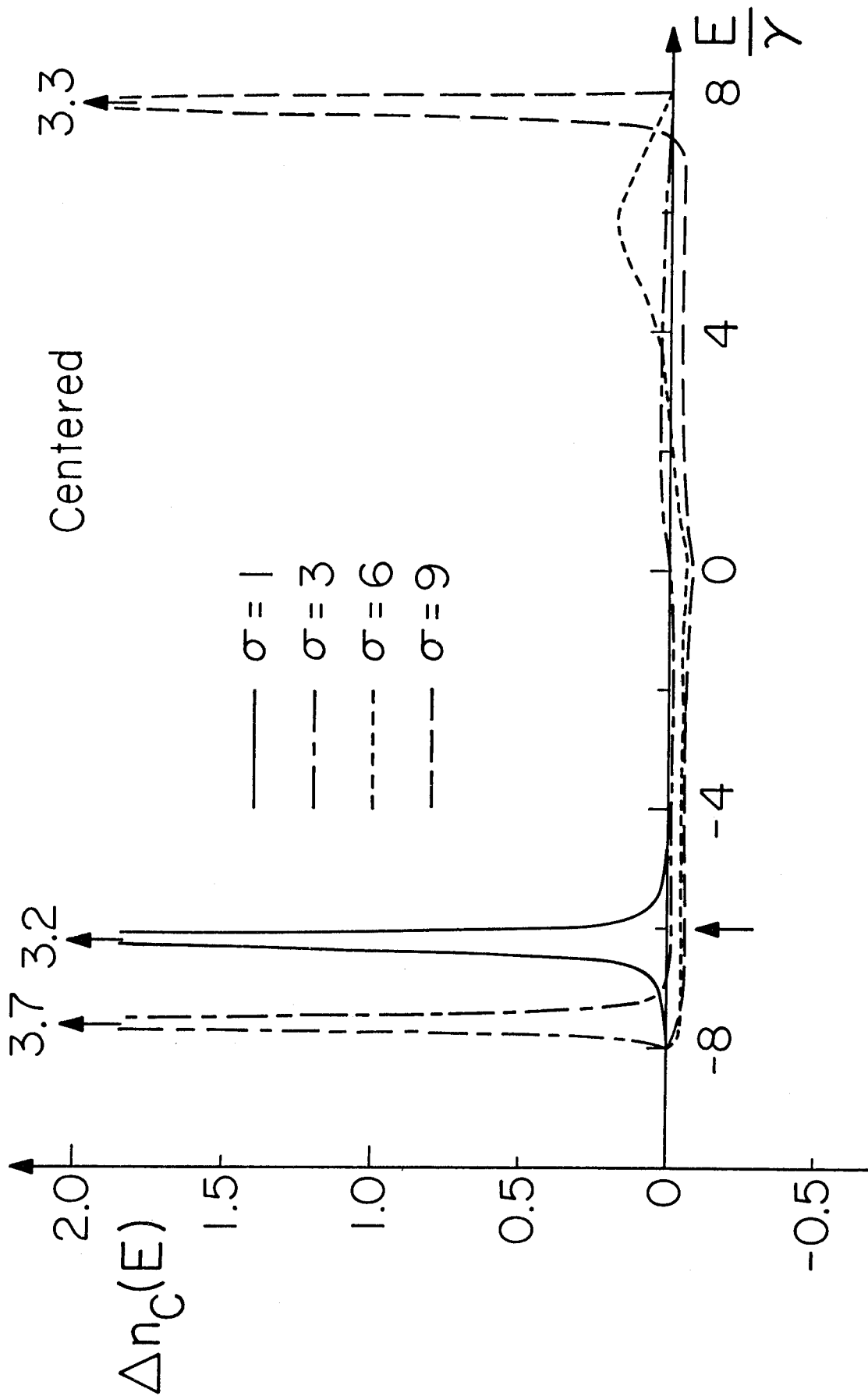


Figure 10

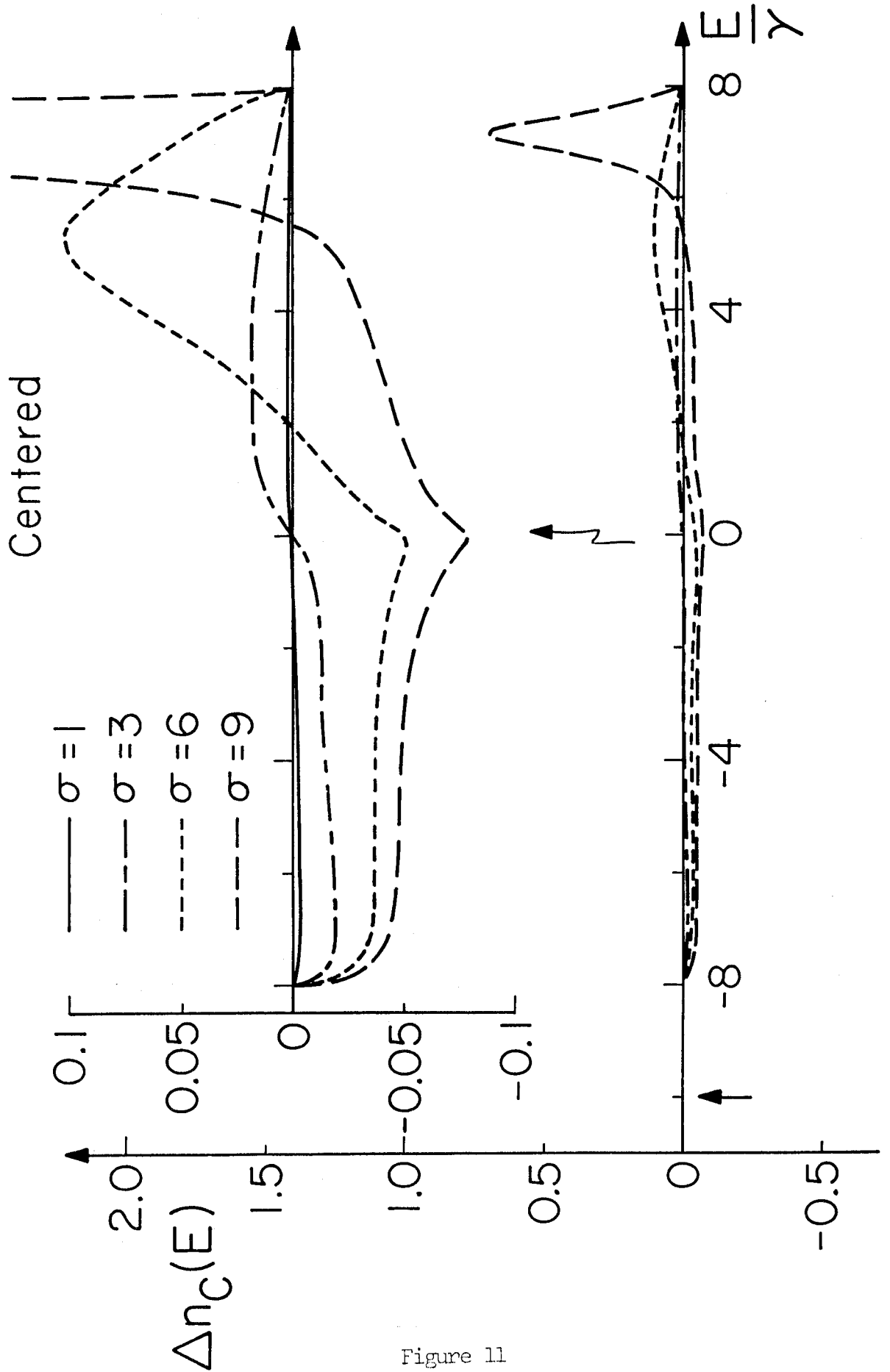


Figure 11

CHAPTER V
CONCLUSIONS

V. CONCLUSIONS

In this thesis, we have investigated, in three parts, the change in the electronic structure due to surface creation, surface reconstruction and single atom chemisorption. These are three of the fundamental problems that one must study before understanding surface phenomena from first principles. The detailed conclusions for each part are summarized at the end of each respective chapter.

The problems were attacked successively, each building on the results of the previous study. We first studied the electronic structure of the clean (001) surface of a two-band crystal with the CsCl structure. The model was used to simulate a semiconductor or insulator surface. We found that the presence of the second empty (conduction) band, separated by the band gap from the valence band, has important effects on the shift in the energy levels during surface creation. The electronic and thermodynamic properties obtained were consistent with the known properties for crystals with a band gap. *These are results which cannot be obtained with a one-band model.*

Once we obtained a wave mechanical description of the surface, we proceeded to investigate the effect of a structural change of the surface on the electronic energy levels. The results were contrasted with those from a one-band calculation. *Again, we found that the qualitative behavior depends critically upon the presence of the empty conduction band.*

From these two studies, we have concluded that the surface properties of semiconductors or insulators depend crucially upon the existence of the conduction band even though it is not occupied. The perturbation due to the surface causes the energy levels in the conduction band to interact

and to affect the energy levels in the valence band for both the case of surface creation and surface reconstruction.

From this observation, we next want to assess the importance of the conduction band when we introduce a discrete energy level into the system as occurs in chemisorption. The novel situation which occurs involves the interaction of the discrete atomic energy level with two continua of states which can in turn interact with each other. However, in order to have a basis for comparison, the calculation in Chapter IV was carried out for a bcc metal. We have found that the results obtained can be expressed in concepts similar to those of chemical bonding in molecules. Calculations for the two-band case are now underway.

Throughout our calculation, we have assumed a simple model analogous to Hückel molecular orbital theory in molecular quantum chemistry. Although the Hückel model is relatively simple compared to an extensive configuration interaction (CI) calculation, it has given a good first order understanding of the electronic structure of molecules. Similarly, we believe that the tight binding approximation we have used can give good physical insight into the electronic structure of surfaces. The calculations become more important in view of the fact that an extensive treatment of these surface phenomena does not exist at the present time. However, it should always be kept in mind that in order to obtain quantitative agreement with experiment, one must include the interaction between the electrons and use a many-body wave function. Unfortunately, the capability of doing this does not presently exist. Consequently, model calculations, such as those in this thesis, are the only method currently practical to advance our understanding of these important surface phenomena.

CHAPTER VI

APPENDICES

Section A: Quantum Molecular Calculation of
the Low Lying States of Cyclobutadiene.

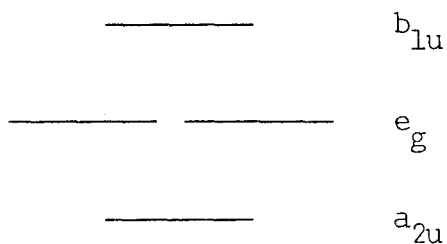
Section B: Picosecond Spectroscopy - A Study of
Nonlinear Optical Phenomena.

APPENDIX A

Low Lying States of Cyclobutadiene

This is a preliminary report of *ab initio* study of the ground state and low lying excited states of cyclobutadiene. Of particular interest is the question of whether the ground state is a singlet or a triplet. Simple MO and VB ideas give rise to different ordering of low lying states.

Simple MO considerations lead to the following MO scheme for the orbitals of cyclobutadiene in a square geometry:



The ground state configuration is $[\sigma \text{ core}](a_{2u})^2(e_g)^2$. Since the degenerate orbitals e_{gx} and e_{gy} are orthogonal, we expect the lowest state to be a triplet

$$\psi_{\text{triplet}} = a \left\{ [\sigma \text{ core}](a_{2u})^2 (e_{gx}e_{gy} - e_{gy}e_{gx})\alpha\beta\alpha\alpha \right\} .$$

In the simple MO picture, four states arise from the $(a_{2u})^2(e_g)^2$ configuration:

$${}^1A_{1g}: (x^2 + y^2)(\alpha\beta - \beta\alpha) \quad ,$$

$${}^1B_{1g}: (x^2 - y^2)(\alpha\beta - \beta\alpha) \quad ,$$

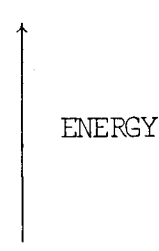
$${}^1B_{2g}: (xy + yx)(\alpha\beta - \beta\alpha) \quad ,$$

$${}^3A_{2g}: (xy - yx)(\alpha\alpha) \quad ,$$

where $x = e_{gx}$, $y = e_{gy}$.

Evaluating the energies for these wavefunctions, we get the following ordering of states:

<u>STATES</u>			
${}^1A_{1g}$	$(x^2 + y^2)$	————	$E_0 + J_{xx} + K_{xy}$
${}^1B_{2g}$	$(xy + yx)$	————	$E_0 + J_{xy} + K_{xy}$
${}^1B_{1g}$	$(x^2 - y^2)$	————	$E_0 + J_{xx} - K_{xy}$
${}^3A_{2g}$	$(xy - yx)$	————	$E_0 + J_{xy} - K_{xy}$



(Energies of the states not ordered to scale.)

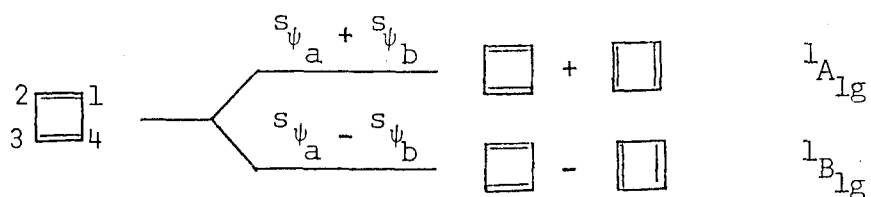
The coulomb repulsion, J_{xx} , between two electrons in the e_{gx} orbital should be greater than the coulomb repulsion, J_{xy} , between an electron in e_{gx} and an electron in e_{gy} . In ordering the B_{1g} and ${}^1B_{2g}$ states, we assumed that $2K_{xy} > J_{xx} - J_{xy}$. E_0 is the energy of the core plus the energy of the doubly occupied a_{2u} orbital and one-electron energies for the e_{gx} and e_{gy} orbitals.

The VB method predicts strikingly different ordering of states. In VB theory, there are two ways to make two double bonds,

$${}^2 \begin{array}{|c|} \hline \square \\ \hline \square \\ \hline \end{array} {}^1_4 \quad {}^S\psi_a = a[(\phi_1\phi_2 + \phi_2\phi_1)(\phi_3\phi_4 + \phi_4\phi_3)]^{\alpha\beta\alpha\beta} ,$$

$${}^2 \begin{array}{|c|} \hline \square \\ \hline \square \\ \hline \end{array} {}^1_4 \quad {}^S\psi_b = a[(\phi_1\phi_4 + \phi_4\phi_1)(\phi_2\phi_3 + \phi_3\phi_2)]^{\alpha\beta\alpha\beta} ,$$

where ϕ_i denotes orbital centered on site i . To get the proper symmetry (D_{4h}), we take resonant and antiresonant combinations (${}^S\psi_a - {}^S\psi_b$), and (${}^S\psi_a + {}^S\psi_b$). This results in two singlet states.



Triplet states arise from making one π bond and triplet coupling the other two P orbitals:

$$\begin{array}{c} 2 \\ \square \\ 3 \end{array} \begin{array}{c} \uparrow \\ \uparrow \end{array} \quad T_{\psi_1} = a[(\phi_2\phi_3 + \phi_3\phi_2)(\phi_4\phi_1 - \phi_1\phi_4)\alpha\beta\alpha\alpha] ,$$

$$\begin{array}{c} \uparrow \\ \uparrow \end{array} \square \quad T_{\psi_2} = a[(\phi_1\phi_4 + \phi_4\phi_1)(\phi_2\phi_3 - \phi_3\phi_2)\alpha\beta\alpha\alpha] ,$$

$$\begin{array}{c} \uparrow \uparrow \\ \square \end{array} \quad T_{\psi_3} = a[(\phi_3\phi_4 + \phi_4\phi_3)(\phi_1\phi_2 - \phi_2\phi_1)\alpha\beta\alpha\alpha] ,$$

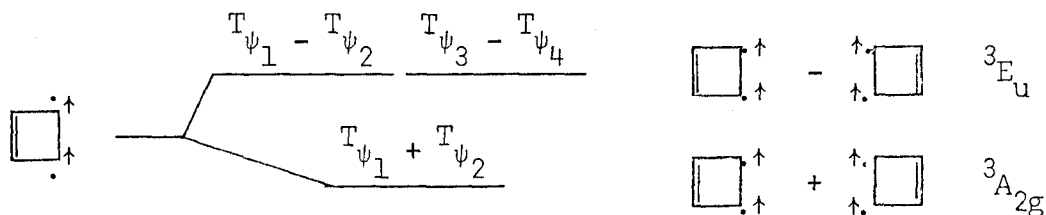
$$\begin{array}{c} \square \\ \uparrow \uparrow \end{array} \quad T_{\psi_4} = a[(\phi_1\phi_2 + \phi_2\phi_1)(\phi_3\phi_4 - \phi_4\phi_3)\alpha\beta\alpha\alpha] .$$

(There are only 3 independent eigenfunctions since $T_{\psi_1} + T_{\psi_2} = T_{\psi_3} + T_{\psi_4}$.)

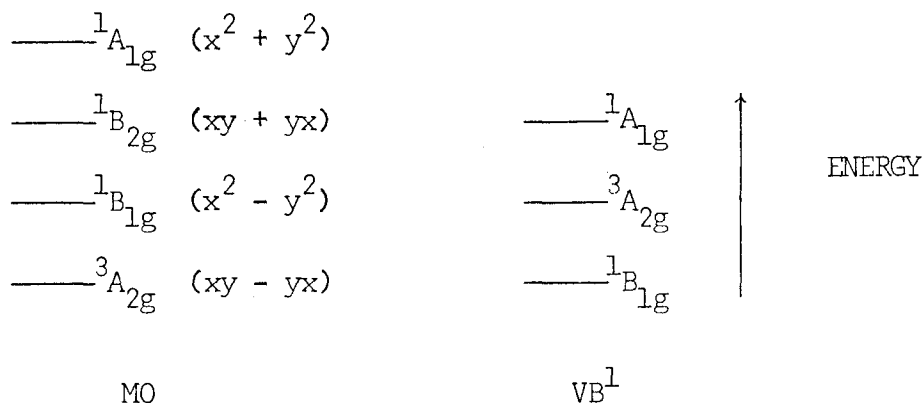
The appropriate symmetry combinations are:

$${}^3A_{2g} \quad \Psi = T_{\psi_1} + T_{\psi_2} = T_{\psi_3} + T_{\psi_4} ,$$

$${}^3E_u \quad \begin{cases} \Psi_x = T_{\psi_1} - T_{\psi_2} \\ \Psi_y = T_{\psi_3} - T_{\psi_4} \end{cases} ,$$



The ordering of the low lying states from the two approaches are:



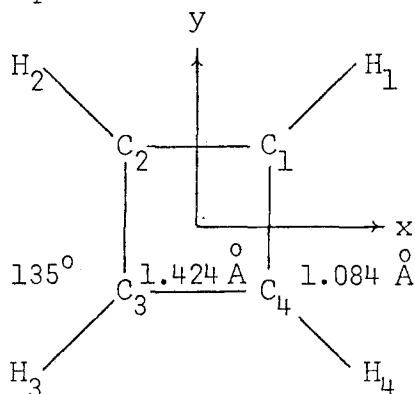
(Energies of the states are not ordered to scale.)

We see that there is a rather drastic disagreement between the VB and MO descriptions at this level. This disagreement makes cyclobutadiene theoretically interesting.

A DESCRIPTION OF THE CALCULATIONS

The basis set used is the Gaussian equivalent of a double zeta basis, the $(9S_C 5P_C / 4S_H)$ basis contracted to $(4S_C 2P_C / 2S_H)$.^{2,3}

Recently, IR spectra of cyclobutadiene have been recorded. The spectra indicate that cyclobutadiene has an effective square geometry (D_{4h}).^{4,5} We have used a fixed D_{4h} geometry throughout our calculation. We used a C-C bond distance of 1.424 Å from the results of a geometry search for cyclobutadiene by Buenker and Peyerimhoff.⁶ We chose 1.084 Å as the C-H bond distance which is the experimental C-H bond distance for benzene.⁷



RESULTS

After the HF calculations on the triplet state had converged, the sigma core was frozen. The core Hamiltonian obtained was used in all subsequent calculations. This reduced the size of the basis to 8π functions. In the GVB calculations, correlations of electrons in the π bonds are taken into consideration.

The configurations for the MBS CI calculations were obtained from all possible excitations among the four lowest π orbitals. For the FULL CI calculations, configurations were obtained from all possible excitations among the 8π orbitals. Total energies for the low lying excited states and the excitation energies are tabulated in Tables I and II.

DISCUSSION

HF calculations predict that the ${}^3A_{2g}$ lies lower than the ${}^1B_{1g}$ by 0.2035 e.V.. The ordering of the states arising from the $(a_{2u})^2(e_g)^2$ configuration agrees qualitatively with that from a simple MO consideration. We would expect that the ${}^1B_{2g}$ is separated from the ${}^3A_{2g}$ ($xy - yx$) by twice the exchange integral, K_{xy} , and similarly for ${}^1A_{1g}$ and ${}^1B_{1g}$. The exchange integral, K_{xy} , obtained from the splitting of ${}^1A_{1g}$ ($x^2 + y^2$) and ${}^1B_{1g}$ ($x^2 - y^2$) is 1.3 e.V., and from the splitting of ${}^1B_{2g}$ and ${}^3A_{2g}$ is 1.2 e.V.. (The ${}^1A_{1g}$ ($x^2 + y^2$) and ${}^1B_{1g}$ ($x^2 - y^2$) were obtained by doing the HF calculation with MO occupation x^2 and then doing the 2 configuration CI, mixing in y^2 . The 2 CI configurations were generated from single excitation among the four lowest orbitals.)

In the GVB calculation, the π bonds are localized, reducing the symmetry of the molecule from D_{4h} to C_{2v} . The GVB calculation on the singlet state was done on the VB structure \square , and for the triplet state, the structure

$\begin{array}{|c|} \hline \uparrow \\ \hline \square \\ \hline \uparrow \\ \hline \end{array}$. Although these states are not symmetry states, the GVB calculations show that the singlet is lower than the triplet by 0.5383 e.V.. The actual singlet and triplet states of the molecule are obtained from a linear combination of the two equivalent VB structures, i.e. $\begin{array}{|c|} \hline \square \\ \hline \end{array} \pm \begin{array}{|c|} \hline \square \\ \hline \end{array}$ and $\begin{array}{|c|} \hline \uparrow \\ \hline \square \\ \hline \uparrow \\ \hline \end{array} \pm \begin{array}{|c|} \hline \uparrow \\ \hline \square \\ \hline \uparrow \\ \hline \end{array}$. The states are split by the resonance and antiresonance energies. From the GVB calculations, the singlet state is lowered in energy more than the triplet state since two pairs are correlated in the singlet whereas only one pair is correlated in the triplet. The HF description of the ${}^1B_{1g}$ is inadequate since the HF wavefunction does not describe correlation of the bonding pairs.

Both the MBS CI and the FULL CI calculations show that the singlet state is lower than the triplet state by about 0.4 eV. We conclude that the ground state of cyclobutadiene in a square (D_{4h}) geometry is ${}^1B_{1g}$.

June, 1974

Wilson Ho

Bob Walkup

(The total energy of the ${}^3A_{2g}$ state obtained from the HF calculation using the 48 basis functions is 0.017 e.V. higher than the energy obtained with the 8π functions after freezing the core, even though the final wavefunctions agree to 4 digits. This indicates a possible flaw in the GVB program.)

We have also carried out a geometry search of cyclobutadiene and found the ground state to be rectangular with energy about 0.2 e.V. lower than the optimum square geometry. The resonance energies of the ground state were obtained as a function of the geometrical distortion by the SOGI method. These results will be reported elsewhere.

REFERENCES

1. R. McWeeny, Proc. Roy. Soc. (London) A227, 288 (1955).
2. S. Huzinaga, J. Chem. Phys. 42, 1293 (1965).
3. T. H. Dunning, J. Chem. Phys. 53, 2823 (1970).
4. O. L. Chapman, C. L. McIntosh and J. Pacansky, J. Amer. Chem. Soc. 95, 614 (1973); O. L. Chapman, D. De La Cruz, R. Roth and J. Pacansky, J. Amer. Chem. Soc. 95, 1337 (1973).
5. A. Krantz, C. Y. Lin and M. D. Newton, J. Amer. Chem. Soc. 95, 2744 (1973).
6. R. J. Buenker and S. D. Peyerimhoff, J. Chem. Phys. 48, 354 (1968).
7. L. Pauling, The Nature of the Chemical Bond, Third Edition, Cornell University Press, Ithaca, N.Y., 1960.

TABLE I

Total Energies for Cyclobutadiene (in hartrees)

	<u>HFSCF</u>	<u>GVB</u>	<u>MBS CI</u>	<u>FULL CI</u>
${}^3A_{2g}(xy - yx)$	-153.5941	-	-153.6306	-153.6417
$\square_{\uparrow\uparrow}^{\uparrow}$ triplet	-	-153.5973	-	-
${}^1B_{1g}(x^2 - y^2)$	-153.5866	-	-153.6476	-153.6577
\square singlet	-	-153.6171	-	-
x^2	-153.5399	-	-	-
${}^1A_{1g}(x^2 + y^2)$	-153.4906	-	-153.5619	-153.5765
${}^1B_{2g}(xy + yx)$	-153.5047	-	-153.5013	-153.5268
$\square_{\uparrow\downarrow}^{\uparrow}$ singlet	-	-153.5079	-	-
${}^5B_{1g}$	-153.3615	-	-	-
3E_u	-	-	-153.4828	-153.4927
1E_u	-	-	-153.2799	-153.3198

TABLE II

Excitation Energies for Cyclobutadiene (in eV)

	<u>HFSCF</u>	<u>GVB</u>	<u>MBS CI</u>	<u>FULL CI</u>
${}^3A_{2g}(xy - yx)$	0	-	0.4675	0.4343
$\square \begin{smallmatrix} \cdot \uparrow \\ \cdot \uparrow \end{smallmatrix}$ triplet	-	0.5383	-	-
${}^1B_{1g}(x^2 - y^2)$	0.2035	-	0	0
\square singlet	-	0	-	-
x^2	1.4751	-	-	-
${}^1A_{1g}(x^2 + y^2)$	2.8151	-	2.3361	2.2082
${}^1B_{2g}(xy + yx)$	2.4326	-	3.9847	3.5612
$\square \begin{smallmatrix} \cdot \uparrow \\ \cdot \downarrow \end{smallmatrix}$ singlet	-	2.9714	-	-
${}^5B_{1g}$	6.3298	-	-	-
3E_u	-	-	4.4893	4.4878
1E_u	-	-	10.0106	9.1936

Figure Caption

Figure 1: The energy levels of the low lying states of cyclobutadiene in four separate calculations with the ground state $^1B_{1g}$ in the Full CI calculation as the zero reference. HF stands for Hartree-Fock, GVB stands for Generalized Valence Bond, MBS CI stands for Minimum Basis Set Configuration Interaction, and FULL CI stands for Full Configuration Interaction.

Low Lying States of Cyclobutadiene

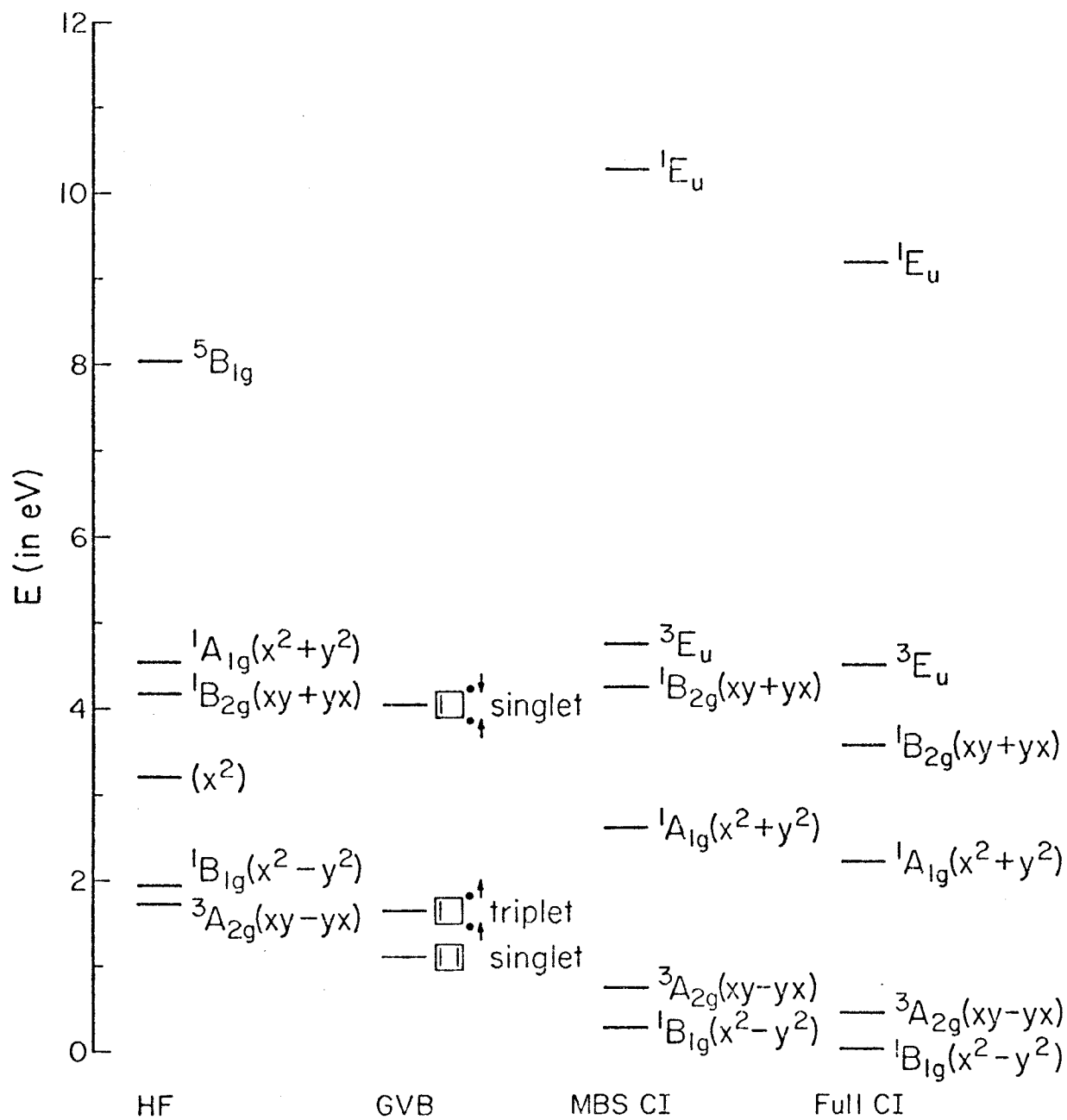


Figure 1

APPENDIX B

The Study of Nonlinear Optical Phenomena with a Picosecond Laser

The time scale in optical spectroscopy has undergone drastic changes in recent years. Flash spectroscopy, devised by Norrish and Porter,¹ has been used to detect short-lived triplet states and has extended conventional spectroscopy from the millisecond into the microsecond region. With the discovery of the laser,² new time domains have become accessible for the study of the interaction of light with matter. Nanosecond pulses are obtainable with a Q-switched laser.³ When the laser is mode-locked, picosecond pulses can be produced,⁴ allowing us to study ultrafast primary processes occurring in molecules.⁵ However, not too many problems in spectroscopy can be studied with these ultrashort pulses due to the limited number of fundamental frequencies available from these solid state lasers, namely 1060 nm from Nd⁺³-glass and 694.3 nm from ruby. Nevertheless, the interaction with matter of these short duration and high intensity pulses has resulted in the observation, for the first time, of nonlinear optical phenomena at optical frequencies.⁶ These highly interesting phenomena include the generation of optical harmonics,⁷ stimulated Raman scattering,⁸ photon echoes,⁹ and the simultaneous absorption of two photons via a virtual state.¹⁰ In this section, we present the two-photon absorption and the subsequent fluorescence of 1,2,5,6-dibenzanthracene (DBA).

In our laboratory, we have a Nd⁺³-glass laser, mode-locked and Q-switched by an Eastman Kodak #9860 bleachable dye diluted to 0.15 optical density with dichloroethane. Basically, the solid state laser consists of a 8" x 1/2" Nd⁺³-glass rod cut and placed at the Brewster angle in a Korad K-1 laser head,

and situated between a 99.99% reflectance mirror and a partially transmitting, 45% reflectance, mirror. The bleachable dye solution is also placed at the Brewster angle. The laser cavity forms a Fabry-Perot interferometer and sustains discrete optical frequencies

$$\nu_n = \frac{nc}{2L} , \quad (1)$$

where n is the number of half wavelengths of light in the resonator, L is the length of the cavity and c is the speed of light in vacuum. Optical pumping is achieved by a flash lamp which coils around the laser rod. The process involved is shown in Figure 1. Energy from the pumping light is used to excite the Nd^{+3} ions to the absorption band. The ions quickly undergo radiationless transitions to the ${}^4\text{F}$ state. The sharp infrared radiation at 1060 nm is due to the stimulated emission from ${}^4\text{F}_{3/2}$ to ${}^4\text{I}_{11/2}$ states. The coherent output, however, consists of random spikes of variable duration. This is overcome by placing a photo-bleachable dye in the cavity. The dye functions as a shutter, or Q-switching, and is kept closed during the initial pumping by absorbing the emission from the laser rod. In this way, it is possible to achieve a large population inversion without oscillation. As the excited state population continues to grow, the intensity of the light becomes great enough to bleach the dye transition. Energy is then released in a "giant" pulse of nanosecond duration. However, if the relaxation time of the dye is very short compared to the round trip time for a pulse to travel between the mirrors, a sharp pulse can be obtained via the bleaching of the dye by the "giant" Q-switched pulse and subsequent rapid relaxation of the dye. Since only intense pulses can bleach the dye, the sharp pulse obtained is also of high intensity. As this pulse propagates

between the mirrors, a fraction of it is transmitted each time it is reflected from the partially transmitting mirror. The dye also serves to lock in phase each of the Fabry-Perot modes. The mode-locking produces pulses of picosecond duration. Thus the output of the laser consists of a train of picosecond pulses separated by the round trip time it takes for a pulse to travel the distance between the mirrors.

The first nonlinear effect obtained with laser light was observed in 1961 by Franken, et al.⁷ at the University of Michigan. They were able to generate the second harmonic light at a wavelength of 347.15 nm by focusing the beam from a ruby laser onto a quartz crystal. They found that the conversion to the second harmonic light is about 1 part in 10^8 , and that the intensity of the second harmonic is approximately proportional to the square of the intensity of the fundamental light. Since then, conversions up to 20% have been obtained. In 1962, Giordmaine¹¹ and Maker et al.¹² reported second-harmonic generation from an unfocused ruby laser light in KDP and quartz. The materials suitable for the generation of optical harmonics must be transparent both to the fundamental light and its harmonics and have nonlinear dielectric constants. In addition, the materials must be anisotropic and cannot have a center of inversion symmetry. Glass which is isotropic may be induced to generate a second harmonic if an external strong bias field is applied. In our laboratory, the unfocused light from the Nd^{+3} -glass laser is passed into a phase-matched potassium dihydrogen phosphate (KDP) crystal. The second harmonic, with a wavelength of 530 nm, lies in the green region of the visible spectrum.

Another nonlinear effect is the simultaneous absorption of two photons by molecules and was first observed in 1961 by Kaiser and Garrett¹⁰ in

$\text{CaF}_2:\text{Eu}^{2+}$. They obtained fluorescence light around 425 nm by focusing ruby-laser light of wavelength 694.3 nm at $\text{CaF}_2:\text{Eu}^{2+}$. This process differs from the process of generating optical harmonics. In the two-photon absorption process, there are four, rather than three, real and virtual levels involved. In addition, the crystal can have a center of inversion, and fluorescence is observed after excitation to a real absorbing state at twice the laser frequency. The absorption of the first photon excites the molecule to a virtual state of approximately zero lifetime, lying at 1/2 the energy of the real absorbing state. Due to the high intensity of the laser, a second photon can be absorbed simultaneously and excite the molecule to the real absorbing state. The intensity of the resulting fluorescence light varies quadratically with the intensity of the excitation light as opposed to the linear relationship found for low intensity excitation light.

In our laboratory, two-photon fluorescence has been observed in various liquids. The method is used to measure the time duration of the laser pulses and to synchronize temporally the various beams traveling different paths in the experiments. The pulse width of a mode-locked laser cannot be measured at the present time with an oscilloscope-photodiode detection system. The fastest oscilloscope, Tektronix 519, has a rise time of 0.3 nsec, two orders of magnitude greater than the pulse duration.

Giordmaine et al.¹³ have reported the observation of two-photon fluorescence of 1,2,5,6-dibenzanthracene (DBA) in benzene. The emission occurs in the 400 - 420 nm region with a lifetime \leq 50 nsec. In their laser resonator, the front reflector is a plane parallel quartz mirror of 0.63 cm thickness. Standing waves are set up within this oscillator medium in addition to those from the main laser resonator. The emission arises via

the simultaneous absorption of two photons from the optical pulses separated by 60 psec, the time it takes to travel a distance twice the thickness of the plane parallel mirror. In our experiment, the front reflector is wedged. The second harmonic of the Nd^{+3} -glass laser is passed through a beam splitter and the two beams are subsequently joined to induce the two-photon fluorescence. In this way, the time separation of the two pulse trains can be accurately determined, and the two pulse trains can be used as exciter and prober in an experiment, respectively. In Figure 2, we show the experimental arrangement.

The 1060 nm Nd^{+3} -glass laser output, simultaneous mode-locked and Q-switched by Kodak #9860 dye solution, is passed through a KDP crystal to generate 530 nm light pulses. The 530 nm light goes through a beam splitter, and the resulting two beams are collimated, intensity matched, and reduced to a diameter of 1 mm throughout the 5.0 cm fluorescence cell containing 10^{-2} M DBA in benzene. Each beam is intense enough to produce two-photon fluorescence by itself. The track produced is recorded with Polaroid 3000 film.

In one of the two beams, a variable delay is set up to vary the temporal separation of the two beams. The variable delay consists of 3 prisms, one of which is mounted on a translational stage with a precision micrometer head covering a range of 0 to 50 mm and read to an accuracy of 0.01 mm. An intensity enhancement results from a simultaneous absorption of two photons due to the dependence of the integrated fluorescence on the integral of the fourth power of the electric field.¹⁴

A typical two-photon fluorescence spot and its photodensitometer trace are shown in Figure 3. The contrast ratio, the ratio of the signal to the

background intensity, is about 1.2. The movement of the two-photon fluorescence spot as a function of the time separation between the two pulses is shown in Figure 4. A V-shaped curve is obtained as the relative temporal position of the two pulses reverses. From the change in the position of the variable delay and the corresponding change in the two-photon fluorescence spot, the index of refraction of the solution is calculated to be 1.50 as compared to 1.54¹⁵ for benzene alone.

The length of the two-photon fluorescence spot l is given by

$$l = \frac{\alpha ct}{n}, \quad (2)$$

where α is a constant depending on the pulse shape, n is the refractive index of the solution, and t is the pulse duration. From the photodensitometer trace, by taking l to be the full-width at half-maximum intensity above the background, and $\alpha = 1$ for a Lorentzian pulse, the 530 nm optical pulse is found to have a duration of about 9 psec.

Other systems were also studied. Solutions of naphthalene in benzene failed to show an enhancement of intensity due to two-photon fluorescence. In this case, the two beams used are the 530 nm and its Raman line at 560 nm scattered from a solution of fluorobenzene.¹⁶ The absence of two-photon fluorescence from solutions of naphthalene in benzene can be attributed to the presence of impurities which quench the fluorescence. If lower concentrations are used, such as 10^{-4} M solutions, it is possible that the fluorescence intensity becomes too weak to be detected due to low concentrations. This was confirmed with concentrations from 10^{-1} to 10^{-5} M.

Another possible difficulty might lie in the difference in the 530 nm and the 560 nm intensities. Since the 560 nm alone produces no

recordable track due to its low intensity, and the 530 nm does, the intensity of the 530 nm should be properly matched to that of the 560 nm. In principle, the brightness of the two photon enhancement spot is proportional to $I_1 I_2$, where I_1 and I_2 are the intensities of the 530 nm and the 560 nm pulses, respectively. On the other hand, the brightness of the background is proportional to I_1^2 . Thus by decreasing the 530 nm intensity, the contrast ratio can be improved. This was tried with 10^{-3} M naphthalene in benzene with 3 laser shots per photograph. However, no noticeable fluorescence spot was observed.

With two 1060 nm photons, fluorescence was observed in Rhodamine 6G, an organic dye, and a much better contrast ratio was obtained. In this case, the two beams collided with one another without either one being reflected from a mirror.

In summary, we have shown a nonlinear optical effect, the simultaneous absorption of two photons, obtained with a picosecond laser. This is one of the numerous interesting phenomena resulting from the large field strength of the light pulses. From the position of the two-photon fluorescence spot, beams traveling different paths in an experiment can be synchronized temporally. With one beam acting as the excitation source and the other as the probe, the time scale in kinetics is reduced to the picosecond range. However, an extensive study of primary chemical processes involving excited electronic states awaits the development of lasers tunable in the U.V. region. Nevertheless, numerous applications have already been made. Recently, lasers have been used successfully for isotope separation.¹⁷ Historically, the field of optics has played an important role in science. The invention of telescopes, diffraction gratings, and the theory of electricity and magnetism have all made great advances in science. The laser has provided us with

a new form of light. Its full potential is yet to be realized.

Summer, 1973

References

1. R. G. W. Norrish and G. Porter, *Nature* 164, 658 (1949); G. Porter, *Proc. Roy. Soc. A* 200, 284 (1950).
2. A. L. Schawlow and C. H. Townes, *Phys. Rev.* 112, 1940 (1958); T. H. Maiman, *Phys. Rev. Lett.* 4, 564 (1960); *Nature* 187, 493 (1960).
3. R. W. Hellwarth, *Adv. in Quantum Electronics*, ed. J. R. Singer, Columbia Univ. Press 334 (1961); F. H. McClung and R. W. Hellwarth, *J. Appl. Phys.* 33, 828 (1962).
4. H. W. Mocker and R. J. Collins, *Appl. Phys. Lett.* 6, 270 (1965); A. J. DeMaria, D. A. Stetser and H. A. Heynau, *Appl. Phys. Lett.* 8, 174 (1966); A. J. DeMaria, *Prog. in Optics* 9, 33 (1971).
5. See, for example, P. M. Rentzepis, *Chem. Phys. Lett.* 2, 117 (1968); 3, 717 (1969); M. M. Malley and P. M. Rentzepis, *Chem. Phys. Lett.* 3, 534 (1969); M. R. Topp, P. M. Rentzepis and R. P. Jones, *J. Appl. Phys.* 42, 3415 (1971); K. B. Eisenthal, *Chem. Phys. Lett.* 6, 155 (1970).
6. A. Yariv, *Quantum Electronics*, J. Wiley and Sons, 1968.
7. P. A. Franken, A. E. Hill, C. W. Peters and G. Weinreich, *Phys. Rev. Lett.* 7, 118 (1961).
8. R. W. Hellwarth, *Phys. Rev.* 130, 1850 (1963).
9. I. D. Abella, N. A. Kurnit and S. R. Hartmann, *Phys. Rev.* 141, 391 (1966); D. Grischkowsky and S. R. Hartmann, *Phys. Rev. Lett.* 20, 41 (1968).
10. W. Kaiser and C. G. B. Garrett, *Phys. Rev. Lett.* 7, 229 (1961).

11. J. A. Giordmaine, Phys. Rev. Lett. 8, 19 (1962).
12. P. D. Maker, R. W. Terhune, M. Nisenoff and C. M. Savage, Phys. Rev. Lett. 8, 21 (1962).
13. J. A. Giordmaine, P. M. Rentzepis, S. L. Shapiro and K. W. Wecht, Appl. Phys. Lett. 11, 216 (1967).
14. W. H. Glenn, IEEE J. Quantum Electronics, vol. QE-6, 510 (1972).
15. Handbook of Chemistry and Physics, Chemical Rubber Publishing Co., Cleveland, Ohio, 49th ed., P. C-146, 1968.
16. J. A. Calviello and Z. H. Heller, Appl. Phys. Lett. 5, 112 (1964).
17. Chem. and Engrg. News, p. 24, July 8, 1974; p. 17, May 12, 1975.

Figure Captions

- Figure 1: The processes involved in a four-level system for Nd^{+3} -glass laser. The excitation is to a band of energy states.
- Figure 2: Experimental arrangement for observing two-photon fluorescence. LC is the laser cavity; F1 is a BG18 filter which transmits only the 530 nm pulses; B is a 530 nm beam splitter; R is a 100% reflector at 530 nm; VD is the variable delay; L is a system of collimating lenses which reduces the size of each beam to 1/2; F2 are filters used to adjust the intensities of the beams; C is a camera using Polaroid 3000 film and set at f/2.8; SC is the solution cell with 10^{-2} M 1,2,5,6-dibenzanthracene (DBA) in benzene; M is a totally reflecting mirror.
- Figure 3: A typical two-photon fluorescence (TPF) spot and its photodensitometer trace for 1,2,5,6-dibenzanthracene (DBA) in benzene. Arrow points to the intensity enhancement at the TPF spot. The contrast ratio is about 1.2, low compared to TPF from other organic molecules, e.g., Rhodamin 6G.
- Figure 4: Positions of the TPF spot from mirror as a function of the variable delay (VD) positions. Arrow points to the position of the VD at which the paths of the two separate beams are exactly equal; the two beams are again synchronized temporally after they rejoin (see Figure 2).

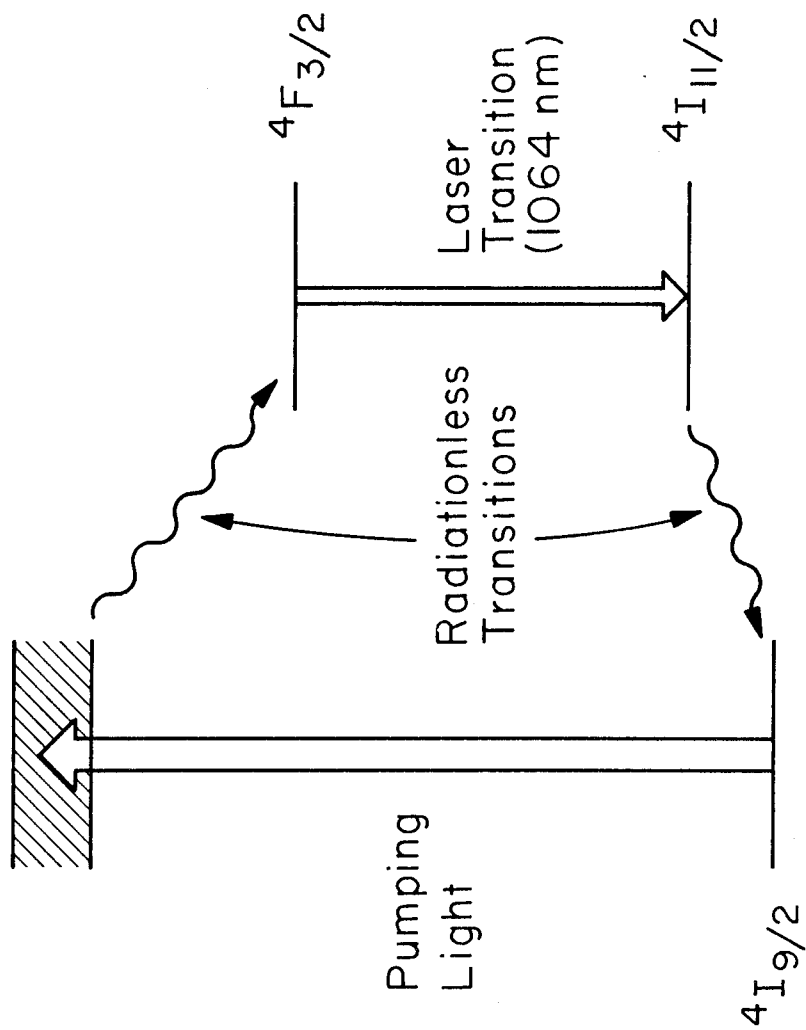


Figure 1

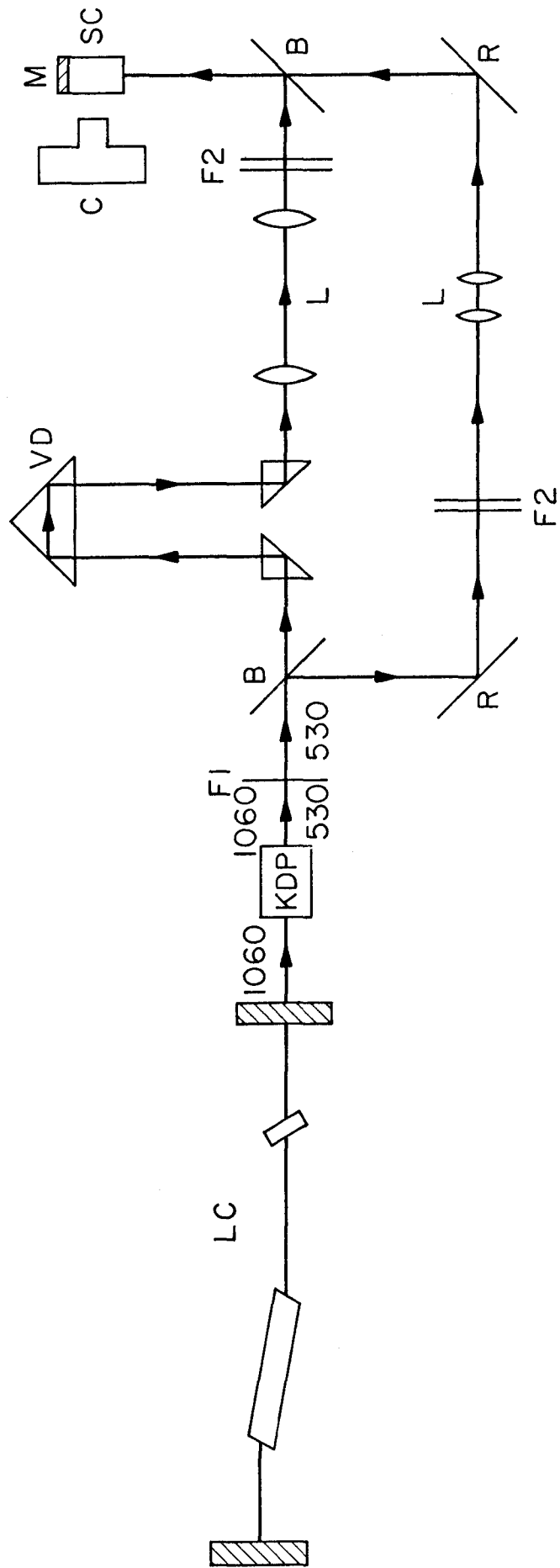


Figure 2

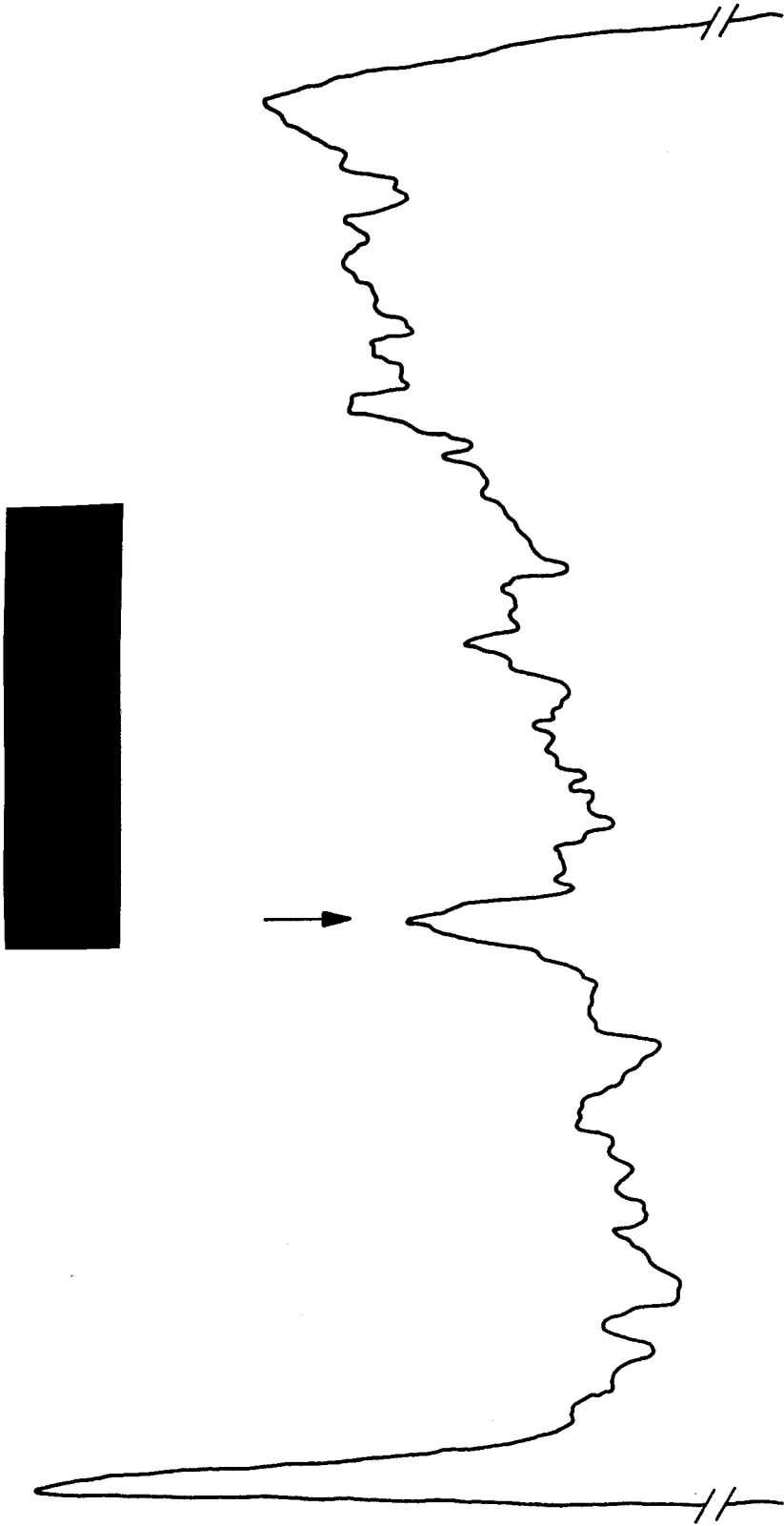


Figure 3

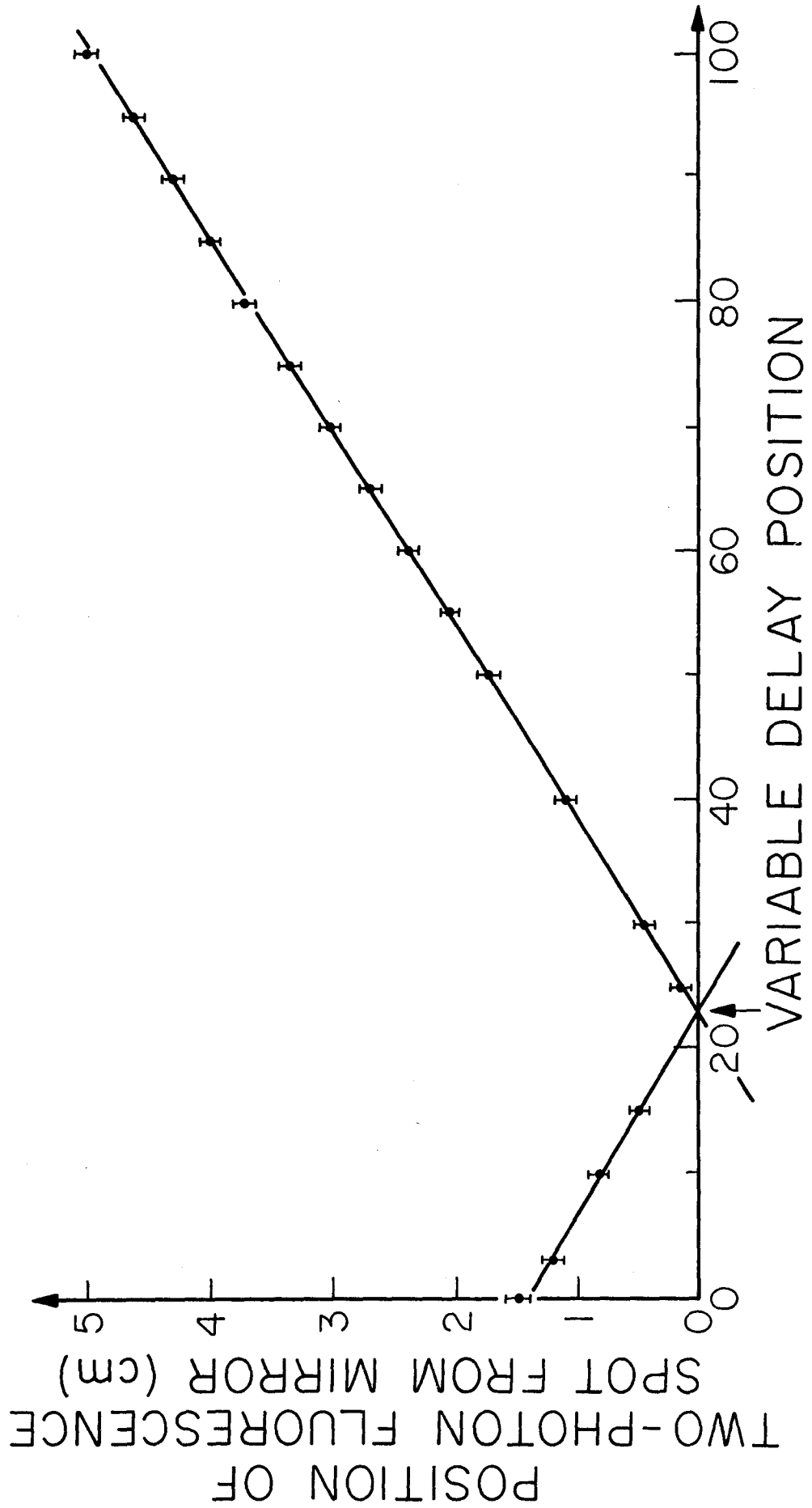


Figure 4